UNIVERSITY OF OKLAHOMA

GRADUATE COLLEGE

# A COUPLED HYDRAULIC-MECHANICAL ELASTOPLASTIC CONSTITUTIVE MODEL FOR UNSATURATED SANDS AND SILTS

A DISSERTATION

SUBMITTED TO THE GRADUATE FACULTY

in partial fulfillment of the requirements for the

Degree of

DOCTOR OF PHILOSOPHY

By

CHUNYANG LIU
Norman, Oklahoma
2009

A COUPLED HYDRAULIC-MECHANICAL ELASTOPLASTIC CONSTITUTIVE MODEL FOR UNSATURATED SANDS AND SILTS

A DISSERTATION APPROVED FOR THE
SCHOOL OF CIVIL ENGINEERING AND ENVIRONMENTAL SCIENCE

BY

Dr. Kanthasamy Muraleetharan, Chair

Dr. Younane Abousleiman

Dr. Tohren Kibbey

Dr. Gerald Miller

Dr. Luther White

# DEDICATION

To my wife and my upcoming son, Dave.

# ACKNOWLEDGEMENTS

I would like to express my deep gratitude and appreciation to my advisor, Professor Kanthasamy K. Muraleetharan, whose guidance, patience, friendship and encouragement over the past years have been invaluable, especially in those periods when I doubted successful completion of this research.

I appreciate the significant guidance and insightful comments from Dr. Younane Abousleiman, Dr. Tohren Kibbey, Dr. Gerald Miller and Dr. Luther White, members of my advisory committee. Their suggestions and comments are greatly valued.

A huge thank you to my beloved wife, Ms. Xuerong Huang. I am deeply indebted to my wife for her unfailing love, endless support and strong encouragement. Not only is she my wife, but she is my life. Finally, I wish to express my deep appreciation to my parents and my friends, whose continuous support provided me with the encouragement to pursue my dreams.

# TABLE OF CONTENTS

# LIST OF TABLES

# LIST OF FIGURES

# ABSTRACT

Unsaturated soils are three-phase porous media consisting of a solid skeleton, pore water, and pore air. It is well known that the behavior of unsaturated soils is influenced heavily by the matric suction (pore air pressure minus pore water pressure). Soil water characteristic curves (SWCCs) describe the relationship between matric suction and water content in unsaturated soils. In terms of constitutive modeling of soils, the relationship between matric suction and water content can be termed the hydraulic behavior of soils. SWCCs show hysteretic behavior depending on wetting/drying history of the soil. Recently geotechnical engineers have begun to notice that SWCCs also depend on the stress-strain history (mechanical behavior) of a soil. The hydraulic behavior of unsaturated soils, on the other hand, influences the mechanical behavior through matric suction. All of these facts, especially the coupling effects between hydraulic and mechanical behavior, demonstrate a very complex behavior of unsaturated soils.

Unsaturated soils are prevalent in many parts of the world and geotechnical engineers are often called to predict the behavior of these structures such as the rainfall induced failure of a compacted soil slope. In order to predict the behavior of unsaturated soil geotechnical engineering structures, a hysteretic SWCCs model is first proposed based on the bounding surface plasticity concept. The hysteresis in SWCCs is modeled using concepts that parallel the elastoplastic theory used to model stress-strain behavior

of soils. Matric suction is used as the stress variable and volume fraction of water or volumetric water content is used as the strain variable in modeling the SWCCs. This hysteretic SWCCs model is incorporated into a simple isotropic constitutive model to verify the proposed concepts that account for the coupling effects between hydraulic and mechanical behavior of unsaturated soils. Then a comprehensive constitutive model for unsaturated soils is developed in the general stress space. The rate equations of the proposed unsaturated soil model are integrated using a fully implicit integration scheme. Two sets of laboratory tests, one for Minco silt and another for Toyoura sand are used to calibrate and validate the model performance. The model is shown to capture the influence of stress-strain history on the SWCCs and the influence of SWCCs on the stress-strain behavior of silts and sands and predict the laboratory tests reasonably well.

# CHAPTER 1

# INTRODUCTION

## 1.1 BACKGROUND

Unsaturated soils are very common in the top layer of the Earth, where most engineering activities occur. Many geohazards like landslides are triggered by swelling and shrinking unsaturated soils. In order to reduce the damage caused by the geohazards or prevent them from happening, it is important and necessary to understand the stress-strain behavior of unsaturated soils. The necessity to evaluate such geohazards motivated the current research.

Unsaturated soils are multi-phase porous media. To keep the problem as simple as possible without losing generality, it is assumed that unsaturated soils are three-phase porous media composed of a solid skeleton, pore air and pore water. Generally speaking, pore water is not pure and some air and ions are dissolved in the water. In the current research, pore air and pore water are assumed to be homogeneous as idealized immiscible fluids. Also, the temperature-related effects are not considered and the stress-strain

behavior of unsaturated soils is assumed to be rate-independent. The microstructure of three-phase unsaturated soils is schematically shown in Fig. 1.1.

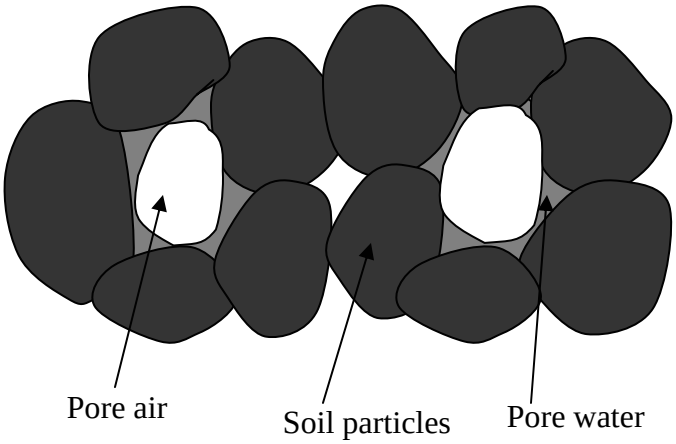


**Fig. 1.1** Microstructure of unsaturated soils

It is well accepted that the stress-strain behavior of both saturated and unsaturated soils is essentially elastoplastic, but unsaturated soils exhibit more complex behavior than saturated soils. Saturated soils are two-phase porous media composed of a solid skeleton and pore water, and the main difference between saturated and unsaturated soils is the existence of pore air in unsaturated soils. The complex engineering properties of unsaturated soils come from pore air and the interactions between pore air and pore water.

Although great efforts have been devoted to modeling unsaturated soils by many researchers, e.g., Alonso *et al*. (1990), Wheeler *et al*. (2003), and Li (2007 a&b), constitutive modeling of unsaturated soils is still a very active field and many fundamental issues, such as the selection of stress-strain variables, are still being researched. The currently available constitutive models for unsaturated soils are not

complete in the sense that some of them do not account for the water content variation (e.g., Alonso *et al*., 1990; Matsuoka *et al*., 2002; Faris *et al*., 2006), some of them can not describe the hysteresis of SWCCs (Thu *et al*., 2007) and some of them provide no information on unsaturated soil behavior under cyclic loadings (Li, 2007b). Increasing amount of experimental evidences (e.g., Cui and Delage, 1996; Rampino *et al*., 2000; Geiser *et al.*, 2006; Miller *et al.*, 2008) show that suction history strongly influences the stress-strain behavior of unsaturated soils and the stress-strain history affects the suction-water content relationship. In terms of constitutive modeling of soils, the suction-water content relationship (i.e., the SWCCs) can be termed the hydraulic behavior of soils. Although SWCCs play a major role in terms of fluid flow through unsaturated soils, the term hydraulic behavior refers to the relationship between water content and suction at a given point in the soil mass in this dissertation. The coupling effects between hydraulic and mechanical mechanisms have not been thoroughly investigated. The dearth of information on the interactions between SWCCs and stress-strain behavior forms a big gap between theoretical research and needs from engineering practice. The current research presents a comprehensive constitutive model to simulate the above-mentioned special features for unsaturated soils.

Minco silt is an Oklahoma soil and the engineering properties of Minco silt have been experimentally investigated in the laboratory at the University of Oklahoma for the last number of years (Ananthanathan, 2002; Vinayagam, 2004; Tan, 2005) and also has been used in centrifuge model tests (Deshpande, 1997). This availability of test results makes Minco silt an ideal soil for investigating analysis procedures such as constitutive

models. Usually, it is time-consuming and very costly to run laboratory tests under complex loading conditions, e.g., drying and wetting suction loops. The current research presents a constitutive model for Minco silt, whose model parameters can be calibrated using relatively simple laboratory tests. This constitutive model can then be used to predict soil behavior under complex loading conditions. Furthermore, this constitutive model and a finite element computer code can also be used to predict initial boundary value problems such as a centrifuge model test or a geotechnical structure in the field. The constitutive model presented here is also appropriate for simulating the engineering properties of other unsaturated silts and sands.

## 1.2 OBJECTIVES

The main objective of the current research is to propose a comprehensive constitutive model for unsaturated silts and sands. The development of unsaturated soil constitutive model so far has focused on clays only. The stress-strain behavior of sands and silts are somewhat similar, but quite distinct from that of clays. The first key aspect of the proposed constitutive model is the choice of stress-strain variables derived based on the theory of mixtures with interfaces (Muraleetharan and Wei, 1999). Another key aspect is the description of SWCCs within the framework of elastoplasticity and fully coupling it with the deformation of the soil skeleton. The elastoplastic description of the SWCCs will allow the model to easily describe the observed hysteresis in the curves. Third, this constitutive model can easily simulate unsaturated sand/silt behavior under cyclic loadings within the framework of elastoplasticity theory. The coupling

mechanisms between the SWCCs and soil deformation will allow the model to describe phenomena such as shrinkage induced by reduction in water content, wetting-induced collapse and the influence of soil deformation on SWCCs. The model has smooth transitions between dry state, unsaturated state and saturated state. Finally, the model parameters are easily calibrated via common triaxial tests and some other simple tests.

## 1.3 OUTLINE OF THE DISSERTATION

Chapter 2 presents a comprehensive literature review on constitutive modeling of unsaturated soils. The emphasis is laid on the evolution of the selection of stress-strain variables. At the same time, the advantages and disadvantages of some representative sand/silt models are analyzed. This chapter also discusses some typical elastoplasticity frameworks for predicting stress-strain behavior of saturated sands/silts under cyclic loadings.

Chapter 3 presents an extensive literature review on the available models for single SWCC and hysteretic SWCCs. After the literature review, this chapter discusses the physical mechanisms behind the hysteresis of SWCCs. Then a simple model based on the bounding surface plasticity concept (Dafalias and Popov, 1975&1976; Dafalias and Herrmann, 1986) is proposed to simulate the hysteresis in SWCCs. A wide range of SWCCs data covering clays, silts, sands and glass beads are used to check the performance of the model for SWCCs. The comparisons between test results and model predictions illustrate the satisfactory performance of the proposed model for SWCCs.

Chapter 4 presents a simple isotropic constitutive model for unsaturated soils. This isotropic model is proposed to check the validity of the idea on how to account for the coupling effects between hydraulic and mechanical mechanisms of unsaturated soils. This isotropic model fully incorporates the hysteretic SWCCs model proposed in Chapter 3. The hardening laws are simple but sufficient to capture the overall behavior of unsaturated soils. Comparisons between test results and model predictions illustrate the reasonable performance of the coupled isotropic model.

Based on the critical state two-surface plasticity model for sand introduced by Manzari and Dafalias (1997) and the modified SANISAND model (Taiebat and Dafalias, 2008), Chapter 5 presents a comprehensive constitutive model for unsaturated silts and sands in the general stress space to fully investigate the coupling effects between hydraulic and mechanical mechanisms. Soil behavior under monotonic/cyclic loading conditions is extensively investigated. A fully implicit integration method is adopted to implement the proposed model on the single element level. Some available test results are compared with the model predictions to check the performance of the proposed unsaturated soil model. Because very limited test results are available, some hypothetical studies are also carried out to investigate the coupled unsaturated soil behavior.

# CHAPTER 2

# LITERATURE REVIEW

## 2.1 INTRODUCTION

This chapter presents a thorough literature review on the constitutive modeling of unsaturated soils, ranging from the models based on the concept of effective stress to the models based on two stress variables. Among the two stress variables models, some use two independent stress variables, e.g., net stress and suction, while some others use dependent stress variables, which are actually (modified) suction and suction-related effective stress. The selection of dependent stress variables is always related to the thermodynamics or the mixture theory of porous media. The selection of stress-strain variables and the related models are extensively discussed in this chapter. Some important concepts for simulating cyclic loadings, e.g., the bounding surface plasticity concept (Dafalias and Popov, 1975&1976; Dafalias and Herrmann, 1986) and subloading surface concept (Hashiguchi, 1989) are also discussed. This is necessary for developing a constitutive model which can be used to predict soil behavior under cyclic loadings, including both external mechanical loadings and hydraulic drying/wetting loadings. Some important saturated soil models, including sand and clay models are also briefly reviewed.

The mechanical behavior of sands and silts are somewhat similar, but quite different from that of clays,

## 2.2 EFFECTIVE STRESS MODELS

Since the concept of effective stress for saturated soils was introduced by Terzaghi (1936), many researchers (e.g., Biot, 1941; Skempton, 1961; Suklje, 1969; Nur and Byerlee, 1971) have proposed different modified equations for effective stress for saturated porous media based on experimental observations or theoretical considerations. Among these definitions of effective stress of saturated soils or rocks, stress variables are total stress and pore water pressure, but the effect of pore water pressure on effective stress is accounted for in different ways. Generally speaking, the difference of effective stress comes from the weighting factor of pore water pressure, which involves the porosity, the compressibility or both. de Boer and Ehlers (1990), Lade and de Boer (1997) and Jardine *et al*. (2004) provided a comprehensive review on the historical development of the effective stress concept. The concept of effective stress is able to successfully predict shear strength characteristics and volume change process of saturated geomaterials (see Skempton and Bjerrum, 1957). Houlsby (1979) presented a different interpretation of the principle of effective stress in terms of continuum mechanics and stated that: "… *the principle of effective stress can be seen as a principle of the independence of the mechanical work input to the soil skeleton and to the pore fluid* …". From available literature, very few people discussed the relationship between water content and effective stress in saturated soils and Henkel (1960) seems to be the only

exception. For normally consolidated clays, Henkel (1960) found that water content is uniquely related to effective stress, irrespective of drainage conditions or stress path. In this way, specific volume is defined as an internal variable controlling soil behavior and this important finding was later used in the critical state soil mechanics (Roscoe *et al*., 1958). In summary, the concept of effective stress for saturated soils is well established and extensively accepted. It captures the stress-strain behavior of saturated soils well, although a unique effective stress may be not suitable for other geomaterials.

Due to the success in modeling saturated geomaterial behavior based on the concept of effective stress, it becomes natural to extend the concept of effective stress to unsaturated soils. In fact, two questions have to be clarified on the effective stress concept for unsaturated soils. First, can a single effective stress be used to describe the entire behavior, including both hydraulic and mechanical ones? If the answer to the first question is *yes*, then the second question is: how to define effective stress for unsaturated soils? The first question is actually related to the validity of the use of the effective stress concept in unsaturated soils. To answer both questions, the second question is discussed first and the first question will be automatically resolved.

Croney *et al*. (1958), Bishop (1959), Jennings (1961), Coleman (1962) and Blight (1967) were among the first who tried to use a single effective stress to describe unsaturated soil behavior. Probably, Croney (1952) was the first one to appreciate the importance of suction in relation to unsaturated soil deformation. Most proposed effective

stress equations for unsaturated soils have similar form to Bishop's equation (1959), which is given below in a modified form:

$$\boldsymbol{\sigma}' = (\boldsymbol{\sigma} - p_a \mathbf{I}) + \chi s_c \mathbf{I} \tag{2.1}$$

where: $\boldsymbol{\sigma}'$ is effective stress tensor; $\boldsymbol{\sigma}$ is total stress tensor; $\chi$ is the Bishop's parameter; $s_c = p_a - p_w$ is matric suction, which is defined as the difference between pore air pressure $p_a$ and pore water pressure $p_w$; $\mathbf{I}$ is the second order unit tensor. The soil mechanics sign convention is used here. That is, compressive stresses are considered positive.

Starting from microstructural analysis, Li (2003) also derived a Bishop-type but much more complicated effective stress for unsaturated soils. In the equation proposed by Li (2003), the coefficient in front of suction is a tensor instead of a scalar. Recently, using the double porosity concept, Khalili *et al*. (2005) suggested another Bishop-type effective stress, which was actually extended from the work done by Khalili and Khabbaz (1998), in which the Bishop parameter was defined as a function of suction. Starting from the conservation laws and mechanical energy for multi-phase porous media, Borja (2006) derived the effective stress for unsaturated soils that equals the difference between the total stress and mean neutral stress, which represents the relative contributions of intrinsic pore water and pore air pressures, weighted according to the degree of saturation. Interestingly, the effective stress derived by Borja (2006) has similar form to what Loret and Khalili (2000) calculated using the theory of mixtures. On the basis of the

consideration of enthalpy, Murray (2002) proposed an equation of state for unsaturated soils. Murray's equation of state is actually another Bishop-type effective stress of unsaturated soils with a complicated coefficient. Although the effective stress equations are based on different theories or experimental observations, they have similar form and the main difference comes from the definition of the Bishop's parameter $\chi$.

Although they agreed that the shear strength of unsaturated soils depends on the Bishop-type effective stress, Jennings and Burland (1962) were among the first to question the validity of Bishop-type effective stress in that it does not provide an adequate relationship between volume change, e.g. collapse and effective stress. Their findings were based on the consolidation tests on unsaturated soils. The samples they tested were supposed to expand upon flooding, because the effective stress should decrease when suction decreased, see Eq. (2.1). The samples, however, collapsed during flooding. The single Bishop-type effective stress failed to predict the collapse behavior. With the help of mixture theory, Bluhm and de Boer (1996) investigated the Terzaghi's principle of effective stress and concluded that the principle of effective stress is valid only in a special case of a mixture of an incompressible porous solid filled with incompressible and inviscid fluids, where the effective stresses of the fluids have been neglected. Li (2003) concluded that it is impossible to define an effective stress for unsaturated soils purely on the basis of continuum stress variables or of any of the combinations that assign a scalar identity to suction effect. Li (2003) introduced a fabric anisotropic tensor to account for the significant shear effect induced by suction. The

practical applicability of the effective stress definition by Li (2003) is questionable, because the fabric of soils is difficult to measure along a given loading path.

Although the difficulties in applying the Bishop-type effective stress have been extensively recognized by many people, e.g., Aichison and Donald (1956), Bishop and Donald (1961) and Fredlund and Morgenstern (1977), the efforts to find an "ultimate" effective stress for unsaturated soils have never been stopped. Recently, Khalili *et al*. (2004) provided some new evidence to prove that effective stress exists in unsaturated soils. Loret and Khalili (2002) introduced an effective stress elastoplastic model for unsaturated soils. Although the model performance on the behavior of solid skeleton looks reasonable, their model is incomplete in that no cyclic loading behavior can be simulated and the effect of soil deformation on the hydraulic behavior is not investigated.

In fact, most of the above listed references just provide effective stress equations, instead of fully implementing them into real constitutive models to describe unsaturated soil behavior. Prior to the 1990s, the concept of effective stress for unsaturated soils was used with fully linear or nonlinear elasticity theory. The difficulties in implementing the effective stress concept to simulate soil behavior are unavoidable, because the soil behavior is essentially elastoplastic instead of purely elastic. Starting from the 1990s, many researchers tried to apply the effective stress for unsaturated soils in the framework of elastoplasticity theory and they achieved some valuable progress.

Kohgo *et al*. (1993 a&b) proposed a new definition of effective stress for unsaturated soils based on microscopic analysis of pore water states. Further, they separated suction effects into two parts: one is that effective stress increases with increasing suction and the other one is that increasing suction induces increases in both yield stress and stiffness of soil skeleton. The two suction effects were accounted for within the framework of the modified Cam Clay model (Schofield and Wroth, 1968) and shear strength characteristics and volume change behavior were simulated in a reasonable manner. Still, no coupling effects between external loading and suction were considered and no water content information was provided. The limitations of Kohgo's model are actually the general problems that are very hard to solve using a single effective stress to simulate the complex behavior of unsaturated soils.

Coussy and Dangla (2002) introduced a very special equation for effective stress of unsaturated soils as follows:

$$\boldsymbol{\sigma}' = \left(\boldsymbol{\sigma} - p_a \mathbf{I} + s_r s_c \mathbf{I}\right) + \left(\frac{\partial (nU)}{\partial \boldsymbol{\varepsilon}}\right)_{s_r, T} \tag{2.2}$$

$$U(n, s_r) = \int_{s_r}^{1} f(n, s_c) ds_c \tag{2.3}$$

where $n$ is porosity; $U$ is the interface energy defined in Eq. (2.3); $\boldsymbol{\varepsilon}$ is the strain tensor of soil skeleton; $s_r$ is the degree of saturation; $T$ is absolute temperature in ºF.

The first bracket in Eq. (2.2) is actually Bishop's effective stress given in Eq. (2.1) with $\chi = s_r$. Eq. (2.3) states that the interface energy is directly related to the relationship between suction and degree of saturation, which actually represents the soil water characteristic curve. To determine the interface energy, the function $f(n, s_c)$ has to be specified. The effect of interface energy on soil skeleton stress is explicitly included in this definition. It seems that this single effective stress definition can predict hydraulic behavior, soil strength and soil deformation, but it is important to notice that the inclusion of interface energy is actually necessary information for describing hydraulic behavior. Of course, if different interface energies are given along same suction path, then the hysteresis of SWCCs will be captured. Although the explicit stress variables are different, this single effective stress definition is actually equivalent to the dependent stress variables, which will be introduced later.

Because of the difficulties in applying single effective stress to describe unsaturated soil behavior, many people (e.g., Bishop and Blight, 1963; Aitchison, 1967; Matyas and Radhakrishna, 1968; Barden *et al*., 1969) starting from the 1960s tried to use different combinations of stress variables to describe the stress-strain behavior of unsaturated soils. Their work and the progress they made will be reviewed next.

## 2.3 MODELS BASED ON INDEPENDENT STRESS VARIABLES

On the basis of the observations from the "null" tests, Fredlund and Morgenstern (1977) presented a theoretical stress analysis using continuum mechanics and concluded

that any two of the three normal stress variables, i.e., $p - p_a$, $p - p_w$ and $p_a - p_w$, can be used as stress state variables for unsaturated soils. Note: $p$ is mean total stress; $p_a$ and $p_w$ are pore air pressure and pore water pressure, respectively. The concept of two stress variables opens a new avenue to modeling unsaturated soil behavior. This eliminates the need to find a single effective stress, on which too much expectation is put to simulate both shear strength and volume change behavior simultaneously. The concept of two stress variables provides a good philosophy to decompose a complex problem into multiple simple sub-problems. Among the three possible combinations of stress variables, mean net stress $p - p_a$ and suction $p_a - p_w$ are the most common combination.

Although some early unsaturated soil models are available in the literature, for example Coleman (1962) and Lloret and Alonso (1985), these models are basically developed within the framework of state surfaces (Matyas and Radhakrishna, 1968) or some other simple method instead of using theory of elastoplasticity and they can only be used to simulate some aspect(s) of simple soil behavior. These models are not an integral scheme for constitutive modeling. The situation was not changed until Alonso *et al*. (1990) introduced the so-called Barcelona Basic Model. In the Barcelona Basic Model, mean net stress, deviatoric stress and suction were selected to be the fundamental stress variables. The Barcelona Basic Model was developed within the framework of the Cam Clay model (Schofield and Wroth, 1968) and one of the remarkable contributions is their definition of the loading collapse (LC) curve, which describes how the preconsolidation stress changes as suction changes. In other words, the effect of suction on the yield stress is captured by the LC curve. The yield locus is enclosed by the LC curve and the

maximum past suction ever experienced by the soil. With the LC curve, the Barcelona Basic Model can simulate many special mechanical behaviors, e.g. swelling or collapse induced by suction change. In the Barcelona Basic Model, change of stiffness and shear strength with suction can also be simulated. However, the Barcelona Basic Model provides no information on irreversible volume change and water content. The latter disadvantage was addressed by Wheeler *et al*. (2003). A thorough investigation on the Barcelona Basic Model was carried out by Wheeler *et al*. (2002). To improve the performance of the Barcelona Basic Model, Gens and Alonso (1992) and Alonso *et al*. (1999) introduced a neutral loading line to separate stress paths causing swelling from those causing compression. In this way, the modified Barcelona model can predict irreversible volume change, which is a great progress. The Barcelona Basic Model does not have the ability to simulate the irreversible change of water content during cyclic drying and wetting loops.

On the basis of suction-controlled triaxial tests on compacted Speswhite Kaolin conducted by Sivakumar (1993), Wheeler and Sivakumar (1995) proposed an elastoplastic critical state framework using mean net stress, deviatoric stress, suction and specific volume as state variables. With four state variables adopted in the model, an isotropic normal compression hyperline, a critical state hyperline and a state boundary hypersurface were defined. Although an associated flow rule was employed, the overall mechanical behavior of unsaturated soils under monotonic loading was well captured. But this model was too complicated in that many model parameters, e.g. the slope of the critical state line, were functions of suction. The difficulties in calibrating the model

parameters should not be underestimated. Realizing the model by Wheeler and Sivakumar (1995) provided no information on the variation of water content, Wheeler (1996) extended that model by introducing a second volumetric state variable, i.e., specific water volume. This model (Wheeler, 1996) is almost complete in the sense that it simulates both hydraulic and mechanical behavior of unsaturated soils, although no cyclic loading is considered. In addition, the selection of state variables is not justified by theoretical proof.

Cui and Delage (1996) performed a series of tests on Jossigny silt. They paid special attention to the effects of suction on the yielding behavior, which were accounted for using the LC concept presented by Alonso *et al*. (1990). Mean net stress and suction were selected to be the stress variables. An inclined elliptical form of the yield surface was adopted to capture the anisotropic stress state during $K_0$ compaction. A non-associated flow rule was adopted for better description of stress-strain behavior under monotonic loadings. Cui and Delage's model (1996) includes the effects of suction on dilatancy of unsaturated soils. Again, their work can only simulate monotonic stress-strain behavior of unsaturated soils without providing any information on the hydraulic behavior.

Starting from the Barcelona Basic Model, Thomas and He (1998) proposed an extended critical state elastoplastic constitutive model based on net stress and suction. Numerical analysis was carried out to provide variations of net stress, suction, specific volume and degree of saturation in unsaturated soils. To account for the degree of

saturation, a general form of state surface similar to Lloret and Alonso (1985) was introduced. Although the hydraulic behavior is incorporated in the modified model, the cyclic loading effects still can not be simulated. It seems that the elastoplastic model proposed by Muraleetharan and Nedunuri (1998) was the first one to account for the cyclic loading effects in unsaturated soils and their model was based on Wheeler's work (1996) and the bounding surface plasticity concept (Dafalias and Herrmann, 1986).

In addition to the above discussed models, Rampino *et al*. (2000), Macari *et al*. (2003), Chiu and Ng (2003) and Thu *et al*. (2007) also proposed different comprehensive models for unsaturated soils. Although these models differ in details, the framework they share is very similar in that the critical state concept is applied and the loading collapse curve is also included. To account for the water content change, soil water characteristics are proposed and SWCCs are incorporated into the constitutive model via suction, which goes into the yield surface as an independent stress variable. Recently, Sheng *et al.* (2008) have introduced a new modeling approach for unsaturated soils using independent stress variables. It is shown that the wetting-induced collapse and plastic shrinkage during initial drying are both directly coming from the suction-related hardening effects. In their model, the hysteretic SWCCs are incorporated into stress-strain relationships and some important questions in unsaturated soil mechanics have been investigated.

Most of the independent two stress variables models for unsaturated soils belong to the Barcelona Basic Model family or its modified version. Some interesting findings need to be pointed out. First, based on the experimental results, the critical state seems to

exist in unsaturated soils, see Maâtouk *et al*. (1995), Wang *et al*. (2002) and Estabragh and Javadi (2008) for silty soils, Adams (1996) and Toll (1990) for sandy clays and Wheeler and Sivakumar (2000) for compacted Speswhite Kaolin. Toll and Ong (2003) presented a comprehensive experimental investigation on the critical state parameters and further discussion on these parameters can be found in Toll and Ong (2004). Tarantino (2007) introduced a generalized critical state framework for unsaturated soils and three critical state equations were used to predict the deviatoric stress, the degree of saturation and the void ratio. Second, although suction can be defined as an independent stress variable, it does not mean the inclusion of suction enables a constitutive model to simulate the hydraulic behavior. A relationship to describe suction and water content, i.e., SWCCs has to be proposed. In this way, it is possible to account for the coupling effects between mechanical and hydraulic behavior. Third, to simulate the soil behavior under cyclic loading, a proper plasticity driver or framework should be selected. Last but not least, experimental investigation on the coupling effects between mechanical and hydraulic behavior of unsaturated soils should be carried out systematically. All the models have to be based on the experimental results. Currently, few experiments on unsaturated soils are available to systematically investigate the coupling effects between mechanical and hydraulic behavior, especially under cyclic loadings for both external loadings and suction. Generally, the models based on the two independent stress variables can capture many of the features of unsaturated soils, such as wetting-induced collapse and dependence of yield surface on suction. As pointed out by Loret and Khalili (2002), these models fail to reproduce some special features of unsaturated soils as noticed by

Fleureau *et al*. (1993), such as the elastic response that follows the plastic behavior in isotropically compressed soils that are subject to increasing suction.

As mentioned earlier, the selection of independent stress variables is not based on solid theoretical justification. It is very interesting to notice that some models, e.g. Alonso *et al*. (1990) have suction as one of the stress variables, but no corresponding strain-like variable is included. Similarly, the stress-strain variables for mechanical behavior are selected without solid basis. Very few people question the validity of the selection of the stress-strain variables used in these constitutive models. Geiser *et al*. (2000) pointed out the selection of net stress and suction could fail to provide a straightforward transition between saturated and unsaturated states. A drawback to select the (mean) net stress and suction as stress variables was also addressed by Sheng *et al*. (2004). Their main concern was on the numerical implementation of constitutive models into existing finite element codes, most of which are based on the concept of effective stress. If net stress and suction are selected to be the stress variables, then extra coding work has to be done to make the transition smooth between saturated and unsaturated states. As mentioned by Nuth and Laloui (2008a), separating the mechanical stress, i.e., net stress completely from the hydraulic stress, i.e., suction prevents a direct accounting of the hydraulic hysteresis effects on the mechanical behavior. On the basis of the above discussion, it is obvious that the appropriate selection of stress-strain variables is important to simulate the unsaturated soil behavior. The more reasonable selection of stress-strain variables for modeling unsaturated soils will be discussed in the next section.

## 2.4 MODELS BASED ON DEPENDENT STRESS VARIABLES

A good constitutive model has to be based on correct selection of stress-strain variables. Although the models reviewed in Section 2.3 provide reasonable simulations, the theoretical justification on the selection of stress-strain variables is not clear. Because the stress variables, e.g., net stress and suction, used for these models are easy to control in the laboratory, it is normal to treat them to be fundamental variables for constitutive modeling. Wheeler and Sivakumar (1995) provided a very brief discussion on the selection of stress-strain variables, but only Houlsby (1997) investigated this issue systematically. Houlsby (1997) derived the work input $W$ to an unsaturated granular material and the work conjugated stress-strain variables for unsaturated soils were defined as:

$$W = \cdots - ns_c \dot{s}_r + \cdots + \boldsymbol{\sigma}' : \dot{\boldsymbol{\varepsilon}} \tag{2.4}$$

$$\boldsymbol{\sigma}' = \boldsymbol{\sigma} - \left[ s_r p_w + (1 - s_r) p_a \right] \mathbf{I} = (\boldsymbol{\sigma} - p_a \mathbf{I}) + s_r s_c \mathbf{I} \tag{2.5}$$

where: $n$ is porosity; $s_c$ is suction; $s_r$ is degree of saturation; $\boldsymbol{\varepsilon}$ is strain tensor of the solid skeleton; $\boldsymbol{\sigma}'$ and $\boldsymbol{\sigma}$ are effective stress and total stress tensors, respectively.

Observations on Eqs. (2.4) and (2.5) indicate that the degree of saturation is conjugated to the modified suction, i.e. $ns_c$ and the conjugated stress to the skeleton strain is the new effective stress. Comparing Eq. (2.5) with Eq. (2.1) and recalling the definition of suction, it is found that Houlsby's new effective stress is nothing new but a

special form of Bishop's definition with $\chi = s_r$. Eq. (2.5) also shows the contribution of suction to the new definition of effective stress. Any change in suction will introduce possible change in effective stress. In this sense, the constitutive models for unsaturated soils using suction and suction-dependent effective stress are classified as dependent stress variables models. Any change in suction will definitely change water content in unsaturated soils as well.

Although Houlsby's work concludes a similar result as Bishop's effective stress definition, the contribution made by Houlsby can not be neglected or underestimated. It demonstrates a theoretical proof on the selection of stress-strain variables for modeling the mechanical and hydraulic behavior of unsaturated soils, although the stress-strain variables derived by Houlsby may not be the best choice. Interestingly, although derived on the basis of work input to the porous media, the effective stress given by Houlsby (1997) is consistent with thermodynamical consideration (Hassanizadeh and Gray, 1990; Hutter *et al*., 1999; Gray and Schrefler, 2001). However, the dynamic compatibility conditions on the interfaces are not enforced in Houlsby's (1997) derivation. Other alternatives of effective stress for unsaturated soils are also available, e.g., Li and Zienkiewicz (1992). Without clear definition of stress-strain variables, the numerical implementation, e.g. the finite element method, of any constitutive model will be awkward.

The saturated soil model proposed by Pastor *et al*. (1990) was extended by Bolzon *et al*. (1996) to simulate unsaturated soil behavior. Suction and Bishop's stress with $\chi$

assumed to be degree of saturation were selected to be stress variables. The emphasis of their work was laid on the soil stiffness change induced by suction. Some important soil behavior, for example collapse on wetting was investigated. Santagiuliana and Schrefler (2006) modified Bolzon *et al*.'s (1996) model by adding a hydraulic constitutive relationship, which was proposed by Sheng *et al*. (2004) to account for the soil water characteristics. The added feature enables the original model (Bolzon *et al*., 1996) to take into account the irreversible deformation during cyclic drying and wetting loadings. Overall, the model proposed by Santagiuliana and Schrefler (2006) provides reasonable predictions on both mechanical and hydraulic behavior, but the simulation of dilation behavior needs improvements. To get better model prediction on dilation, good silt/sand base model should have been selected. Santagiuliana and Schrefler (2006) validated their model based on experimental results from Sion silt, while Bolzon *et al*.'s (1996) model was originally developed for clays.

Gallipoli *et al*. (2003b) introduced an improved constitutive model to predict the degree of saturation incorporating dependence on suction and specific volume as well. In this way, the effects of soil deformation on the degree of saturation are fully considered, but no hydraulic hysteresis during wetting and drying is discussed. Later, to account for the magnitude of the interparticle bondings due to water menisci, Gallipoli *et al*. (2003a) introduced a new constitutive parameter $\xi = f(s_c)(1 - s_r)$, which was related to suction $s_c$ and degree of saturation $s_r$. The parameter $\xi$ accounts for the contributions from the intensity of the stabilizing normal force from the interparticle contact by a single water meniscus and the number of water menisci. Through connecting the parameter $\xi$ to soil

deformation parameters, e.g., the void ratio, the effects of hydraulic behavior on mechanical behavior are considered. Although this elastoplastic soil model is very simple, the overall performance is good. The coupling effects in unsaturated soils are taken into account. Further discussion on this model can be found in Gallipoli *et al*. (2004).

With the emphasis laid on the different roles of pore air pressure and pore water pressure, Wheeler *et al*. (2003) presented a comprehensive constitutive model for unsaturated soils, which captures the coupling effects between hydraulic hysteresis and the mechanical behavior. Based on experimental observations, the loading collapse curve, suction increase yield curve and suction decrease yield curve were assumed to be straight lines in the mean Bishop's stress with $\chi = s_r$ and modified suction space. The mean Bishop's stress can be actually regarded as the mean effective stress. The three yield lines are related to each other. The movement of any yield line will introduce the corresponding changes on the other two. In this way, the coupling effects between hydraulic and mechanical behavior is fully considered. Although this model captures some basic behavior of unsaturated soils, the soil water characteristics are too simple and the model need to be modified for better predictions on the soil behavior under cyclic loadings. Later, Sun *et al.* (2007a&b) adopted similar simplified hysteretic SWCCs and yield suction curves to Wheeler *et al.* (2003) in the framework of the Barcelona Basic Model to investigate the unsaturated Pearl clay behavior.

On the basis of thermodynamical consideration, Li (2007a) systematically investigated some important concepts, e.g., critical state and SWCCs in unsaturated soils

and a demonstrative model for unsaturated soils was proposed. Since Li's (2007a) work was based on Houlsby (1997) and Collins and Kelly (2002), the stress-strain variables were the same as given by Houlsby (1997). Both the effective stress increment and modified suction increment were functions of the strain increment and the degree of saturation increment. The coupling effects between hydraulic and mechanical behavior were proved using the thermodynamics laws. In addition, it was proven that the hysteresis of SWCCs at a given strain of solid skeleton was not in conflict of the fundamental laws (Wei and Dewoolkar, 2006). Also, if a unique SWCC was assumed, the critical state lines and the isotropic consolidation lines for the soil skeleton were proved to exist and they could be treated as state functions. Following his thermodynamics-based constitutive framework, Li (2007b) presented a basic model, in which the coupling effects were fully considered and the hysteresis of SWCCs was also addressed. His model was not used for predicting soil behavior under cyclic shearing or compression. The impact of volume change on SWCCs was not considered either. Overall, the constitutive framework set up by Li (2007a) provides a strong theoretical justification on the selection of the stress-strain variables, the existence of critical state and the coupling effects between hydraulic and mechanical behavior in unsaturated soils.

In fact, Houlsby (1997) pointed out that any linear combination of the stress variables is possible for soil modeling, as long as the new stress-strain variables meet the work input definition. Eq. (2.6) illustrates such a treatment:

$$
\begin{aligned}
W &= \cdots - n s_c \dot{s}_r + \cdots + \boldsymbol{\sigma}' : \dot{\boldsymbol{\varepsilon}} \\
&= \cdots + s_c \left( - n \dot{s}_r + s_r \dot{\varepsilon}_v \right) + \cdots + \left( \boldsymbol{\sigma} - p_a \mathbf{I} \right) : \dot{\boldsymbol{\varepsilon}} \\
&= \cdots + s_c \dot{v}_w / v + \cdots + \left( \boldsymbol{\sigma} - p_a \mathbf{I} \right) : \dot{\boldsymbol{\varepsilon}}
\end{aligned}
\tag{2.6}
$$

where: $v_w = 1 + s_r e$ is the specific water volume, which was also used by Wheeler and Sivakumar (1995); $v = 1 + e$ is the specific volume and $e$ is the void ratio; $\varepsilon_v$ is the volumetric strain.

As noticed by Sheng *et al*. (2004), if dependent stress variables $s_c$ and $\boldsymbol{\sigma}'$ are adopted, then their conjugated strain variables $s_r$ and $\boldsymbol{\varepsilon}$ are independent; if independent stress variables $s_c$ and $\left( \boldsymbol{\sigma} - p_a \mathbf{I} \right)$ are used, then their conjugated strain variables are dependent. It means the selection of stress-strain variables is not absolute and any linear algebraic operation on the work input equation can always provide some alternatives. More discussion on the selection of stress-strain variables for unsaturated soil modeling can be found in Lu and Likos (2006), Sheng *et al.* (2008) and Laloui and Nuth (2009). Generally speaking, the selection of stress-strain variables depends on many factors, for example the compressibility of soil skeleton and pore fluid, the consideration on the interfaces between pore fluids and the validity of the averaging process (Gray and Hassanizadeh, 1989).

Based on the discussion by Wilmanski (1995) and Hassanizadeh and Gray (1990), the dynamic compatibility conditions on the interfaces have to be satisfied. Following the Laws of thermodynamics and enforcing the dynamic compatibility conditions on the

interfaces between different phases in multi-phase porous media, Muraleetharan and Wei (1999), Wei (2001), Wei and Muraleetharan (2002 a&b) obtained the energy dissipation inequality in unsaturated soils as:

$$D_p = \left[n_s\left(\mathbf{t}_s - p_a\mathbf{I}\right):\dot{\boldsymbol{\varepsilon}}^p + \xi\dot{\chi}\right] + \left[-s_c\dot{n}_w^p + \zeta\dot{\gamma}\right] \geq 0 \qquad (2.7)$$

where: $n_s$ is the volume fraction of solid component, i.e., the ratio between volume of solids and total volume of soil; $\mathbf{t}_s$ is the intrinsic Cauchy stress tensor of solid component, which is assumed positive in compression; $p_a$ is the pore air pressure; $\mathbf{I}$ is the unit tensor $\delta_{ij}$ ; $\boldsymbol{\varepsilon}^p$ is the plastic strain tensor of the solid component; $s_c$ is the matric suction, which equals $\left(p_a - p_w\right)$ with $p_w$ the pore water pressure; $n_w^p$ is the irrecoverable volumetric water content or volume fraction of water ; $\xi$ and $\zeta$ are internal forces associated with $\chi$ and $\gamma$, which account for the hardenings of solid skeleton and water phase, respectively.

From Eq. (2.7), the plastic deformation of the solid skeleton and the irrecoverable water content change posses similar energy dissipation forms, but the microscopic mechanisms behind the two plastic behavior are totally different. Plastic deformation of solid skeleton comes from the slipping and rolling of solid grains and driven by external forces. The irrecoverable moisture content change is controlled by the surface energy dissipation during changes in shape of the air-water menisci. More restrictively, the two

different mechanisms of energy dissipation can be decomposed and Eq. (2.7) can be rewritten as follows:

$$D_s = n_s\left(\mathbf{t}_s - p_a\mathbf{I}\right):\dot{\boldsymbol{\varepsilon}}^p + \xi\dot{\chi} \geq 0 \tag{2.8}$$

$$D_w = -s_c\dot{n}_w^p + \zeta\dot{\gamma} \geq 0 \tag{2.9}$$

An important observation based on Eq. (2.8) is that the plastic deformation can be described using the following stress measure, because it is conjugated with the plastic strain rate $\dot{\boldsymbol{\varepsilon}}_p$ of the solid skeleton:

$$\boldsymbol{\sigma}' = n_s\left(\mathbf{t}_s - p_a\mathbf{I}\right) = \left(\boldsymbol{\sigma} - p_a\mathbf{I}\right) + n_w s_c\mathbf{I} \tag{2.10}$$

where: $n_w$ is the volume fraction of water.

Although same notation is adopted here, $\boldsymbol{\sigma}'$ in Eq. (2.10) is different from $\boldsymbol{\sigma}'$ in Eq. (2.1). Here, $\boldsymbol{\sigma}'$ is referred to as *the intergranular stress tensor*, which plays the similar role to the effective stress as defined earlier in the sense the intergranular stress tensor governs the energy dissipation of soil skeleton. For fully saturated conditions, $\boldsymbol{\sigma}'$ becomes the Terzaghi's effective stress. Note that the proposed intergranular stress is equivalent to the Bishop's effective stress when the Bishop parameter $\chi_w$ equals $n_w$. In Eq. (2.9), the minus sign in front of $s_c$ means the volume fraction of water decreases when suction increases or *vice versa*. In the intergranular stress tensor, it is not necessary

to *a priori* evaluate $n_w$, since $n_w$ is already described by the relationship between moisture content and suction, which is actually the soil water characteristic curves (SWCCs). The energy dissipation of SWCCs is given in Eq. (2.9). With the dissipation inequalities given in Eqs. (2.8) and (2.9), the evolution equations for $\dot{\boldsymbol{\varepsilon}}^p$ and $\dot{n}_w^p$ can be derived using the standard procedure from the theory of plasticity. One of the key deviations of Muraleetharan and Wei (1999) and Wei (2001) from other thermodynamics related works for unsaturated soils is their fundamental assumption that free energy densities of phases depend on the volume fractions of these phases.

In the intergranular stress, volume fraction of water is actually a weighting factor of suction. The selection of volume fraction of water to be the weighting factor is more appropriate than degree of saturation or an empirical parameter $\chi$, see Eq. (2.1). Recall the volume fraction of water is equal to the product of degree of saturation and porosity, i.e., $n_w = s_r \times n$. In this sense, the inclusion of volume fraction of water in the intergranular stress accounts for effects from both the porosity and the degree of saturation. In the current research, the intergranular stress and suction are selected to be the stress variables and they are conjugated with the plastic strain rate $\dot{\boldsymbol{\varepsilon}}^p$ and the rate of the irreversible volume fraction of water $\dot{n}_w^p$, respectively.

To investigate the advantages introduced by the intergranular stress, the critical state concept is examined within two different frameworks as shown in Figs. 2.1. If suctions are different, the critical state line for Kaolin (Sivakumar, 1993) is different when the critical state is plotted in the mean net stress and deviatoric stress space. In

other words, the critical state is not unique and it is related to the suction in the mean net stress and deviatoric stress space. However, if the critical state is plotted in the mean intergranular stress, i.e., $p' = (\sigma'_{11} + \sigma'_{22} + \sigma'_{33})/3$ and deviatoric stress space, the critical state line becomes unique. The existence of a unique critical state line for unsaturated soils is one of the advantages of using the intergranular stress.

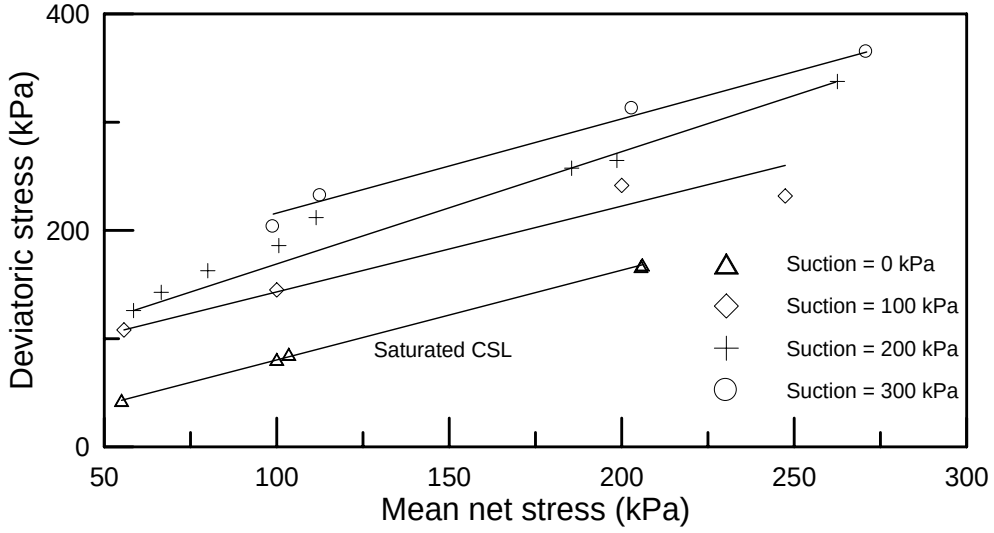


**Fig. 2.1a** Critical state lines for Kaolin in mean net stress vs. deviatoric stress plane

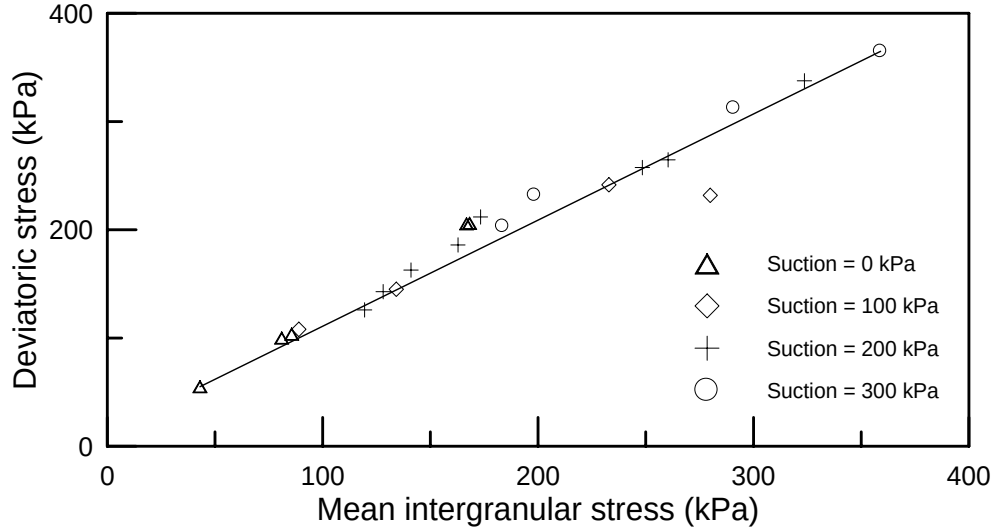


**Fig. 2.1b** Critical state line for Kaolin in mean intergranular stress vs. deviatoric stress plane

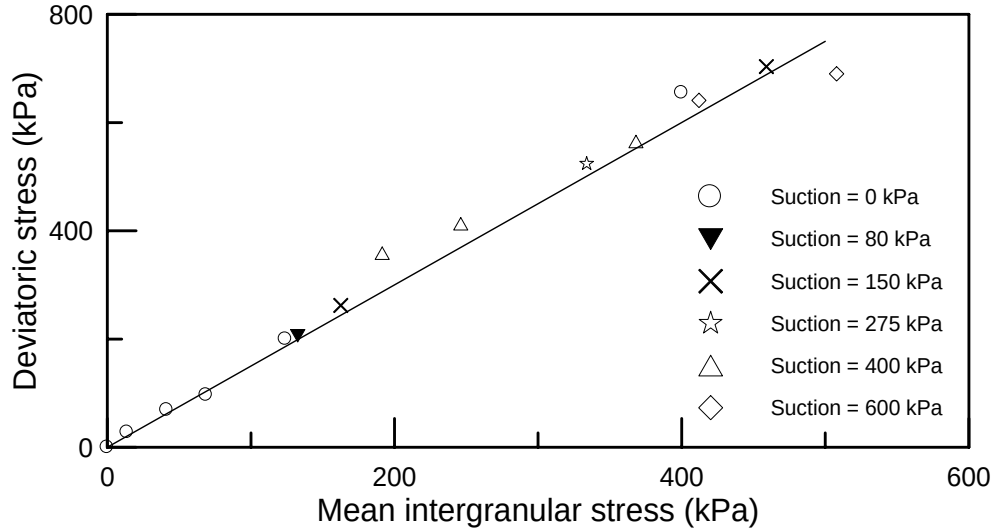


**Fig. 2.2** Critical state line for Trois-Rivières silt in mean intergranular stress vs. deviatoric stress plane

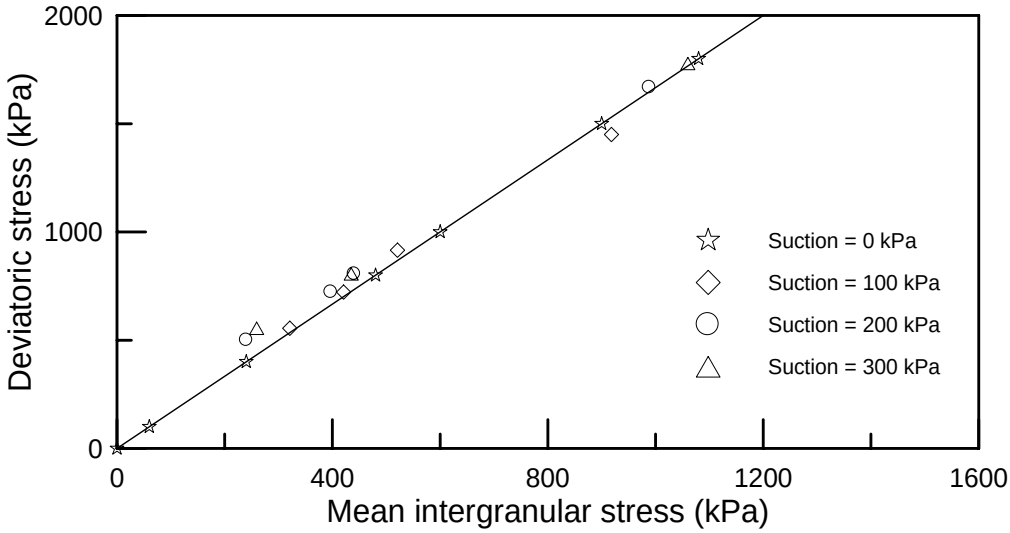


**Fig. 2.3** Critical state line for a silty sand in mean intergranular stress vs. deviatoric stress plane

Similar procedure was carried out on different soils to justify the validity of the critical state concept in unsaturated soils. Maâtouk *et al.* (1995) reported some valuable test results measured under a wide range of suctions on Trois-Rivières silt. The critical

state of Trois-Rivières silt was plotted in Fig. 2.2 in the mean intergranular stress vs. deviatoric stress space. Rampino *et al.* (2000) reported the mechanical responses of a silty sand. Fig. 2.3 also illustrates the critical state of the silty sand in the mean intergranular stress vs. deviatoric stress space. As is shown in the above figures, the adoption of the intergranular stress ensures a unique critical state line for not only clays, but also silts and sands. The extension of the critical state concept from saturated soils to unsaturated soils is valid with the introduction of the intergranular stress. To calibrate the parameters for the critical state line for an unsaturated soil, any test on saturated soils should work, since both saturated and unsaturated soils have the same critical state line.

## 2.5 ELASTOPLASTICITY THEORY ON CYCLIC LOADING

One of the main objectives of the current research is to simulate unsaturated soil behavior under cyclic loading, including both cyclic suction and cyclic external loadings. Most of the models reviewed in the last sections are not appropriate to predict soil behavior under cyclic loadings. The main objective of this section is to review some representative theories for cyclic loadings.

By introducing the concept of 'a field of hardening moduli', Mrŏz (1967 & 1969) generalized the hardening rules to better simulate metal behavior for complex loading histories, such as cyclic loading. The work hardening model was termed as multi-surface plasticity model. By taking into account both isotropic hardening and kinematic hardening, Mrŏz *et al*. (1978) extended the implementation of multi-surface plasticity

model from metal to soils. To account for the isotropic hardening, the yield condition is assumed to depend on stress state and some internal variables of soil, such as irreversible void ratio. For cyclic loading processes, hysteretic phenomena are of essential importance. Due to the initial preconsolidation, kinematic hardening has to be taken into account. The original multi-surface plasticity model is composed of one yield surface, one bounding surface and a finite number of nesting surfaces. The hardening modulus on the yield surface depends on the relative configuration of the yield surface and bounding surface. The nesting surfaces can translate and expand or contract due to the internal variables, such as irreversible density change. Certain nesting surface becomes active when the current stress state reaches it and the corresponding hardening modulus will be calculated based on this nesting surface and certain translational rule. Since the nesting surfaces are different, the hardening moduli vary in a piecewise linear manner between nesting surfaces. By assuming an infinite number of nesting surfaces, continuous evolution of the hardening modulus can be achieved, see Mrŏz *et al*. (1978 & 1981). Based on the multi-surface plasticity theory, a uniform formulation was proposed by Mrŏz and Pietruszczak (1983) for sands and Pietruszczak and Mrŏz (1983) for clays. Mrŏz *et al*. (1978 & 1979) also presented a simplified two-surface (i.e., the yield surface and bounding surface) model as a special version of multi-surface model to avoid tracing the evolution of all nesting surfaces. The hardening modulus depends on the distance between the current stress state and its associated point on the bounding surface. This simplified two-surface model is similar to the bounding surface plasticity model, which will be reviewed next.

The classical isotropic or kinematic hardening plasticity models are reasonably good for simple loading histories. For complex loading histories, such as cyclic loadings in plastic range, these models are incapable of simulating the hysteretic behavior, which is important to account for the damage accumulation or stabilization of hysteresis loops after a certain number of cyclic loadings. The bounding surface plasticity theory (Dafalias and Popov, 1975 & 1976; Krieg, 1975) is an attempt to generalize the conventional flow theory to account for the cyclic behavior of materials. The idea behind the bounding surface plasticity concept is very simple: for any current stress state inside the quasi-elastic domain, there is an associated point on the bounding surface by means of a certain mapping rule. The plastic modulus of current stress state depends on the distance between current stress state and its associated point on the bounding surface. A salient feature which differentiates the bounding surface concept from the multi-surface plasticity model is that the bounding surface plasticity theory allows plastic deformation to occur even for stress state inside the quasi-elastic domain. Dafalias and Herrmann (1982) stated that: *the quasi-elastic domain is not a yield surface since the stress may move first elastically inwards and then introduce plastic loading before it reaches this surface again; the quasi-elastic domain is not a loading surface either, since no associated consistency condition is required*. The mathematical foundation and formulation of the bounding surface plasticity model can be found in Dafalias and Herrmann (1982) and Dafalias (1986). Dafalias and Herrmann (1986) and Anandarajah and Dafalias (1986) presented the applications of the bounding surface plasticity to isotropic and anisotropic cohesive soils, respectively. A time-dependent version of bounding surface model was introduced by Kaliakin *et al*. (1987). Because the concept

behind the bounding surface plasticity is reasonable and simple, many applications to model geomaterials and refinements to the bounding surface plasticity can be found in literature, such as Bardet (1986 & 1990), Wang *et al*. (1990), Kaliakin and Dafalias (1990), Crouch and Wolf (1994 a&b), Crouch *et al*. (1994), Ling *et al*. (2002) and Datcheva and Schanz (2003).

Among these works, it is worth to mention the sand model proposed by Crouch *et al*. (1994). To define a reasonable loading surface, both radial and deviatoric mapping rules are used. A non-associated flow rule is incorporated into a sub-elliptic plastic potential surface. The critical-state line is also special because of its bi-linear kinked shape. An 'effective' normal consolidation line is used to link the loose state and dense state, instead of using different sets of model parameters to simulate sand behavior when their densities are different. Although this model is capable of simulating many special characteristics, such as plastic stiffening during cyclic loadings, this model is too complicated in the sense that too many model parameters need to be calibrated and the continuity condition between two mapping regions is sometimes violated. In addition, as stated by Mrŏz (1980), the translational rule proposed by Dafalias and Popov (1977) is nothing new but a limiting case of the multi-surface model formulation.

As noticed by Prevost (1982), although the multi-surface model provides great versatility and flexibility to describe material behavior, it suffers inherent storage inconvenience, because the theory requires that the field calculations, the positions, the sizes and plastic moduli of each yield surface be stored at each integration point in a

finite element implementation. Meanwhile, the bounding surface plasticity model requires *a priori* selection of the evolution laws.

While the multi-surface model and the bounding surface plasticity concept attracted many researchers' attention, a similar model named subloading surface model was introduced by Hashiguchi and Ueno (1977). Hashiguchi (1978, 1980, 1985, 1989, 1993 & 2000) published a series of papers on refining and implementing the subloading surface model. The subloading surface model is composed of two surfaces: an inner sub-loading surface on which the current stress state lies and the outer yield surface. In the subloading surface model, the subloading surface passing through the current stress point and similar to the normal-yield surface is incorporated and the plastic modulus is assumed to depend on the measure of degree of approaching the yield surface, called the *normal-yield ratio*, which is the ratio of the size of the subloading surface to that of the yield surface. While Dafalias (1986) stated that no consistency condition is needed for stress point inside the bounding surface in the bounding surface model, the consistency condition for the subloading surface model is explicitly introduced and the plastic modulus is rationally derived based on the consistency condition for the subloading surface. The subloading surface model fulfills the continuity condition, the smoothness condition and the work rate-stiffness relaxation requirements. The Masing effect, which is required to simulate cyclic loading behavior, is also satisfied. To better simulate soil behavior, Hashiguchi and Chen (1998) formulated the evolution rule of rotational hardening to describe the inherent anisotropy of $K_0$-consolidated soils. Although the

subloading surface model formulation is very complicated, the basic idea is very similar to those of the multi-surface model and the bounding surface model.

Starting from the single surface isotropic hardening model (Kim and Lade, 1988; Lade and Kim, 1988 a&b), Lade and Inel (1997) and Inel and Lade (1997) added the rotational kinematic mechanisms to develop a constitutive model accounting for the soil behavior during cyclic loadings. Here both the yield surface and plastic potential surface involve a combination of isotropic and kinematic hardenings. Their model preserves the soil behavior of isotropic hardening under monotonic loadings and the added rotational kinematic hardening enables the model to simulate the soil behavior under cyclic loadings. Within the combined frameworks of kinematic hardening and bounding surface plasticity, Gajo and Muir Wood (1999) introduced a kinematic hardening model for sands. Similarly, Manzari and Dafalias (1997) developed a critical state two-surface plasticity model for sands and their work will be reviewed in detail in Chapter 5, since the current research is based on their work.

Some other representative frameworks for simulating soil behavior under cyclic loadings include Desai (1974), Lade and Duncan (1975), Nova and Muir Wood (1979), Nova and Hueckel (1981), Zienkiewicz *et al*. (1985) and Pastor *et al*. (1985). At the same time, the experimental investigation on the soil behavior under cyclic loadings was progressing as well. The main contribution belonged to Tatsuoka and Ishihara (1974), Ishihara *et al*. (1975 & 1980), Hyodo *et al*. (1991 & 1994), Arumoli *et al*. (1992), Ishihara (1993), Verdugo and Ishihara (1996), Uchida and Stedman (2001) and so on.

This section presented a thorough literature review on the constitutive modeling of saturated soil behavior under cyclic loadings. The plasticity driver and hardening laws are the main topics covered. The multi-surface plasticity model, the bounding surface plasticity model and the subloading surface model share many similar characteristics in that different surfaces are used to carry out different tasks. Different hardening laws are also proposed to simulate soil behavior under cyclic loadings. These important concepts will be adopted for unsaturated soil constitutive modeling in the current research.

## 2.6 SUMMARY

This chapter first reviewed the concept of effective stress in saturated soils. The extension of the concept of effective stress from saturated soils to unsaturated soils was then discussed. Although the idea to use a single effective stress to simulate unsaturated soil behavior is attractive, it is very difficult to recover all the complex coupling effects between mechanical and hydraulic behavior of unsaturated soils using a single effective stress. The historical development of constitutive models from stress-suction-strain to stress-suction-strain-water content was also briefly discussed. The inclusion of the soil water characteristics in unsaturated soil modeling will definitely improve the model performance. The models based on independent stress variables capture some special features of unsaturated soils, including the coupling effects, but the selection of stress-strain variables is not based on theoretical justification. It seems reasonable to predict the

unsaturated soil behavior using the dependent stress variables within an appropriate elastoplasticity framework.

# CHAPTER 3

# SOIL WATER CHARACTERISTIC CURVES

## 3.1 INTRODUCTION

Unsaturated soils are composed of three phases: soil skeleton (solid), pore water (liquid), and pore air (gas). The air-water interface plays a major role in the behavior of unsaturated soils. Sometimes, the air-water interface is treated as a fourth phase (Fredlund and Rahardjo, 1993). The distinctive property of the air-water interface is its ability to exert a tensile pull. From a macroscopic viewpoint, the pressure difference (i.e., pore air pressure minus pore water pressure) across the air-water interface is called the matric suction. In soil mechanics, the water content information is usually correlated to suction through the soil water characteristic curves (SWCCs). It is important to know that the SWCCs have a close relationship to many soil properties, such as shear strength, permeability, diffusion and adsorption. In practice, the SWCCs provide useful information for modern agriculture, geoenvironmental engineering, petroleum engineering and many other fields.

The relationship between water content and suction is not unique and exhibits hysteresis (e.g., Poulovassilis, 1970a; Topp, 1971a). Using the Laws of thermodynamics, Hassanizadeh and Gray (1993) investigated the thermodynamic basis of capillary pressure in porous media and they hypothesized that the hysteretic phenomenon in SWCCs is indeed the result of projecting a complex capillary function onto a single plane. Further suggestion was given by Hassanizadeh and Gray (1993) that a complete functional dependence of capillary pressure should include the specific area of the air-water interface in addition to the water content. Following the hypothesis given by Hassanizadeh and Gray (1993), some researchers proposed theoretical models (e.g., Reeves and Celia, 1996; Held and Celia, 2001) or designed laboratory experiments (e.g., Cheng *et al.*, 2004; Chen, 2006) to investigate the relationship between capillary pressure, water content and interfacial area. The results show that the relationship is not unique and the hypothesis by Hassanizadeh and Gray (1993) does not hold. It was suggested that some new internal variables may have to be introduced to establish a unique functional dependence of capillary pressure. Using the thermodynamic theory, Morrow (1970) even developed a detailed mechanism of immiscible displacement in porous media in terms of a quantized model. The theoretical investigation, including the above efforts, on the capillary hysteresis will make this problem more and more complicated and the complex situation can significantly impede the application of the hysteresis model in practice. In this chapter, the discussion on the capillary hysteresis, i.e. SWCCs is limited to the relationship between suction and water content for simplification. No more (internal) variables are considered.

A typical set of hysteretic SWCCs (Chen *et al*., 2007) for a fine sand ($D_{50}$ = 0.14 mm, SP) is shown in Fig. 3.1.

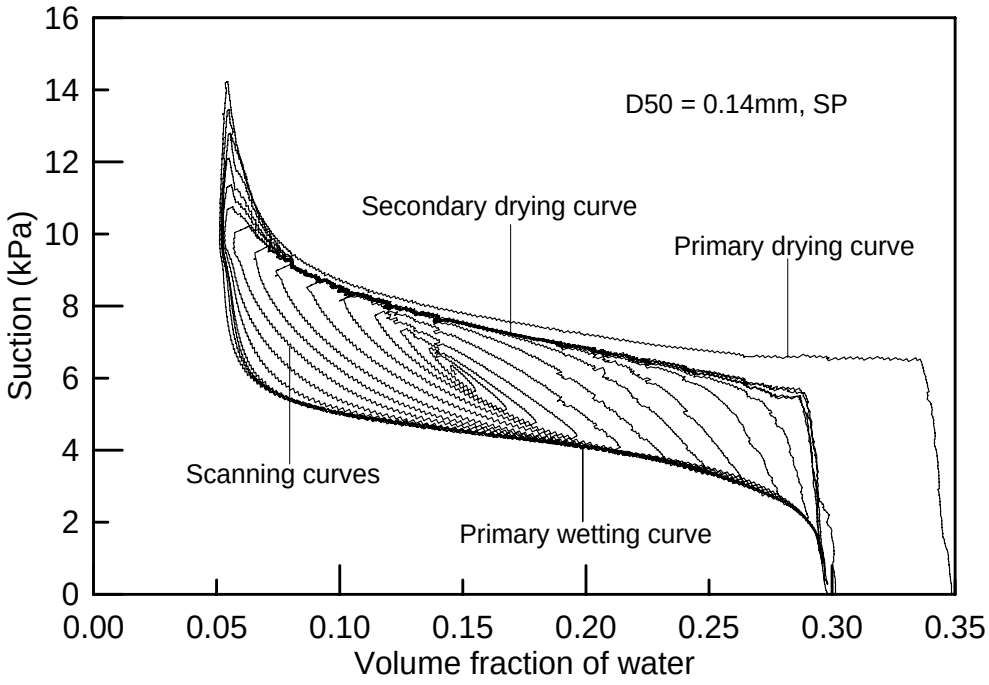


**Fig. 3.1** Measured SWCCs for a fine Ottawa sand (after Chen *et al*., 2007)

Generally speaking, to get a complete hysteretic loop of SWCCs in the laboratory is very time consuming. For example, obtaining the primary wetting and drying portions of the SWCCs for a sand using conventional methods based on ceramic capillary barriers can take as long as 2 to 4 months. These curves in Fig. 3.1 were obtained using an innovative automated parallel miniature pressure cell system (Chen *et al*., 2007). They made use of a novel experimental setup that can obtain the primary wetting and drying curves for a sand within 1.5 to 6.5 hours, and a complete set of SWCCs, including detailed scanning loops, within 13 to 19 hours. The primary drying curve, the primary wetting curve, the secondary drying curve, and selected scanning curves are presented.

The secondary drying curve is different from the primary drying curve due to air entrapment. For completeness, the particle size distribution curve of the fine Ottawa sand used by Chen *et al*. (2007) is given in Fig. 3.2:

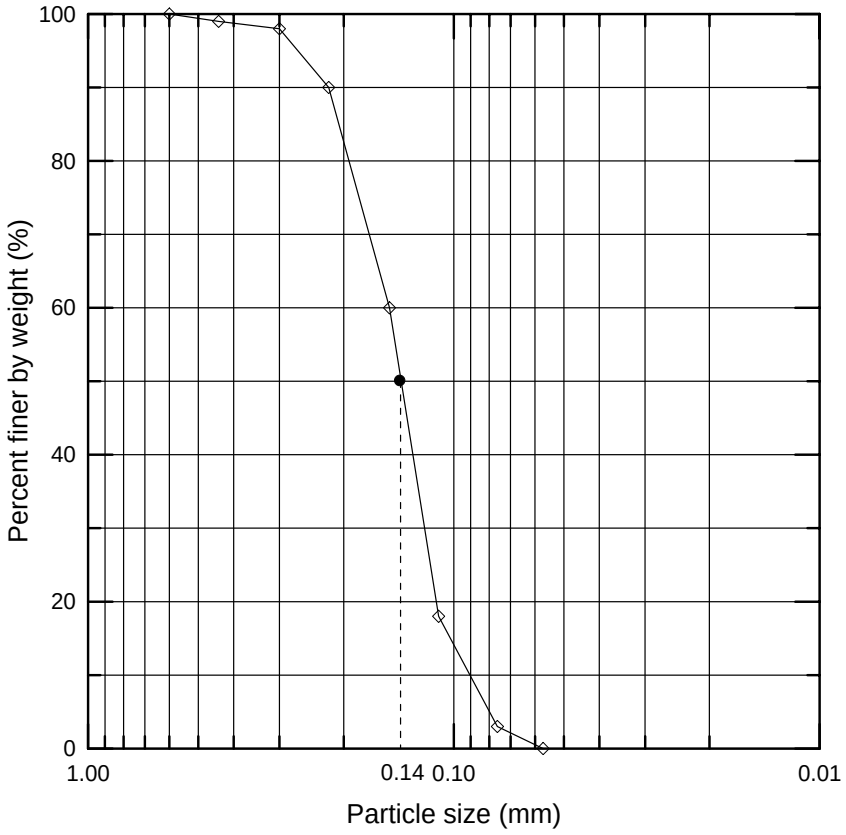


**Fig. 3.2** Particle size distribution curve for a fine Ottawa sand

After the general properties of SWCCs are discussed, it is very instructive to take a look at the physical explanation on the hysteresis of SWCCs. Because the free interfacial energy present between pore air and pore water, a discontinuity in pressure exists across the interface separating pore air and pore water. The pressure difference across the interface depends on the interface curvature. The so-called Young-Laplace equation, which is given below, comes directly from the force balance condition on the

interface. Fig. 3.3 illustrates the equilibrium state at a curved interface between pore air and pore water.

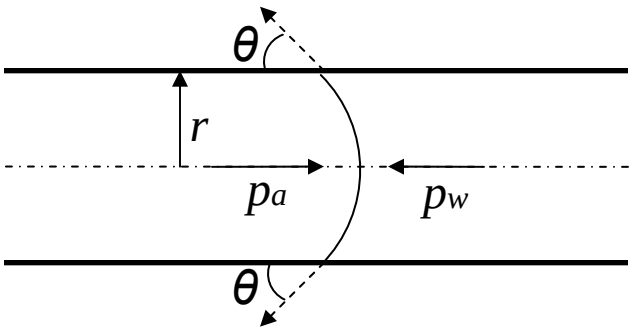


**Fig. 3.3** Equilibrium at a curved interface between pore air and pore water in a tube

The equilibrium condition on the interface along the horizontal direction reads:

$$\sum F_x = p_a \pi r^2 - p_w \pi r^2 - \gamma 2\pi r \cos\theta = 0 \tag{3.1}$$

$$s_c = p_a - p_w = \frac{2\gamma \cos\theta}{r} \tag{3.2}$$

where: $p_a$ and $p_w$ are pore air pressure and pore water pressure, respectively; $\gamma$ is air-water interfacial surface tension; $s_c$ is suction or capillary pressure; $\theta$ is contact angle and $r$ is pore radius. Suction is actually a measure of the tendency of a porous medium to suck in the pore water or to repel the pore air. At a given pore radius, when suction increases, the contact angle has to decrease to satisfy the balance condition. This means the pore water is pushed back by pore air and the water content decreases. For the same reason, water content increases when suction decreases. At a given suction in practice,

the contact angle may be different due to many factors. The mechanisms behind the hysteresis in SWCCs have been extensively investigated by many researchers (e.g. Bear, 1972; Adamson, 1990; Lenhard *et al.*, 1991; Lu and Likos, 2004). From a microscopic viewpoint, the main factors attributing to the hysteresis in SWCCs are nonwetting fluid (e.g., pore air) entrapment (e.g., Poulovassilis, 1970b), contact angle changes associated with wetting/drying paths, and irregular pore geometry. The hysteresis of SWCCs due to pore air entrapment is not our main concern and the effect of air entrapment on hysteresis of SWCCs is assumed to be neglected. The last two factors are illustrated in Fig. 3.4 as follows:

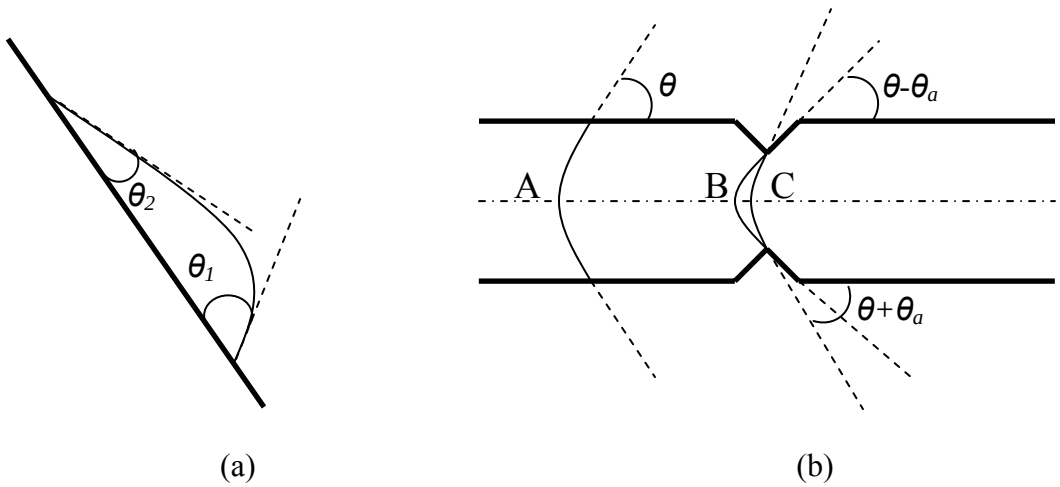


**Fig. 3.4** Hysteresis in (a) contact angle and (b) pore geometry

Fig. 3.4(a) shows the effect of drying or wetting paths on contact angle. $\theta_1$ is the advancing contact angle corresponding to the wetting phase as it moves over a new surface, which is similar to the wetting process. $\theta_2$ is the receding contact angle corresponding to the wetting phase moves off a previously covered surface, the similar

process to drying. The same wetting phase on the same surface introduces different contact angles depending on the movement of the wetting phase. Sometimes, this phenomenon is called rain drop effect (Bear, 1972). Obviously, the contact angle on the wetting side is larger than the one on the drying side. On the basis of Eq. (3.2), the difference in the contact angle between wetting and drying sides explains why the suction is different at a given water content. Actually, the hysteresis of the contact angle during the wetting-drying process also explains the hysteresis of SWCCs. Fig. 3.4(b) illustrates the effect of pore geometry, especially the effect of some small irregular asperities on the hysteresis of soil water characteristics. The geometric non-uniformity of individual pores results from the so-called ink bottle effect. The meniscus A stands for the equilibrium state of wetting and nonwetting phases within the pore channel and the contact angle is given as $\theta$. On the asperity, if the local suction is increased, the meniscus will move to the left and reach balance at B. As shown in Fig. 3.4(b), the contact angle decreases to $\theta - \theta_a$, where $\theta_a$ represents the contact angle change due to the asperity. Similarly, if suction decreases on the asperity, the meniscus will migrate to the right ending at C and the contact angle will change to $\theta + \theta_a$. Of course, it is possible for the meniscus to leave the asperity if suction is high or low enough. The migration of meniscus in the pore channel is corresponding to the drying-wetting process. Similar discussion can be found in Pride and Flekkøy (1999). Physical explanation of hysteresis in SWCCs for clays is further complicated and is still not very well understood due to the physicochemical interactions between clay particle surfaces and pore fluids.

Inclusion of hysteresis effects is essential to simulating the infiltration related problems in unsaturated soils (e.g. Beese and van der Ploeg, 1976; Stauffer and Dracos, 1984; Kool and Parker, 1987). Proper simulation of infiltration processes in unsaturated soils is important to analyze the failure of earth slopes during or after heavy rainfall events and other complex phenomena. The inclusion of hysteresis effects of suction is also important to investigate the shear strength of unsaturated soils. How to correlate the shear strength to SWCCs was discussed by many people, such as Fredlund *et al.* (1995). In fact, many factors, such as soil type and compaction conditions have strong influence on the shape of SWCCs. The related discussion on the impact of soil type and compaction conditions on soil water characteristics can be found in Miller *et al.* (2002). The relationship between pore size, particle size, aggregate size and soil water characteristics is referred to in the work done by Wu *et al.* (1990).

Some special features of soil water characteristics were briefly discussed. This section also introduced the mechanisms behind the hysteresis of soil water characteristics. Attention is next turned to a method to predict the hysteresis in soil water characteristics in unsaturated soils. The literature review is carried out first and then a phenomenological model based on the bounding surface plasticity concept is presented. The performance of the proposed SWCCs model is extensively validated using available data.

## 3.2 LITERATURE REVIEW

### 3.2.1 MODELS FOR SINGLE SWCC

In this section, the models for predicting single SWCC are reviewed. Some important concepts in single SWCC are discussed. A typical single SWCC is given in Fig. 3.5. Basically, a single SWCC model ignores the hysteresis in the SWCCs and represents any one of these curves with an equation. The shapes of SWCC of different soils, i.e., clays and sands are different. The general shape of SWCC is sigmoidal as given in Fig. 3.5. The SWCCs of some gap-graded soils show bimodel or multimodel distribution, see de F.N. Gitirana and Fredlund (2004) and Zhang and Chen (2005). Minco silt is not gap-graded, so only sigmoidal or S-shaped SWCC is discussed here. In practice, water content can be given in volume fraction of water, degree of saturation or other convenient choices.

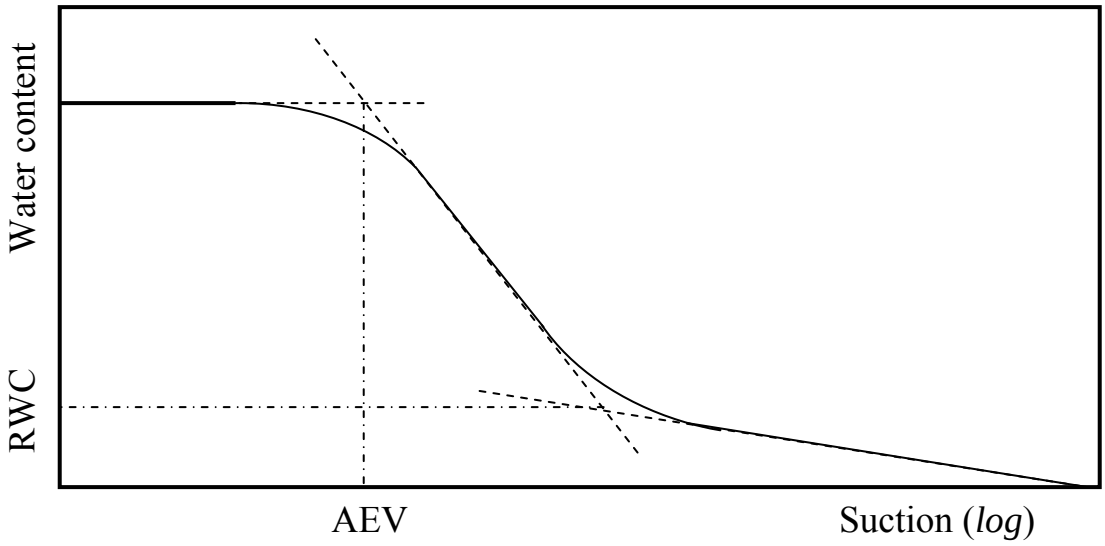


**Fig. 3.5** A typical soil water characteristic curve

How to determine the air-entry value (AEV) and residual water content (RWC) is graphically illustrated in Fig. 3.5. AEV is the suction value where air starts to enter the

largest pores in the soil. RWC stands for the residual water content, which is the water content where large suction change is required to remove additional water from the soil. If current suction is lower than the AEV, then the soil behaves like saturated soils, although the suction is not zero. This means the concept of effective stress for saturated soils works well to predict stress-strain behavior of unsaturated soils when the suction is lower than the AEV. Based on experimental observation (e.g., Croney and Coleman, 1961) and thermodynamical considertations (e.g., Richards, 1965), a suction slightly lower than $10^6$ *kPa* can bring almost any soils to near zero relative humidity.

Many researchers, such as Brooks and Corey (1964), van Genuchten (1980) and Fredlund and Xing (1994), have proposed functional forms to describe the single SWCC. Some popular models for single SWCC are given in their modified forms as follows:

Brooks and Corey (1964): $n_w = n_{res} + (n_{sat} - n_{res})(a \times s_c^n)$ (3.3.1)

van Genuchten (1980): $n_w = n_{res} + \frac{n_{sat} - n_{res}}{\left[1 + (a \times s_c)^n\right]^m}$ (3.3.2)

Fredlund and Xing (1994): $n_w = n_{sat}\left[\frac{1}{\ln\left(e + (s_c / a)^n\right)}\right]^m$ (3.3.3)

Feng and Fredlund (1999): $n_w = \frac{n_{sat} + n_{res}(s_c / a)^m}{1 + (s_c / a)^m}$ (3.3.4)

where: $n_w$ is volume fraction of water; $n_{res}$ and $n_{sat}$ are residual and saturated volume fraction of water, respectively; $s_c$ is suction; $a$, $m$ and $n$ are model parameters.

These models are essentially curve fitting equations, found through best fit of test data. The pros and cons of those SWCC equations have been extensively investigated by Leong and Rahardjo (1997), Barbour (1998) and Sillers *et al.* (2001). Overall, the SWCC equations have enough accuracy to fit test results. Their main difference comes from the number of model parameters. Some equations have RWC as a model parameter, while others do not. Although the inclusion of RWC gives more physical meaning, it is not necessary to have RWC in the SWCC equations since most of those equations are just based on curve fitting techniques. Especially, it is not always easy to find out RWC, because suction can not easily reach very high value in practice. Recently, Pham and Fredlund (2008) have proposed two equations for single SWCC and both equations fit the test data very well of soil state from slurry state to completely dry condition. Although the volume change of soils is observed in the drying process, both curve fitting equations can still capture the evolution of gravimetric water content with suction change. These two equations are too complicated to be applied in practice easily.

### 3.2.2 MODELS FOR HYSTERETIC SWCCS

To better simulate the stress-strain behavior of unsaturated soils, it is desirable to include the soil water characteristics in the constitutive model. Since SWCCs exhibit strong hysteretic behavior, there is no reason to simplify the hysteretic SWCCs into single SWCC. The hysteretic phenomenon has been widely observed (e.g., Morrow and

Harris, 1965; Talsma, 1970; Vachaud and Thony, 1971; Nimmo and Miller, 1986) and many models have been proposed to simulate hysteretic capillary behavior since 1960s.

Mualem (1973, 1974 & 1984), Haverkamp *et al.* (2002), Pham *et al.* (2003), Rojas and Rojas (2005), Maqsoud *et al.* (2006) and many others proposed different methods to simulate the hysteresis in SWCCs. Generally speaking, the available models for simulating hysteretic SWCCs can be classified into different categories, such as geometric scaling models (e.g., Parker and Lenhard, 1987; Gandola *et al.*, 2004), independent domain models (e.g., Everett, 1954 & 1955; Mualem, 1973), dependent domain models (e.g., Topp, 1971b; Mualem, 1974 & 1984; Poulovassilis and El-Ghamry, 1978; Mualem and Miller, 1979) and rational extrapolation models (e.g., Parlange, 1976; Braddock *et al.*, 2001; Haverkamp *et al.*, 2002). Excellent review on the available models for hysteretic SWCCs can be found in Viaene *et al.* (1994) and Maqsoud *et al.* (2004).

Using the similarity hypothesis, Mualem (1973) assumed that pore water distribution function of soils is a product of two independent functions that are difficult to obtain. By considering a different integration domain, Mualem (1974 & 1984) improved his independent domain model (Everett, 1954 & 1955; Mualem, 1973). The separate description of primary drying scanning curve, primary wetting scanning curve and the higher-order wetting/drying curves after a series of alternating processes of drainage and imbibition makes the model very complicated. In addition, the integration process to find out the drying function and wetting function in different integration domain impedes the application of Mualem's model in practice.

Although the independent domain theory of hysteresis is useful in describing the hysteretic behavior of soil water characteristics in some cases, the theory is not general enough to describe all soil water characteristics of porous media (e.g., Topp and Miller, 1966). By introducing the hypothesis that the domain accumulation or removal depends on the values of the variables at reversal, Poulovassilis and Childs (1971) extended the concept of domains and the primary scanning curves can be well described using their domain theory. Later, Poulovassilis and El-Ghamry (1978) extended the primitive domain theory of Poulovassilis and Childs (1971) to cover scanning curves of any order. Comparisons between the predictions based on the domain theory and test results show the good model performance.

The representative models based on the concept of rational extrapolation were introduced by Parlange (1976) and Haverkamp *et al.* (2002). Mualem and Morel-Seytoux (1978) investigated the model proposed by Parlange (1976) and pointed out Parlange's (1976) model is mathematically complicated. In addition, as pointed by Parlange (1976) himself, the actual wetting boundary curve is seldom obtained in the determination of the moisture retention characteristic. Compared with Mualem's dependent model, Parlange's model is incomplete in that his model only considered even drying and uneven wetting scanning curves without providing even wetting and uneven drying scanning curves. Haverkamp *et al.* (2002) also proposed a method to simulate the SWCCs based on the concept of rational extrapolation and geometric scaling of various curves. It is assumed that the water retention curve is described by three parameters. One of the three

parameters defines the shape of the water retention curve and the other two parameters scale the soil water pressure head and volume fraction of water, respectively. Correspondingly, three conditions to determine the three parameters are introduced. Although only one curve is needed to predict all the other water retention curves, the proposed method requires information such as the drying and wetting sequence numbers that are difficult to determine for practical applications.

Pham *et al.* (2003) proposed empirical equations to model only the main drying and wetting curves. Maqsoud *et al.* (2006) extended Kovacs' (1981) model and predicted the main drying and wetting curves and a scanning curve that originated on the main curves for sands using certain assumptions about the contact angle for the air-water interface. Rojas and Rojas (2005) proposed a model based on detailed description of the pore geometry. It is, however, difficult to determine the parameters describing the pore geometry. Recently more rigorous models based on different theoretical grounds have been presented to describe the hysteresis in SWCCs (e.g. Li, 2004; Wei and Dewoolkar, 2006; Kohgo, 2008). It is also very interesting to note that there is a trend to use the bounding surface plasticity concept (Dafalias and Popov, 1975 & 1976) to simulate the hysteretic soil water characteristic curves. However, experimental validations of these models are still limited.

In summary, the above mentioned hysteretic SWCCs models either involve complex mathematics calculations or deserve deep physical understanding behind the hysteretic phenomenon. Another disadvantage of those models is the difficulty related to

the calibration of model parameters, because some models are based on the microscopic consideration and some parameters do not have explicit physical meanings. In fact, a close look at the typical SWCCs in Fig. 3.1 indicates the hysteretic phenomenon in soil water characteristics is nothing new but a similar phenomenon to Bauschinger effect in metals. This means the hysteresis of SWCCs can be described using classical elastoplasticity theory, which is familiar to most geotechnical engineers. A simple SWCCs model based on the bounding surface plasticity concept (Dafalias and Popov, 1975 & 1976) is presented in the next section.

## 3.3 SWCCS MODEL BASED ON THE BOUNDING SURFACE PLASTICITY CONCEPT

In section 2.4, the energy dissipation mechanisms of soil skeleton and pore water are given in Eqs. (2.8) and (2.9). Comparison between the two equations indicates that the two energy dissipation mechanisms have identical form except the energy dissipation of soil skeleton is given in tensors while the energy dissipation related to suction is in scalars. Stress-strain behavior of the soil skeleton and SWCCs of unsaturated soils have many features in common. Both stress-strain curves and SWCCs exhibit hysteresis during loading-unloading and drying-wetting cycles and the behavior is path dependent. Since elastoplasticity theory has been successfully used to predict the stress-strain behavior of soils, it is possible to propose a model for SWCCs using elastoplasticity theory to simulate the hysteresis of SWCCs.

Motivated by the observation that all scanning curves are bounded by primary wetting curve and the second drying curve (see Fig. 3.1), the bounding surface plasticity theory, which was reviewed in Chapter 2, is selected to be the elastoplastic framework for hysteretic SWCCs prediction. Due to its ability to predict plastic deformations within the bounding surface, the bounding surface plasticity theory is a good choice to simulate cyclic loading such as drying and wetting. Li (2004) also presented a simplified bounding surface model for SWCCs, but without validation against experimental data. Part of the following work was published by Liu and Muraleetharan (2006) and Muraleetharan *et al.* (2008). Here, some modifications are adopted and more validations on the proposed SWCCs model are carried out.

### 3.3.1 BOUNDING CURVES

Observations on Fig. 3.1 indicate that the primary drying curve is not appropriate to be selected as one of the bounding curves because of the air entrapment. Therefore, it is convenient to select the primary wetting curve and the secondary drying curve as bounding curves and the equation proposed by Feng and Fredlund (1999) may be used to describe these two curves as given below:

The primary wetting curve: $$n_{w1} = \frac{n_{sat} + n_{res}\left(s_c / b_1\right)^{d_1}}{1 + \left(s_c / b_1\right)^{d_1}} \tag{3.4.1}$$

The secondary drying curve: $$n_{w2} = \frac{n_{sat} + n_{res}\left(s_c / b_2\right)^{d_2}}{1 + \left(s_c / b_2\right)^{d_2}} \tag{3.4.2}$$

where: $n_{sat}$ is the water content at zero suction (= porosity, $n$), $n_{res}$ is the residual water content at very high suction. $b_1$, $d_1$, $b_2$ and $d_2$ are four material parameters and $b_1$ and $b_2$ have the same unit as suction in this study. The adoption of Eqs. (3.4) to simulate the bounding curves is based on the observation that $n_w = n_{sat}$ when suction $s_c = 0\,kPa$ and $n_w = n_{res}$ when suction is very high. Any other appropriate equations for the bounding curves can also be used as long as they provide enough accuracy for curve-fitting the test results.

### 3.3.2 CAPILLARY ELASTIC AND PLASTIC MODULI

Because suction is the stress variable and it is a scalar, the description of SWCCs can be treated as a one-dimensional problem. Volume fraction of water is regarded as the conjugated strain-like variable to suction. In this way, the relationship between suction and volume fraction of water, i.e., SWCCs is an equivalent problem as the classical elastoplastic problem. At the beginning of any drying/wetting cycle, purely capillary elastic behavior is expected. That is, the volume fraction change will be totally recoverable upon suction reversal. During other parts of drying/wetting cycles the behavior will be capillary elastoplastic. Similar to the elastoplastic theory, the capillary elastic and plastic moduli, $\Gamma^e$ and $\Gamma^p$, can be respectively defined as:

$$ds_c = \Gamma^e dn_w^e \tag{3.5}$$

$$ds_c = \Gamma^p dn_w^p \tag{3.6}$$

where: $ds_c$ is the increment in suction and $dn_w^e$ and $dn_w^p$ are the increments in recoverable (elastic) and irrecoverable (plastic) volume fraction of water.

Generally speaking, a constant capillary elastic modulus $\Gamma^e$ can provide sufficient accuracy. Usually, $\Gamma^e$ is a large number and this means the elastic behavior of SWCCs is not dominant and purely elastic behavior of SWCCs just occurs at the very beginning portion of each scanning curve. Actually, it is convenient to assume that the yielding of SWCCs starts at the beginning of each suction path change without losing any accuracy. In addition, the capillary elastic modulus can be related to suction if enough test data are available for such a treatment. According to Dafalias and Popov (1976), capillary plastic modulus $\Gamma^p$ on the current stress state point can be assumed to have the following functional form:

$$\Gamma^p = \Gamma^p(\delta, \delta_{in}) \tag{3.7}$$

where: $\delta$ is the vertical distance (in suction units) between the current stress state point and its corresponding bounding curve; $\delta_{in}$ is the value of $\delta$ at the initiation of yielding for each drying/wetting process. Fig. 3.6 illustrates the meanings of $\delta_{in}$ and $\delta$.

In Fig. 3.6, the calibration scanning curve is a drying curve, starting from the lower bound and ending at the upper bound. $\delta$ is the vertical distance between the current state point and the drying bound. It is also possible that the scanning curve does

not start from either bound, because suction path can change anytime and anywhere between two bounds. Similarly, to predict the scanning curve during wetting process, the wetting bound is used to calculate the plastic modulus. For each drying or wetting path, a new $\delta_{in}$ needs to be calculated. $\delta_{in}$ does not change until the suction path is changed from wetting to drying or from drying to wetting.

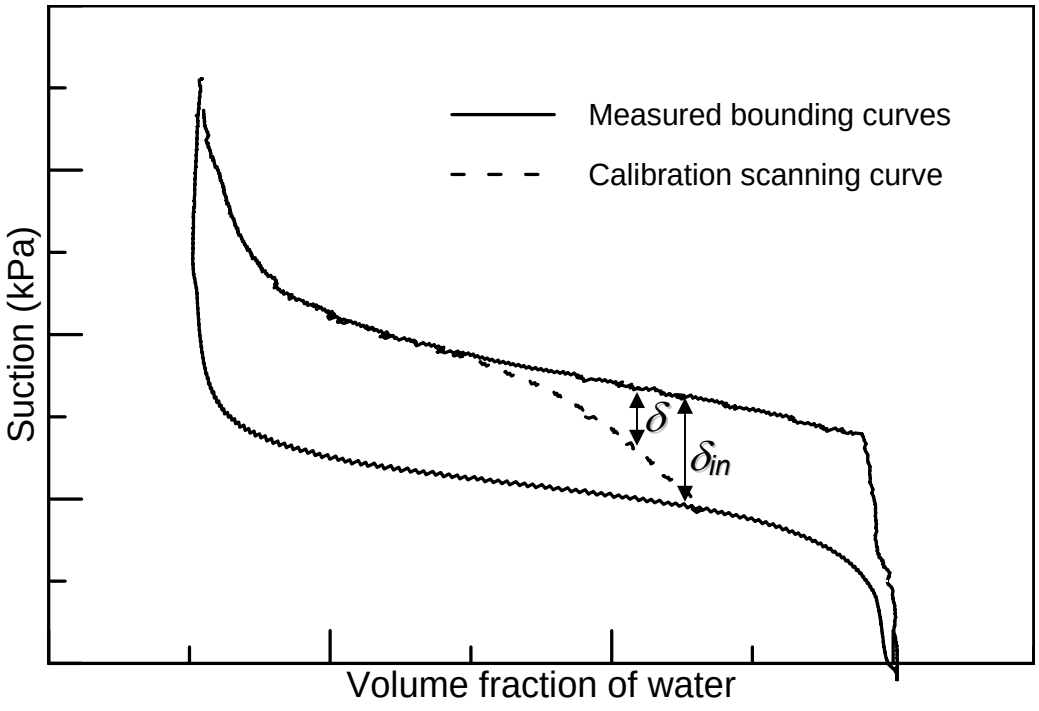


**Fig. 3.6** Illustration of $\delta$ and $\delta_{in}$ for the SWCCs model

Assuming the standard additive decomposition, the following relationships hold for all state points on SWCCs.

$$dn_w = dn_w^e + dn_w^p \tag{3.8}$$

$$1/\Gamma = 1/\Gamma^e + 1/\Gamma^p \tag{3.9}$$

where: $\Gamma$ is the tangent capillary modulus in $s_c - n_w$ space.

Dafalias and Popov (1976) proposed a possible evolution equation for $\Gamma^p$. With some modifications this evolution equation can be expressed as:

$$\Gamma^p = \Gamma_0^p \left(1 + h \cdot \delta / < \delta_{in} - g\delta >\right) \tag{3.10}$$

where: $\Gamma_0^p$ is the value of $\Gamma^p$ when $\delta = 0$, i.e., the value of $\Gamma^p$ on the bounding curves. $g$ is a model parameter, which typically ranges from 1.0 to 2.0. In this study, it is set to be 1.0. $< >$ is the Macaulay brackets. When $\delta = \delta_{in}$, $\Gamma^p = \infty$ and it means the elastic behavior dominates, which occurs at the beginning of each drying or wetting process. When $\delta = 0$, $\Gamma^p = \Gamma_0^p$ and it means the scanning curve merges onto the corresponding bounding curve and develops along that bounding curve. $h$ is a shape parameter, which can be a constant or can be made to be a function of $\delta$ and $\delta_{in}$ as follows:

$$h = \rho / \left(1 + f \cdot r^m\right) \tag{3.11}$$

$$r = \delta / \delta_{in} \tag{3.12}$$

where: $\rho$, $f$ and $m$ are three other parameters. In fact, a constant shape parameter $h$ provides enough accuracy. For simplicity, a constant $h$ is used in this study.

Based on the bounding surface plasticity concept, a simple SWCCs model is developed for simulating the hysteretic behavior of SWCCs. The model is described within the framework of classical elastoplasticity theory. The only difference in this SWCCs model is the selection of stress and strain variables to be suction and volume fraction of water, respectively. All other concepts are identical, for example the capillary elastic and plastic moduli correspond to the elastic and plastic moduli used in the description of the stress-strain behavior.

### 3.3.3 SWCCS MODEL CALIBRATION

Because of air entrapment, the primary drying curve generally gives unstable soil water characteristics if the soil starts drying from a saturated state (see Fig. 3.1). To apply the proposed SWCCs model, the secondary drying and the primary wetting curves (i.e., bounding curves) and a scanning curve are required to calibrate the model parameters. As to the bounding curves, there are six parameters to be calibrated. $n_{res}$ and $n_{sat}$ can be determined very easily from the bounding curves. $b_1$, $d_1$, $b_2$ and $d_2$ should be determined using a trial-and-error procedure. Any scanning curve can be used to calibrate $\Gamma^e$ and $h$. The initial portion of the scanning curve will be used to find out $\Gamma^e$ while the shape parameter $h$ has to be calibrated in a trial-and-error way.

## 3.4 SWCCS MODEL PERFORMANCE

To check the performance of the proposed SWCCs model, available test results for several different soils are compared with the model predictions. The test results cover a wide range of soil samples, including different sands (e.g. Topp, 1969; Poulovassilis, 1970a; Gillham *et al.*, 1976; Dane and Hruska, 1983; Chen *et al.*, 2007), silt loam (e.g. Topp, 1971 a & b; Clothier and Smettem, 1990; Haverkamp *et al.*, 1997), clay loam (e.g. Dane and Hruska, 1983) and some glass-bead medium (e.g. Topp and Miller, 1966). All the model parameters are calibrated and given in Table 3.1. In this study, the SWCCs data from six different sands, three different silts, one clay and two glass-bead media are used to check the validity of the proposed SWCCs model. For the convenience to compare the predictions with the original test results, all the units in the model are modified according to the original units used in the corresponding test programs. For example, the suction unit may be given in *cm* (centimeter) of water, instead of *kPa*. In some cases, degree of saturation, not volume fraction of water is used to represent the water content information. The model predictions are, however, carried out using suction and volumetric water content as stress-strain variables as described before.

Fig. 3.7 illustrates the comparison between measured and predicted scanning curves for the U.S. Silica (Berkeley Springs, West Viginia) F-95 sand (Chen *et al.*, 2007). Using the calibrated model parameters, predictions are made for a complex suction path given by 8.62 *kPa* (A) → 4 *kPa* (B) → 9.2 *kPa* (C) → 4.1 *kPa* (D) → 8.0 *kPa* (E) with the starting point at (0.06, 8.62 *kPa*). These scanning curves were not used in the calibration of the model parameters. The scanning curve used for the calibration is shown in Fig. 3.6. Although not shown here the same set of model parameters can be used to

predict all the other scanning curves. The detailed material information and experimental setup can be found in Chen *et al.* (2007). The refined treatment of $\Gamma^e$ and $h$ may significantly improve the model performance for certain soils, but in this study constant values for these parameters provided sufficient accuracy.

Fig. 3.8 compares the predicted scanning drying curve (SDC) and wetting curve (PWC) with the measurements for Las Cruces sand (Dane and Hruska, 1983). The model accurately predicts all the other scanning curves. In addition, the equations of the bounding curves work very well too.

The next example illustrates the predictions and measurements of the hysteretic behavior of Rubicon sandy loam (Topp, 1969). Although the simulation of the drying/upper bound at low suction is not good, the overall model performance is satisfactory. The shape of the drying/upper bound is too much different from that of the wetting/lower bound. Recall that all the drying scanning curves are predicted based on the slope at each point on the dry bound and the distances between suction states on the scanning curves and the dry bound. Because of the discrepancy in some portion of the dry bound, the simulations of the wetting scanning curves are better than those of the drying scanning curves. Of course, a more accurate bounding curve equation other than the one proposed by Feng and Fredlund (1999) can be used for better simulation of the bounding curves and then of the scanning curves. Although related research is not carried out, it is even possible that totally different forms of the drying bound and the wetting bound can be used to predict the scanning curves. Generally speaking, better bounding curve

equations will give better simulations of scanning curves. For some special soils, the bounding curves can even be divided into different pieces and piecewise functions can be used to carry out the analysis to obtain better predictions.

Fig. 3.10 compares the measurements and predictions of scanning curves of Wray dune sand (Gillham *et al.*, 1976) and reasonable predictions are achieved. Fig. 3.11 and Fig. 3.12 deal with the hysteretic behavior of two different porous bodies I and II (Poulovassilis, 1970a). Both porous bodies are essentially sand. Porous body I has a slightly wider pore size distribution than porous body II. From Table 3.1, the calibrated model parameters are very close for porous body I and body II. All the predictions, including the bounding curves are satisfactory.

Figs. 3.13 through 3.15 present the model predictions for three silts, i.e., Caribou silt loam (Topp, 1971 a & b), silt loam (Haverkamp *et al.*, 1997) and Manawatu silt loam (Clothier and Smettem, 1990). Because silts have smaller size particles than sands, it takes a longer time to reach equilibrium whenever suction changes. To run SWCCs tests on silts is time consuming. Especially, the soil water characteristic data of silts do not provide smooth evolution curves and this phenomenon has been observed by many researchers, e.g., Chen (2006). For the three silts given here, only very limited data are available. Although there are only limited data available, the overall performance of the SWCCs model is satisfactory.

Fig. 3.16 illustrates the capillary hysteresis of Rideau clay loam (Topp, 1971a). This is the only case study dealing with the hysteretic SWCCs of clay. Clays generally have very fine particles and suction can reach high levels. Too many uncertainties, such as organic components make the investigation of soil water characteristics of clays difficult. SWCCs tests on clays can take couple of months or even years. New techniques to measure SWCCs are badly needed to provide complete results in a reasonable time period. Considering the time-consuming process to get complete SWCCs of clay, the SWCCs model provides an alternative way to account for the suction effects on clay hydraulic behavior when limited test data are available. The overall performance of the simple SWCCs model on predicting SWCCs behavior of clays is reasonably shown in Fig. 3.16.

Figs. 3.17 and 3.18 show the model performance for man-made glass-bead media (Topp and Miller, 1966). The two glass samples have different pore-space geometries. The glass-bead media I is composed of relatively uniform glass spheres of about 180 $\mu m$ in diameter, while the glass-bead media II is composed of much smaller aggregated glass beads. As expected, Figs. 3.17 and 3.18 clearly show that the model yields very good predictions of the hysteretic scanning curves.

## 3.5 SUMMARY

In this chapter, a thorough literature review on modeling both single SWCC and hysteretic SWCCs was presented. The physical explanation for the hysteresis in SWCCs

in porous media was briefly discussed. Within the framework of classical elastoplasticity theory, a simple SWCCs model based on the bounding surface plasticity concept was proposed. An extensive validation study of the proposed model was carried out using test results for different porous media and satisfactory comparisons between model predictions and test results are obtained. This simple SWCCs model will be implemented into the constitutive model of unsaturated soils to investigate the coupling effects between mechanical and hydraulic behavior in the next two chapters.

**Table 3.1** Model parameters for SWCCs model validation

| | Sand[1] | Sand[2] | Sand[3] | Sand[4] | Sand I[5] | Sand II[5] | Silt[6] | Silt[7] | Silt[8] | Clay[9] | Glass-Bead A[10] | Glass-Bead B[10] |
|---|---|---|---|---|---|---|---|---|---|---|---|---|
| $b_1$ | 4.2 | 16.2 | 38.0 | 19.9 | 19.3 | 21.1 | 40.0 | 443 | 27.0 | 28.0 | 29.2 | 26.4 |
| $d_1$ | 8.0 | 4.4 | 1.5 | 4.4 | 3.1 | 3.1 | 1.2 | 3.7 | 2.8 | 1.5 | 7.7 | 7.1 |
| $b_2$ | 7.2 | 33.7 | 98.0 | 33.8 | 26.9 | 29.7 | 139 | 881 | 52.5 | 73.0 | 47.4 | 40.2 |
| $d_2$ | 8.0 | 4.3 | 4.0 | 8.6 | 4.5 | 6.1 | 2.6 | 3.7 | 2.8 | 2.2 | 14.9 | 9.9 |
| $\Gamma^e$ | $-100$ | -1800 | -1500 | -1700 | -1200 | -1200 | -5000 | -14000 | -1000 | -5500 | -150 | -150 |
| $h$ | 7.0 | 5.0 | 7.0 | 7.0 | 3.0 | 2.0 | 10.0 | 7.0 | 5.0 | 7.0 | 15.0 | 16.0 |
| $n_{sat}$ | 0.3 | 0.386 | 0.38 | 0.3 | 0.2725 | 0.258 | 0.402 | 0.443 | 0.293 | 0.415 | 0.833 | 0.9 |
| $n_{res}$ | 0.053 | 0.006 | 0.157 | 0.1 | 0.05 | 0.05 | 0.306 | 0.01 | 0.015 | 0.285 | 0.1 | 0.2 |



**Note 1:**

1: U.S. Silica F-95 sand (Chen *et al.*, 2007)
2: Las Cruces sand (Dane and Hruska, 1983)
3: Rubicon sandy loam soil (Topp, 1969)
4: Wray dune sand (Gillham *et al.*, 1976)
5: Porous body I and porous body II (Poulovassilis, 1970a)
6: Caribou silt loam (Topp, 1971 a & b)
7: Silt loam (Haverkamp *et al.*, 1997)
8: Manawatu silt loam (Clothier and Smettem, 1990)
9: Rideau clay loam (Topp, 1971a)
10: Glass-bead media (Topp and Miller, 1966)

**Note 2:**

Only suction in sand[1] is in *kPa* and other suctions are in *cm* (centimeter) of water. $b_1$, $b_2$ and $\Gamma^e$ have the same unit as suction. Only water content in glass-beads[10] is in degree of saturation, while others are in volume fraction of water.

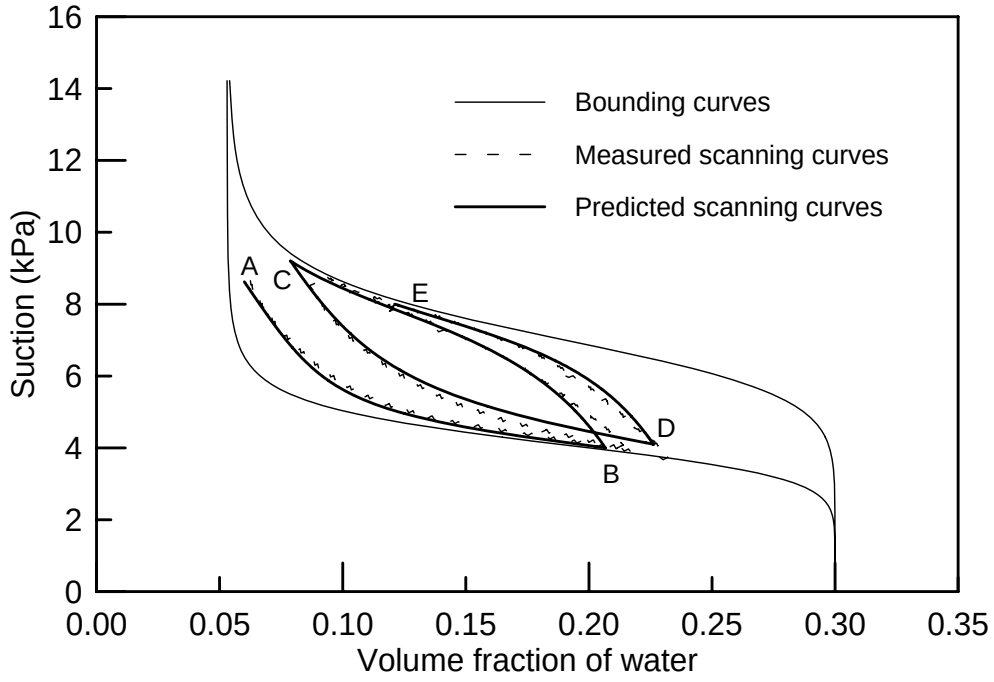


**Fig. 3.7** Comparison between measured and predicted scanning curves for the U.S. Silica F-95 sand (test results from Chen *et al.*, 2007)

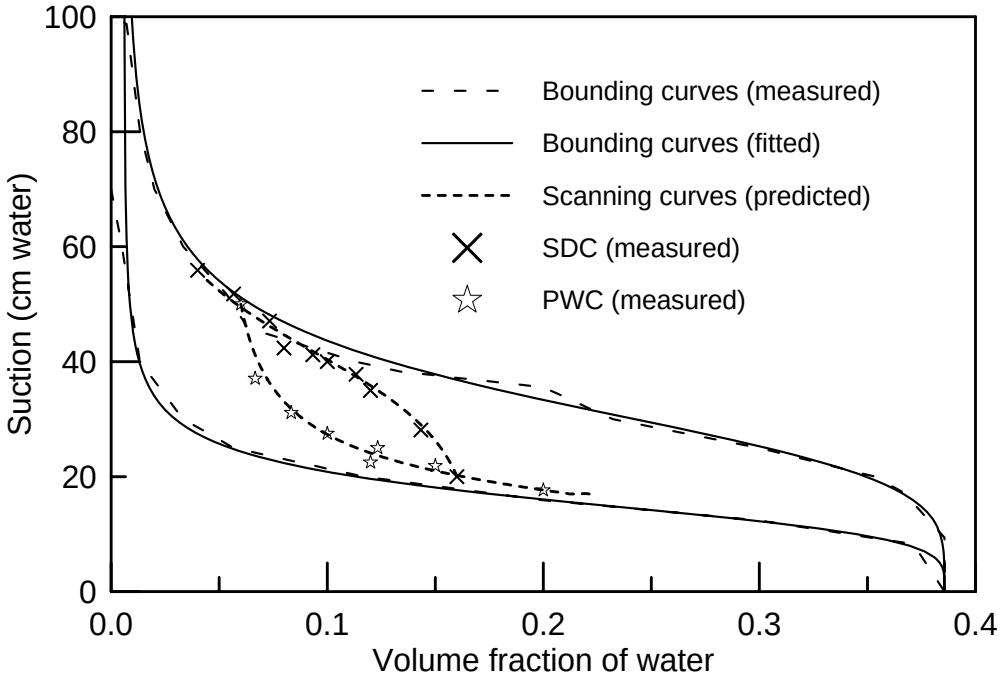


**Fig. 3.8** Comparison between measured and predicted scanning curves for Las Cruces sand (test results from Dane and Hruska, 1983)

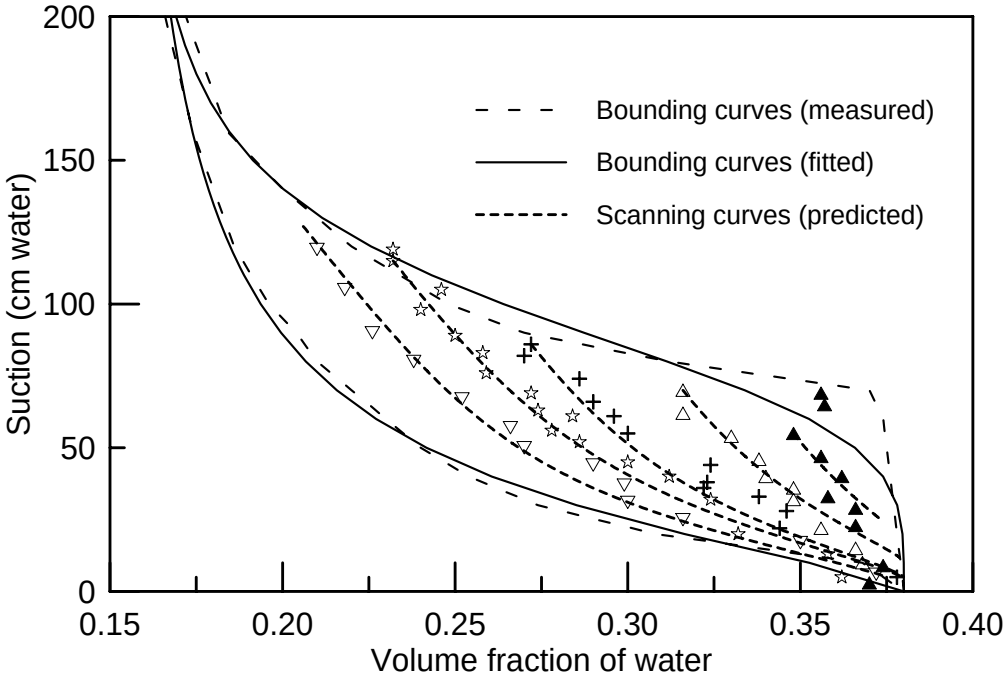


(a) Wetting scanning curves

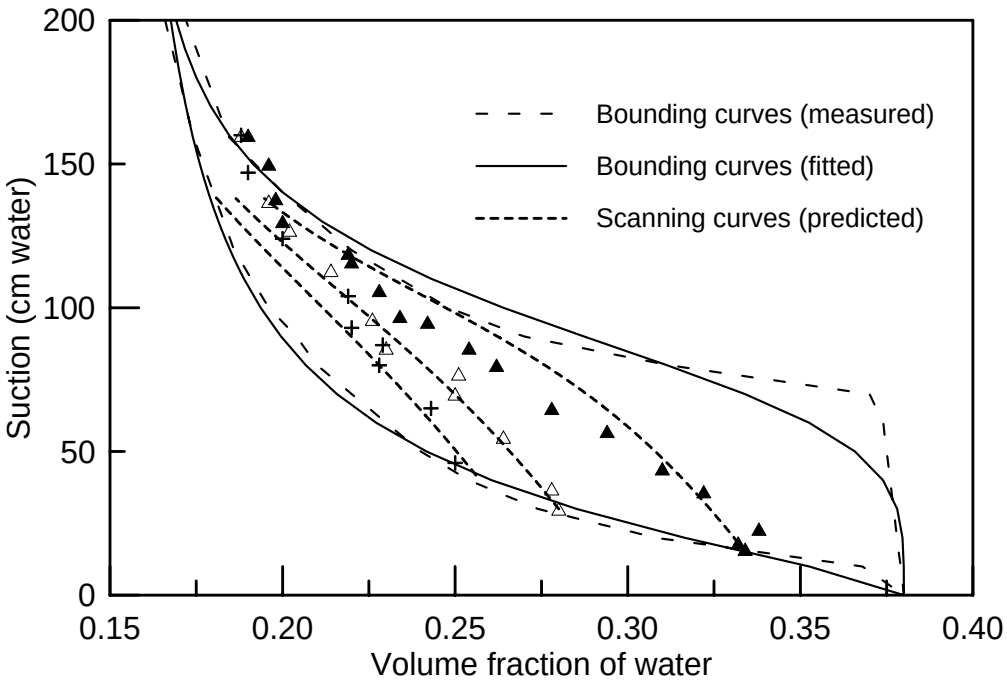


(b) Drying scanning curves

**Fig. 3.9** Comparison between measured and predicted scanning curves for Rubicon sandy loam soil (test results from Topp, 1969)

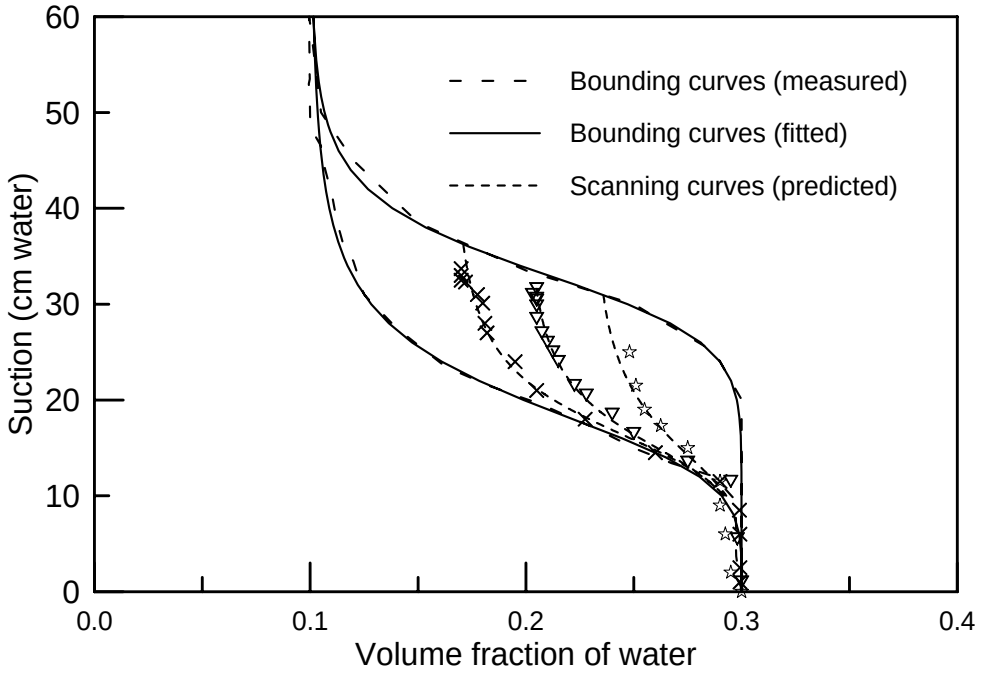


(a) Wetting scanning curves

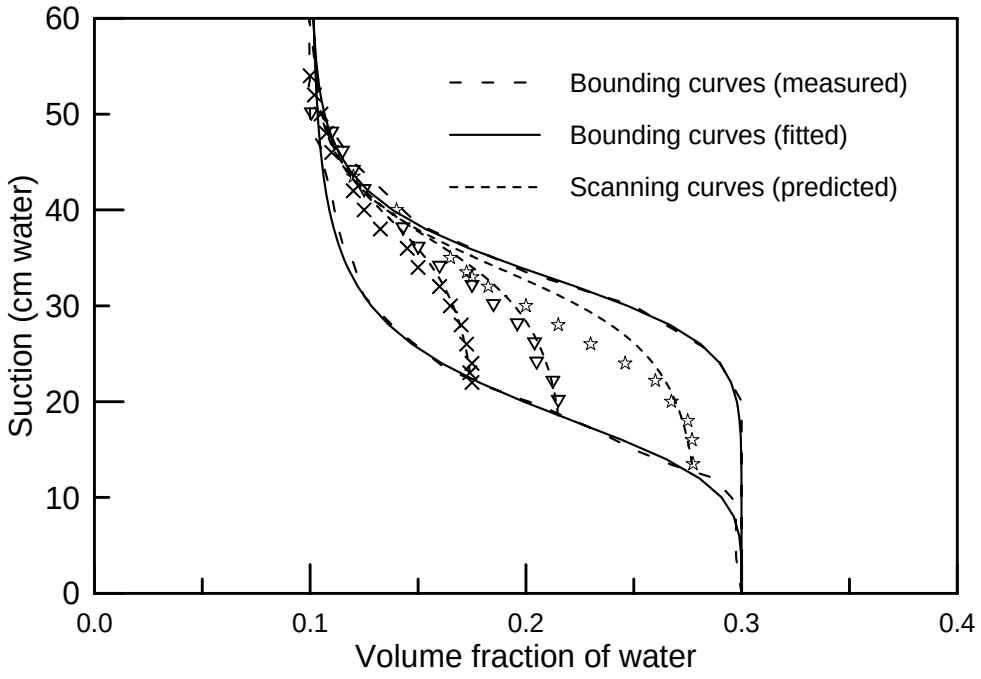


(b) Drying scanning curves

**Fig. 3.10** Comparison between measured and predicted scanning curves for Wray dune sand (test results from Gillham *et al.*, 1976)

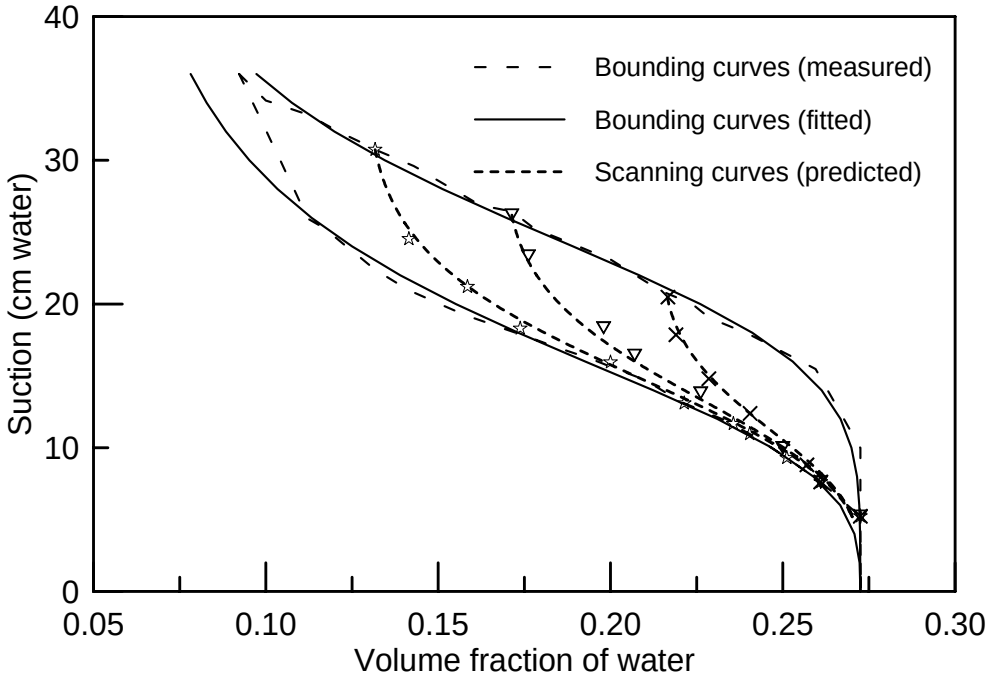


(a) Wetting scanning curves

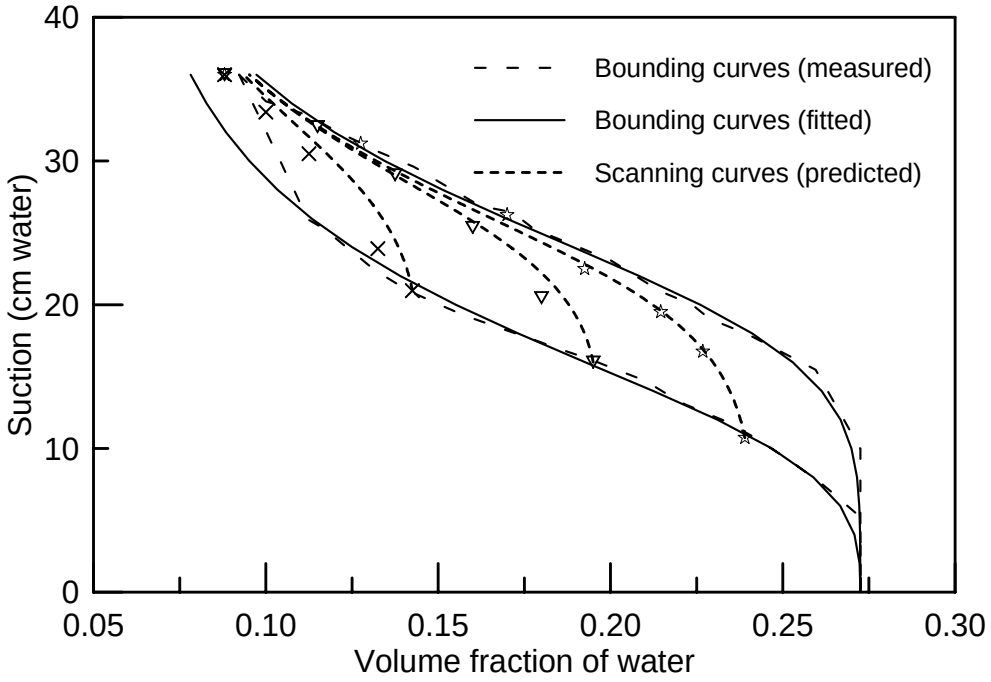


(b) Drying scanning curves

**Fig. 3.11** Comparison between measured and predicted scanning curves for porous body I (test results from Poulovassilis, 1970a)

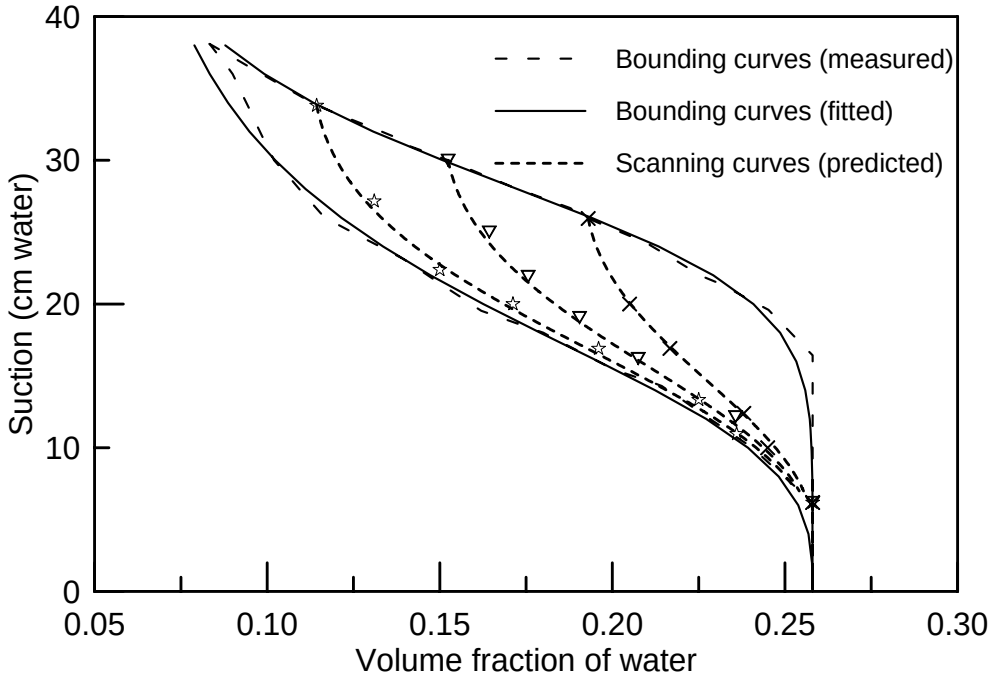


(a) Wetting scanning curves

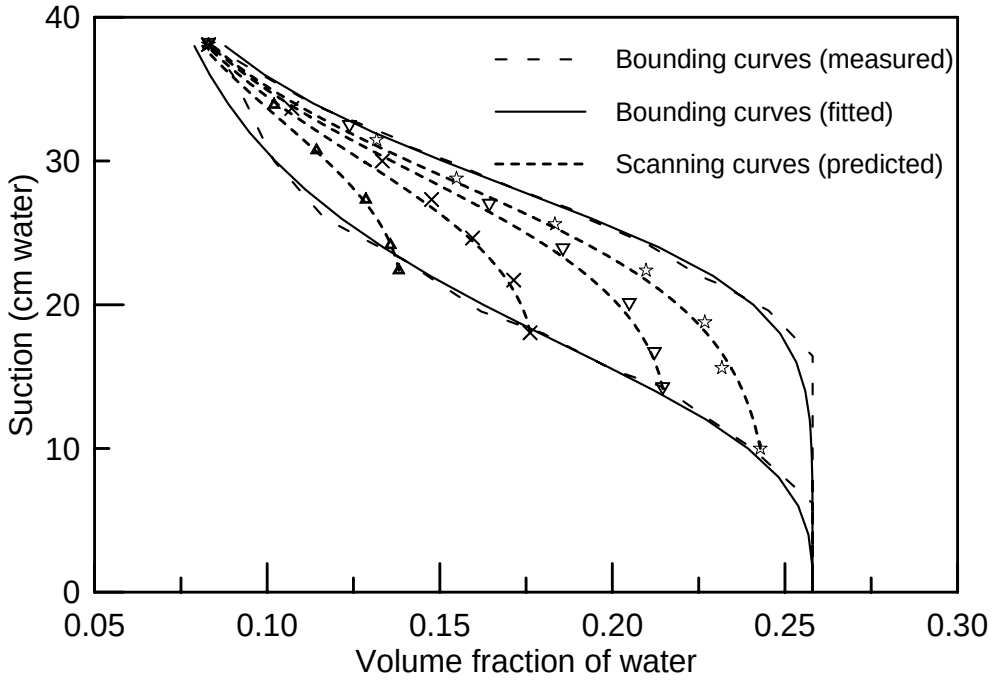


(b) Drying scanning curves

**Fig. 3.12** Comparison between measured and predicted scanning curves for porous body II (test results from Poulovassilis, 1970a)

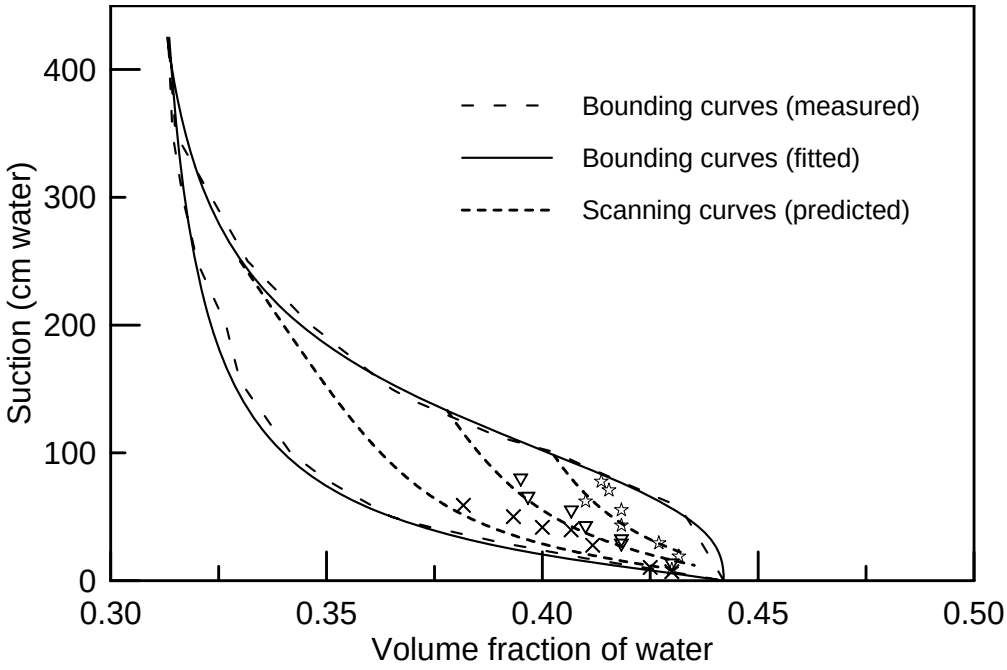


(a) Wetting scanning curves

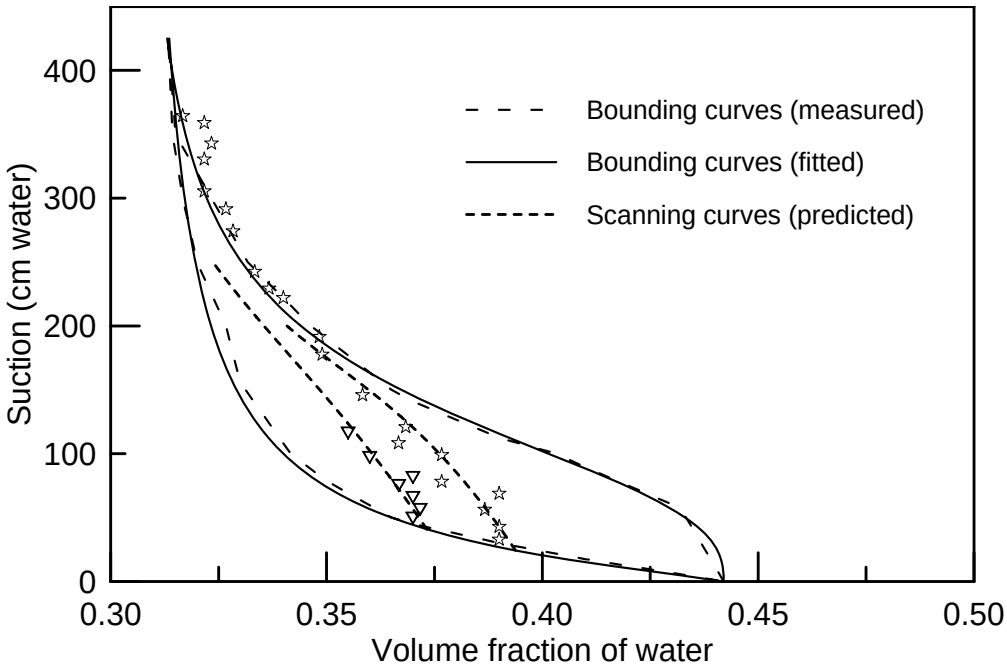


(b) Drying scanning curves

**Fig. 3.13** Comparison between measured and predicted scanning curves for Caribou silt loam (test results from Topp, 1971 a & b)

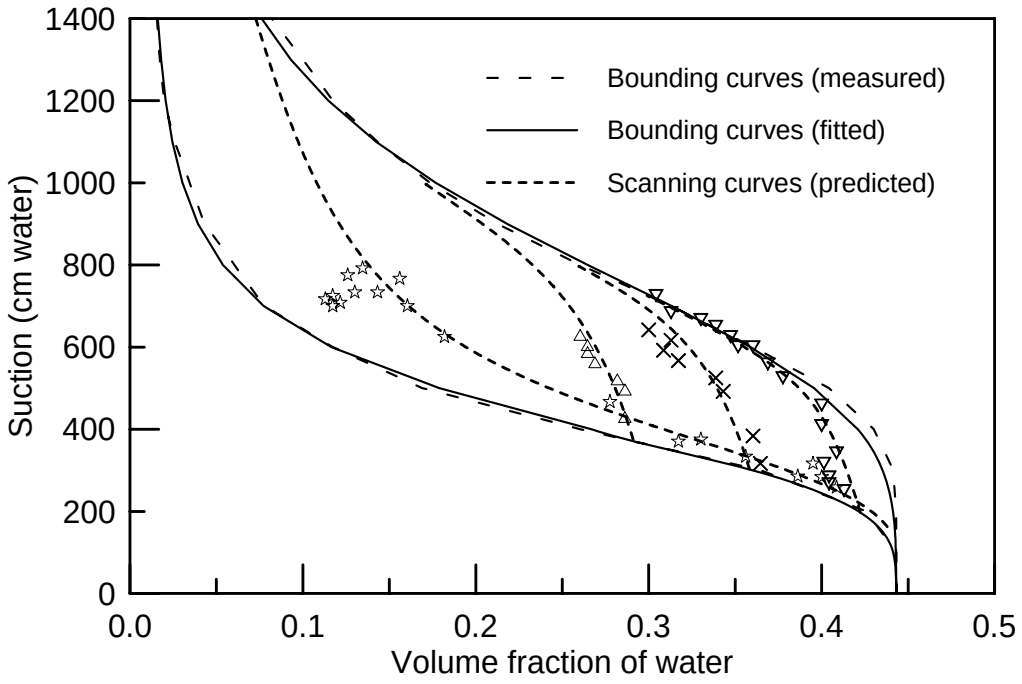


**Fig. 3.14** Comparison between measured and predicted scanning curves for a silt loam (test results from Haverkamp *et al.*, 1997)

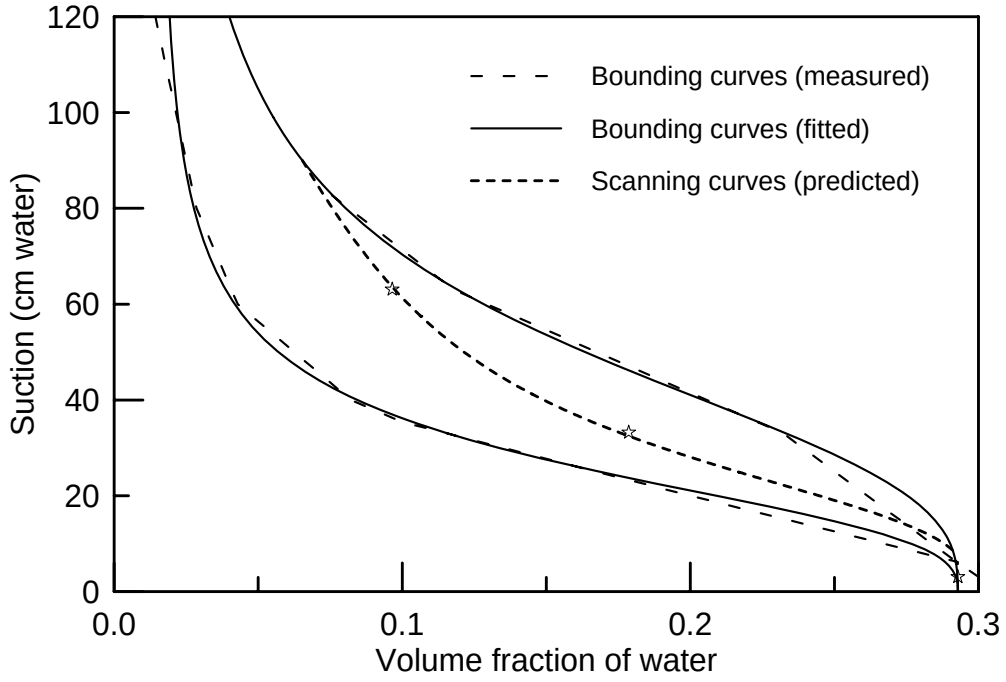


**Fig. 3.15** Comparison between measured and predicted scanning curves for Manawatu silt loam (test results from Clothier and Smettem, 1990)

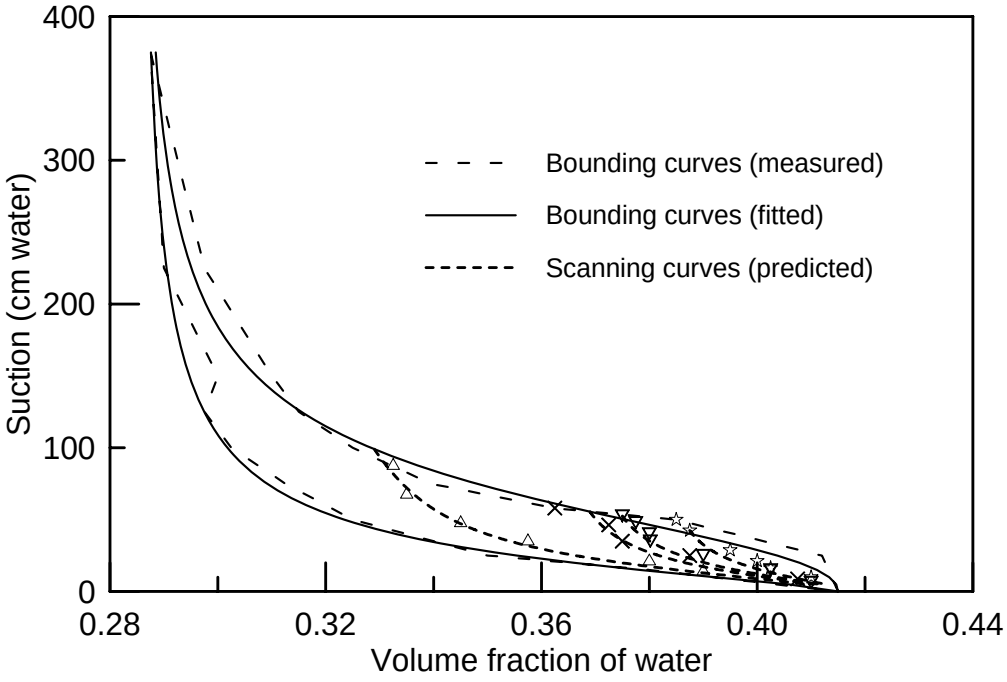


(a) Wetting scanning curves

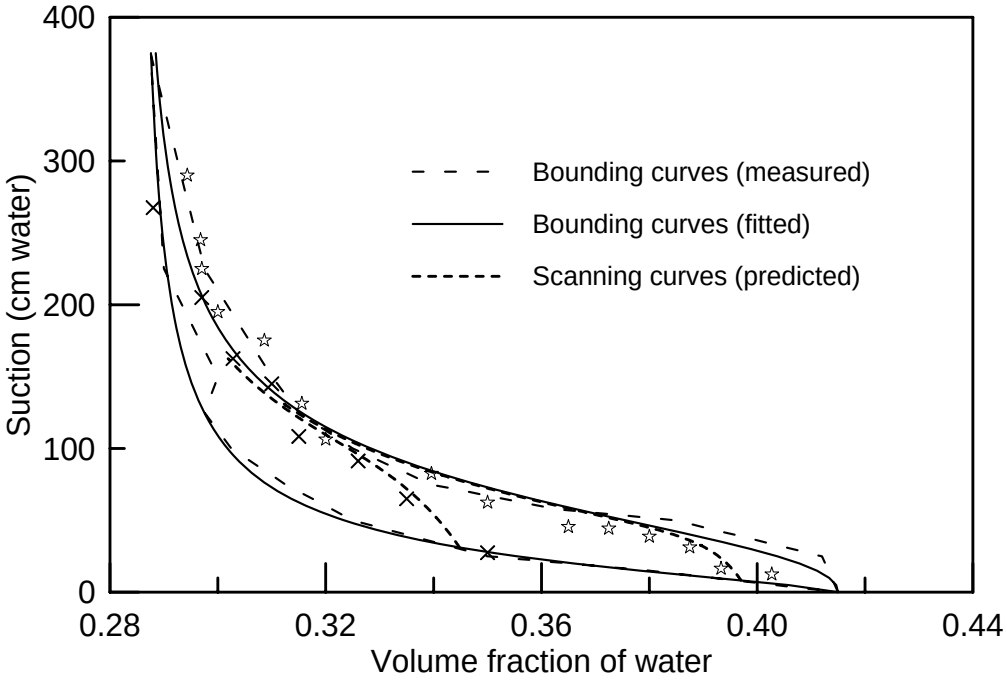


(b) Drying scanning curves

**Fig. 3.16** Comparison between measured and predicted scanning curves for Rideau clay loam (test results from Topp, 1971a)

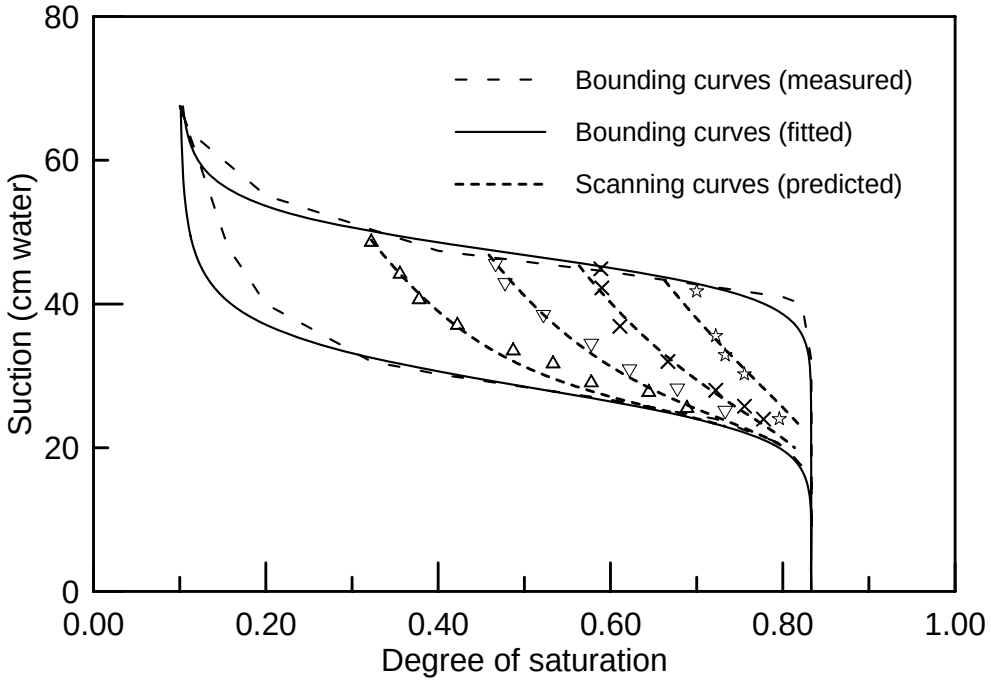


(a) Wetting scanning curves

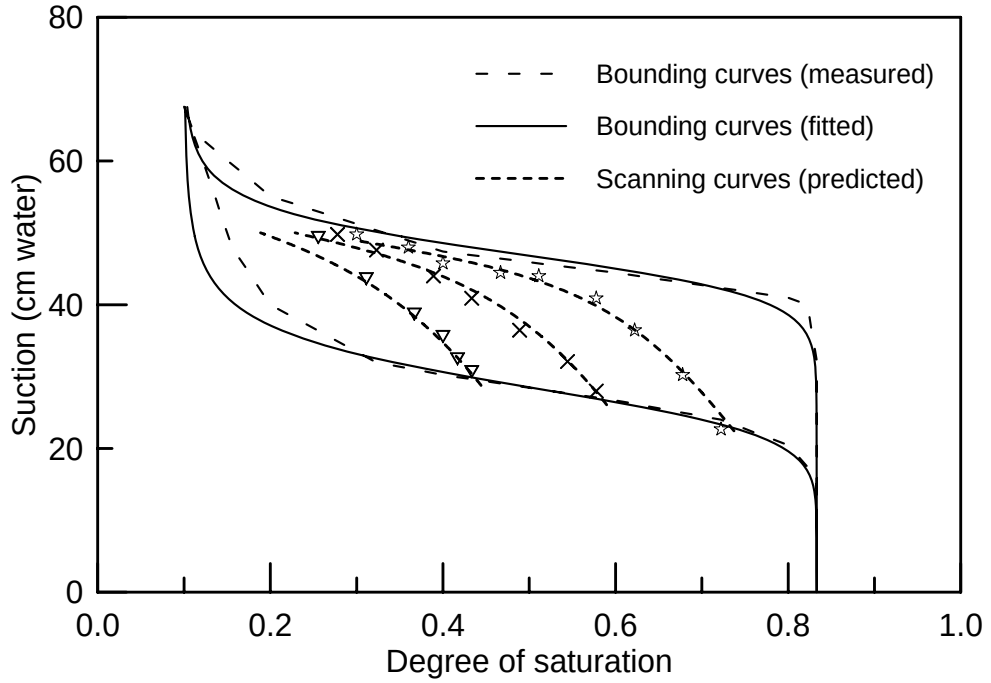


(b) Drying scanning curves

**Fig. 3.17** Comparison between measured and predicted scanning curves for glass-bead media I (test results from Topp and Miller, 1966)

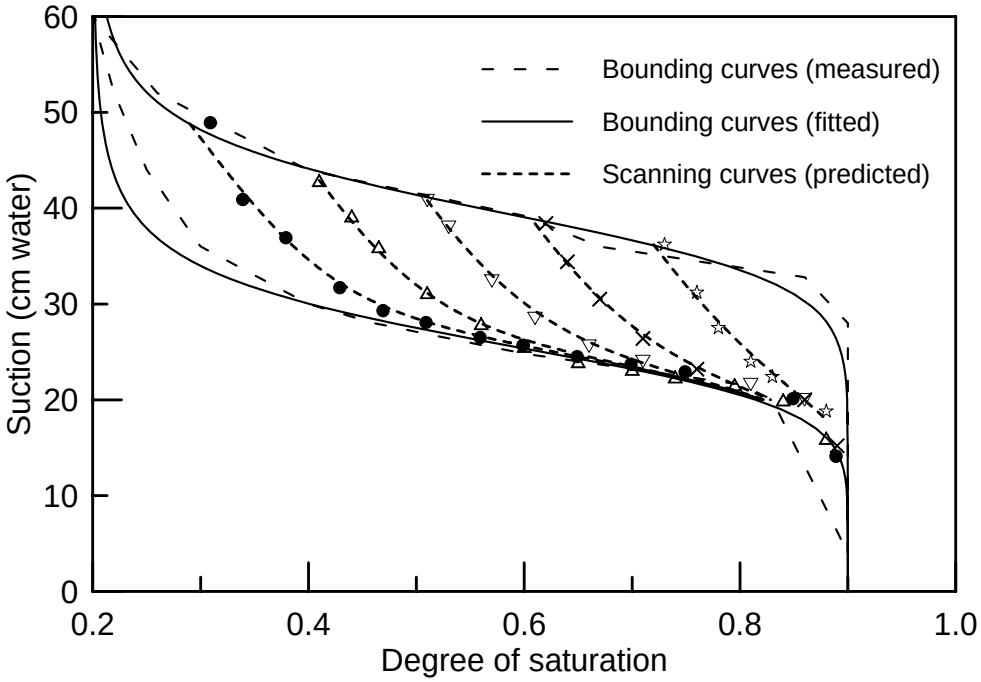


(a) Wetting scanning curves

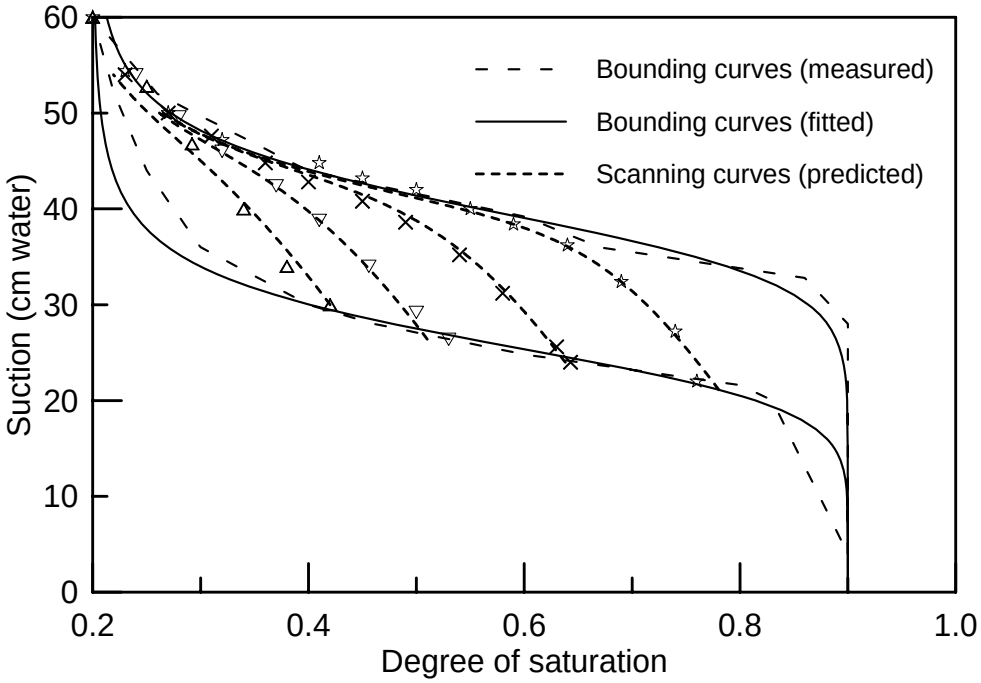


(b) Drying scanning curves

**Fig. 3.18** Comparison between measured and predicted scanning curves for glass-bead media II (test results from Topp and Miller, 1966)

# CHAPTER 4

# AN ISOTROPIC MODEL FOR UNSATURATED SOILS

## 4.1 INTRODUCTION

In Chapter 2, a thorough literature review was carried out to investigate the selection of stress-strain variables and constitutive modeling of unsaturated soil behavior. From Eq. (2.10) in Chapter 2, it is clear that the intergranular stress is directly related to both suction and water content, so it stands to reason that the mechanical behavior of unsaturated soil is strongly dependent on the soil state relative to the SWCCs. Although many either simple or complicated models have been proposed in the past decades, most of these models have focused on the mechanical behavior and neglected the coupling effects between the mechanical and hydraulic mechanisms. In Chapter 3, a simple SWCCs model was presented to show that the suction path has a strong effect on the hysteretic relationship between suction and water content. In fact, not only the wetting and drying history, but also the stress history of the soil has strong influence on SWCCs. Besides the stress or strain history, both the suction history and water content influence the stress-strain behavior of unsaturated soils as well. To simulate the unsaturated soil behavior in a complete sense, it is necessary to incorporate both mechanical and

hydraulic behavior in the constitutive model. Both mechanisms are not independent and they affect each other in an interactive way and this idea is supported by laboratory work, such as Sun *et al.* (2007c) and Miller *et al*. (2008).

In recent years, the important role of SWCCs in unsaturated soil mechanics has come to the forefront of geotechnical research. Although major progress has been made, it is apparent that additional research is needed to improve existing models and develop new models. As discussed in Chapter 2, there are very few models that incorporate hysteresis in SWCCs and none are widely accepted. This is partly because there are very little experimental data available that reveals the detailed relationship between the SWCCs and externally applied stress. It is worth to note that some valuable data do exist (e.g., Ng and Pang, 2006; Ho *et al.*, 2006; Miller *et al.*, 2008), but they are relatively limited in terms of the number of tests and variables examined. To investigate the coupling effects between mechanical and hydraulic behavior of unsaturated soils is a relatively new topic and it is still under development.

In this chapter, a simple isotropic constitutive model for unsaturated soils is proposed. The coupling effects between mechanical and hydraulic behavior are fully considered. The hysteretic SWCCs model presented in Chapter 3 is incorporated in this isotropic model to account for the coupling effects between hysteretic SWCCs and stress-strain behavior of unsaturated soils. The main purpose of this chapter is to present a general idea on how to describe the coupling effects between stress-strain behavior and SWCCs. The proposed isotropic model will be validated via comparing the model

predictions against available laboratory test results. A hypothetical soil is also used to predict some special characteristics of unsaturated soils under complex suction and stress paths.

## 4.2 ISOTROPIC MODEL FORMULATION

This section presents a coupled hydraulic-mechanical constitutive model for unsaturated soils by combining the elastoplastic SWCCs presented in Chapter 3 with an isotropic elastoplastic stress-strain model for the solid skeleton. While the SWCCs are described using a bounding surface plasticity model as detailed earlier, the isotropic stress-strain behavior is described using a classical, yield surface-based, plasticity model in a manner similar to the one proposed by Wheeler *et al.* (2003). The coupled model is presented here to illustrate the capabilities of the elastoplastic framework described. The framework and the concepts presented are general enough to allow the use of more sophisticated models to describe the stress-strain behavior as shown in Chapter 5.

In this isotropic model, the stress variables are the mean intergranular stress from Eq. (2.10) and matric suction. Their conjugated strain variables are volumetric strain and volume fraction of water. The model formulation and all the calculations are expressed using these conjugated stress-strain variables. For convenience, the stress-strain variables shown in the figures are those typically used in unsaturated laboratory tests. For example, net stress and degree of saturation are common variables for external loading and water content used in laboratory tests, respectively. Volumetric strain is generally given in

terms of specific volume or void ratio change.

The discussion on the theory of this isotropic model is part of the work by Muraleetharan *et al.* (2008). The case studies in Section 4.3 used to validate the isotropic model performance are part of Muraleetharan *et al.* (2008) and Miller *et al.* (2008).

### 4.2.1 HARDENING LAWS

The hardening laws define the modification of the yield surfaces during the process of plastic flow. Since the irrecoverable volume fraction of water and plastic volumetric strain are treated as plastic strain variables, the evolution of all the bounding surfaces, including the bounding suction curves and the yield mean intergranular stress is affected by both the irrecoverable volume fraction of water and plastic volumetric strain. The effect of soil deformation on the hysteresis of SWCCs has been extensively discussed by many researchers, such as Li (2007 a&b), Gallipoli *et al.* (2008) and Nuth and Laloui (2008b). In the current research, it is assumed that the plastic volumetric strain of soil skeleton has a direct effect on the bounding suctions. The history of soil skeleton deformation therefore affects the bounding suctions. Once the bounding suctions change, any scanning SWCC curve shifts. In this way, the effect of soil deformation on the SWCCs can be appropriately accounted for. Simultaneously, the irrecoverable volume fraction of water also influences the yield stress of the soil skeleton. Essentially, the irrecoverable volume fraction of water represents a joint effect from both the stress-strain history and the suction history. Any volumetric deformation of soil skeleton during drying or wetting process can be captured well through this method. With fully

consideration of the coupling effects between the mechanical and hydraulic mechanisms, the coupled hardening laws for SWCCs and soil skeleton are defined as follows:

$$ds_{c0} = \Gamma_0^p dn_w^p + \Gamma_v^p d\varepsilon_v^p \tag{4.1}$$

$$dp_0' = K_0^p d\varepsilon_v^p + K_1^p dn_w^p \tag{4.2}$$

The hardening laws given above describe the change in bounding suction ( $s_{c0}$ ) and yield mean intergranular stress ( $p_0'$ ) with respect to changes in plastic volumetric strain ( $\varepsilon_v^p$ ) and irrecoverable volume fraction of water ( $n_w^p$ ). The bounding suction refers to values on two different curves, the wetting bounding curve and the drying bounding curve. The coefficients in Eqs. (4.1) and (4.2) are defined as 'plastic moduli'. $\Gamma_0^p$ is the value of capillary plastic modulus $\Gamma^p$ on the bounding curves and it is defined in Eq. (3.10) in Chapter 3. The other three moduli are defined as: $\Gamma_v^p = s_{c0}\zeta v$, $K_0^p = p_0'\eta_0 v$ and $K_1^p = -p_0'\eta_1$, where $\zeta$, $\eta_0$ and $\eta_1$ are three material parameters and $v$ is the specific volume, which is defined in terms of porosity *n* as: $v = \frac{1}{1-n}$. Both Eqs. (4.1) and (4.2) state that the plastic volumetric strain and irrecoverable volume fraction of water have effects on the bounding suctions and the yield mean intergranular stress. In addition, the inclusion of specific volume $v$ in $\Gamma_v^p$ and $K_0^p$ has similar function to the capillary bonding function proposed by Gallipoli *et al.* (2003a). The hardening laws in Eqs. (4.1) and (4.2) are one of the special features that differentiate the current model from other

models. The coupling effects between the mechanical and hydraulic mechanisms are fully accounted for using the hardening laws.

### 4.2.2 YIELD FUNCTIONS

Similar to what Wheeler *et al.* (2003) assumed, the yield surface, which is plotted in Fig. 4.1, is composed of three curves, i.e., the drying bound BC, the wetting bound AD and the yield mean intergranular stress AB.

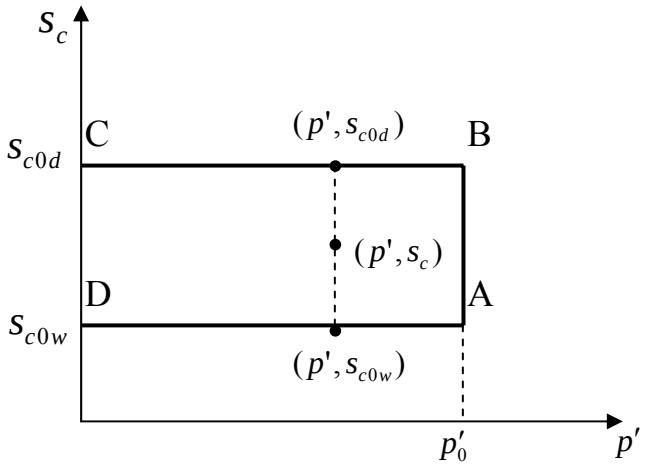


**Fig. 4.1** Yield surfaces of the isotropic model

The bounding/yield curves are described by the following three functions:

$$p' = p'_0 \tag{4.3}$$

$$s_c = s_{c0w} \tag{4.4}$$

$$s_c = s_{c0d} \tag{4.5}$$

where: $s_{c0w}$ and $s_{c0d}$ stand for bounding suctions on the primary wetting and secondary drying curves, respectively. Rearranging Eq. (3.4) in Chapter 3, $s_{c0w}$ and $s_{c0d}$ can be calculated as follows:

The primary wetting curve: $$s_{cow} = b_1 \left( \frac{n_{sat} - n_w}{n_w - n_{res}} \right)^{\frac{1}{d_1}} \tag{4.6}$$

The secondary drying curve: $$s_{cod} = b_2 \left( \frac{n_{sat} - n_w}{n_w - n_{res}} \right)^{\frac{1}{d_2}} \tag{4.7}$$

where: $n_{sat}$ is the water content at zero suction ( = porosity $n$). $n_{res}$ is the residual water content at very high suction. $n_w$ is current water content. $b_1$, $d_1$, $b_2$ and $d_2$ are four material parameters and $b_1$ and $b_2$ have the same unit as suction in this study. $p'$ is the mean intergranular stress, which is the first invariant of the intergranular stress tensor (see Eq. (2.10)) and is given by:

$$p' = \frac{1}{3}\left(\sigma'_{11} + \sigma'_{22} + \sigma'_{33}\right) = (p - p_a) + n_w s_c \tag{4.8}$$

where: $p$ and $p_a$ are the mean total stress and pore air pressure, respectively.

$p = \frac{1}{3}\left(\sigma_{11} + \sigma_{22} + \sigma_{33}\right)$, where $\sigma_{11}$, $\sigma_{22}$ and $\sigma_{33}$ are the total stresses. $s_c$ is the suction.

### 4.2.3 ELASTIC RESPONSES

Elastic responses of the solid skeleton and water content are given by:

$$d\varepsilon_v^e = \frac{k dp'}{v p'} \tag{4.9}$$

$$dn_w^e = \frac{ds_c}{\Gamma^e} \tag{4.10}$$

where: $k$ is a constant standing for the slope of an elastic swelling line in the $v - \ln p'$ space. $\Gamma^e$ is the capillary elastic modulus.

### 4.2.4 FLOW RULES

A flow rule is the necessary kinematic assumption postulated for plastic deformation or plastic flow. Flow rules define how the plastic volumetric strain and irrecoverable water content change with yield intergranular stress and yield suction. A general form of yield function and its consistency condition are given as follows:

$$F\left(s_{c0},\, p_0',\, \varepsilon_v^p,\, n_w^p\right) = 0 \tag{4.11}$$

$$dF = \frac{\partial F}{\partial s_{c0}} ds_{c0} + \frac{\partial F}{\partial p_0'} dp_0' + \frac{\partial F}{\partial \varepsilon_v^p} d\varepsilon_v^p + \frac{\partial F}{\partial n_w^p} dn_w^p = 0 \tag{4.12}$$

According to the bounding surface plasticity concept (Dafalias and Herrmann, 1975&1976), the loading index can be written as:

$$L = \frac{1}{K_p}\left(\frac{\partial F}{\partial s_c} ds_c + \frac{\partial F}{\partial p'} dp'\right) = \frac{1}{\overline{K}_p}\left(\frac{\partial F}{\partial s_{c0}} ds_{c0} + \frac{\partial F}{\partial p'_0} dp'_0\right) \tag{4.13}$$

where: $K_p$ and $\overline{K}_p$ are the actual plastic modulus and the bounding plastic modulus, respectively. Recall the yield surface in Eqs. (4.3) to (4.5) and the loading indices along AB and BC or AD can be written as follows:

Along AB: $$L = \frac{1}{K_p}\frac{\partial F}{\partial p'} dp' = \frac{1}{\overline{K}_p}\frac{\partial F}{\partial p'_0} dp'_0 = \frac{1}{K_p} dp' = \frac{1}{\overline{K}_p} dp'_0 \tag{4.14}$$

Along BC or AD: $$L = \frac{1}{K_p}\frac{\partial F}{\partial s_c} ds_c = \frac{1}{\overline{K}_p}\frac{\partial F}{\partial s_{c0}} ds_{c0} = \frac{1}{K_p} ds_c = \frac{1}{\overline{K}_p} ds_{c0} \tag{4.15}$$

The plastic volumetric strain and irrecoverable volume fraction of water are treated as internal variables and the flow rules can be given as follows:

$$d\varepsilon_v^p = < L > \frac{\partial F}{\partial p'} = < L > = \frac{1}{\overline{K}_p} dp'_0 = \frac{1}{\eta_0 \nu}\frac{dp'_0}{p'_0} \tag{4.16}$$

$$dn_w^p = < L > \frac{\partial F}{\partial s_c} = < L > = \frac{1}{K_p} ds_c = \frac{1}{\overline{K}_p} ds_{c0} = \frac{ds_c}{\Gamma^p} = \frac{ds_{c0}}{\Gamma_0^p} \tag{4.17}$$

Recall the definition of the capillary plastic modulus:

$$\Gamma^p = \Gamma_0^p \left(1 + h \cdot \delta / < \delta_{in} - g\delta >\right) \tag{4.18}$$

Eq. (4.16) is consistent with the flow rule $dn_p^w / d\varepsilon_v^p = 0$ and Eq. (4.17) is consistent with the flow rule $d\varepsilon_v^p / dn_p^w = 0$. The definitions of plastic moduli $\Gamma^p$ and $\Gamma_0^p$ are given in Eq. (3.10) in Chapter 3.

These flow rules imply that the yield curve given by $p' = p_0'$ and the bounding curve(s) given by $s_c = s_{c0w}$ (or $s_{c0d}$) are perpendicular to each other on the $p' - s_c$ plane. At the intersection of the bounding curve(s) and the yield curve, $d\varepsilon_v^p$ and $dn_w^p$ are calculated by solving two simultaneous equations given by Eqs. (4.1) and (4.2):

$$d\varepsilon_v^p = \frac{\eta_1}{v\left(\eta_0 \Gamma_0^p + \eta_1 s_{c0} \zeta\right)} ds_{c0} + \frac{\Gamma_0^p}{v\left(\eta_0 \Gamma_0^p + \eta_1 s_{c0} \zeta\right)} \frac{dp_0'}{p_0'} \tag{4.19}$$

$$dn_w^p = \frac{\eta_0}{\left(\eta_0 \Gamma_0^p + \eta_1 s_{c0} \zeta\right)} ds_{c0} - \frac{s_{c0} \zeta}{\left(\eta_0 \Gamma_0^p + \eta_1 s_{c0} \zeta\right)} \frac{dp_0'}{p_0'} \tag{4.20}$$

So far, the isotropic model formulation has been completely presented in terms of mean intergranular stress and suction. The coupling effects between mechanical and hydraulic behavior of unsaturated soils are fully described and the hysteretic SWCCs model is included in this isotropic coupled model. Although the definitions of yield surface, flow rules and hardening laws are simple, the idea to investigate the coupling effects is fully described.

### 4.2.5 ISOTROPIC MODEL CALIBRATION

How to calibrate the SWCCs model parameters is given in Chapter 3 and the procedure is not repeated here. Besides the six parameters of SWCCs model, four additional parameters, $k$, $\zeta$, $\eta_0$ and $\eta_1$ are required to describe the coupled hydraulic-mechanical behavior. The parameter $k$ can be obtained from an unloading-reloading portion of a constant suction oedometer test and $k$ is the slope of that portion of the curve in $e - \ln p'$ space. With $k$ obtained the parameter $\eta_0$ can be calibrated by matching the loading curves during a constant suction oedometer test in $e - \ln p'$ space. The calibration of the parameters $\zeta$ and $\eta_1$ will require coupled hydraulic-mechanical tests where the soil undergoes plastic volume and irrecoverable water content changes. A wetting-induced collapse test is one such test. To calibrate all the model parameters, SWCCs with bounding curves and a scanning curve, a constant suction oedometer test and a constant external loading flooding test are needed. Although these tests are not trivial, they are becoming common in terms of studying the behavior of unsaturated soils. Some important progress in accelerating the measurement of SWCCs is described by Chen *et al.* (2007) and Miller *et al.* (2008).

## 4.3 ISOTROPIC MODEL VALIDATION

Very limited experimental results are available in the literature to investigate the coupling effects between hydraulic and mechanical behavior of unsaturated soils. The

dearth of test data on this topic is mainly due to the time-consuming procedure to run tests to obtain hysteretic SWCCs. The other possible reason for the lack of test data is that the earlier researchers did not pay enough attention to the coupling effects. Most of the available test programs dealt with the mechanical behavior of unsaturated soils under constant or different suctions, but very few studies investigated the effects of external loading on the soil water characteristics, especially the hysteretic property of SWCCs. Simple isotropic collapse tests conducted by Sun *et al.* (2007c) on Pearl clay are first used to illustrate the capabilities of the proposed model. Then predictions for three different hypothetical, but complex tests with varying stresses and suctions that can be carried out in the laboratory are presented to give further insight into the capabilities of the model. Finally, another valuable set of laboratory results from the University of Oklahoma (Miller *et al.*, 2008) are used to check the validity of the proposed isotropic constitutive model for unsaturated soils. In unsaturated laboratory tests, stress quantities traditionally reported are net stress and suction. Traditional stress strain quantities are used to report the predictions to provide insight for the readers into the behavior predicted by the model. The model calculations are, however, carried out using intergranular stress and suction as illustrated in the model development. All the model parameters used in these predictions are given in Table 4.1.

### 4.3.1 PEARL CLAY: CONSTANT MEAN NET STRESS COLLAPSE TESTS

This series of suction-controlled triaxial tests (Sun *et al.*, 2007c) were designed to investigate the collapse behavior of unsaturated compacted clay. Pearl clay reported by

Sun *et al.* (2007c) has a liquid limit of 49, a plasticity index of 22, and a specific gravity of 2.71. As shown in Fig. 4.2a, only the primary wetting curve is available. The measured curve shown in Fig. 4.2a is obtained at a mean net stress $(p - p_a)$ of 20 *kPa*. This curve is used to calibrate the parameters $b_1$, $d_1$, $n_{sat}$, and $n_{res}$. Typical values are used for rest of the SWCCs parameters and these values are given in Table 4.1. Predicted secondary drying curve and a scanning curve with this set of parameters are also shown in Fig. 4.2a and the predictions appear reasonable. Next, the coupling parameters and the stress-strain parameter $k$ are calibrated using an isotropic collapse test. $k$ comes directly from the initial portion of $v - \ln p'$ at constant suction of 147 *kPa*, which is Loading Phase #1 given below. Loading Phases #2 and #3 are used to calibrate $\zeta$, $\eta_0$ and $\eta_1$. The test results and the calibrated model predictions are shown in Fig. 4.2b. The stress path for this test involves three different loading phases as given below:

Loading Phase #1: Constant suction 147 *kPa*, mean net stress: 20 *kPa* (A) → 98 *kPa* (B);
Loading Phase #2: Constant mean net stress 98 *kPa*, suction: 147 *kPa* (B) → 0 *kPa* (C);
Loading Phase #3: Constant suction 0 *kPa*, mean net stress: 98 *kPa* (C) →196 *kPa* (D).
Initial conditions at A are as follows: $n_w = 0.314$; mean yield intergranular stress, $p_0' = 95.0$ kPa.

Finally, using the calibrated model parameters another collapse test results are predicted as shown in Fig. 4.2c. Compared with the test used for model calibration, the only difference of the validation test lies in the mean net stress when wetting occurs. For the calibration test, the suction is reduced from 147 *kPa* to 0 *kPa* at a mean net stress of

98 *kPa*, while for the validation test, the wetting occurs at mean net stress of 49 *kPa*. Model predictions compare reasonably well with the measured results.

### 4.3.2 HYPOTHETICAL SOIL: CONSTANT-SUCTION ISOTROPIC LOADING TESTS

The soil experiences isotropic loading at a constant suction $s_c = 50\ kPa$ and initial volume fraction of water, $n_w = 0.35$. Initial specific volume of the soil sample, $v = 1.8$ corresponding to a porosity ($n$) of 0.44. The mean net stress path is given as: 10 *kPa* (A) → 200 *kPa* (C) → 10 *kPa* (D) → 1000 *kPa* (G). The mean yield intergranular stress is initially set at $p_0' = 141\ kPa$. The results are presented in Figs. 4.3a and 4.3b. In Fig. 4.3b and several other figures, degree of saturation, $s_r$, is used to clearly illustrate the behavior after the soil becomes a two-phase material. For the predictions presented here, the soil is treated as a two-phase material when $s_r \geq 0.999$.

During the loading from A to B, only elastic volumetric strains are calculated. At point B, the yield surface is reached and the elastoplastic behavior begins. The elastoplastic behavior is sustained until the mean net stress increase ends at point C. From C to D unloading occurs and the soil exhibits purely elastic behavior. During the reloading phase the yield surface is reached again at point E. As the mean net stress keeps increasing, the soil becomes compressed and the degree of saturation keeps increasing simultaneously. Finally, the soil reaches a saturated state at point F, resulting in a change in slope of the specific volume-mean net stress curve after point F as shown in Fig. 4.3a.

### 4.3.3 HYPOTHETICAL SOIL: MOVEMENT OF THE SWCCS DUE TO CHANGES IN NET STRESS

Wetting-drying curves are predicted for two different mean net stresses, 60 and 600 *kPa* as shown in Figs 4.4a and 4.4b. The initial conditions at Point A are: $p - p_a = 60\ kPa$, $s_c = 120\ kPa$, $n_w = 0.16$, $v = 2.2$, $s_r = 0.29$, and $p_0' = 141\ kPa$. First, at a constant mean net stress of 60 *kPa* a wetting-drying cycle is carried out given by the suction path: 120 *kPa* (A) → 30 *kPa* (C) → 120 *kPa* (D). For the second simulation starting with the same initial conditions at Point A, the mean net stress is increased from 60 *kPa* to 600 *kPa* while keeping the suction at 120 *kPa* (A to E). This loading is then followed by a wetting-drying cycle 120 *kPa* (E) → 30 *kPa* (F) → 120 *kPa* (G).

For the simulation at a mean net stress of 60 *kPa*, starting at point A, the degree of saturation increases during the wetting process and the soil becomes saturated. During the initial part of this wetting phase (A → B), due to the reduction in the intergranular stress, the soil experiences increase in volume. Towards the end of the wetting phase (B → C), however, slight reduction in volume can be observed. The reason for this reduction in volume is the change in $p_0'$ due to the coupling effect given by Eq. (4.2) during the wetting process. Although suction keeps decreasing from A to B and then to C, swelling is observed during AB portion while collapse occurs during BC. After the mean net stress is increased from 60 *kPa* to 600 *kPa*, the same suction path (see EFG) is applied onto the soil. Similar behavior of volume change occurs, but the magnitudes of swelling and

collapse during EF are much smaller than those during ABC. The large volume decrease observed from A to E prevents further volume change during the wetting process from E to F. Additional volume change can be observed during subsequent drying from F to G. The hysteresis in SWCCs and the influence of the net stress on the SWCCs are clearly shown in Fig. 4.4a. In this case study, the effects of external loading (i.e., mechanical behavior) on hydraulic behavior are presented.

### 4.3.4 HYPOTHETICAL SOIL: COMPLEX STRESS PATHS

This simulation involves three different loading phases:

Loading Phase #1: Constant suction 100 *kPa*, mean net stress: 50 *kPa* (A) → 200 *kPa* (C) → 50 *kPa* (D);

Loading Phase #2: Constant mean net stress 50 *kPa*, suction: 100 *kPa* (D) → 60 *kPa* (E) → 100 *kPa* (F);

Loading Phase #3: Constant suction 100 *kPa*, mean net stress: 50 *kPa* (F) → 800 *kPa* (H).

Initial state: $v = 2.2$, $n_w = 0.16$, $s_r = 0.29$, $p_0' = 141\ kPa$.

The predictions are illustrated in Figs. 4.5a and 4.5b. During the Loading Phase #1, the soil behavior is very similar to what is shown in Fig. 4.3a. The yield surface is reached at Point B and elastoplastic strains are predicted from B to C. When the mean net stress experiences a reduction from 200 *kPa* to 50 *kPa*, only elastic volumetric strains are predicted.

During the wetting-drying cycle in Loading Phase #2, the soil experiences elastic swelling from D to E and then elastic compression from E to F (Fig. 4.5a). During this phase the degree of saturation changes from point D to point E and then comes back to point F as shown in Fig. 4.5b. During the Loading Phase #3, the yield surface is reached at point G, different from the point C reached during the Loading Phase #1. The wetting-drying cycle in Loading Phase #2 leads to a change in yield pint from C to G.

### 4.3.5 OU MIXTURE: LOADING HISTORY EFFECTS ON SWCCS

This series of laboratory tests conducted by Miller *et al.* (2008) seems to be one of the first sets of data investigating the coupling effects between mechanical and hydraulic behavior of unsaturated soils in a systematic way. The OU mixture is a mixture of two commercially available manufactured porous media, Sil-Co-Sil 250 (U.S. Silica Company) and Glass Beads, Size BT-9 (Zero Products). Its grain size distribution is similar to that of fine sandy silt having about 48% fine sand, 46% silt and 6% clay. Details on the mixture can be found in Miller *et al.* (2008). The SWCCs conducted for net vertical stress of 10 *kPa* and 200 *kPa* are presented in Figs. 4.6a and 4.6b, respectively. The bounding curves for these two net vertical stresses are compared in Fig. 4.6c. The SWCCs model parameters are calibrated from the 10 *kPa* net vertical stress results. This calibration and all the subsequent predictions are made using a coefficient of earth pressure at rest, $K_0$ of 1.0. That is, the vertical stress is assumed to be same as the

mean stress. The measured and predicted SWCCs for net vertical stress of 10 *kPa* are presented in Fig. 4.6d.

The four additional isotropic model parameters were calibrated from the test results given in Fig. 4.6e. With these calibrated model parameters, the SWCCs for 200 *kPa* net vertical stress are predicted following a stress/suction change path that simulates the stress/suction change path for a portion of the experiment. Specifically, starting with as compacted conditions, loading and wetting paths as shown in Fig. 4.6e are first simulated. Then the following wetting/drying cycles are simulated: start at zero suction and follow the secondary drying curve to near residual saturation at a suction of 70 *kPa*, wet back to a point along the primary wetting curve at a suction of 20 *kPa*, followed by a complete drying and wetting path (suction increase to 60 *kPa* then decrease back to 20 *kPa*) to establish a scanning curve loop. The measured and predicted portions of the SWCCs for 200 *kPa* net vertical stress are shown in Fig. 4.6f. The only parameter that needed adjustment was the residual saturation. A value of $n_{res} = 0.06$ is used to predict the behavior at 200 *kPa* net vertical stress. The comparison in Fig. 4.6f demonstrates that the proposed model is well suited to capture the hysteretic nature of the SWCCs and reasonable agreement with experimental results was obtained. To further appreciate the potential of the model to capture the coupled mechanical-hydraulic behavior, the predicted SWCCs for net vertical stress of 10 and 200 *kPa* are shown together alongside a similar graph depicting the experimental data in Fig. 4.6g. In this figure it is apparent that the model is capturing some of the essential features demonstrated by the experimental data. In particular, the shape and position of the model SWCCs for 10 and

200 *kPa* net vertical stress is similar to that exhibited by the experimental curves. That is, the model SWCC for a net vertical stress of 200 *kPa* is slightly steeper and positioned slightly above the model SWCC for a vertical stress of 10 *kPa*. However, the model does not show the slight difference in the air-entry value observed in the experimental results.

## 4.4 SUMMARY

A simple isotropic constitutive model for unsaturated soils was presented and its ability to simulate the coupling effects between mechanical and hydraulic behavior was investigated. Both the effects of external loading history on the SWCCs and the effects of SWCCs on soil deformation were extensively studied and the proposed isotropic model provided reasonable predictions. Although the model formulation is very simple, it does capture most of the special characteristics of unsaturated soils. In addition, the model is able to simulate the transition from unsaturated to saturated behavior exhibited by the isotropic collapse that occurs during sample flooding and subsequent saturated compression. Due to its success in simulating the soil behavior, the general idea behind this isotropic model will be implemented into a comprehensive constitutive model for unsaturated soils in general stress space in the next chapter.

**Table 4.1** Model parameters for Pearl clay, hypothetical soil and OU mixture

| | Symbol | Pearl Clay | Hypothetical Soil | OU Mixture |
|---|---|---|---|---|
| SWCCs parameters | $b_1$ | 22 $kPa$ | 40 $kPa$ | 19 $kPa$ |
| | $d_1$ | 1.6 | 5.0 | 1.4 |
| | $b_2$ | 100 $kPa$ | 60 $kPa$ | 32 $kPa$ |
| | $d_2$ | 5.0 | 5.0 | 1.7 |
| | $\Gamma^e$ | $-3000$ $kPa$ | $-1100$ $kPa$ | $-1700$ $kPa$ |
| | $h$ | 15.0 | 7.0 | 7.0 |
| | $n_{sat}$ | 0.492 | 0.5 | 0.384 |
| | $n_{res}$ | 0.305 | 0.15 | 0.042 |
| Coupling parameters | $\eta_0$ | 17.5 | 7.69 | 50.0 |
| | $\eta_1$ | 10.0 | 7.0 | 15.5 |
| | $\zeta$ | 16.0 | 6.15 | 16.0 |
| | $k$ | 0.07 | 0.02 | 0.001 |

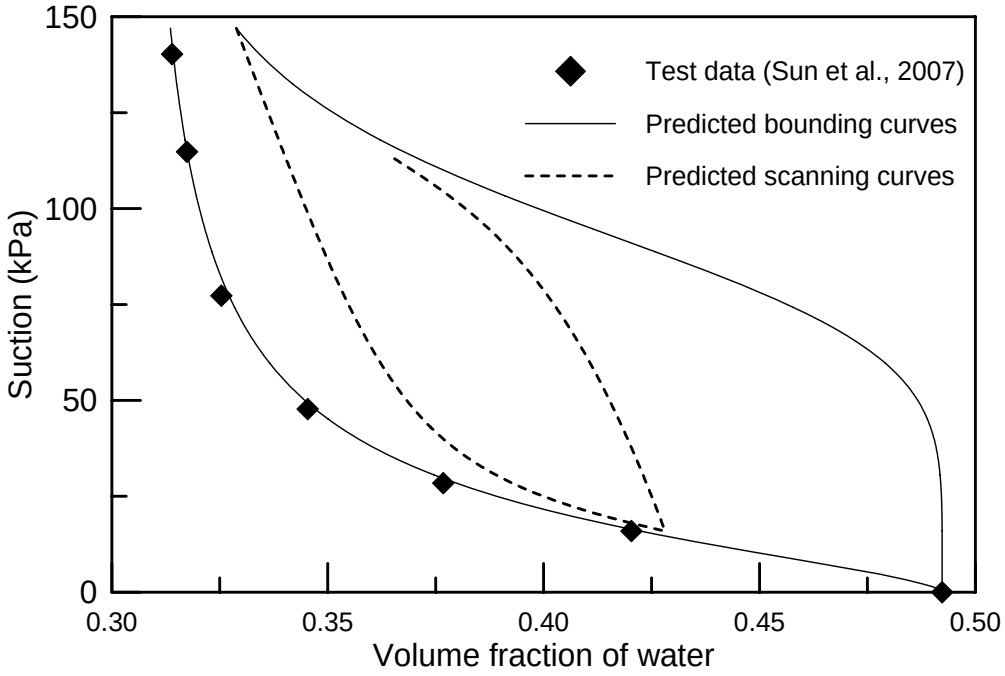


**Fig. 4.2a** Measured and predicted SWCCs for Pearl clay

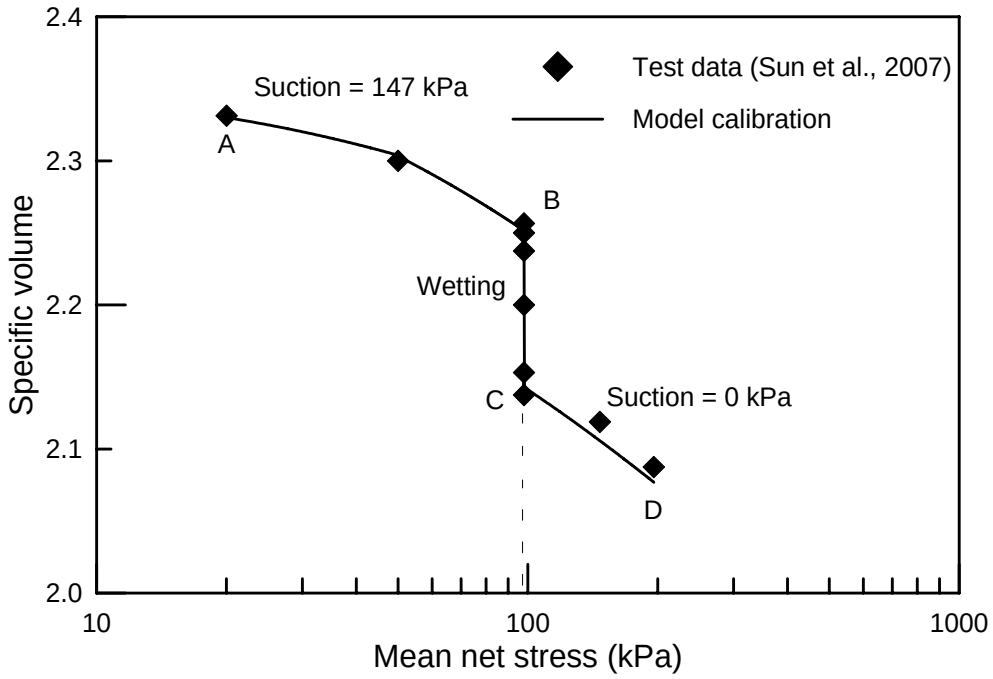


**Fig. 4.2b** Change of specific volume with mean net stress for Pearl clay: Wetting at 98 *kPa* mean net stress

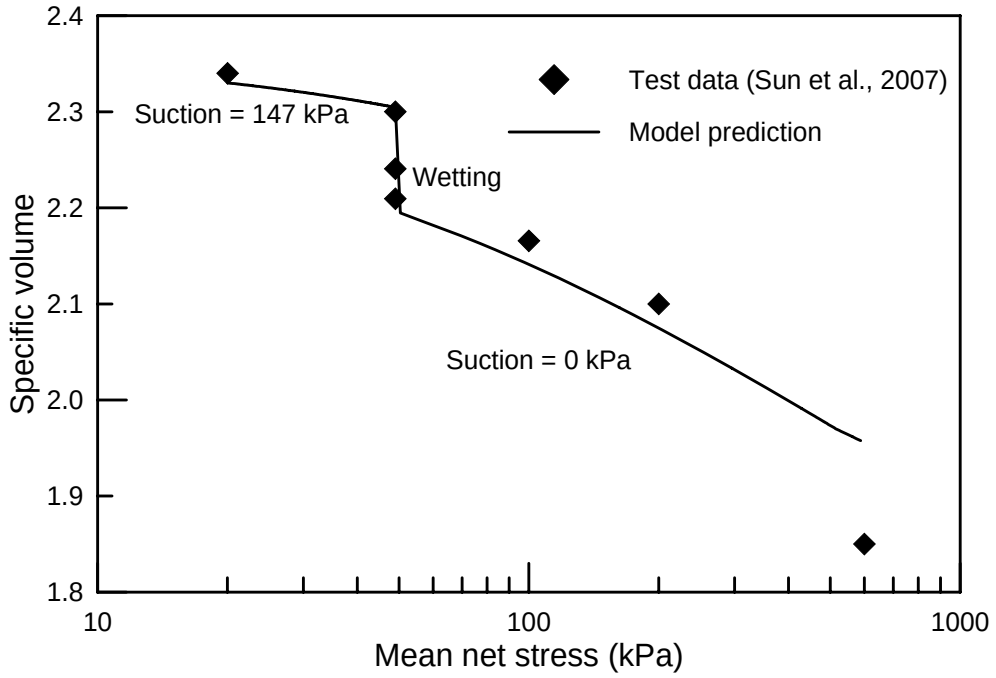


**Fig. 4.2c** Change of specific volume with mean net stress for Pearl clay: Wetting at 49 *kPa* mean net stress

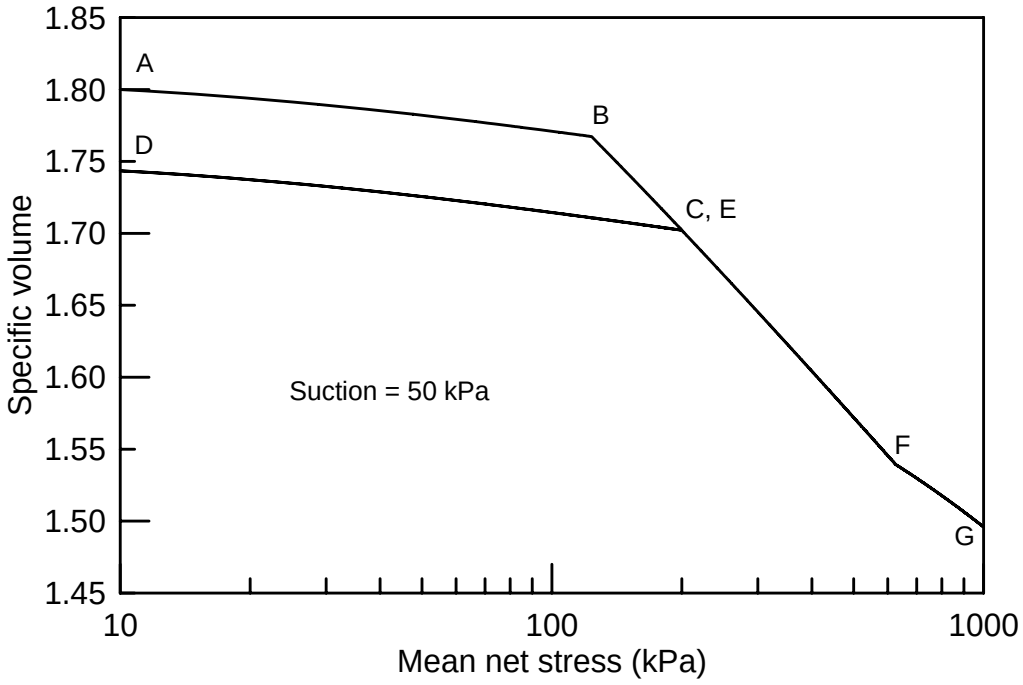


**Fig. 4.3a** Change of specific volume with mean net stress for the hypothetical soil

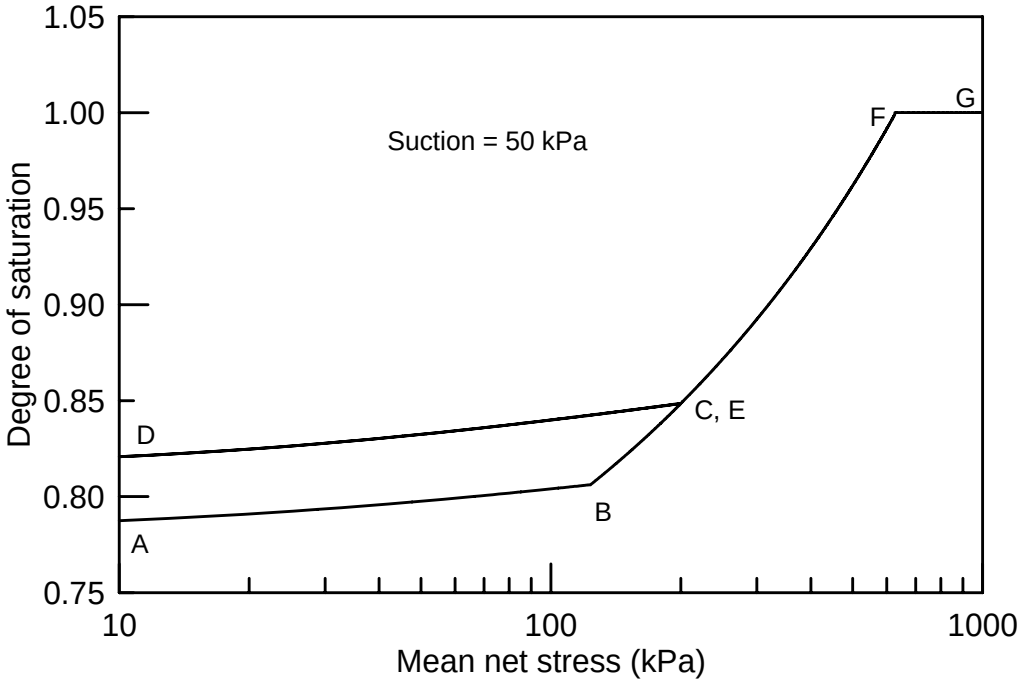


**Fig. 4.3b** Change of saturation with mean net stress for the hypothetical soil

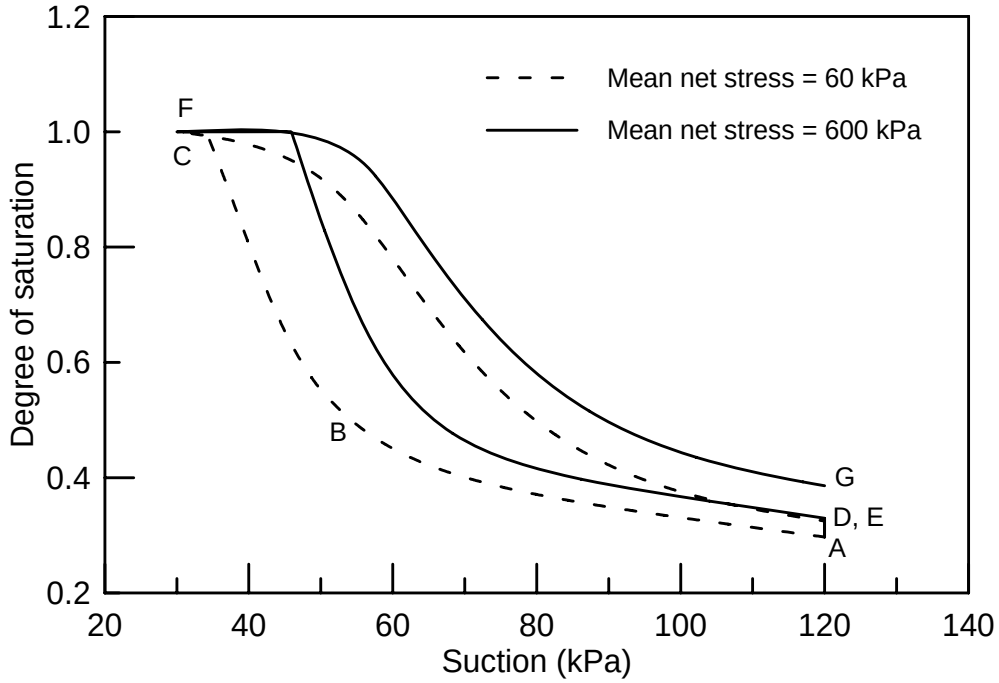


**Fig. 4.4a** Change of saturation with suction under different mean net stresses for the hypothetical soil

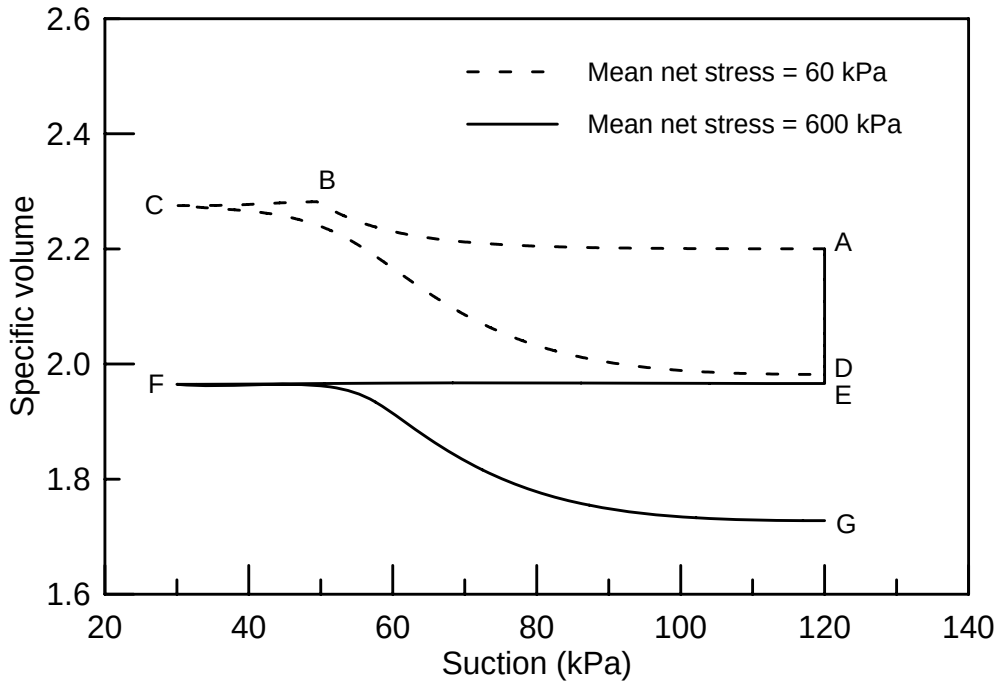


**Fig. 4.4b** Change of specific volume with suction under different mean net stresses for the hypothetical soil

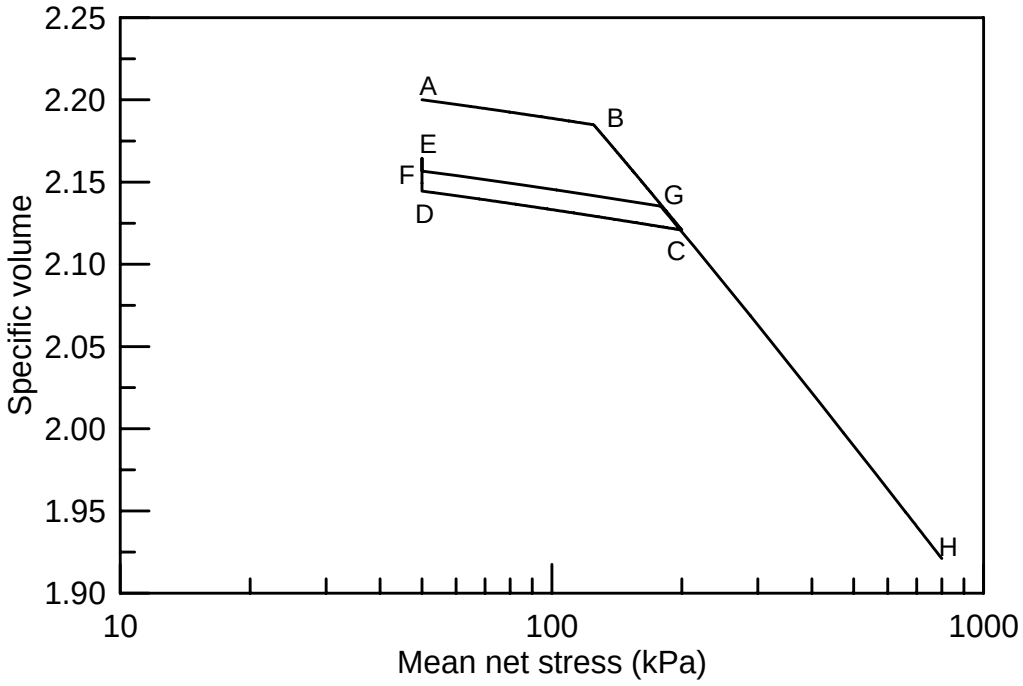


**Fig. 4.5a** Variation of specific volume with mean net stress for the hypothetical soil

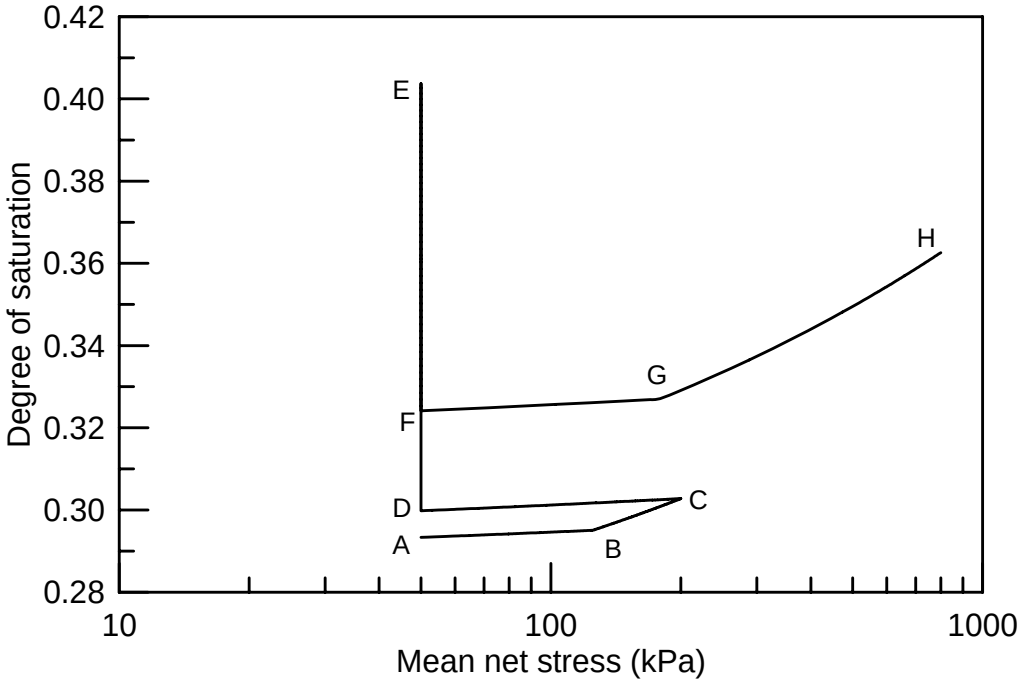


**Fig. 4.5b** Variation of saturation with mean net stress for the hypothetical soil

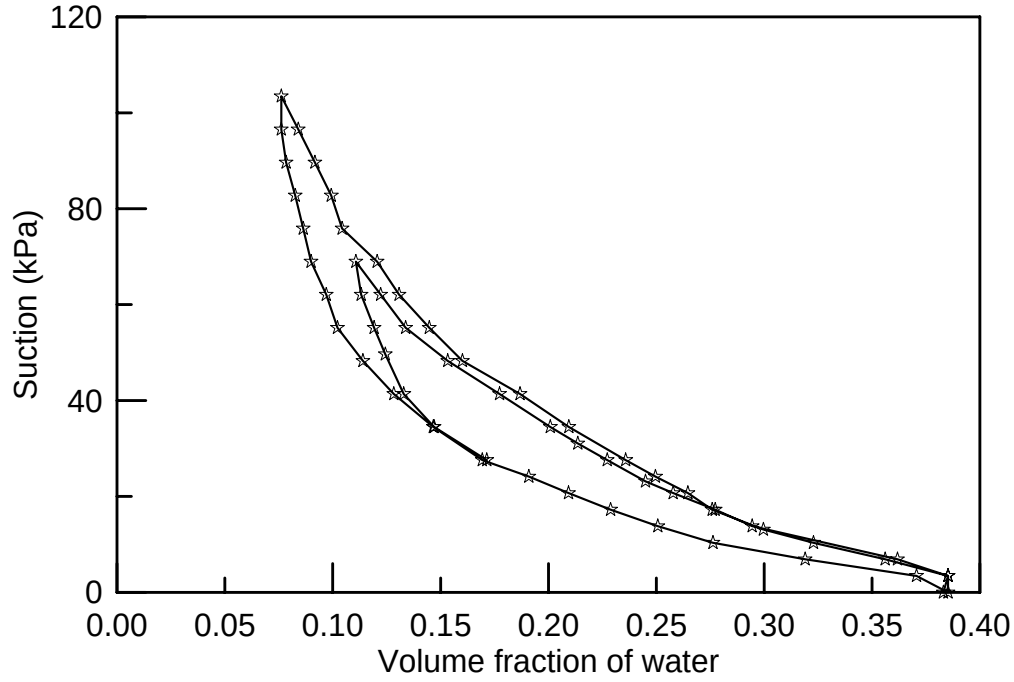


**Fig. 4.6a** Soil water characteristic curves for net vertical stress of 10 *kPa*

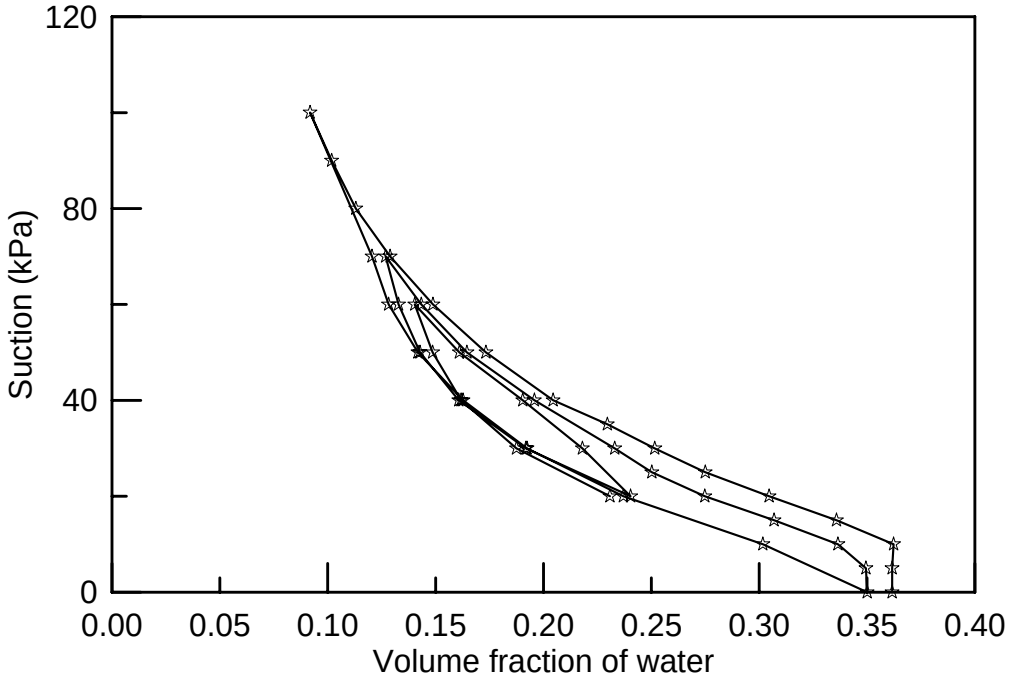


**Fig. 4.6b** Soil water characteristic curves for net vertical stress of 200 *kPa*

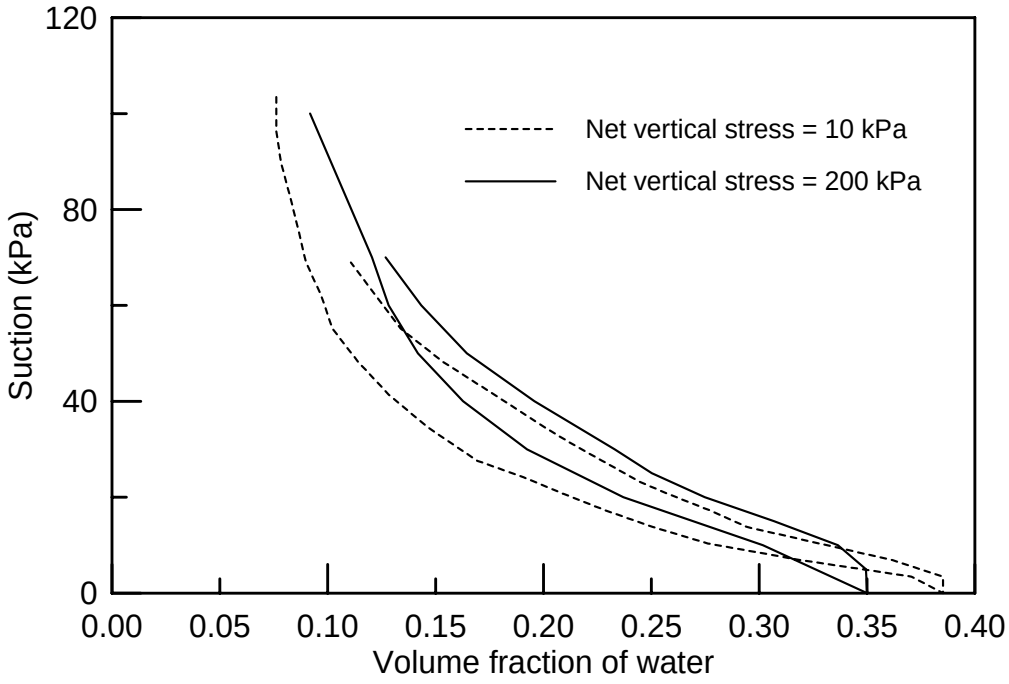


**Fig. 4.6c** Comparison of SWCCs for net vertical stresses of 10 *kPa* and 200 *kPa*

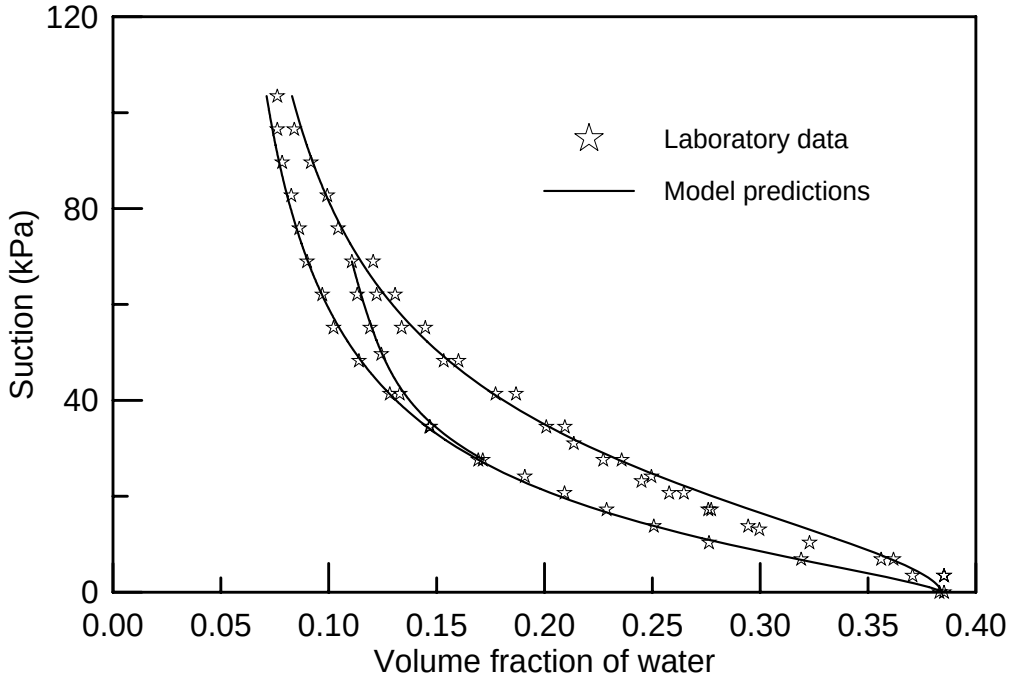


**Fig. 4.6d** Measured and predicted SWCCs for net vertical stress of 10 *kPa*

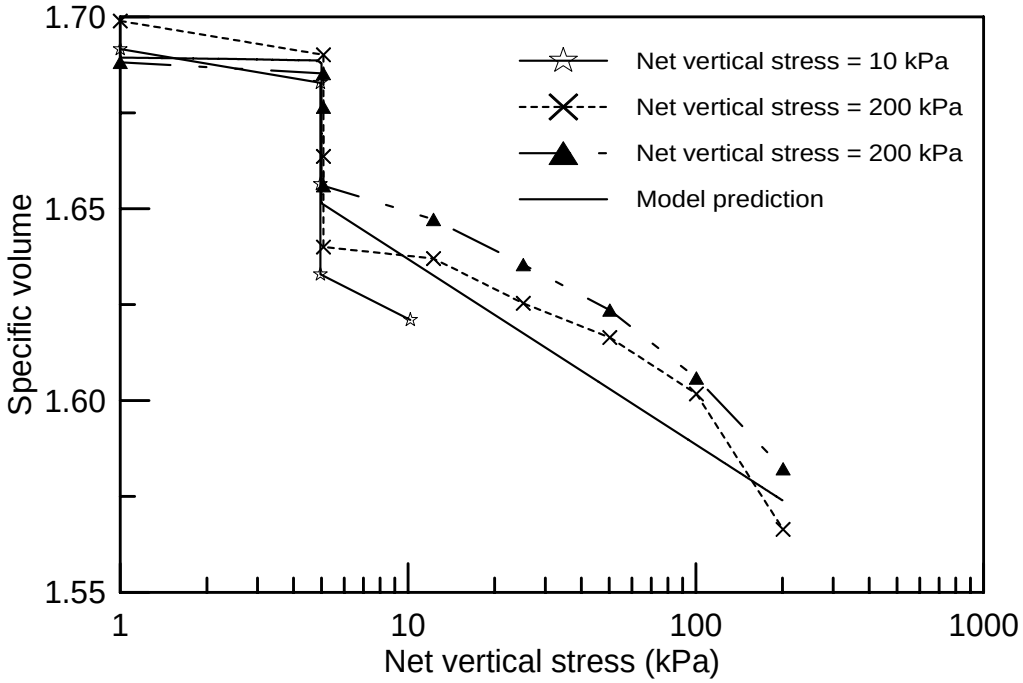


**Fig. 4.6e** Specific volume vs. net vertical stress: test results and model calibration

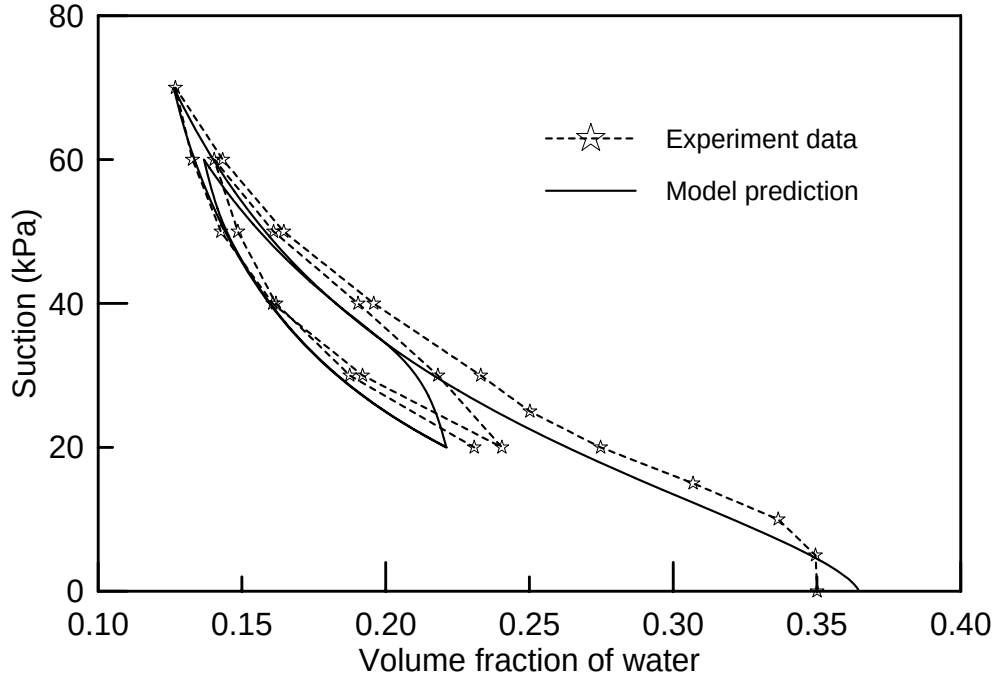


**Fig. 4.6f** Measured and predicted scanning SWCCs for net vertical stress of 200 *kPa*

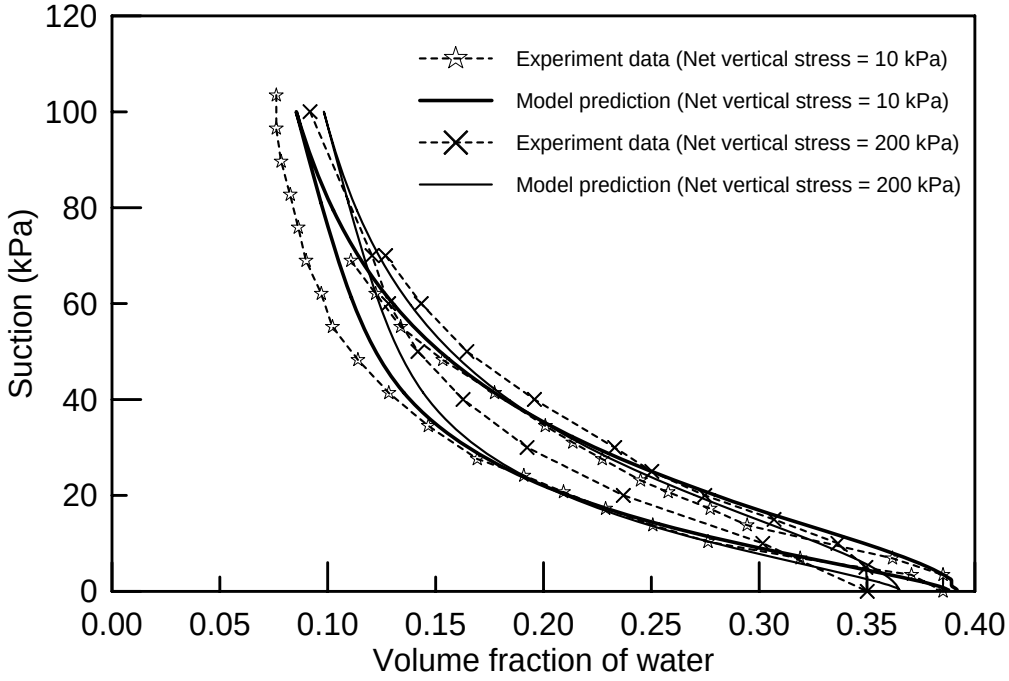


**Fig. 4.6g** Comparison of measured and predicted scanning SWCCs for net vertical stresses of 10 *kPa* and 200 *kPa*

# CHAPTER 5

# 3-D MODEL FOR UNSATURATED SANDS AND SILTS

## 5.1 INTRODUCTION

To fully investigate unsaturated silt or sand behavior, it is very useful to look into saturated silt or sand behavior. In fact, saturated silt or sand behavior can be treated as a special case for unsaturated soils when the suction reduces below the air entry value. The incorporation of the hysteresis SWCCs and the coupling effects between the mechanical and hydraulic behavior of unsaturated sands or silts differentiate the model developed in the current research from previously developed unsaturated soil models.

It is well known that the behavior of sand or silt depends not only on the density of the material, but also on the confining stress applied. Subjected to shear loadings, loose sands contract, while medium or dense sands dilate. To account for the effects of soil density on soil behavior, earlier models (e.g., Lade, 1977; Vermeer, 1978; Wang *et al.*, 1990; Crouch and Wolf, 1994a) generally used different sets of model parameters to capture the sand behavior, treating the same sands with different initial densities as

different soils. The limitation raised from this approach is obvious and this approach does not provide good control over the soil state during loading or unloading.

To treat the effects of density and confining stress on sand behavior in a unified way, some important concepts, such as the state parameter (Been and Jefferies, 1985), the phase transformation line or PTL (Ishihara *et al.*, 1975) and the state index (Ishihara, 1993), have been proposed over the last two decades. The state parameter, $\psi = e - e_c$, is defined to be the difference between the current void ratio $e$ and the corresponding critical void ratio $e_c$ at the same effective stress. In fact, the concept of the state parameter opens a new window for simulating the special behavior of sands. The introduction of the state parameter makes it possible to use a unique set of model parameters to simulate sand behavior under various loading conditions. Many researchers (e.g., Nova and Muir Wood, 1979; Been *et al.*, 1986; Yu, 1994, 1996 & 1998; Manzari and Dafalias, 1997; Gajo and Muir Wood, 1999; Li *et al.*, 1999) have proposed different saturated sand models on the basis of the concept of the state parameter and great progress on sand modeling has been achieved. Although the concept of the state parameter is attractive to simulate the sand behavior, the limitations on application of the state parameter are also obvious. For example, Bardet (1986) and Li *et al.* (1999) only correlated the state parameter to their dilatancy rules. Although the state parameter is explicitly included in both the dilatancy surface and the bounding surface in the model proposed by Manzari and Dafalias (1997), this model has to resort to some special treatments to prevent purely elastic deformation under constant stress ratio paths and to avoid initial dilation of loose samples under certain loading conditions. To overcome

these limitations, Taiebat and Dafalias (2008) introduce a modified SANISAND model, which enables the prediction of plastic strains during any type of constant stress-ratio loadings. Different techniques are also introduced by several other researchers (e.g., Desai, 1974; Pastor *et al.*, 1985 & 1990; Yang, 2003; Yang and Muraleetharan, 2003) to simulate saturated sand behavior, but these ideas are generally very complicated and the application of these models into practice is not easy.

One of the most important topics related to saturated sands is dilatancy, which can be defined as $D = \dot{\varepsilon}_v^p \Big/ \left|\dot{\varepsilon}_q^p\right|$ (e.g., Roscoe and Burland, 1968) in the triaxial space with $\dot{\varepsilon}_v^p = \left(\dot{\varepsilon}_1^p + 2\dot{\varepsilon}_3^p\right)$ to be the change rate of the plastic volumetric strain and $\dot{\varepsilon}_q^p = 2\left(\dot{\varepsilon}_1^p - \dot{\varepsilon}_3^p\right)/3$ to be the change rate of the plastic deviatoric strain, respectively. $\dot{\varepsilon}_1^p$ and $\dot{\varepsilon}_3^p$ are the plastic principal strain increments. In the earlier works the dilatancy was assumed to be a function of stress ratio $\eta = q/p'$ as $D = D(\eta, C)$ (e.g., Rowe, 1962; Roscoe and Schofield, 1963 ) with $q = \sigma_1' - \sigma_3'$ and $p' = \left(\sigma_1' + 2\sigma_3'\right)/3$. $\sigma_1'$ and $\sigma_3'$ are the effective principal stresses. $C$ can be some other material constant, such as the friction angle (Rowe, 1962) or the critical state constant $M$ (Roscoe and Schofield, 1963). In fact, experimental observations demonstrate dilatancy is not only a function of stress ratio, but also many other internal variables, such as the shear strain (Kabilamany and Ishihara, 1990), plastic volumetric strain (Li, 1997) and critical void ratio (Wan and Guo, 1999). Later, Li *et al.* (1999) and Li and Dafalias (2000) proposed some generalized state-dependent forms for the sand dilatancy. This means the dilatancy should be related not only to the stress ratio and plastic volumetric strain, but also to many other state-

dependent variables, such as void ratio, the state parameter, critical void ratio and even anisotropic parameters. The correct description of dilatancy is critical to capturing the phase transformation behavior of sand before it reaches the ultimate critical state. The phase transformation behavior is also one of the most obvious properties which differentiate sands from clays. By differentiating the restrictions on dilative shear failure from those on the critical state, Li (1997) defined a dilative shear failure mode between the phase transformation state and the critical state. Li's (1997) work captured the evolution of shear stiffness well and explicitly considered the termination of dilative tendency along the limiting deviatoric stress ratio path. On the basis of the basic structure of Wang *et al.* (1990), Li (2002) also developed a double-hardening bounding surface sand model with a state-dependent dilatancy (Li and Dafalias, 2000). A similar idea was introduced by Manzari and Dafalias (1997), who show that the proposed state-dependent dilatancy is equivalent to an interpretation that the phase transformation stress ratio is variable with the state parameter. The physical explanation of dilatancy should be carried out on the microscopic level (see Goddard and Didwania, 1998; Wan and Guo, 2001), but the microscopic interpretation is beyond the scope of current research. Recently, Dafalias and Manzari (2004) investigated sand behavior under cyclic undrained loading conditions and concluded that the inclusion of the fabric change is critical to capture the reduction of shear modulus under cyclic loadings. The introduction of fabric-dilatancy internal variables improves the model performance, such as the prediction of liquefaction, so that the inclusion of fabric-dilatancy variables in sand modeling is well justified.

Another very important topic related to sand is its anisotropic properties, either the structural anisotropy or the stress/strain-induced anisotropy. Microscopic investigations on the sand anisotropy have been carried out over the last two decades (Tobita, 1988 & 1989; Oda and Nakayama, 1988; Yoshimine *et al.*, 1998). Mooney *et al.* (1998) found that the critical state line in the $e - \ln p'$ space is not unique and Yoshimine *et al.* (1998) pointed out that this contradiction to the critical state soil mechanics is due to the anisotropic fabric. As pointed out by Li and Dafalias (2002) and Dafalias *et al.* (2004), the dependence of the critical state line on the fabric anisotropic does not invalidate the framework of the critical state soil mechanics, but rather expands the critical state concept for sands. On the basis of micromechanical considerations, Li and Dafalias (2002) defined an anisotropic state variable, which is incorporated into both the critical state equation and plastic modulus, to characterize the influence of the sand fabric on the stress-strain-strength responses. Later, motivated by the observation that rotations of principal stresses yield non-coaxial plastic deformations, Li and Dafalias (2004) generalized the anisotropic parameter to involve a properly defined loading direction relevant to the stress reversal process. This model is able to describe sand behavior under either proportional or non-proportional loading conditions. Ling *et al.* (2002) have proposed an anisotropic elastoplastic bounding surface model, which accounts for the isotropic hardening, kinematic hardening and distortional hardening as well. Similarly, within the framework of anisotropic bounding surface plasticity, Datcheva and Schanz (2003) developed an unsaturated soil model accounting for the isotropic and kinematic hardening effects. The above mentioned work provides insight understanding of the sand/silt behavior.

Great efforts have been taken to model sand behavior for the last four decades and major progress has been achieved on saturated sand modeling. Although unsaturated clay modeling has attracted attention from many researchers, for example Alonso *et al.* (1990), Wheeler and Sivakumar (1995) and Li (2007b), the investigation of unsaturated silts and/or sands is relatively new. This lack of progress in unsaturated silt/sand modeling is mainly due to the lack of systematical laboratory investigation of the engineering properties of unsaturated silts/sands, especially the coupling effects between mechanical and hydraulic mechanisms. The already complicated (saturated) sand behavior discussed above is another factor contributing to the slow progress in extending saturated sand/silt models to unsaturated ones.

Recently, in an investigate of the capillary effects on unsaturated soil behavior, Gallipoli *et al.* (2008) revisited the test data on Jossigny silt and Barcelona clayey silt and confirmed that a unique capillary bonding function linking the ratio between unsaturated and saturated void ratios at the same mean average skeleton stress exists. Further, their analysis also confirmed that the capillary bonding function applies to both the normal consolidation state and the critical stress state. The main contribution from Gallipoli *et al.* (2008) is that the volumetric changes of soil samples can be accounted for during either wetting or drying. Although Gallipoli *et al.* (2008) addressed the effect of hydraulic mechanism on soil deformation, they did not pay attention to the effect of soil deformation on the hydraulic behavior. Khalili *et al.* (2008) also proposed a comprehensive constitutive model for unsaturated soils, fully considering the coupling

effects between hydraulic and mechanical hysteresis. Because Khalili *et al.*'s (2008) model is based on the bounding surface clay plasticity, their model is essentially a clay model and it is not appropriate for simulating sand or silt behavior. Also, Sun *et al.* (2008) and Yang *et al.* (2008) introduced unsaturated soil models to simulate the hydro-mechanical behavior under undrained conditions. Both models belong to the Barcelona Basic Model framework (Alonso *et al.*, 1990), so some of the drawbacks of the Barcelona Basic Model still remain. To capture the unsaturated soil behavior under cyclic loadings, Yang *et al.* (2008) integrated their model into the bounding surface plasticity theory framework (Dafalias and Herrmann, 1982), so the model proposed by Yang *et al.* (2008) is also essentially for clay, not silt or sand.

In this chapter, the main objective is to propose a comprehensive constitutive model for unsaturated sands/silts. This model should be kept as simple as possible yet still have the ability to simulate most of the special features of unsaturated silts/sands, such as wetting-induced collapse and shearing-induced dilation, and especially the coupling effects between mechanical and hydraulic behavior under monotonic or cyclic loadings. To achieve a smooth transition between saturated and unsaturated states, this unsaturated soil model should become a saturated soil model when suction becomes lower than the air entry value, the matric suction value that must be exceeded before air enters the largest soil pores. The air entry value of sand is generally very low, because the soil particles are large compared to clays and silts. The typical air entry value of sand is a couple of *kPa*. Formulation of this unsaturated sand/silt model is presented in the next section.

## 5.2 3-D MODEL FORMULATION

The unsaturated sand/silt model is developed on the basis of available saturated sand/silt models with necessary modifications. The coupling effect between mechanical and hydraulic behavior in the 3-D model is handled similarly to that of the isotropic model as described in Chapter 4. In this chapter, the superscripts *e* and *p* stand for elastic and plastic variables, respectively. Variables in bold font are tensors and overdotted variables stand for the changes of these variables with respect to time. The operator "**:**" between two tensors denotes the trace of their product. The operator "$\otimes$" between two tensors represents the tensor product. Following the discussion of the selection of stress-strain variables in Chapter 2, the stress variables are selected as follows:

The intergranular stress: $\boldsymbol{\sigma}' = (\boldsymbol{\sigma} - p_a \mathbf{I}) + n_w s_c \mathbf{I}$; $\sigma'_{ij} = (\sigma_{ij} - p_a \delta_{ij}) + n_w s_c \delta_{ij}$ (5.1)

The matric suction: $s_c = p_a - p_w$ (5.2)

where: $p_a$ and $p_w$ are the pore air pressure and pore water pressure, respectively; $\boldsymbol{\sigma}$ is the total stress tensor; $\mathbf{I}$ is the second-order unit tensor and $\delta_{ij}$ is the Kronecker delta. The conjugated strain variables are the regular strain tensor $\boldsymbol{\varepsilon}$ (or $\varepsilon_{ij}$) of the soil skeleton and the volume fraction of water $n_w$, respectively. As discussed in detail in Chapter 2, alternative stress-strain variables may be used. The basis for the selection of stress-strain

variables is that the selected variables should be consistent with the thermodynamic theory and be easily measured.

### 5.2.1 ELASTIC RESPONSES

The elastic responses of soil skeleton and water content are given as follows:

$$\dot{\varepsilon}_v^e = \frac{\dot{p}'}{K};\ \dot{\boldsymbol{\varepsilon}}_q^e = \frac{\dot{\mathbf{s}}}{2G} \tag{5.3}$$

$$\dot{n}_w^e = \frac{\dot{s}_c}{\Gamma^e} \tag{5.4}$$

where: $p' = \left(\sigma'_{11} + \sigma'_{22} + \sigma'_{33}\right)/3$ and $\mathbf{s}$ are the hydrostatic intergranular stress and the deviatoric stress tensor, respectively; $\varepsilon_v$ and $\boldsymbol{\varepsilon}_q$ are the volumetric strain and deviatoric strain of soil skeleton; $K$, $G$ and $\Gamma^e$ are the bulk modulus, shear modulus and capillary elastic modulus, respectively. As mentioned in Chapter 3, the capillary elastic modulus $\Gamma^e$ can be assumed to be a constant or a function of suction if experimental data warrant such a treatment. For simplicity, $\Gamma^e$ is assumed to be a constant in the current study. Although the effect of suction on the elastic deformation of soil skeleton is not explicitly provided, the inclusion of suction in the intergranular stress accounts for the suction effects on soil deformation. Since the purely recoverable component of water content is not significant, as discussed in Chapter 3, the effect of soil deformation on the recoverable water content change is not accounted for here and the recoverable

component of water content change is only related to the change of suction. The related definitions of stress-strain variables and moduli are given as below:

$$p' = \left(\sigma'_{xx} + \sigma'_{yy} + \sigma'_{zz}\right)/3 = \left(\sigma_{xx} + \sigma_{yy} + \sigma_{zz}\right)/3 - p_a + n_w s_c \tag{5.5}$$

$$\mathbf{s} = dev\left(\sigma'_{ij}\right) = dev\left(\sigma_{ij}\right) \tag{5.6}$$

$$\varepsilon_v = tr\left(\varepsilon_{ij}\right) = \varepsilon_{xx} + \varepsilon_{yy} + \varepsilon_{zz},\ \boldsymbol{\varepsilon}_q = dev\left(\varepsilon_{ij}\right) \tag{5.7}$$

$$K = K_0\left(\frac{p'}{p_{ref}}\right)^{b_1};\ G = G_0\left(\frac{p'}{p_{ref}}\right)^{d_1} \tag{5.8}$$

where: $\sigma_{ij}$ and $\sigma'_{ij}$ are the total stress and intergranular stress tensors, respectively. $K_0$, $G_0$, $b_1$ and $d_1$ are four model parameters. $p_{ref}$ is a reference pressure, which is usually assumed to be the atmospheric pressure for convenience. Any other value rather than the atmospheric pressure can also be assigned to $p_{ref}$ as long as it provides reasonable simulations. Although the bulk and shear moduli may be proposed to be functions of the hydrostatic intergranular stress $p'$ and the current void ratio $e$, see Richart *et al.* (1970), Pestana and Whittle (1995) and Taiebat and Dafalias (2008), a simple form of the bulk modulus and shear modulus are adopted in Eq. (5.8) providing a hypoelastic description of soil skeleton response. Such a definition in Eq. (5.8) does not guarantee the existence of a potential and both moduli are simply defined to best match the test results.

### 5.2.2 YIELD, CRITICAL, BOUNDING AND DILATANCY SURFACES

Following the work by Manzari and Dafalias (1997) and Taiebat and Dafalias (2008), the yield surface is defined in such a way that both isotropic and kinematic hardening effects are fully considered. For the convenience of visualization, the surfaces will be schematically described in the triaxial stress space first, and then all the surfaces will be generalized from the triaxial stress space to the general stress space. The yield surface in the triaxial stress space is defined as follows:

$$f(\boldsymbol{\sigma}', s_c; \alpha, m) = (q - p'\alpha)^2 - m^2 p'^2 \left[1 - (p'/p'_0)^\beta\right] = 0 \tag{5.9.1}$$

$$\eta = \alpha \pm m\sqrt{1 - (p'/p'_0)^\beta} \tag{5.9.2}$$

where: $p' = (\sigma'_1 + 2\sigma'_3)/3$, $q = \sigma'_1 - \sigma'_3$. $\alpha$, which is the kinematic hardening parameter, defines the center of the yield surface in the triaxial stress space. In the generalized stress space, $\alpha$ will be extended to be a tensor localizing the center of the yield surface and it captures the kinematic hardening behavior. $m$ is the isotropic hardening parameter, which is generally a small constant. $p'_0$ represents a high mean effective stress, which should not be lower than the highest mean effective stress at which the sand sample bears during a loading process. $\beta$ is a model parameter, which can be set to 20 as a default value as suggested by Taiebat and Dafalias (2008) or calibrated from experimental results. A desirable property of this yield surface is its closed cap-like shape at the tip of the yield surface, where the stress level becomes close to $p'_0$. Without this closed cap at the tip of the yield surface, it is possible that no plastic deformation will occur if $p'$ and $q$ increase at a constant stress ratio $\eta$. Eq. (5.9.2) defines the stress ratio on the yield

surface as $\eta = q/p' = \alpha \pm m\sqrt{1-(p'/p'_0)^{\beta}}$ . When $p'$ is small or $p'_0$ is large, $(p'/p'_0)^{\beta}$ can be assumed very close to be zero and $\eta \doteq \alpha \pm m$ , which becomes the yield surface proposed by Manzari and Dafalias (1997), a special form of Eq. (5.9.1). Under a constant stress ratio, i.e., constant $\eta = q/p'$ loading conditions, the loading path can reach the yield surface and plastic deformation will occur. This special property of the yield surface overcomes the limitation of the yield surface discussed in Manzari and Dafalias (1997).

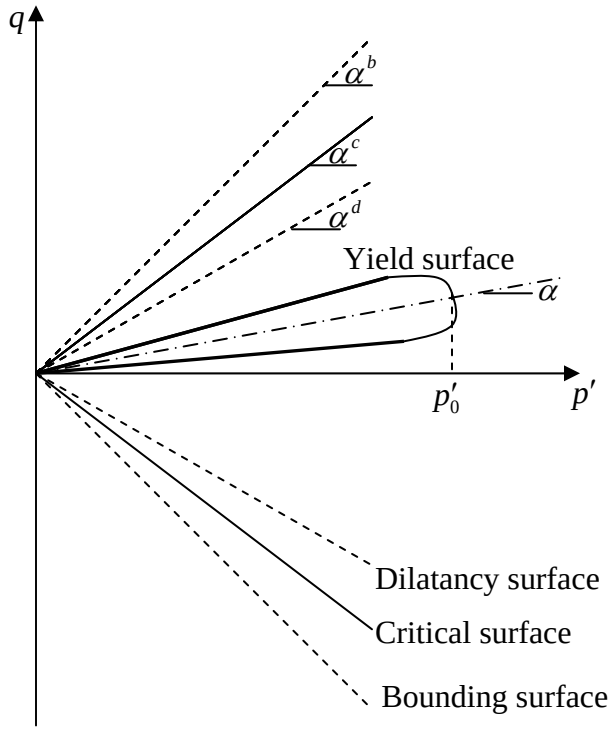


**Fig. 5.1** Model surfaces in triaxial stress space (after Taiebat and Dafalias, 2008)

The yield surface in the triaxial stress space is schematically illustrated in Fig. 5.1. Fig. 5.1 also shows the other three surfaces, i.e., the dilatancy surface, the critical surface and the bounding surface. Following Muir Wood *et al.* (1994), Manzari and Dafalias (1997) proposed simple definitions for all the three surfaces in the triaxial stress space.

Similar to the definition of the yield surface in stress ratio, the stress ratios of the dilatancy, critical and bounding surfaces can be defined in a modified form as follows:

$$M_c^b = \alpha_c^b + m\sqrt{1-\left(p'/p_0'\right)^\beta} = M_c^c + k_c^b < -\psi > \tag{5.10.1}$$

$$M_e^b = \alpha_e^b + m\sqrt{1-\left(p'/p_0'\right)^\beta} = M_e^c + k_e^b < -\psi > \tag{5.10.2}$$

$$M_c^c = \alpha_c^c + m\sqrt{1-\left(p'/p_0'\right)^\beta} \tag{5.10.3}$$

$$M_e^c = \alpha_e^c + m\sqrt{1-\left(p'/p_0'\right)^\beta} \tag{5.10.4}$$

$$M_c^d = \alpha_c^d + m\sqrt{1-\left(p'/p_0'\right)^\beta} = M_c^c + k_c^d \psi \tag{5.10.5}$$

$$M_e^d = \alpha_e^d + m\sqrt{1-\left(p'/p_0'\right)^\beta} = M_e^c + k_e^d \psi \tag{5.10.6}$$

where: superscripts *b*, *c* and *d* represent variables for the bounding surface, the critical surface and the dilatancy surface, respectively. Subscripts *c* and *e* stand for variables under compression and extension, respectively. $M$ 's are stress ratios on the three surfaces and $\alpha$ 's are slopes as given in Fig. 5.1. < > is the Macauley brackets. The slopes of the four surfaces, including the yield surface, on the extension side are actually negative. Eqs. (5.10) just provide absolute values of the stress ratios of the surfaces on the extension side. $k_c^b$, $k_e^b$, $k_c^d$ and $k_e^d$ are positive model parameters. $\psi = e - e_c$ is the state parameter and it is defined to be the difference between the current void ratio $e$ and the critical void ratio $e_c$ at the same stress state. When $\psi = 0$, $\alpha_c^b = \alpha_c^d = \alpha_c^c$ and $\alpha_e^b = \alpha_e^d = \alpha_e^c$. It means all the three surfaces merge when the critical state is reached.

When $\psi < 0$, a state denser than the critical state, $\alpha_c^b > \alpha_c^c > \alpha_c^d$ and $\alpha_e^b > \alpha_e^c > \alpha_e^d$. It means that the stress ratio can pass the dilatancy surface, showing phase transformation behavior before the critical state is reached. When $\psi > 0$, a state looser than the critical state, $\alpha_c^b = \alpha_c^c < \alpha_c^d$ and $\alpha_e^b = \alpha_e^c < \alpha_e^d$. Under this condition, sands/silts show no dilatancy. The multisurfaces capture the sand behavior well, accounting for the density and stress state in a unified manner. Taiebat and Dafalias (2008) defined an exponential, instead of linear relationship of the surfaces with the state parameter.

To describe the unsaturated soil behavior in the general stress space, the yield surface should be generalized from the triaxial stress space to the multiaxial stress space. The hydrostatic intergranular stress $p'$ in the triaxial stress space is now written as $I$ and the new yield surface in the general stress space is given as follows:

$$f(\boldsymbol{\sigma}', s_c; \boldsymbol{\alpha}, m) = \sqrt{(\mathbf{s} - I\boldsymbol{\alpha}) : (\mathbf{s} - I\boldsymbol{\alpha})} - \sqrt{2/3} m I \sqrt{1 - (I / I_0)^{\beta}} = 0 \qquad (5.11)$$

where: $\boldsymbol{\alpha}$ stands for the center of the yield surface. *m* is the isotropic hardening parameter, which stands for the size of the yield surface. $I_0$ plays a similar role as $p_0'$ in the yield surface defined in the triaxial stress space, see Eq. (5.9). The coefficient $\sqrt{2/3}$ has been introduced for convenience of interpretation in the standard triaxial stress space. As can be seen, the yield surface in the general stress space is a modified $J_2$-plasticity yield surface. Fig. 5.2 illustrates the yield surface and the other three surfaces, i.e., the bounding surface, the critical surface and the dilatancy surface in the general stress space.

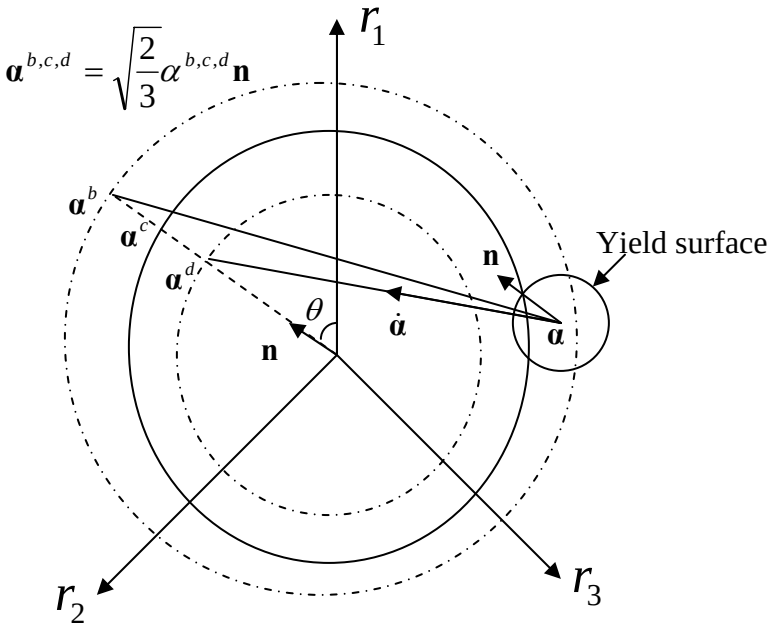


**Fig. 5.2** Model surfaces in multiaxial stress space (after Taiebat and Dafalias, 2008)

The tensor $\boldsymbol{\alpha}$ in the multiaxial stress space is equivalent to $\alpha = \alpha_1 - \alpha_2$ in the triaxial stress space, where $\alpha_1$ and $\alpha_2 = \alpha_3$ are the principal values of $\boldsymbol{\alpha}$. With the definition of a modified Lode angle $\theta$ given below, all the variables defined in the triaxial space can be generalized to the general stress space.

$$\mathbf{r} = \mathbf{s} - I\boldsymbol{\alpha}\,,\ \bar{\mathbf{r}} = \frac{\mathbf{r}}{I} = \left(\frac{\mathbf{s}}{I} - \boldsymbol{\alpha}\right),\ \mathbf{n} = \frac{\mathbf{r}}{\sqrt{\mathbf{r} : \mathbf{r}}} \tag{5.12}$$

$$\bar{J} = \left[\frac{1}{2}tr\left(\bar{\mathbf{r}}^2\right)\right]^{1/2},\ \bar{S} = \left[\frac{1}{3}tr\left(\bar{\mathbf{r}}^3\right)\right]^{1/3},\ \cos 3\theta = \frac{3\sqrt{3}}{2}\left(\frac{\bar{S}}{\bar{J}}\right)^3 \tag{5.13}$$

$$g(\theta, c) = \frac{2c}{(1+c) - (1-c)\cos 3\theta},\ c = \frac{M_e^c}{M_c^c},\ c_b = \frac{k_e^b}{k_c^b},\ c_d = \frac{k_e^d}{k_c^d} \tag{5.14}$$

where: $\bar{J}$ and $\bar{S}$ are the second and third stress invariants. $\theta$ is the Lode angle, ranging from 0º to 60º. Note: $g\left(0^{\circ},c\right)=1$ and $g\left(60^{\circ},c\right)=c$. $c$ is the conversion factor between a quantity in extension and compression. $\mathbf{n}$ is the unit deviatoric stress ratio tensor.

The stress ratios in the triaxial stress space can now be generalized in the general stress space as follows:

$$\boldsymbol{\alpha}_{\theta}^{b}=\sqrt{2/3}\alpha_{\theta}^{b}\mathbf{n},\ \boldsymbol{\alpha}_{\theta}^{d}=\sqrt{2/3}\alpha_{\theta}^{d}\mathbf{n},\ \boldsymbol{\alpha}_{\theta}^{c}=\sqrt{2/3}\alpha_{\theta}^{c}\mathbf{n} \tag{5.15}$$

$$\alpha_{\theta}^{b}=g\left(\theta,c\right)M_{c}^{c}+g\left(\theta,c_{b}\right)k_{c}^{b}<-\psi>-m\sqrt{1-\left(I/I_{0}\right)^{\beta}} \tag{5.16}$$

$$\alpha_{\theta}^{d}=g\left(\theta,c\right)M_{c}^{c}+g\left(\theta,c_{d}\right)k_{c}^{d}\psi-m\sqrt{1-\left(I/I_{0}\right)^{\beta}} \tag{5.17}$$

$$\alpha_{\theta}^{c}=g\left(\theta,c\right)M_{c}^{c}-m\sqrt{1-\left(I/I_{0}\right)^{\beta}} \tag{5.18}$$

When the state parameter $\psi=0$, the three surfaces, i.e., the bounding surface, dilatancy surface and critical surface become identical.

### 5.2.3 HARDENING LAWS

The kinematic hardening parameter $\boldsymbol{\alpha}$ is assumed to be a function of current stress state and plastic deviatoric strain of the soil skeleton. The suction is assumed to affect the kinematic hardening only through its contribution to the intergranular stress tensor. The isotropic hardening parameter $m$ is not only a function of stress state, but also plastic

volumetric strain and irrecoverable water content. The assumption on the isotropic hardening is based on the fact that the change of effective stress and/or suction will change the stiffness of the soil skeleton. This can change the size of the yield surface.

$$\boldsymbol{\alpha} = \boldsymbol{\alpha}\left(\boldsymbol{\sigma}', s_c; \boldsymbol{\varepsilon}_q^p\right),\ m = m\left(\boldsymbol{\sigma}', s_c; \varepsilon_v^p, n_w^p\right) \tag{5.19}$$

$$\dot{\boldsymbol{\alpha}} = \sqrt{\frac{3}{2}} h \left[\frac{2}{3}\alpha_\theta^b \dot{\boldsymbol{\varepsilon}}_q^p - \dot{e}_q^p \boldsymbol{\alpha}\right] =< \Lambda > h\left(\boldsymbol{\alpha}_\theta^b - \boldsymbol{\alpha}\right) =< \Lambda > h\mathbf{b} \tag{5.20}$$

$$\dot{m} = \frac{\partial m}{\partial \varepsilon_v^p}\dot{\varepsilon}_v^p + \frac{\partial m}{\partial n_w^p}\dot{n}_w^p = c_m\left(1+e_0\right)\dot{\varepsilon}_v^p + c_v\left(\frac{s_c n_w}{p_{ref}}\right)^{\varpi}\dot{n}_w^p \tag{5.21}$$

$$h = h_0 \frac{|\mathbf{b}:\mathbf{n}|}{b_{ref} - |\mathbf{b}:\mathbf{n}|},\ \dot{e}_q^p = \sqrt{2/3\dot{\boldsymbol{\varepsilon}}_q^p : \dot{\boldsymbol{\varepsilon}}_q^p},\ b_{ref} = 2\sqrt{2/3}\alpha_c^b \tag{5.22}$$

where: $\Lambda$ is the loading index, which will be defined in the next section. $e_0$ is the initial void ratio. $c_v$, $c_m$ and $\varpi$ are model parameters. The rate of change of the kinematic hardening parameter $\dot{\boldsymbol{\alpha}}$ is dependent on $\left(\boldsymbol{\alpha}_\theta^b - \boldsymbol{\alpha}\right)$, which is the distance between $\boldsymbol{\alpha}$ and its image on the bounding surface $\boldsymbol{\alpha}_\theta^b$. This is exactly what the bounding surface plasticity concept (Dafalias and Popov, 1975; Krieg, 1975) states. The added feature of $h$ depending on $|\mathbf{b}:\mathbf{n}|$ was proposed by Dafalias (1986) and its performance was verified for sand behavior by Manzari and Dafalias (1997). It is assumed that the elastic soil deformation and the recoverable water content change will not affect the isotropic hardening parameter. Only the plastic volumetric strain of soil skeleton and the irrecoverable water content change have influence on the isotropic hardening parameter. Observations on the SWCCs show that $s_c n_w$ is an increasing function of suction. When

suction increases, $n_w^p$ also increases. The suction-induced hardening effects are accounted for in this way. The hardening laws defined in Eqs. (5.20) and (5.21) are one of the special features of the proposed model. The inclusion of suction in the intergranular stress tensor and the effects of suction and irrecoverable water content change on the size of the yield surface differentiate the current model from most of the available unsaturated soil models.

To investigate the coupling effects between the mechanical and hydraulic behavior of unsaturated sands or silts, the evolution of the bounding suctions on the drying bound and wetting bound ($s_{c0d}$ and $s_{c0w}$) are given below.

Wetting: $\dot{s}_{c0w} = \Gamma_{vw}^p \dot{\varepsilon}_v^p + \Gamma_{0w}^p \dot{n}_w^p,\ \Gamma_{vw}^p = s_{c0w}\zeta v$ (5.23.1)

Drying: $\dot{s}_{c0d} = \Gamma_{vd}^p \dot{\varepsilon}_v^p + \Gamma_{0d}^p \dot{n}_w^p,\ \Gamma_{vd}^p = s_{c0d}\zeta v$ (5.23.2)

The equations of the two bounding curves are given by:

Wetting: $n_w = \dfrac{n_{ws} + n_{wr}\left(s_{c0w}/b_2\right)^{d_2}}{1+\left(s_{c0w}/b_2\right)^{d_2}}$ (5.24.1)

Drying: $n_w = \dfrac{n_{ws} + n_{wr}\left(s_{c0d}/b_3\right)^{d_3}}{1+\left(s_{c0d}/b_3\right)^{d_3}}$ (5.24.2)

where: $b_2$, $d_2$, $b_3$, $d_3$ and $\zeta$ are material parameters and $v$ is the specific volume, which is defined in terms of the porosity $n$ as: $v = \frac{1}{1-n}$. $n_{ws}$ and $n_{wr}$ are the saturated and residual volumetric water contents, respectively. $s_{c0w}$ and $s_{c0d}$ are suctions on the wetting and drying bounds, respectively. $\Gamma_{0w}^{p}$ and $\Gamma_{0d}^{p}$ are the capillary plastic moduli on the wetting and drying bounds, respectively. The capillary plastic moduli, $\Gamma_{0w}^{p}$ and $\Gamma_{0d}^{p}$, are calculated in the next section.

### 5.2.4 FLOW RULES AND PLASTIC MODULI

With the assumptions in Eq. (5.19), the consistency condition $\dot{f} = 0$ leads to:

$$\begin{aligned}
\dot{f} &= \frac{\partial f}{\partial \mathbf{s}} : \dot{\mathbf{s}} + \frac{\partial f}{\partial I}\dot{I} + \frac{\partial f}{\partial \boldsymbol{\alpha}} : \dot{\boldsymbol{\alpha}} + \frac{\partial f}{\partial m}\dot{m} \\
&= \frac{\partial f}{\partial \mathbf{s}} : \dot{\mathbf{s}} + \frac{\partial f}{\partial I}\dot{I} + \left[ \frac{\partial f}{\partial \boldsymbol{\alpha}} : \left( \frac{\partial \boldsymbol{\alpha}}{\partial \boldsymbol{\varepsilon}_q^p} \otimes \dot{\boldsymbol{\varepsilon}}_q^p \right) + \frac{\partial f}{\partial m}\frac{\partial m}{\partial \varepsilon_v^p}\dot{\varepsilon}_v^p \right] + \frac{\partial f}{\partial m}\frac{\partial m}{\partial n_w^p}\dot{n}_w^p \\
&= \left( \frac{\partial f}{\partial \mathbf{s}} : \dot{\mathbf{s}} + \frac{\partial f}{\partial I}\dot{I} \right) - K_s^p < \Lambda > - K_m^p \dot{n}_w^p \\
&= 0
\end{aligned} \tag{5.25}$$

where: $K_s^p$ and $K_m^p$ are two plastic moduli, representing the two mechanisms related to the yield surface. $K_s^p$ is equivalent to the traditional plastic modulus in the elastoplasticity theory, while $K_m^p$ is a new plastic modulus accounting for the effects of the hydraulic mechanism on the yield surface.

The loading index $\Lambda$ in Eq. (5.25) is given below:

$$\begin{aligned}\Lambda &= \frac{1}{K_s^p}\left(\frac{\partial f}{\partial \mathbf{s}}:\dot{\mathbf{s}} + \frac{\partial f}{\partial I}\dot{I}\right) - \frac{K_m^p}{K_s^p}\dot{n}_w^p \\ &= \frac{1}{K_s^p}\left\{\frac{(\mathbf{s}-I\boldsymbol{\alpha}):\dot{\mathbf{s}}}{\sqrt{(\mathbf{s}-I\boldsymbol{\alpha}):(\mathbf{s}-I\boldsymbol{\alpha})}} + \frac{\partial f}{\partial I}\dot{I} - \frac{K_m^p}{\Gamma^p}\dot{s}_c\right\}\end{aligned} \tag{5.26}$$

$$\frac{\partial f}{\partial I} = -\left[\frac{(\mathbf{s}-I\boldsymbol{\alpha}):\boldsymbol{\alpha}}{\sqrt{(\mathbf{s}-I\boldsymbol{\alpha}):(\mathbf{s}-I\boldsymbol{\alpha})}} + \sqrt{2/3}m\left(\frac{2-(2+\beta)(I/I_0)^\beta}{2\sqrt{1-(I/I_0)^\beta}}\right)\right] \tag{5.27}$$

where: $\Gamma^p$ is the capillary plastic modulus, which was defined in Chapter 3. The above loading index clearly shows the coupling effects coming from both the intergranular stress and matric suction. With the definition of the loading index, the strain tensor of the soil skeleton can be decomposed into hydrostatic and deviatoric components as follows:

$$\dot{\boldsymbol{\varepsilon}}^p = <\Lambda>\mathbf{R},\ \mathbf{R} = \mathbf{n} + \frac{1}{3}D\mathbf{I},\ \dot{\boldsymbol{\varepsilon}}_q^p = <\Lambda>\mathbf{n},\ \dot{\varepsilon}_v^p = <\Lambda>D \tag{5.28}$$

$$\dot{n}_w^p = \dot{s}_c/\Gamma^p \text{ with } \Gamma^p = \Gamma_0^p\left(1 + H\delta/<\delta_{in} - g\delta>\right) \tag{5.29}$$

where: $\mathbf{R}$ is the direction of $\dot{\boldsymbol{\varepsilon}}^p$, consisting of a deviatoric component $\mathbf{n}$ and a volumetric component $\frac{1}{3}D\mathbf{I}$. $\Gamma_0^p$ can be either $\Gamma_{0w}^p$ or $\Gamma_{0d}^p$, depending on the suction path to be wetting or drying.

$$K_s^p = -\frac{\partial f}{\partial \boldsymbol{\alpha}} : \left( \frac{\partial \boldsymbol{\alpha}}{\partial \boldsymbol{\varepsilon}_q^p} \otimes \mathbf{n} \right) - \frac{\partial f}{\partial m} \frac{\partial m}{\partial \varepsilon_v^p} D$$

$$= \frac{I(\mathbf{s} - I\boldsymbol{\alpha})}{\sqrt{(\mathbf{s} - I\boldsymbol{\alpha}) : (\mathbf{s} - I\boldsymbol{\alpha})}} : \left( \frac{\partial \boldsymbol{\alpha}}{\partial \boldsymbol{\varepsilon}_q^p} \otimes \mathbf{n} \right) + \sqrt{\frac{2}{3}} I \sqrt{1 - (I / I_0)^\beta} c_m (1 + e_0) D \tag{5.30}$$

$$= \frac{hI(\mathbf{s} - I\boldsymbol{\alpha})}{\sqrt{(\mathbf{s} - I\boldsymbol{\alpha}) : (\mathbf{s} - I\boldsymbol{\alpha})}} : \left( \sqrt{\frac{2}{3}} \alpha_\theta^b \mathbf{n} - \boldsymbol{\alpha} \right) + \sqrt{\frac{2}{3}} I \sqrt{1 - (I / I_0)^\beta} c_m (1 + e_0) D$$

$$K_m^p = -\frac{\partial f}{\partial m} \frac{\partial m}{\partial n_w^p} = \sqrt{\frac{2}{3}} I \sqrt{1 - (I / I_0)^\beta} c_v \left( \frac{s_c n_w}{p_{ref}} \right)^{\varpi} \tag{5.31}$$

where: $\Gamma_{0w}^p$ and $\Gamma_{0d}^p$ are the capillary plastic moduli on the primary wetting bound and the secondary drying bound, respectively. Similar to the isotropic model presented in Chapter 4, the two capillary plastic moduli are calculated as follows:

$$\text{Wetting: } \Gamma_{0w}^p = \frac{\partial s_c}{\partial n_w} = -\frac{1}{d_2} \frac{(n_{ws} - n_{wr}) s_c}{(n_{ws} - n_w)(n_w - n_{wr})} \Big|_{s_c = s_{c0w}} \tag{5.32}$$

$$\text{Drying: } \Gamma_{0d}^p = \frac{\partial s_c}{\partial n_w} = -\frac{1}{d_3} \frac{(n_{ws} - n_{wr}) s_c}{(n_{ws} - n_w)(n_w - n_{wr})} \Big|_{s_c = s_{c0d}} \tag{5.33}$$

In the above-calculated capillary plastic moduli, both $n_{ws}$ and $n_{wr}$ are directly related to the soil configuration. As soil deformation develops, $n_{ws}$ and $n_{wr}$ will definitely change. $n_{ws}$ always equals the ratio between the volume of pore voids and the volume of soil sample. $n_{wr}$, which represents the residual volume fraction of water, can not be calculated similar to $n_{ws}$. To find out the evolution of $n_{wr}$, some microscopic variables representing the soil configuration have to be introduced. This procedure will

tremendously increase the complication of the proposed model. For simplicity, it is assumed $n_{wr}$ is a constant for a given soil.

### 5.2.5 DILATANCY COEFFICIENT AND CRITICAL STATE LINE

As suggested by Nova and Muir Wood (1979), the dilatancy coefficient is assumed to be proportional to $\left(M_c^d - \eta\right)$ or $\left(M_e^d - \eta\right)$, which is the difference between the stress ratio on the dilatancy surface and the current stress ratio. In the triaxial stress space, the dilatancy coefficient is defined as: $D = \sqrt{2/3}A\left(M_c^d - \eta\right)$ for compression or $D = \sqrt{2/3}A\left(M_e^d - \eta\right)$ for extension. In the general stress space, the dilatancy coefficient is directly generalized from the triaxial stress space as:

$$D = B\left(\boldsymbol{\alpha}_\theta^d - \boldsymbol{\alpha}\right) : \mathbf{n} = B\mathbf{d} : \mathbf{n} \tag{5.34}$$

$$B = B_0\left(1 + < \mathbf{F} : \mathbf{n} >\right) \tag{5.35}$$

$$\dot{\mathbf{F}} = - < \Lambda > c_f \, < -D > \left(F_{\max}\mathbf{n} + \mathbf{F}\right) \tag{5.36}$$

where: $B_0$ and $c_f$ are model parameters. $F_{\max}$ is another model parameter, representing the maximum value the fabric tensor $\|\mathbf{F}\|$ can attain. Similar definitions of the dilatancy coefficient are adopted by Manzari and Dafalias (1997) and Taiebat and Dafalias (2008). As discussed by Dafalias and Manzari (2004), the consideration of fabric change effects is very important to reach low effective stress of sand under cyclic loading under undrained condition. This scenario is related to many of the behavioral characteristics of

sand, such as liquefaction and large permanent deformation. The fabric tensor in Eq. (5.36) is used to facilitate the modeling of sand behavior during loading-unloading cycles, see Dafalias and Manzari (1999) and Manzari and Prachthananukit (2001).

To account for the inherent fabric anisotropy on the mechanical response of Toyoura sand, Dafalias *et al.* (2004) introduced the dependence of critical state line on the fabric anisotropy. Because the correlation between the fabric anisotropy and the critical state line is difficult to calibrate, a simple and useful critical state line (Li, 1997) is adopted:

$$e_c = e_{cr} - \lambda\left(\frac{I}{p_{ref}}\right)^{\xi} \tag{5.37}$$

$$\psi = e - e_c \tag{5.38}$$

where: $\lambda$ and $\xi$ are two model parameters. $e_c$ is the void ratio at critical state. Although many other alternatives to define the critical state line have been proposed (e.g. Scofield and Wroth, 1968), Eq. (5.37) has the advantage of capturing the critical state for sand or silt under high effective stress utilizing model parameters that are readily calibrated. The state parameter, $\psi$, is defined to be the difference between current void ratio, $e$, and the critical void ratio, $e_c$, at the same mean effective stress.

## 5.3 NUMERICAL INTEGRATION OF THE MODEL

To put the proposed unsaturated silt/sand model into practice and use the model to simulate silt/sand behavior under complex loading conditions, it is necessary and critical to integrate the rate equations presented in the last section and determine the evolution of the stiffness matrix. Different integration schemes (e.g., Simo and Taylor, 1985; Ortiz and Popov, 1985; Simo and Ortiz, 1985), such as the explicit integration method and the implicit integration method are available. Further, the explicit integration method can be divided into the forward Euler method and the Vemeer method. The implicit integration method includes the backward Euler method, the generalized mid-point method and the generalized trapezoidal method. In selecting between different integration methods, primary concern includes simplicity, efficiency, stability and accuracy. As to the $J_2$-plasticity models, extensive investigation on the implicit integration method was carried out by many researchers (e.g., Manzari and Prachathananukit, 2001; Yang *et al.*, 2008) and it is concluded that the closest point projection method (CPPM) is accurate and stable in all simulations including those conducted by using relatively large strain increments without the need for global sub-increments. The CPPM is a generalization of the backward Euler return rule for an arbitrary convex yield surface. The application of the CPPM to integrate different soil models is abundant in the literature (Alawaji *et al.*, 1991; Macari *et al.*, 1997 & 2003). In the current research, the CPPM is adopted to carry out the model integration process.

Before the consistent tangent stiffness matrix was introduced by Simo and Taylor (1985) and Braudel *et al.* (1986), the continuum tangent stiffness matrix was prevalently used. The superiority of the consistent tangent stiffness matrix to the continuum tangent

stiffness matrix was proved by many applications and comparisons (Borja, 1990 & 1991; Jeremic and Sture, 1997). The consistent tangent stiffness matrix is consistent with the integration process of the model equations and beneficially the quadratic rate of the asymptotic convergence of the consistent tangent stiffness matrix can save tremendous computational resources for large problems. However, the consistent tangent stiffness matrix is more complex than the continuum tangent stiffness matrix in the sense that there is no analytical solution for many models and numerical methods have to be used to develop the consistent tangent stiffness matrix. Given the highly nonlinear property of the proposed model, it is impossible to find a closed-form solution for the consistent tangent stiffness matrix in the current research, thus the consistent tangent stiffness matrix will be developed numerically.

The formulation of the unsaturated silt/sand model was presented in detail in the last section. The main purpose of this section is to numerically implement the model to simulate the silt/sand behavior under complex loading conditions. At the current step *n*, it is assumed that all the model quantities and the strain increments, including the change of the volume fraction of water are given. The integration process is used to solve all the quantities at step *n*+1 based on the model formulation and the strain increments. The superscript *m* stands for the local iteration number. It is important to realize that it is not necessary to integrate all the model equations under all possible loading conditions. The selection on the equations to carry out the integration process depends on the loading conditions. For example, if the current skeleton stress state is on the yield surface under constant suction, then the integration of suction related equations, i.e., $\overline{R}_5$, $\overline{R}_6$, $\overline{R}_{10}$ and

$\overline{R}_{11}$ (see below), do not have to be carried out during further loading. It is also possible that only the suction related equations have to be integrated, as long as the stress state is inside the yield surface and suction or water content keeps changing. The coupling effects between the mechanical and hydraulic behavior will be accounted for during the stress-strain update algorithm.

In this section, the main purpose is to integrate the model equations and derive the consistent tangent stiffness matrix using the closest point projection method. To account for the most general situation, i.e., the mechanical and hydraulic loadings exerting simultaneously when the current stress state is on the yield surface, the model equations that need to be integrated are given as follows:

$$\overline{R}_1 = I_{n+1}^{(m)} - \left[ \left( I_n \right)^{(1-b_1)} + \frac{K_0 \left(1-b_1\right)}{p_{ref}^{b_1}} \left( \Delta\varepsilon_{v,n+1} - \Delta\varepsilon_{v,n+1}^{p(m)} \right) \right]^{1/(1-b_1)} \tag{5.39}$$

$$\overline{R}_2 = \Delta\varepsilon_{v,n+1}^{p(m)} - \Lambda_{n+1}^{(m)} D_{n+1}^{(m)} \tag{5.40}$$

$$\overline{\mathbf{R}}_3 = \mathbf{s}_{n+1}^{(m)} - \mathbf{s}_n - 2G_{n+1}^{(m)} \left( \Delta\boldsymbol{\varepsilon}_{q,n+1} - \Delta\boldsymbol{\varepsilon}_{q,n+1}^{p(m)} \right) \tag{5.41}$$

$$\overline{\mathbf{R}}_4 = \Delta\boldsymbol{\varepsilon}_{q,n+1}^{p(m)} - \Lambda_{n+1}^{(m)} \mathbf{n}_{n+1}^{(m)} \tag{5.42}$$

$$\overline{R}_5 = s_{c,n+1}^{(m)} - s_{c,n} - \Gamma^e \left( \Delta n_{w,n+1} - \Delta n_{w,n+1}^{p(m)} \right) \tag{5.43}$$

$$\overline{R}_6 = \Delta n_{w,n+1}^{p(m)} - \left( s_{c,n+1}^{(m)} - s_{c,n} \right) / \Gamma_{n+1}^{p(m)} \tag{5.44}$$

$$\overline{\mathbf{R}}_7 = \boldsymbol{\alpha}_{n+1}^{(m)} - \boldsymbol{\alpha}_n - \Lambda_{n+1}^{(m)} h_{n+1}^{(m)} \mathbf{b}_{n+1}^{(m)} \tag{5.45}$$

$$\overline{R}_8 = m_{n+1}^{(m)} - m_n - c_m \left(1+e_0\right) \Lambda_{n+1}^{(m)} D_{n+1}^{(m)} - c_v \left( \frac{s_{c,n+1}^{(m)} n_{w,n+1}^{(m)}}{p_{ref}} \right)^{\varpi} \Delta n_{w,n+1}^{p(m)} \tag{5.46}$$

$$\overline{\mathbf{R}}_9 = \mathbf{F}_{n+1}^{(m)} - \mathbf{F}_n + \Lambda_{n+1}^{(m)} c_f < -D_{n+1}^{(m)} > \left( F_{\max} \mathbf{n}_{n+1}^{(m)} + \mathbf{F}_{n+1}^{(m)} \right) \tag{5.47}$$

Wetting bound:

$$\overline{R}_{10} = s_{c0w,n+1}^{(m)} - s_{c0w,n} \exp\left[ \zeta v_{n+1}^{(m)} \Delta \varepsilon_{v,n+1}^{p(m)} - \frac{1}{d_2} \frac{\left( n_{ws,n+1} - n_{wr,n+1} \right) \Delta n_{w,n+1}^{p(m)}}{\left( n_{ws,n+1} - n_{w,n+1}^{(m)} \right) \left( n_{w,n+1}^{(m)} - n_{wr,n+1} \right)} \right] \tag{5.48}$$

Drying bound:

$$\overline{R}_{11} = s_{c0d,n+1}^{(m)} - s_{c0d,n} \exp\left[ \zeta v_{n+1}^{(m)} \Delta \varepsilon_{v,n+1}^{p(m)} - \frac{1}{d_3} \frac{\left( n_{ws,n+1} - n_{wr,n+1} \right) \Delta n_{w,n+1}^{p(m)}}{\left( n_{ws,n+1} - n_{w,n+1}^{(m)} \right) \left( n_{w,n+1}^{(m)} - n_{wr,n+1} \right)} \right] \tag{5.49}$$

$$\overline{R}_{12} = \sqrt{\mathbf{r}_{n+1}^{(m)} : \mathbf{r}_{n+1}^{(m)}} - \sqrt{2/3} m_{n+1}^{(m)} I_{n+1}^{(m)} \sqrt{1 - \left( I_{n+1}^{(m)} / I_0 \right)^{\beta}} \tag{5.50}$$

All the variables in the above equations are defined in the last section. The residuals and the unknowns needed to be solved in the above system of equations are:

$$\overline{\mathbf{R}} = \{ \overline{R}_1, \overline{R}_2, \overline{\mathbf{R}}_3, \overline{\mathbf{R}}_4, \overline{R}_5, \overline{R}_6, \overline{\mathbf{R}}_7, \overline{R}_8, \overline{\mathbf{R}}_9, \overline{R}_{10}, \overline{R}_{11}, \overline{R}_{12} \} \tag{5.51}$$

$$\mathbf{U} = \{ I_{n+1}^{(m)}, \Delta \varepsilon_{v,n+1}^{p(m)}, \mathbf{s}_{n+1}^{(m)}, \Delta \boldsymbol{\varepsilon}_{q,n+1}^{p(m)}, s_{c,n+1}^{(m)}, \Delta n_{w,n+1}^{p(m)}, \boldsymbol{\alpha}_{n+1}^{(m)}, m_{n+1}^{(m)}, \mathbf{F}_{n+1}^{(m)}, s_{c0w,n+1}^{(m)}, s_{c0d,n+1}^{(m)}, \Lambda_{n+1}^{(m)} \} \tag{5.52}$$

To solve the highly nonlinear system, the Newton-Raphson algorithm is used:

$$-\mathbf{T} \Delta \mathbf{U} = -\frac{\partial \overline{\mathbf{R}}}{\partial \mathbf{U}} \Delta \mathbf{U} = \Delta \overline{\mathbf{R}} \tag{5.53}$$

The differentiation of $\overline{\mathbf{R}}$ with respect to $\mathbf{U}$, which is the tangent stiffness matrix $\mathbf{T}$, is presented in detail in Appendix II. The initial value of $\mathbf{U}$ is determined using the elastic predictor with the assumption that no plastic strains and no irrecoverable water

content change occur. With the given loading conditions, the trial stress state based on the elastic assumption can be easily calculated. If the trial stress state is located within the yield surface, then it means the elastic assumption holds. However, if the trial stress state is located on or outside of the yield surface, then it is necessary to use the plastic corrector to modify the predictions by simultaneously satisfying all the rate equations from (5.39) through (5.50). The iteration process will not stop until certain error control criteria are met. As mentioned earlier, the selection of the rate equation(s) and how to update the stress strain state depend on the loading conditions. The stress update algorithm is presented in Appendix I.

It is well known that the performance of the closest point projection method is greatly enhanced when a consistent tangent stiffness matrix, which is consistent with the integration scheme, is used in the solution of the global finite element equations. The consistent tangent stiffness matrix is derived in Appendix III.

## 5.4 CALIBRATION OF MODEL PARAMETERS

The proposed model is basically composed of three components: the soil skeleton part or the mechanical part, the SWCCs part or the hydraulic part and the coupling effects between the mechanical and hydraulic behavior. Most of the model parameters can be easily calibrated from common laboratory tests, while some of them have to be determined using a trial-and-error procedure. All the related parameters are listed below:

Elastic parameters: $K_0$, $G_0$, $b_1$, $d_1$, $p_{ref}$

Critical state parameters: $e_{cr}$, $\lambda$, $\xi$, $M_c^c$, $M_e^c$

State parameters: $k_c^b$, $k_c^d$, $k_e^b$, $k_e^d$

Hardening parameters: $h_0$, $m$, $c_m$, $I_0$, $\beta$, $c_v$, $\varpi$

Dilatancy parameter: $B_0$

Fabric parameters: $c_f$, $F_{\max}$

SWCCs model parameters: $b_2, d_2, b_3, d_3, \Gamma^e, g, H, n_{ws}, n_{wr}, \varsigma$

In the above-listed parameters, most of them can be easily calibrated from convention triaxial tests. As to the elastic parameters, i.e., $K_0$, $G_0$, $b_1$, $d_1$ and $p_{ref}$, the elastic modulus and shear modulus at different effective stresses should be calculated for saturated soils. Although some purely elastic behavior is expected at the beginning portion of loading, it is common and convenient to calibrate the elastic parameters during the unloading process. Generally, the unloading process during undrained triaxial tests can be used to find the shear modulus and the unloading process during drained tests can be used for the bulk modulus.

The critical state parameters, i.e., $e_{cr}$, $\lambda$, $\xi$, $M_c^c$ and $M_e^c$ can also be easily calibrated. Undrained triaxial tests on saturated soils can be used to calibrate $M_c^c$ and $M_e^c$, which are the ratios between deviatoric stresses and effective mean stresses during compression and extension, respectively. To get a good estimation of $M_c^c$ and $M_e^c$, it is

always desirable to increase axial strain to reach the phase transformation line. Drained triaxial tests on saturated soils can be used to calibrate $e_{cr}$, $\lambda$ and $\xi$, which are calibrated using curve-fitting technique from the $e - p'$ relationships. Here $e$ is the critical void ratio under certain effective mean stress $p'$.

The state parameters, $k_c^b$, $k_c^d$, $k_e^b$ and $k_e^d$ are special parameters used in the proposed model. $k_c^b$ and $k_e^b$ relate to the bounding stress ratio, while $k_c^d$ and $k_e^d$ relate to the dilatancy stress ratio. Eqs. (5.10) should be used to calculate $k_c^b$, $k_c^d$, $k_e^b$ and $k_e^d$. For example, in order to calculate the coefficient $k_c^b$, a constant confining stress drained test can be used. It is not difficult to measure the stress ratio $M_c^b$ and $M_c^c$ during the test. Once the state parameter $\psi$ is known, $k_c^b$ can be easily calculated from Eq. (5.10.1). Similar procedures can be adopted for calibration of $k_c^d$, $k_e^b$ and $k_e^d$. To find out the dilatancy stress ratio, the confining stress has to be high enough to warrant dilation.

If stress-dilatancy data are available, it is not difficult to find out the dilatancy parameter $B_0$. One alternative is to run a constant confining stress drained test, in which the relationship between the volumetric strain and the axial strain can be determined. Because the dilatancy coefficient deals with the plastic strains, a fine-tuned procedure has to be carried out for a best fit $B_0$.

No explicit physical meaning is defined for the hardening parameter $h_0$ and the calibration of $h_0$ can be carried out by a trial-and-error procedure. As is shown in the model formulation, $h_0$ is directly related to the evolution of the kinematic hardening parameter, so $h_0$ may be calibrated by matching the model predictions to the $q$-$\varepsilon_1$ curve in a drained compression test. The yield surface-related parameters, i.e., $m$, $I_0$ and $\beta$ are usually calibrated based on observation. The size of the yield surface, $m$, is generally small at the beginning of loading. From Fig. 5.1, it shows that $I_0$ is the effective confining stress at the tip of the yield surface. $p_0$ in the triaxial stress space is equivalent to $I_0$ in the general stress space. A reasonable $p'$-$q$ curve will provide a good estimation of $I_0$. As discussed earlier, $\beta$ can be assumed to be 20 or calibrated from test results. Generally, $\beta$ does not introduce too much difference to the model predictions if it is large enough.

$c_m$ is related to the evolution of the isotropic hardening parameter. If $c_m = 0$, it means the size of the yield surface has nothing to do with the plastic volumetric strain of the soil skeleton. Generally speaking, $c_m$ is a small number. A trial-and-error procedure can give a good estimation of $c_m$. Now, $c_v$ and $\varpi$ have to be determined. $c_v$ and $\varpi$ contribute the evolution of the size of the yield surface when suction changes. It is beneficial to realize that the effect of suction on the size of the yield surface is not significant, so $c_v$ is always a small number.

The fabric tensor is important for sand and silt behavior. Soil dilation and liquefaction are significantly affected by the fabric tensor. Calibration of the fabric parameters, $c_f$ and $F_{\max}$, has to be done using a trial-and-error procedure, since no test results directly related to the fabric tensor are provided for most studies. Considering that sands and silts generally have a high strength, the fabric parameters $c_f$ and $F_{\max}$ are large numbers.

The SWCCs model parameters, i.e., $b_2$, $d_2$, $b_3$, $d_3$, $\Gamma^e$, $g$, $H$, $n_{ws}$ and $n_{wr}$, can be easily calibrated from any drying and wetting process. To make sure the calibration curves are close enough to the real drying and wetting bounds, it is always good to apply very high suction during the drying process and start the wetting process from high suction as well. The bounding curves are used to calibrate $b_2$, $d_2$, $b_3$, $d_3$, $n_{ws}$ and $n_{wr}$. Any scanning curve can be used to calibrate $\Gamma^e$, $g$ and $H$. As mentioned in Chapter 3, $g$ can be always assumed to be 1 with satisfying accuracy. Of course, any value of $g$ different from 1 is also possible, if a better accuracy for the SWCCs model is required. $\Gamma^e$, the slope of the initial portion of any scanning curve, is usually a large number. $\varsigma$ is a coupling parameter to demonstrate the effect of soil deformation on the soil water characteristic curves. To determine $\varsigma$, at least two sets of SWCCs under different confining stresses or a wetting-collapse test are required. $\varsigma$ is usually a small number and it can be calibrated using a trial-and-error process. Given the fact that it is time-consuming to run laboratory tests to determine complete SWCCs, it is common that only part of the SWCCs information is available and assumptions have to be made to

determine all of the SWCCs parameters. This procedure is demonstrated in the following section.

## 5.5 MODEL PERFORMANCE

Very limited test results are available to investigate the coupling effects between the mechanical and hydraulic behavior of unsaturated soils. Generally, the cyclic drying-wetting process influences the elastoplastic behavior of unsaturated soils and the soil skeleton deformation introduces shift in the soil water characteristic curves. To validate the predictions of the proposed comprehensive constitutive unsaturated silt/sand model, the available test results from Minco silt (Vinayagam, 2004) and a series of tests on Toyoura sand (Verdugo and Ishihara 1996; Uchida and Stedman 2001; Unno *et al*. 2008) are used. Next, some hypothetical examples are used to demonstrate the coupling effects between the mechanical and hydraulic behavior of unsaturated soils.

### 5.5.1 MINCO SILT

Minco silt is an Oklahoma silt and the engineering properties of Minco silt have been experimentally investigated at the University of Oklahoma over the last decade (Deshpande, 1997; Ananthanathan, 2002; Vinayagam, 2004; Tan, 2005). According to the USCS classification, Minco silt belongs to CL with a liquid limit of 28%, plastic limit of 20% and specific gravity of 2.68. Minco silt is composed of 27% of sand and 73% of

fines. The maximum dry unit weight of Minco silt is about 17.9 $kN/m^3$ and its optimum moisture content is about 12.8%.

Vinayagam (2004) carried out a systematic investigation on Minco silt. All the tests on Minco silt were carried out on two different automated triaxial apparatuses, the GDS and the GCTS, available at the University of Oklahoma. Different test conditions, including different densities, different stresses and different initial suctions were used to investigate the stress-strain behavior of Minco silt. In addition, the specimens were loaded monotonically and cyclically under different drainage conditions as well. Two types of compression tests were run: constant water content tests (CW) and undrained tests (CU). During the shearing period, the water line connected to the triaxial cell was shut off to keep gravimetric water content constant during the constant water content tests (CW), while the air line was set at pressure control. The pore air pressure was constant, while the pore water pressure changed during the CW tests. For the undrained tests (CU), both the water line and the air line were closed, so pore air pressure and pore water pressure changed according to the external loadings. If the soil sample is compressed and the volumetric strain is positive, both pore air pressure and pore water pressure will increase. If the soil sample changes from contraction to dilation, the pore air pressure and pore water pressure will stop increasing and start decreasing. During the shearing process of CW and CU tests, the gravimetric water content is constant. With the assumption that the temperature is constant during the CU tests, the product of the pore air pressure $p_a$ and its volume $V_a$ is a constant, i.e. $p_a \times V_a = const.$

No hysteretic SWCCs data for Minco silt is available. Fig. 5.3 presents all the initial soil water characteristic points for Minco silt by Vinayagam (2004). Deshpande (1997) provided a single wetting SWCC for Minco silt with a dry density that was very close to the one used by Vinayagam (2004) and this curve is treated as the wetting bounding curve in current study. To apply the hysteretic SWCCs model in Chapter 3, all the initial soil water characteristic points should be inside the bounding curves, so the drying bounding curve is hypothetically proposed for Minco silt as plotted in Fig. 5.3.

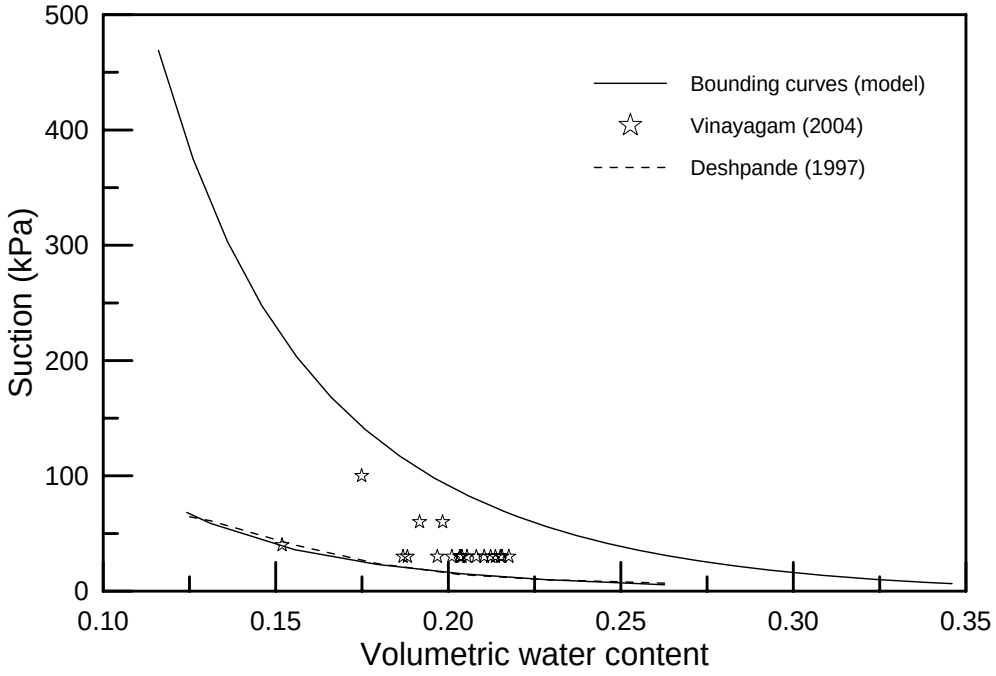


**Fig. 5.3** SWCCs for Minco silt

All the model parameters for Minco silt are calibrated and they are given in Table 5.1. The model parameters related to the mechanical behavior are calibrated using Test No. 2, while the SWCCs model parameters are calibrated using Test No. 5. The parameters dealing with the coupling effects are calibrated using a trial-and-error

procedure. Tests No. 1 through No. 10 are constant water content tests (CW), while all the other tests presented here, including Tests No. 11, 12, 14, 15, 20 and 22 are undrained tests (CU). The test conditions, i.e., the compaction conditions and initial conditions for shearing on the soil samples are given in Table 5.2 as well.

Fig. 5.4 presents the comparisons between the model predictions and test results with the initial suction of 30 *kPa* in a CW test. The comparisons show that the model can capture the stress-strain behavior well, including volumetric strain, deviatoric stress and mean net normal stress. The suction change is not well simulated and the test results of the suction change show that suction initially decreases and then increases. However, test results show that the volumetric strain is always positive, which means the soil sample contracted during shearing. Since the water line is closed during the shearing process, the pore water pressure should keep increasing, while the pore air pressure is kept constant. This means the suction, which is the difference between the pore air pressure and the pore water pressure should keep decreasing. Especially, the SWCCs model states that the increase in the volumetric water content corresponds to a decrease in suction and since the water volume does not change during CW tests, the volumetric water content increases when the soil sample contracts. This further shows that the suction should decrease with axial loading in this CW test.

The pore water pressure was measured by Vinayagam (2004) only at the bottom of the soil sample. A potential reason for this inaccurate measurement of pore water pressure is the shearing rate. If the loading rate is not slow enough, the pore water

pressure inside the sample will not come to equilibrium with the bottom drainage where pore water pressures are measured. Celes (1996) reported the permeability of Minco silt was as low as $4.0\times10^{-8}$ *cm/sec* when the gravimetric moisture content was 13~14%, at which most of the soil samples were compacted by Vinayagam (2004). Vinayagam (2004) used a strain rate of 0.18%/hour for all triaxial tests. Although she attempted to calculate a suitable rate of loading, this rate may not have been slow enough for Minco silt. Similar discrepancies can be seen in the simulations of other tests as well.

Fig. 5.5 presents the test results of Test No. 2. The test results were used in the model calibration for the mechanical parameters. Although the suction is again 30 *kPa*, the absolute values of pore air pressure and pore water pressure are different from Test No. 1. The stress-strain behavior is again simulated well, but there exists a discrepancy between measured and predicted suction changes as described before.

As can be seen, most of the model simulations for soil behavior under monotonic loadings, including both CW and CU tests are reasonable. The suction changes in Fig. 5.8 and Fig. 5.15 are simulated reasonably well. The test results reported in Fig. 5.8 were used to calibrate the coupling model parameters. For the CU tests, in which both the air line and the water line are closed, both pore air pressure and pore water pressure should increase during shearing-induced compaction. When the soil sample contracts, most of the deformation is translated into volume change of pore air, with a small amount of volume change in pore water. Because pore water is undrained, the volumetric water content increases as the soil sample contracts. As volumetric water content increases, the

suction decreases. This means that the magnitude of the pore water pressure change should be higher than that of the pore air pressure. This explanation on the SWCCs evolution is confirmed from the test results and the model simulations as well. From the deviatoric stress vs. axial strain curves, it can be seen that the maximum deviatoric stress increases with increasing net confining stress, given the identical initial suction.

As to the unsaturated Minco silt behavior under cyclic loadings, only two sets of data are examined and they are presented in Fig. 5.16 and Fig. 5.17. The main difference between the two tests is their initial suctions, one is 30 *kPa* and the other is 60 *kPa*. Their initial net stresses and void ratios are very close. Higher suction means higher intergranular stress if the net stress is the same. The model well captures the suction changes and the volumetric strains in both tests. Another very important behavior of Minco silt under cyclic loadings is that the stress-strain cycles stabilize after certain loading cycles. The suction change and volumetric strain also show similar stabilization.

The proposed model has been tested under different loading conditions. The overall performance of the proposed model for simulating the Minco silt behavior is reasonable. The model can reproduce most of the Minco silt behavior. Some discrepancies can be seen in the model predictions of pore water pressure and pore air pressure, but the potential reason may come from the loading rate and measurement.

### 5.5.2 TOYOURA SAND

Toyoura sand is a uniform fine sand consisting of 75% quartz, 22% feldspar and 3% magnetite (Oda *et al.*, 1978). The minimum and maximum void ratios of Toyoura sand are about 0.6 and 0.97, respectively. Toyoura sand has a specific gravity of 2.65 and $D_{50} = 0.17\ mm$.

As discussed earlier, the unsaturated soil model becomes a saturated soil model when the suction drops below the air entry value. In this section, model parameters for Toyoura sand are calibrated and used to simulate saturated sand behavior under monotonic loading conditions and unsaturated sand behavior under cyclic loadings. It is important to notice that the stresses applied to test Toyoura sand (Verdugo and Ishihara, 1996; Unno *et al.*, 2008) cover a very wide range from 30 *kPa* to 3000 *kPa*. The stress used for cyclic loading tests (Unno *et al.*, 2008) on Toyoura sand was very low. To better simulate the sand behavior under both saturated and unsaturated conditions, the model parameters are calibrated using low-stress test results. Because of the compromise between low and high stresses, some discrepancies between model simulations and test results under high stress can be seen. The overall model performance is still reasonable. Unno *et al.* (2008) only provided a single drying SWCC and this curve is used as the drying bounding curve. All the other SWCCs parameters are assumed. Most of the mechanical parameters are calibrated from saturated sand test results (Verdugo and Ishihara, 1996; Uchida and Stedman, 2001) under low confining stresses. The coupling parameters are calibrated using a trial-and-error method. In this way, the proposed model can be examined in a comprehensive manner. The model parameters are given in Table 5.1. A series of undrained tests on Toyoura sand with different void ratios has been

carried out by Verdugo and Ishihara (1996). Model predictions are compared to the test results in Fig. 5.19 to Fig. 5.23.

When the Toyoura sand is very dense (i.e., the void ratio $e$ = 0.735), compression is expected at the beginning of axial strain loading. The pore water pressure is accumulated and the effective stress decreases. However, as the strain loading continues the Toyoura sand experiences dilation. The process from compression to dilation is a special property for sand and it is called the phase transformation behavior. The proposed model can capture the phase transformation property of sand very well. As dilation continues, the accumulated pore water pressure starts decreasing and the effective stress increases.

The initial density of the sand sample plays an important role in determining how the sand behaves during the loading process. When the initial state is loose (i.e., the void ratio $e$ = 0.907), compression is dominant while no obvious dilation can be observed under given loading conditions. Fig. 5.23 clearly illustrates the pure contraction during axial strain loading. As the soil contracts, the pore water pressure accumulates and the effective stress decreases. However, for a medium density sand (i.e., the void ratio $e$ = 0.833), the effective confining stress plays a significant role. When the effective confining stress is low, dilation occurs at an early stage, while if the intergranular confining stress is high, the soil will experience contraction and then dilation. In this study for saturated Toyoura sand, the sand behavior is demonstrated to be strongly related to soil density and stress magnitude.

Limited research on unsaturated Toyoura sand is available in the literature. Unno *et al.* (2008) seems to be the first who systematically investigated unsaturated Toyoura sand behavior. Unfortunately, the strain they applied is small and the effective stress only reaches 30 *kPa*. In that stress range, little plastic response can be expected. Figs. 5.24 to 5.26 present the test results and the model simulations. Fig. 5.24 shows that as the cyclic loading continues, the soil sample experiences contraction and the intergranular stress decreases. It is of great interest to notice that the effective intergranular stress becomes very low at the end of the test. This phenomenon is of great importance in both theory and practice, because liquefaction may occur at the end of the test. In other words, liquefaction not only occurs in saturated sand, but also in unsaturated sand. In addition, the proposed model can also capture the changes in the pore water pressure and pore air pressure very well, as illustrated in Fig. 5.26.

### 5.5.3 HYPOTHETICAL SOIL

Since no test results are available on the coupling effects between the mechanical and hydraulic mechanisms in unsaturated soils, some hypothetical investigation is carried out in this section. All the model parameters are the same as calibrated for Toyoura sand in section 5.5.2.

SWCCs obtained for two different mean total stresses are shown in Figure 5.27. The simulation was conducted as follows. The suction path A (4 *kPa*) → B (20 *kPa*) → C

(4 *kPa*) is simulated keeping the mean total stress at 120 *kPa*. At point C, the mean total stress is increased from 120 *kPa* to 300 *kPa*. Then the suction is changed from C (4 *kPa*) → D (20 *kPa*) → E (4 *kPa*) while the mean total stress is kept constant at 300 kPa. The effects of soil deformation on the SWCCs can be clearly seen in Figure 5.27. When the mean total stress is higher, greater suction has to be exerted to hold the same amount of water in the soil sample. Following the analysis in Chapter 3, higher suction means smaller pore radius, if the contact angle and air-water interface energy are assumed to be constant. In other words, the soil sample contracts under higher mean total stress. It is the volumetric strains under different confining stresses that introduce the shift of the SWCCs. Not only the location of the SWCCs changes, but the shape of the SWCCs also changes as shown in Fig. 5.27.

Figs 5.28 through 5.32 present hypothetical analyses of drained stress-strain behavior of unsaturated Toyoura sand. One group of the hypothetical analysis is carried out under mean total stress of 200 *kPa*, two suctions of 6 *kPa* and 96 *kPa* and different initial void ratios, i.e., 0.74, 0.80 and 0.99. Another group of hypothetical analysis is carried out with the assumption that mean total stress is 800 *kPa*, while two suctions, i.e, 6 *kPa* and 96 *kPa* and two initial void ratios, i.e, 0.74 and 0.99 are adopted. All the hypothetical analyses are assumed to be strain-controlled tests with the axial strain going up to 20%.

Fig. 5.28 presents the relationships between mean intergranular stress and deviatoric stress. Under a given mean total stress, the deviatoric stress increases when the

suction is higher. Figs. 5.29 and 5.30 clearly demonstrate the relationship between deviatoric stress and suction and they show that the soil has a higher strength as higher suction is applied onto the soil. Figs. 5.31 and 5.32 illustrate the effect of the initial density on the soil behavior, with the soil sample contracting initially and then dilating when the soil has a high density, i.e, $e_0 = 0.74$ and 0.80. However, loose sand ($e_0 = 0.99$) contracts from the beginning of the loading process. The hypothetical analysis on the unsaturated Toyoura sand is consistent with the general properties of sand. How the mechanical behavior affects the SWCCs and how the SWCCs affect the mechanical responses are hypothetically analyzed in this section.

## 5.6 SUMMARY

Starting from the saturated sand models proposed by Manzari and Dafalias (1997) and Taiebat and Dafalias (2008), a comprehensive constitutive model for unsaturated sand and silt was presented in this chapter. Some special properties of the proposed model include: 1) a hysteretic SWCCs model based on the bounding surface plasticity concept was implemented to fully capture the soil water characteristic curves during cyclic wetting-drying process; 2) the adoption of the intergranular stress tensor was critical to the development of the unsaturated soil model; 3) a modified yield surface was adopted with a closed cap at its end to improve the model performance when the stress acting on the soil is high; 4) special hardening laws were proposed to account for the coupling effects between the mechanical and hydraulic behavior; 5) the model had been generalized from triaxial stress space to the general stress space. Finally, the rate

equations were integrated using a fully implicit integration scheme and the consistent tangent stiffness was also developed to enhance the model performance. Available test results on Minco silt and Toyoura sand were extensively examined using the proposed model and the overall performance of the model was reasonable.

**Table 5.1** Model parameters for Minco Silt and Toyoura sand

| Parameter list | | Minco Silt | Toyoura sand |
|---|---|---|---|
| Elastic parameters | $K_0$ $(kPa)$ | 20000 | 20000 |
| | $G_0$ $(kPa)$ | 30000 | 10000 |
| | $b_1$ | 0.5 | 0.5 |
| | $d_1$ | 0.5 | 0.5 |
| Critical state parameters | $e_{cr}$ | 0.75 | 0.935 |
| | $\lambda$ | 0.1 | 0.019 |
| | $\xi$ | 0.7 | 0.7 |
| | $M_c^c$ | 1.45 | 1.29 |
| | $M_e^c$ | 1.45 | 1.29 |
| Other state parameters | $k_c^b$ | 2.0 | 0.5 |
| | $k_c^d$ | 1.5 | 3.0 |
| | $k_e^b$ | 2.0 | 2.0 |
| | $k_e^d$ | 3.0 | 0.07 |
| Hardening parameters | $h_0$ | 30 | 500 |
| | $m$ | 0.25 | 0.40 |
| | $c_m$ | 1.0 | 0.0 |
| | $I_0$ $(kPa)$ | 5000 | 5000 |
| | $\beta$ | 20 | 20 |
| | $c_v$ | 0.5 | 0.5 |
| | $\varpi$ | 10 | 10 |
| | $\varsigma$ | 10 | 10 |
| Dilatancy parameters | $B_0$ | 0.1 | 0.5 |
| Fabric parameters | $c_f$ | 5.0 | 100 |
| | $F_{\max}$ | 500 | 100 |
| SWCCs model parameters | $b_2$ | 8.6 | 2.3 |
| | $d_2$ | 0.7 | 1.05 |
| | $b_3$ | 100 | 4.0 |
| | $d_3$ | 0.5 | 1.3 |
| | $\Gamma^e$ $(kPa)$ | -2500 | -100 |
| | $H$ | 5.0 | 7.0 |
| | $n_{ws}$ | 0.413 | 0.95 |
| | $n_{wr}$ | 0.001 | 0.03 |

**Table 5.2** Test conditions for tests on Minco silt (after Vinayagam, 2004)

| Test No. | Test type | After sample preparation | | | After isotropic consolidation | | | Stress state after isotropic consolidation | | |
|---|---|---|---|---|---|---|---|---|---|---|
| | | Water content (%) | $\gamma_{dry}$ ($kN/m^3$) | Void ratio $e_o$ | Water content (%) | $\gamma_{dry}$ ($kN/m^3$) | Void ratio $e$ | Mean net stress ($kPa$) | Suction ($kPa$) | $p_a$ ($kPa$) |
| 1 | CW | 14.00 | 14.28 | 0.842 | 13.81 | 14.49 | 0.814 | 50 | 30 | 60 |
| 2 | CW | 14.20 | 14.25 | 0.845 | 13.95 | 15.16 | 0.733 | 150 | 30 | 45 |
| 3 | CW | 14.04 | 14.19 | 0.852 | 13.50 | 15.63 | 0.682 | 300 | 30 | 45 |
| 4 | CW | 14.06 | 14.30 | 0.838 | 13.72 | 14.54 | 0.808 | 50 | 30 | 60 |
| 5 | CW | 14.19 | 14.28 | 0.841 | 11.87 | 14.45 | 0.819 | 50 | 100 | 120 |
| 6 | CW | 14.23 | 14.23 | 0.847 | 13.57 | 15.21 | 0.728 | 150 | 30 | 50 |
| 7 | CW | 14.03 | 14.18 | 0.854 | 13.29 | 15.01 | 0.752 | 150 | 30 | 50 |
| 9 | CW | 8.50 | 15.90 | 0.654 | 8.13 | 16.13 | 0.630 | 100 | 30 | 50 |
| 10 | CW | 8.17 | 16.03 | 0.639 | 9.13 | 16.31 | 0.612 | 100 | 40 | 70 |
| 11 | CU | 14.20 | 14.15 | 0.858 | 13.59 | 15.32 | 0.716 | 150 | 30 | 50 |
| 12 | CU | 14.18 | 14.16 | 0.857 | 13.76 | 15.51 | 0.695 | 150 | 30 | 50 |
| 14 | CU | 14.08 | 14.25 | 0.845 | 12.72 | 14.78 | 0.779 | 150 | 60 | 80 |
| 15 | CU | 14.23 | 14.18 | 0.854 | 13.53 | 15.09 | 0.742 | 150 | 30 | 50 |
| 20 | CU | 14.11 | 13.97 | 0.881 | 12.75 | 15.26 | 0.723 | 150 | 60 | 80 |
| 22 | CU | 14.14 | 14.23 | 0.847 | 13.60 | 15.41 | 0.71 | 150 | 30 | 50 |

**Note:**

Water contents in Table 5.2 are referred to gravimetric water content.

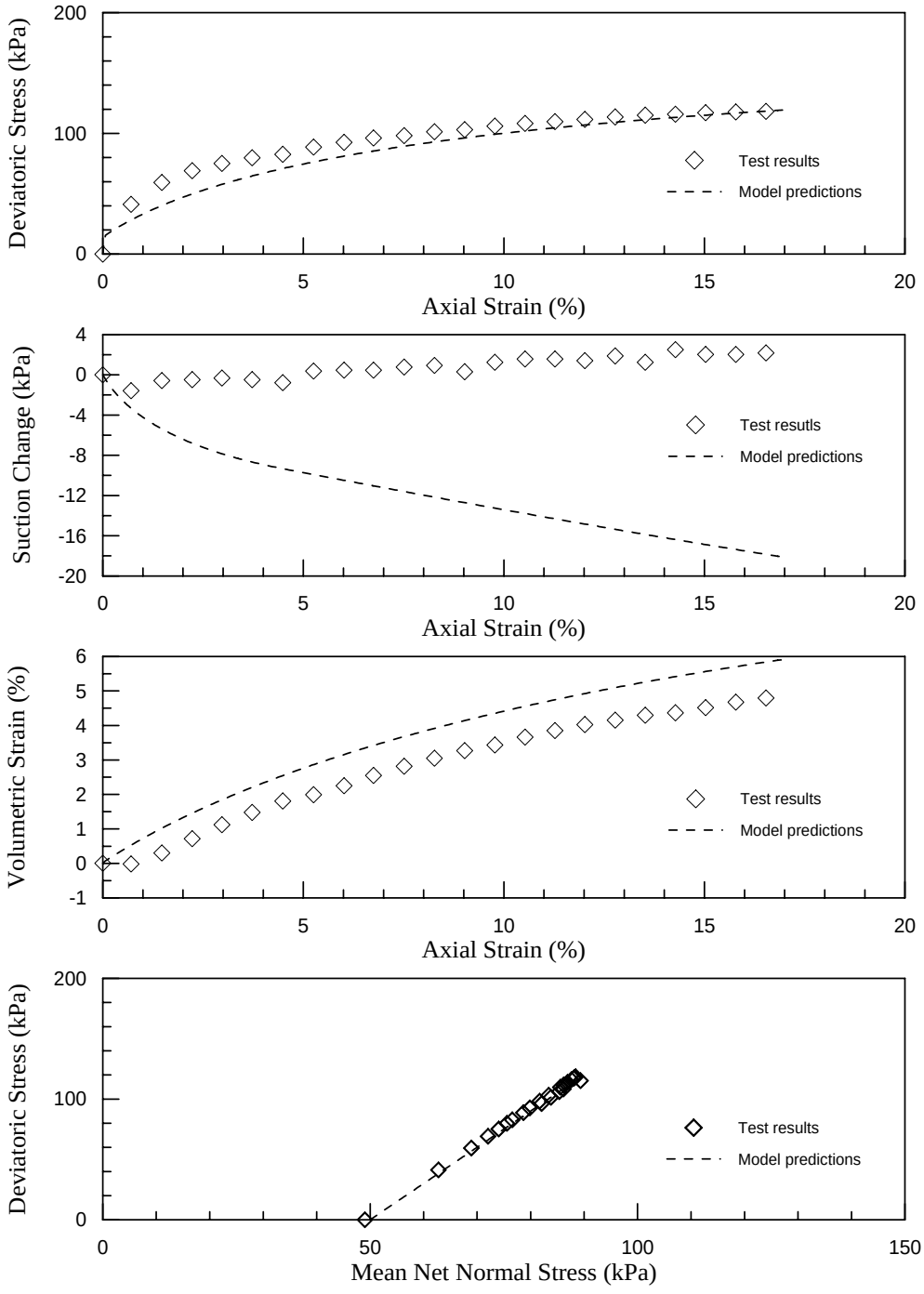


**Fig. 5.4** Model predictions and CW test results for Test No.1 on Minco silt

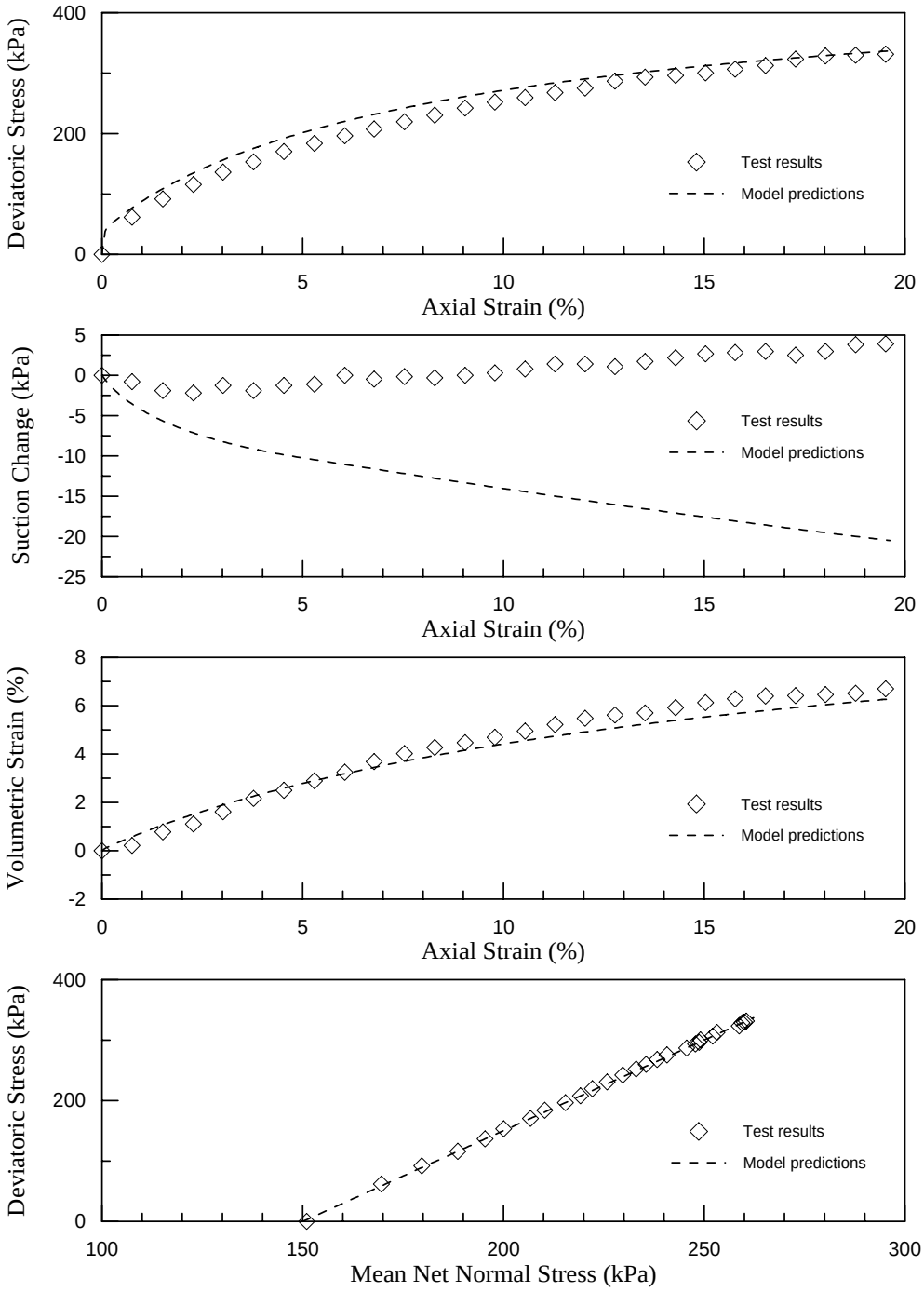


**Fig. 5.5** Model predictions and CW test results for Test No.2 on Minco silt

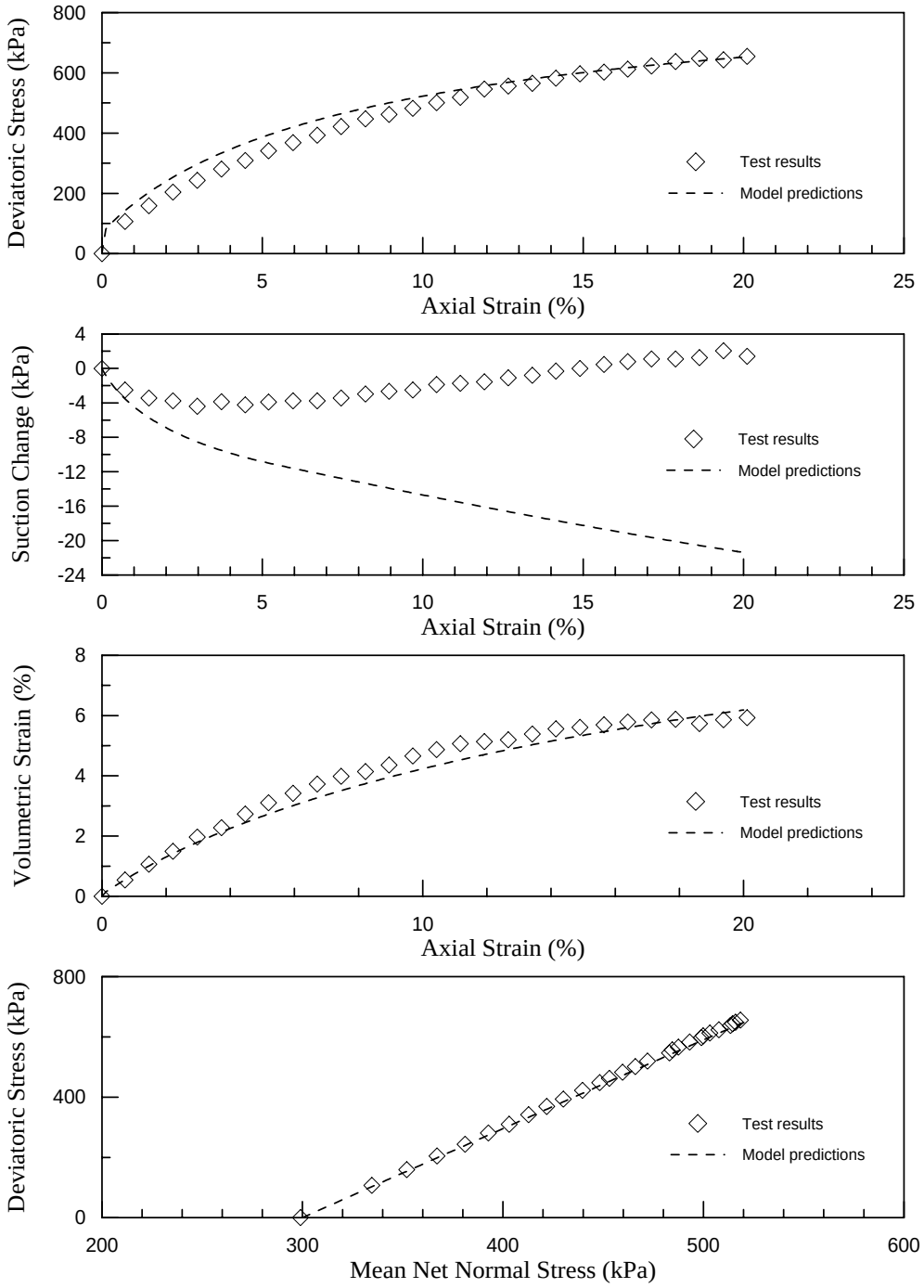


**Fig. 5.6** Model predictions and CW test results for Test No.3 on Minco silt

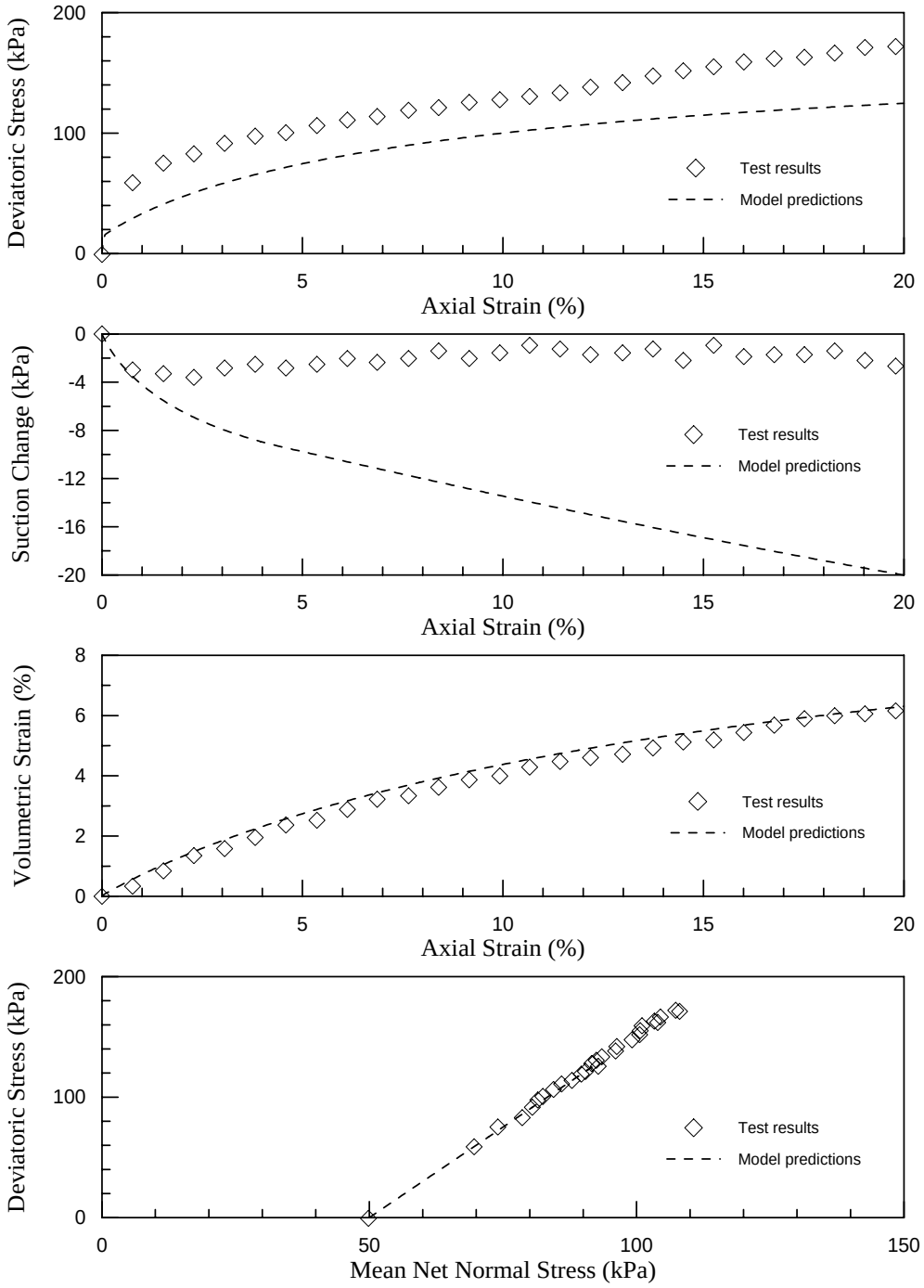


**Fig. 5.7** Model predictions and CW test results for Test No.4 on Minco silt

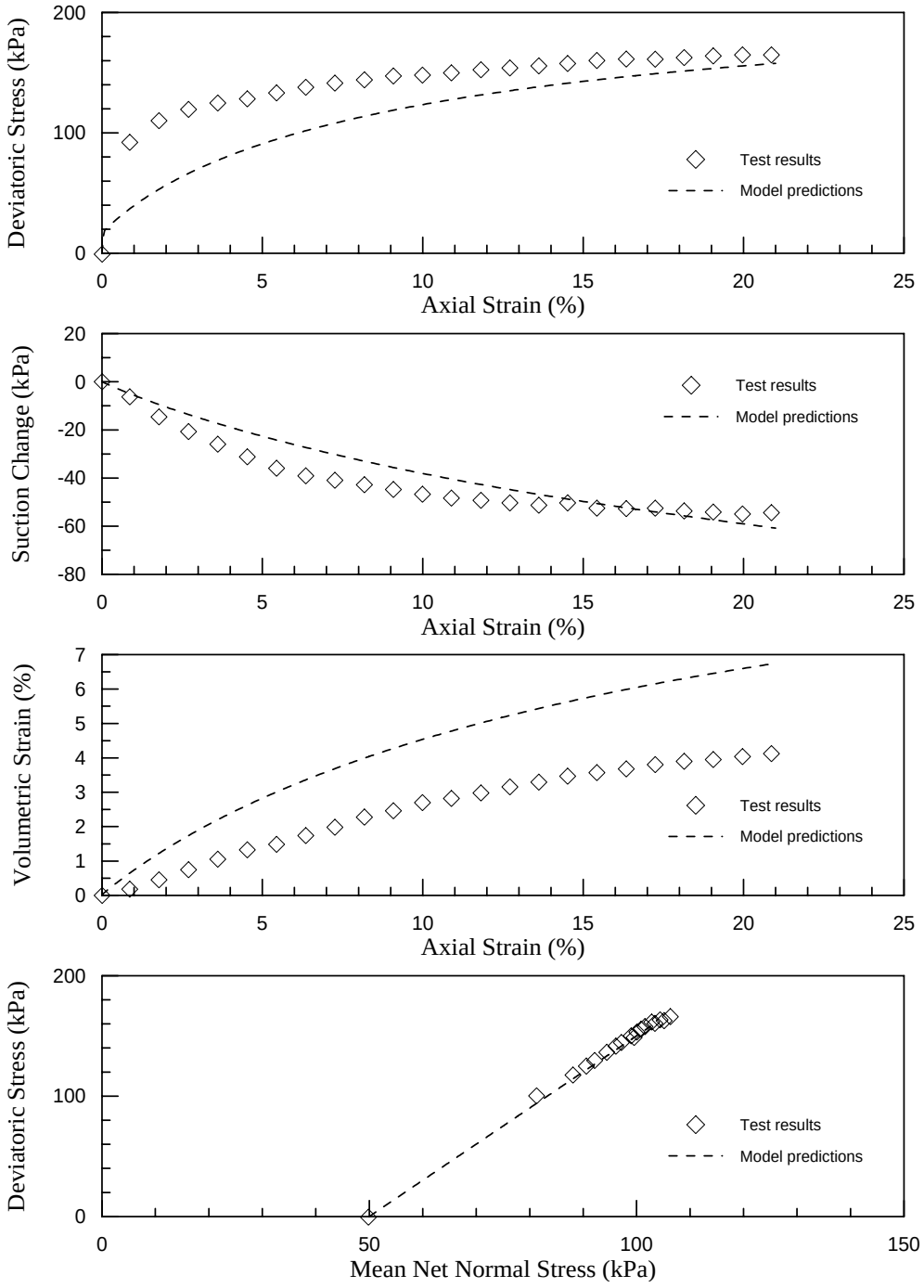


**Fig. 5.8** Model predictions and CW test results for Test No.5 on Minco silt

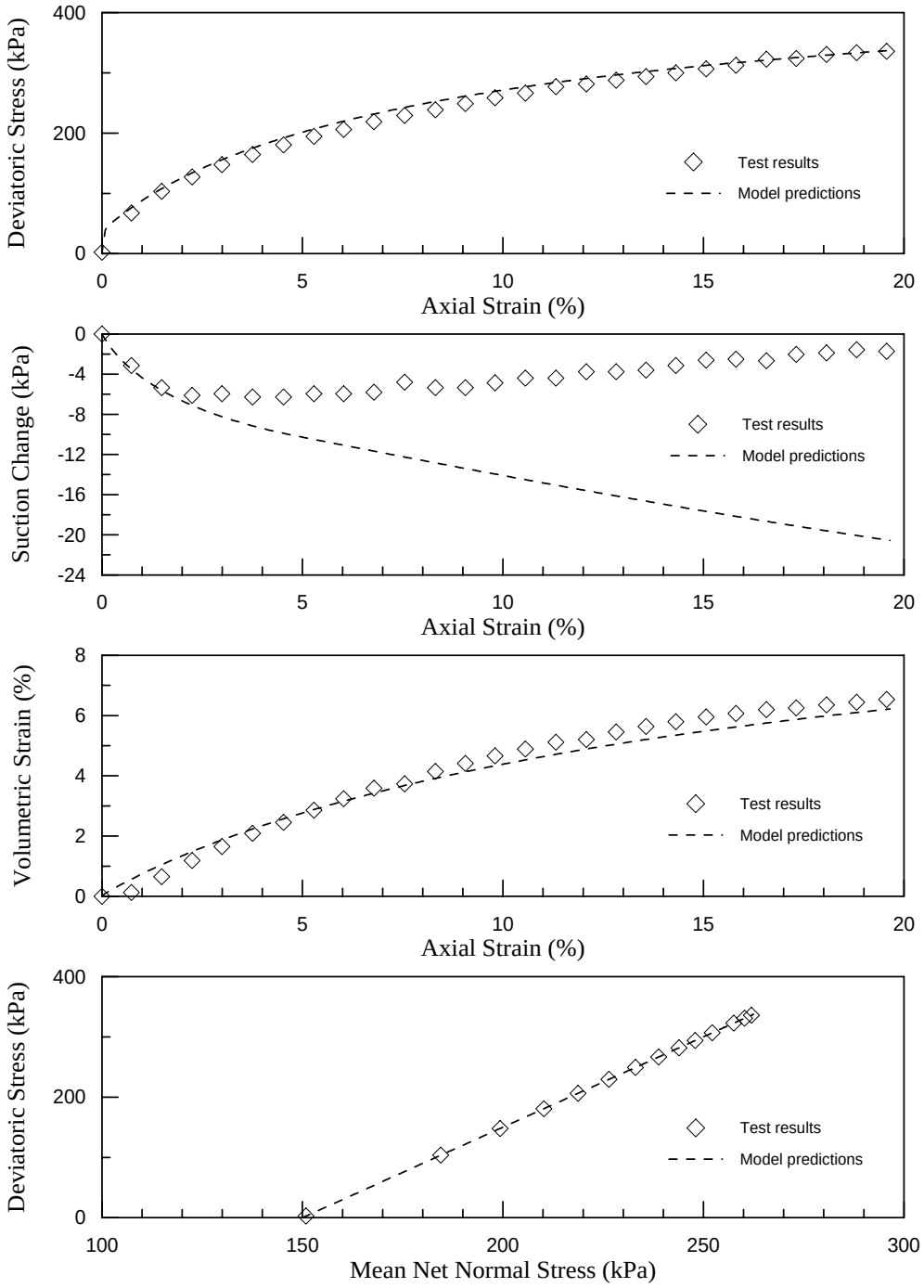


**Fig. 5.9** Model predictions and CW test results for Test No.6 on Minco silt

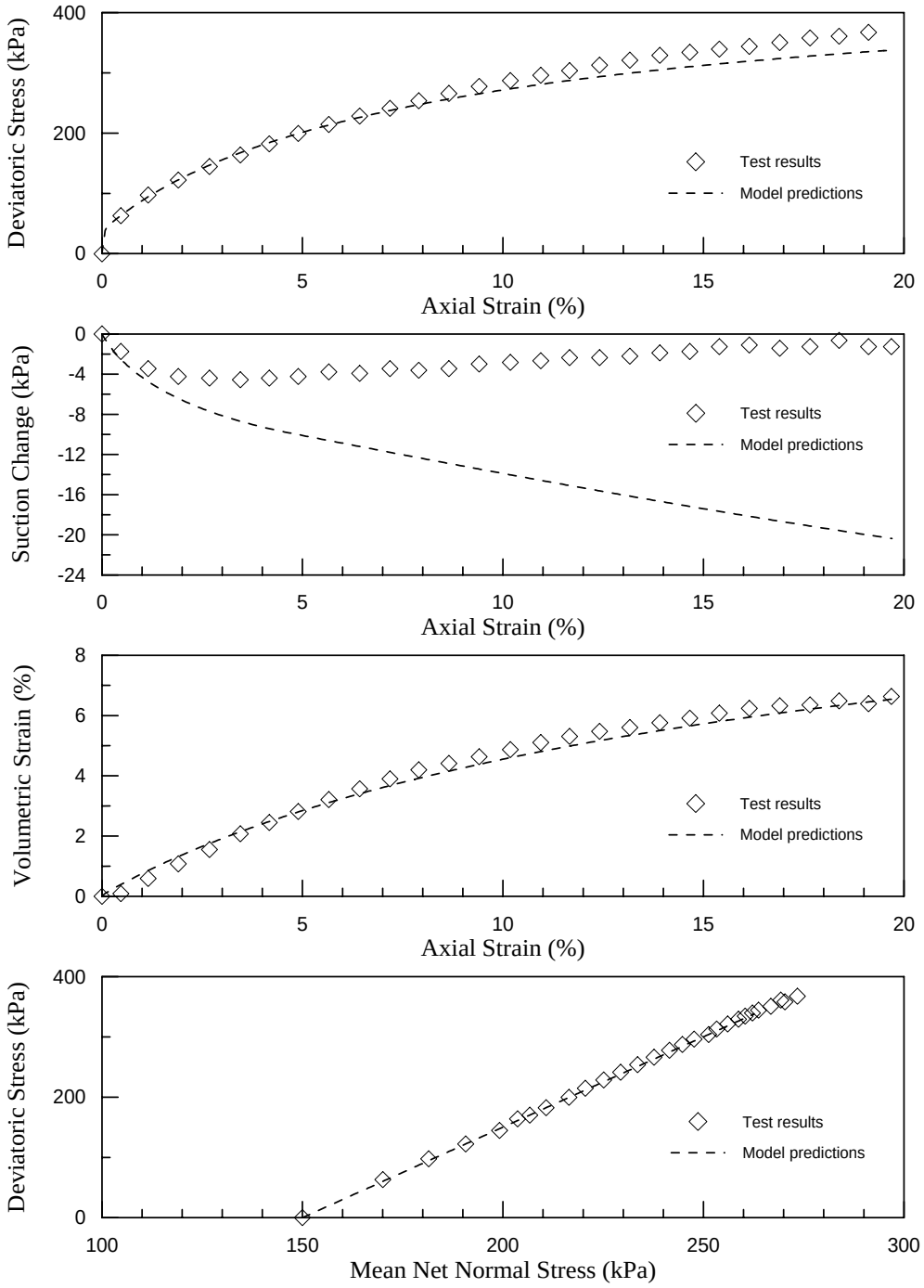


**Fig. 5.10** Model predictions and CW test results for Test No.7 on Minco silt

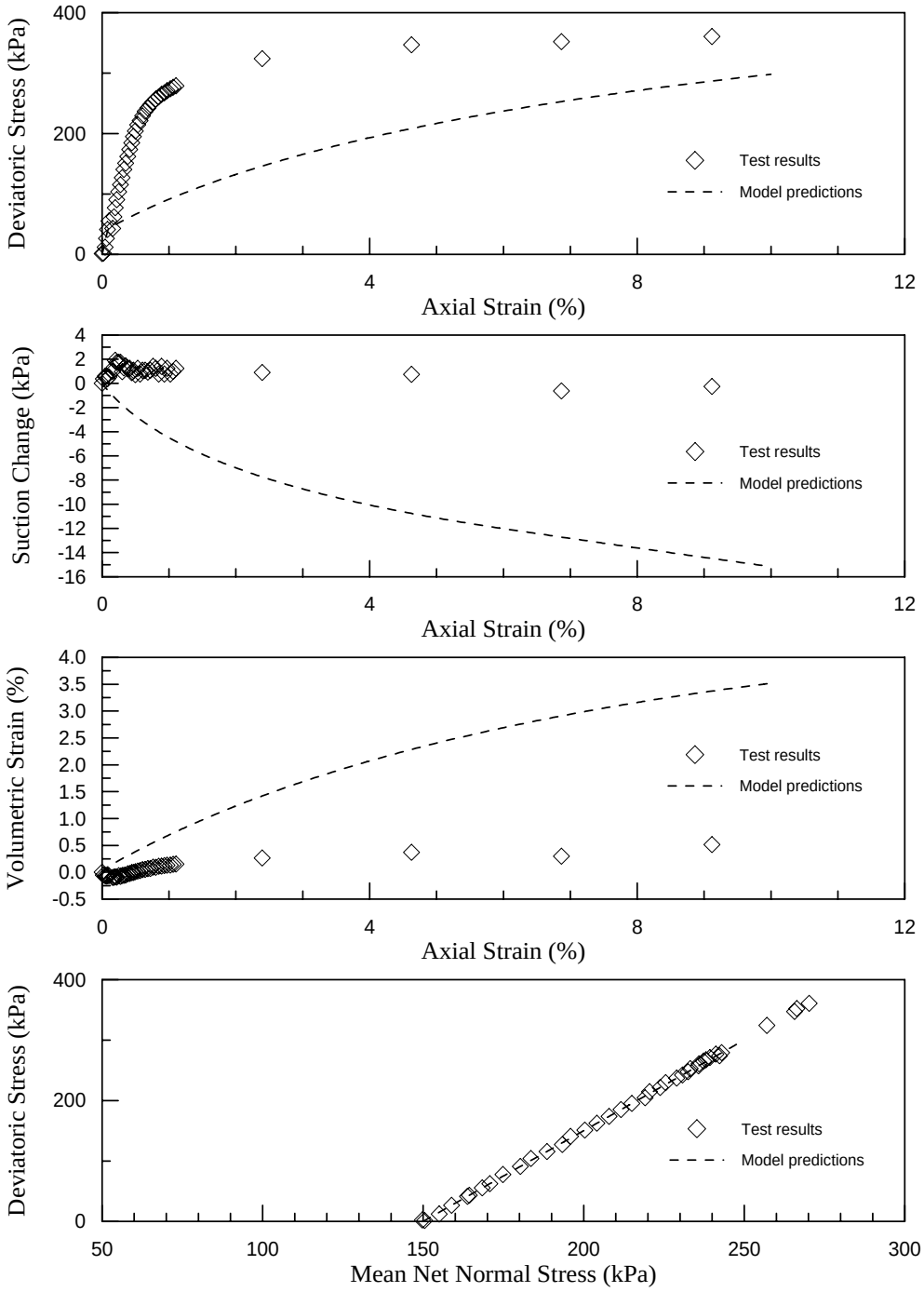


**Fig. 5.11** Model predictions and CW test results for Test No.9 on Minco silt

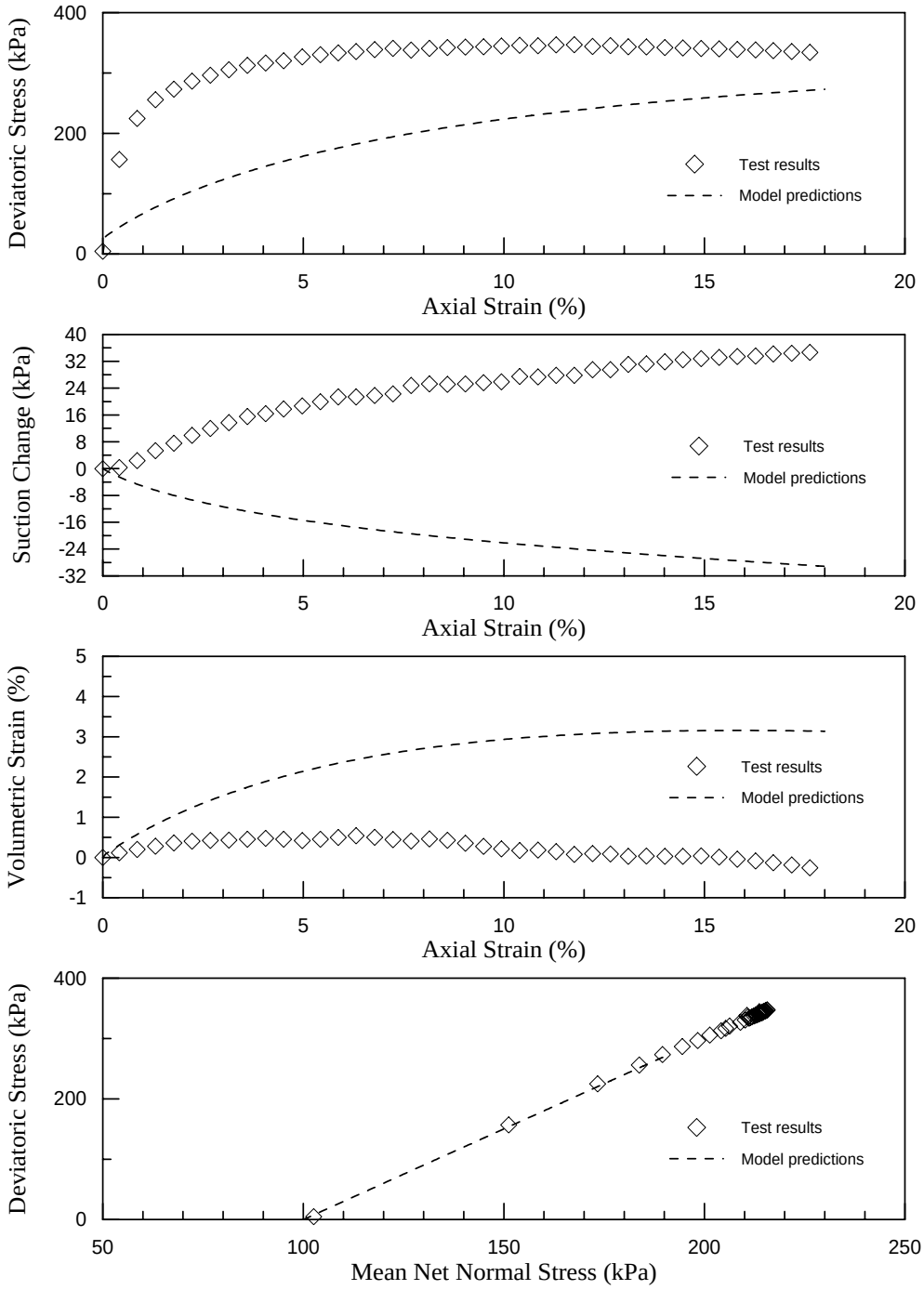


**Fig. 5.12** Model predictions and CW test results for Test No.10 on Minco silt

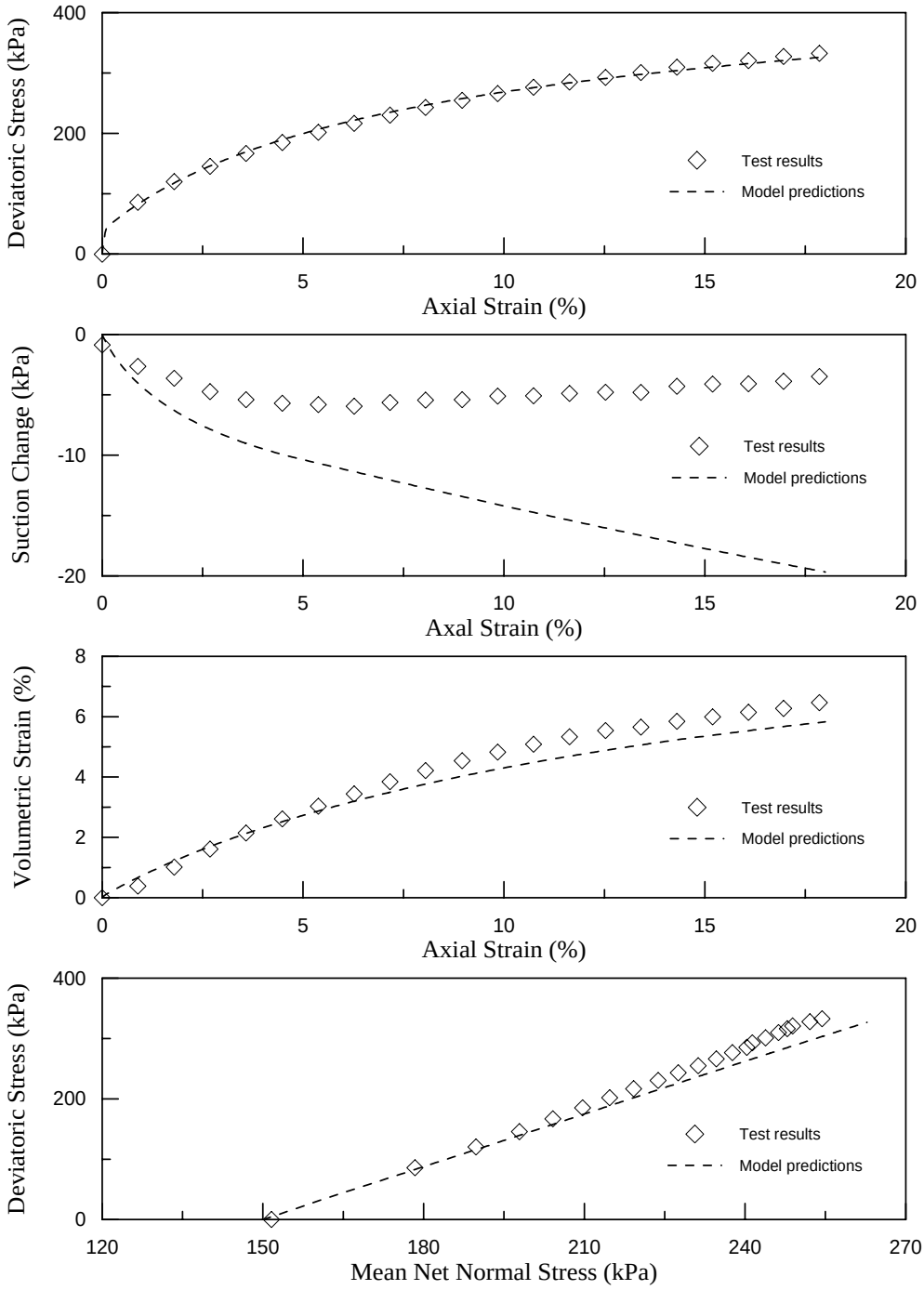


**Fig. 5.13a** Model predictions and CU test results for Test No.11 on Minco silt

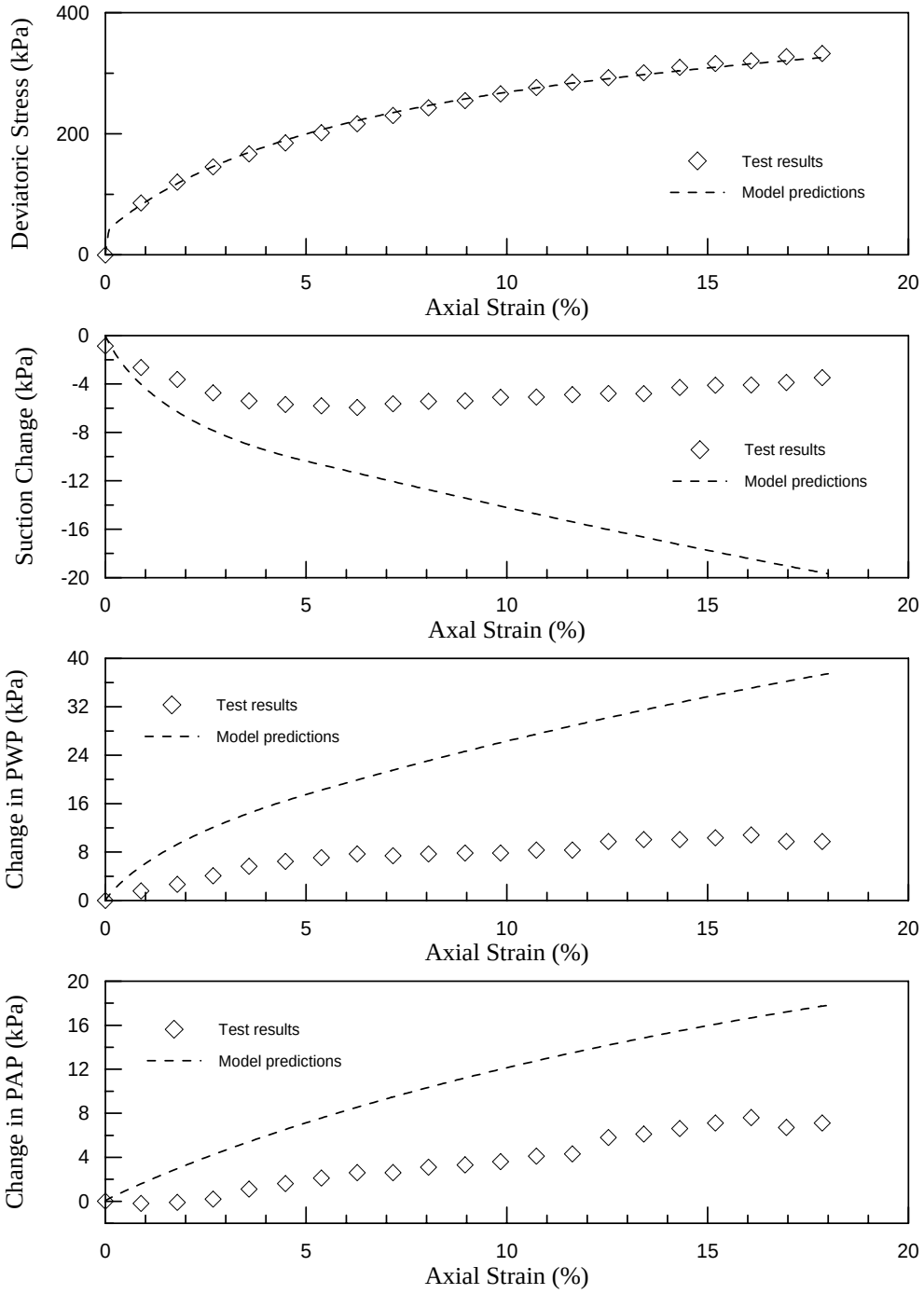


**Fig. 5.13b** Model predictions and CU test results for Test No.11 on Minco silt

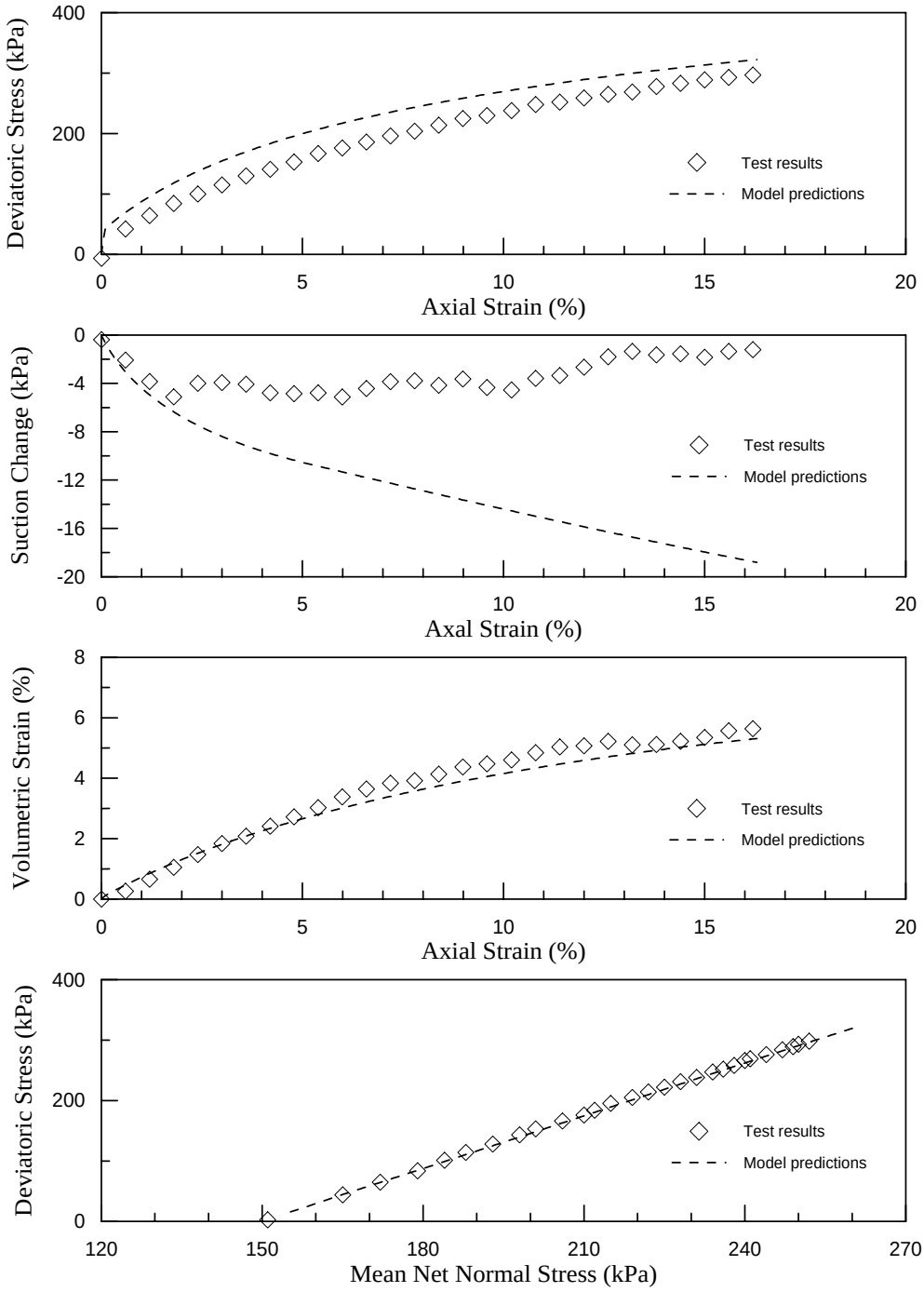


**Fig. 5.14a** Model predictions and CU test results for Test No.12 on Minco silt

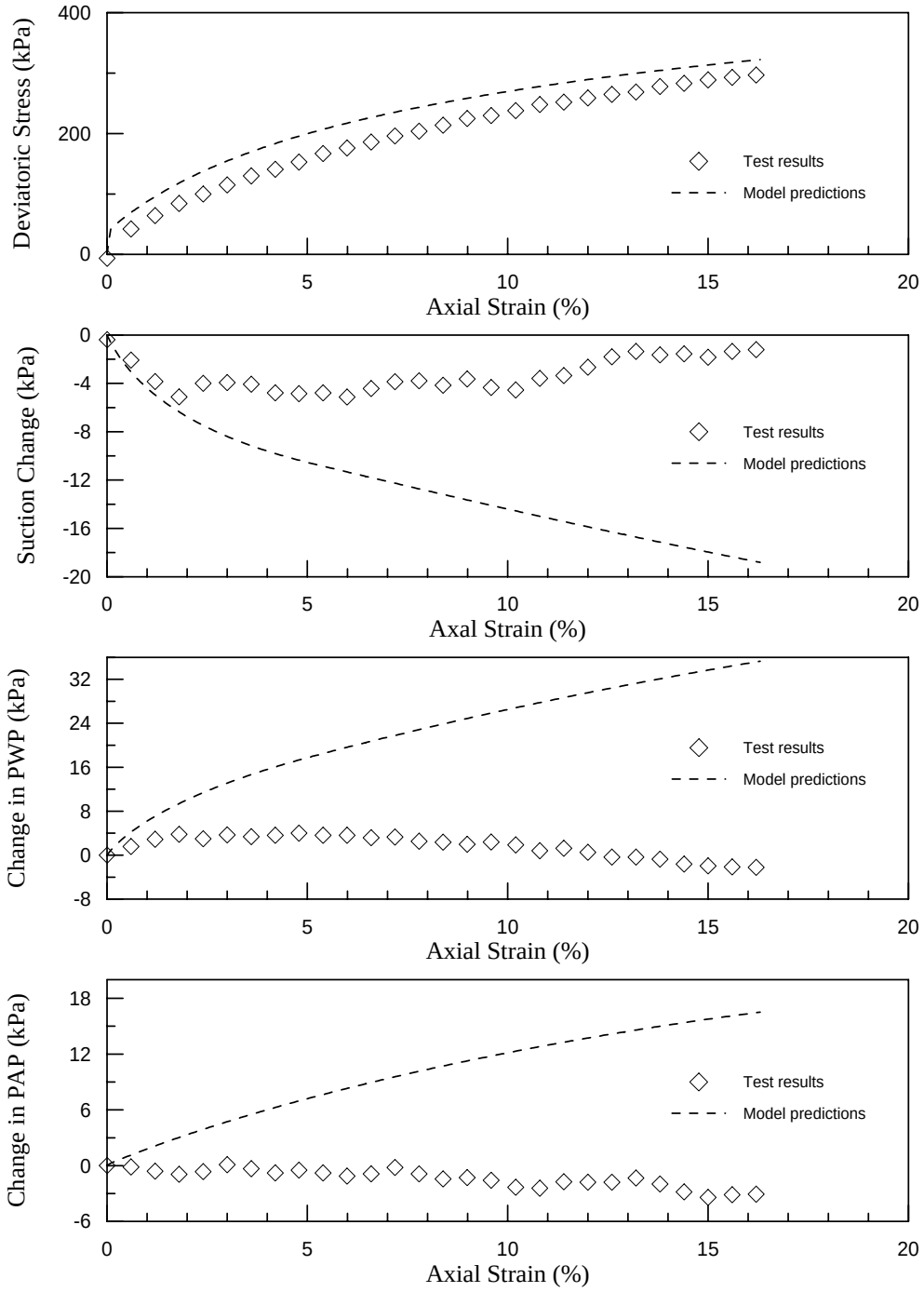


**Fig. 5.14b** Model predictions and CU test results for Test No.12 on Minco silt

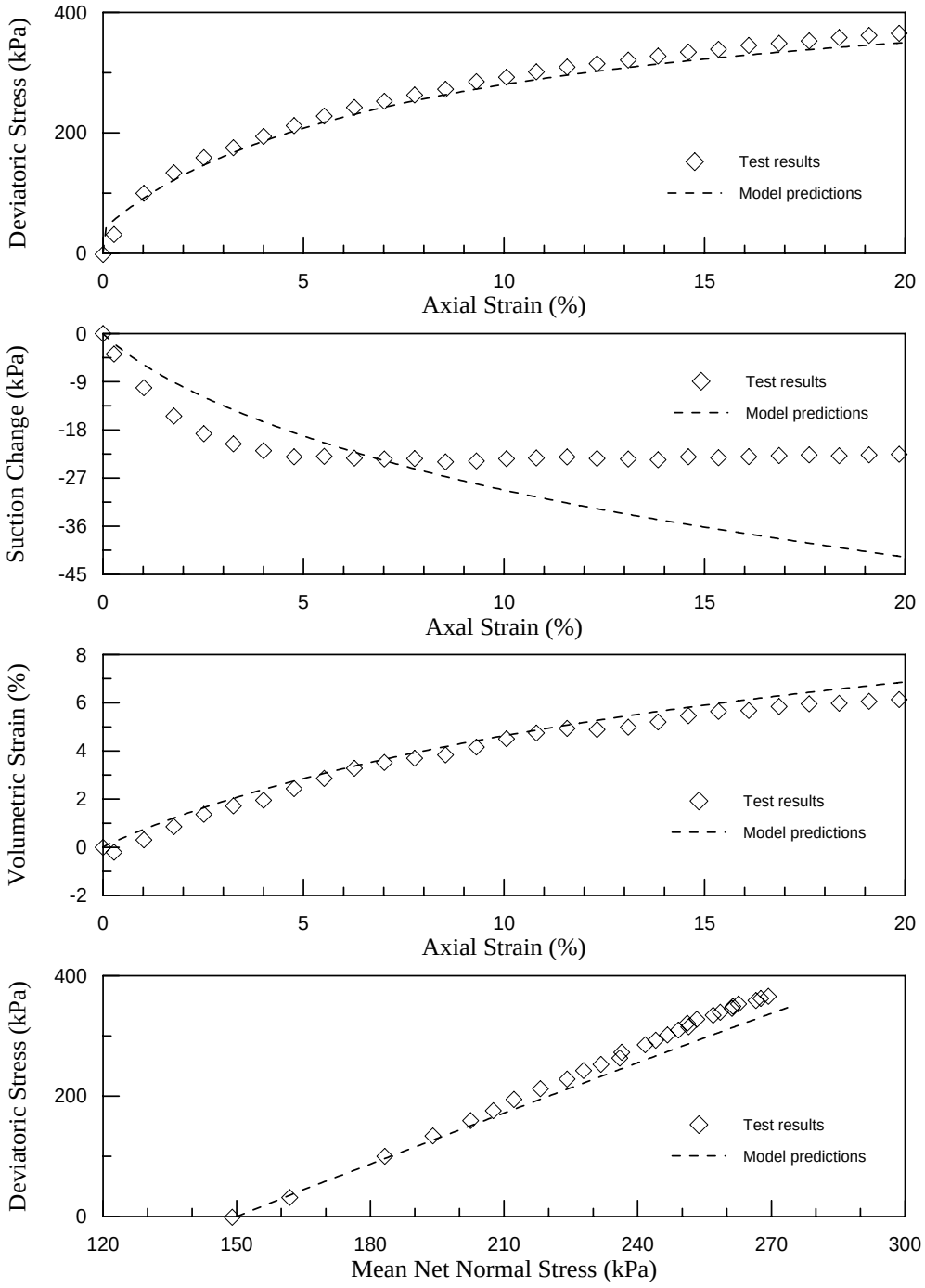


**Fig. 5.15a** Model predictions and CU test results for Test No.14 on Minco silt

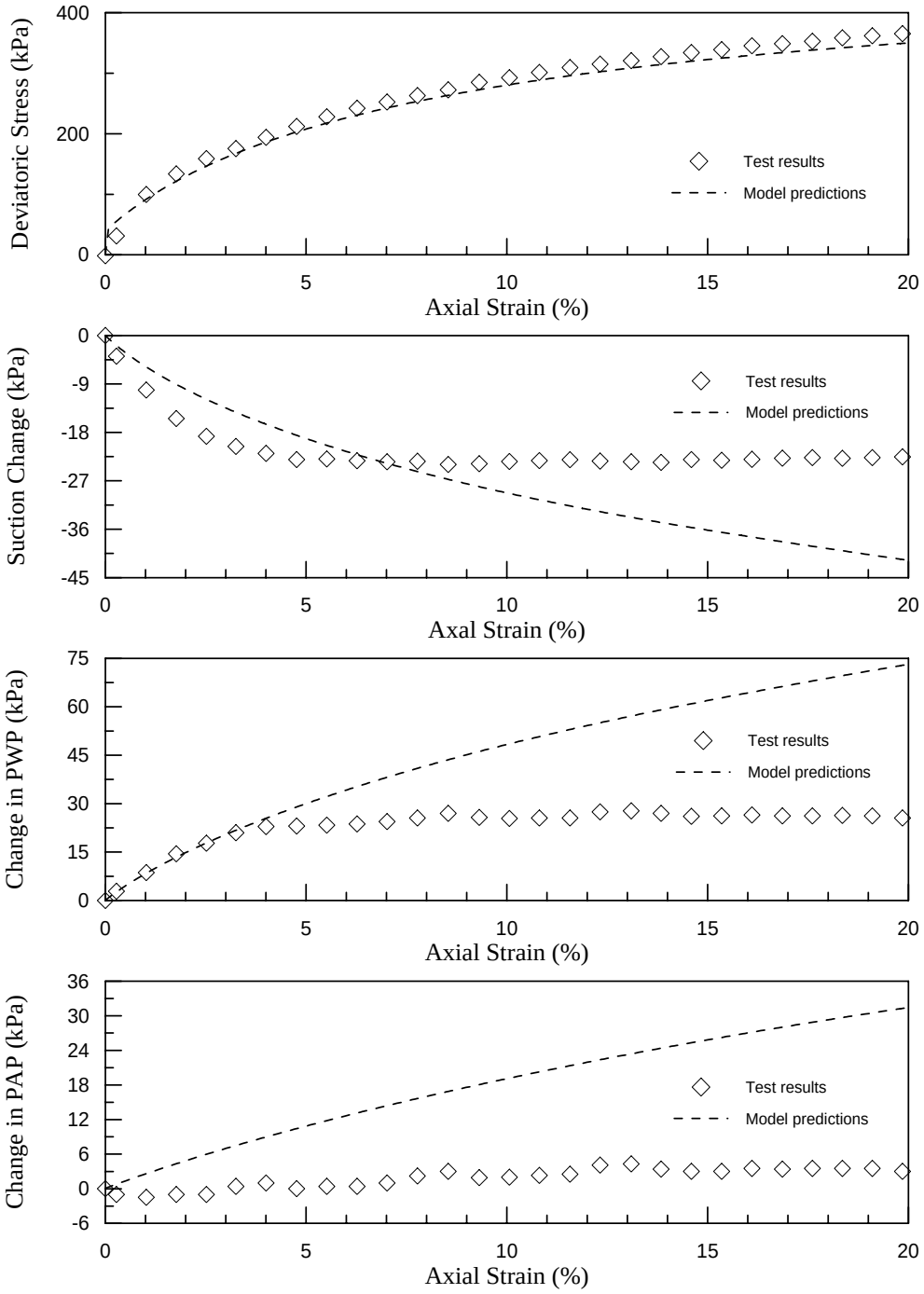


**Fig. 5.15b** Model predictions and CU test results for Test No.14 on Minco silt

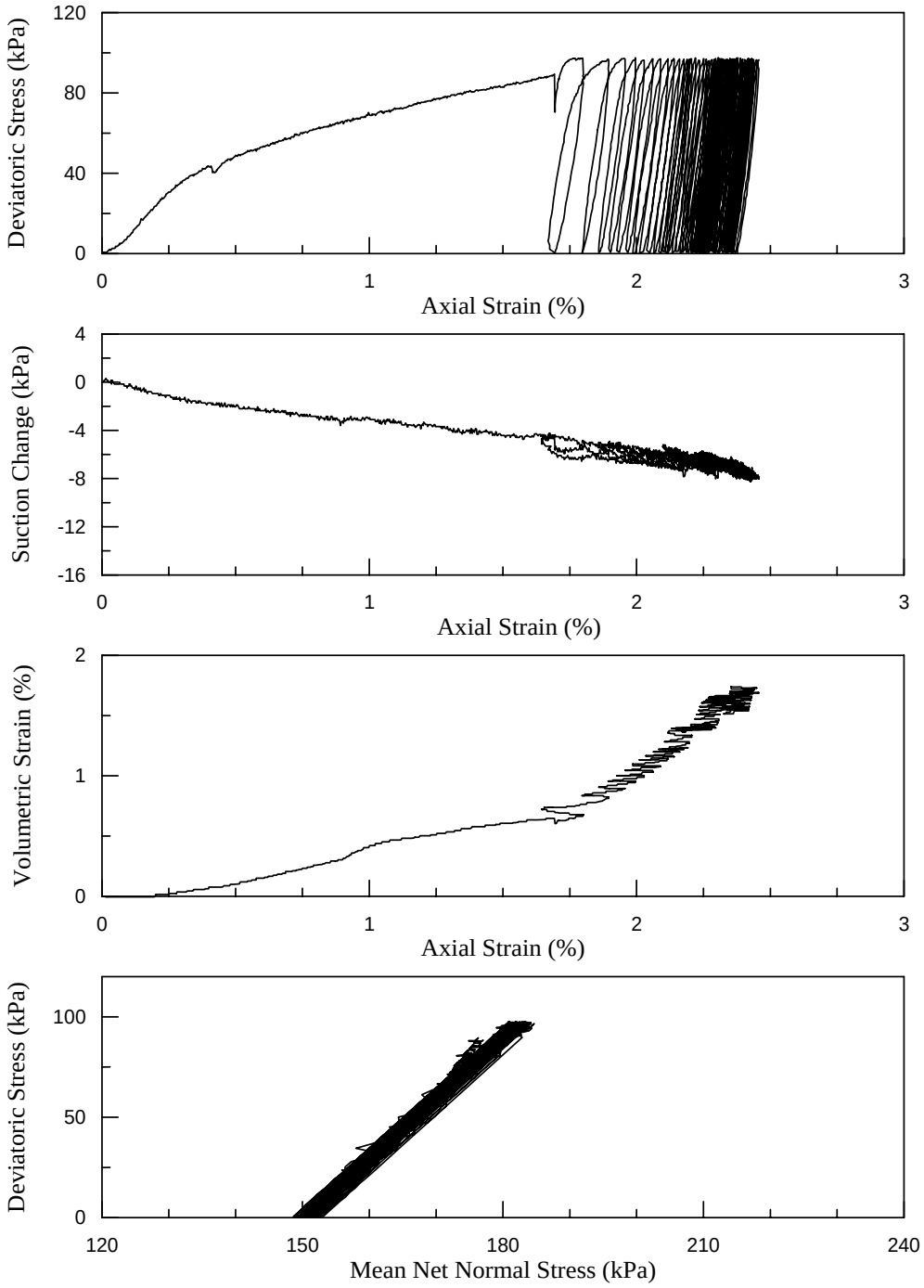


**Fig. 5.16a** CU cyclic test results for Test No.15 on Minco silt (Vinayagam, 2004)

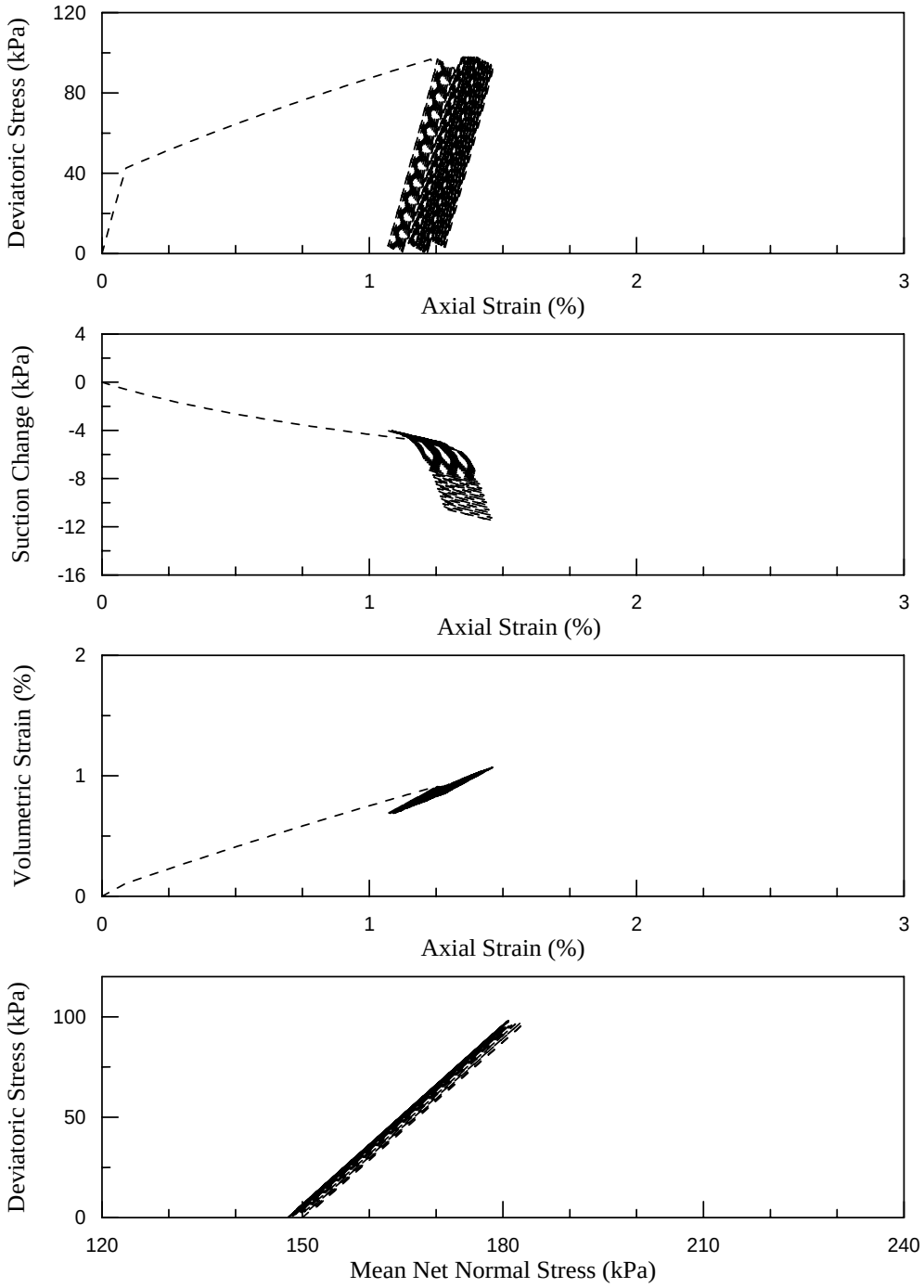


**Fig. 5.16b** Model predictions for CU cyclic Test No.15 on Minco silt

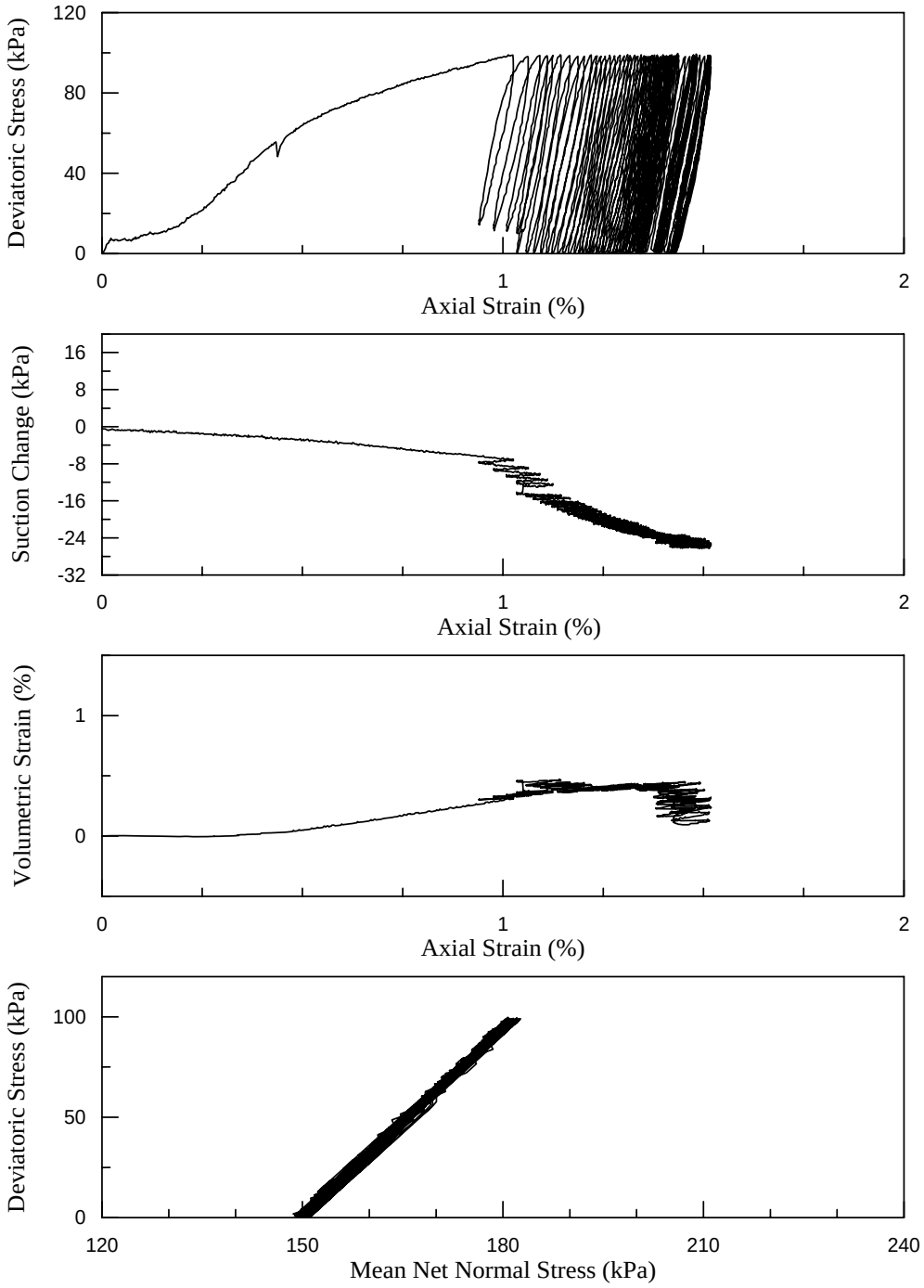


**Fig. 5.17a** CU cyclic test results for Test No.20 on Minco silt (Vinayagam, 2004)

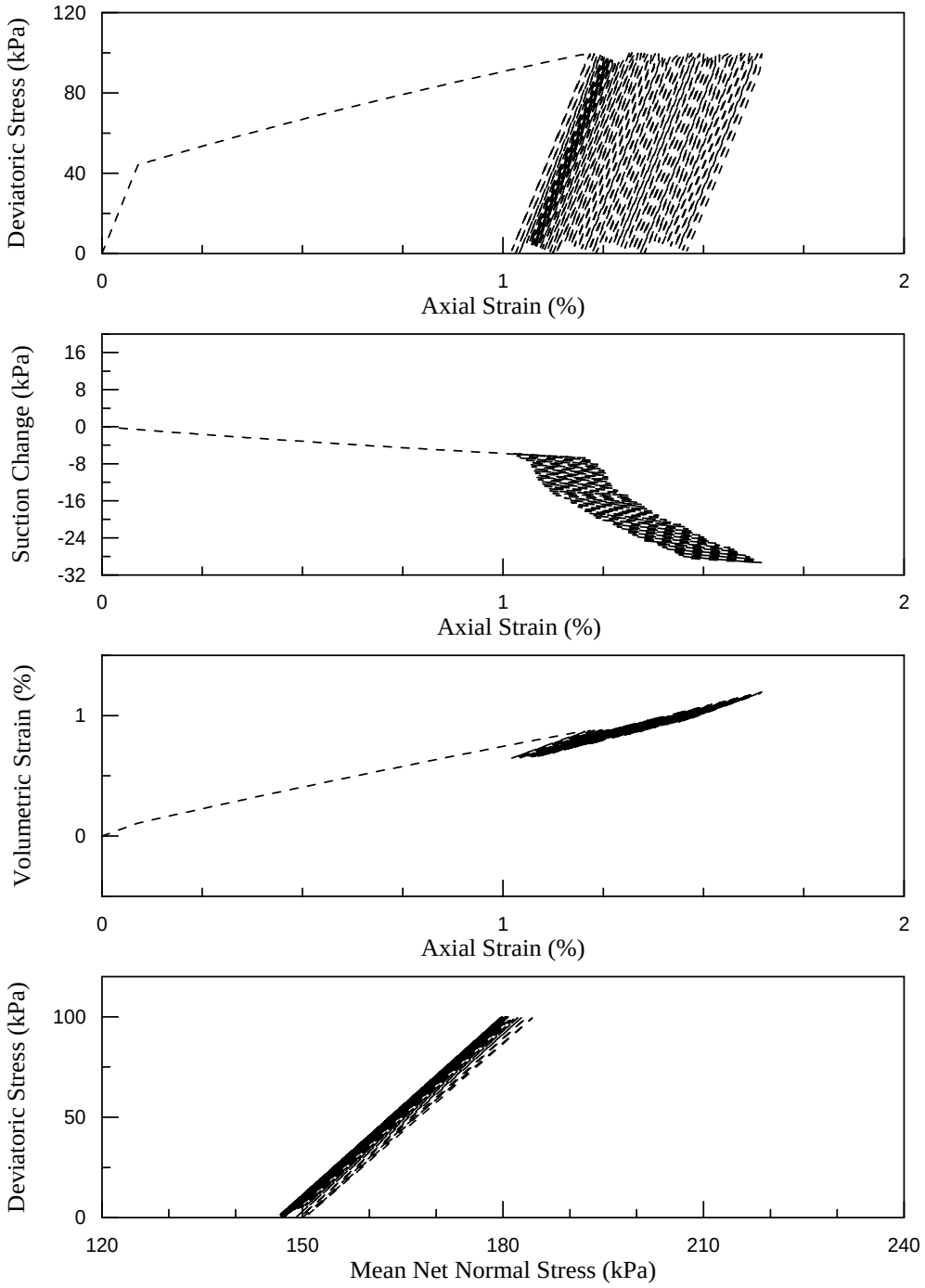


**Fig. 5.17b** Model predictions for CU cyclic Test No.20 on Minco silt

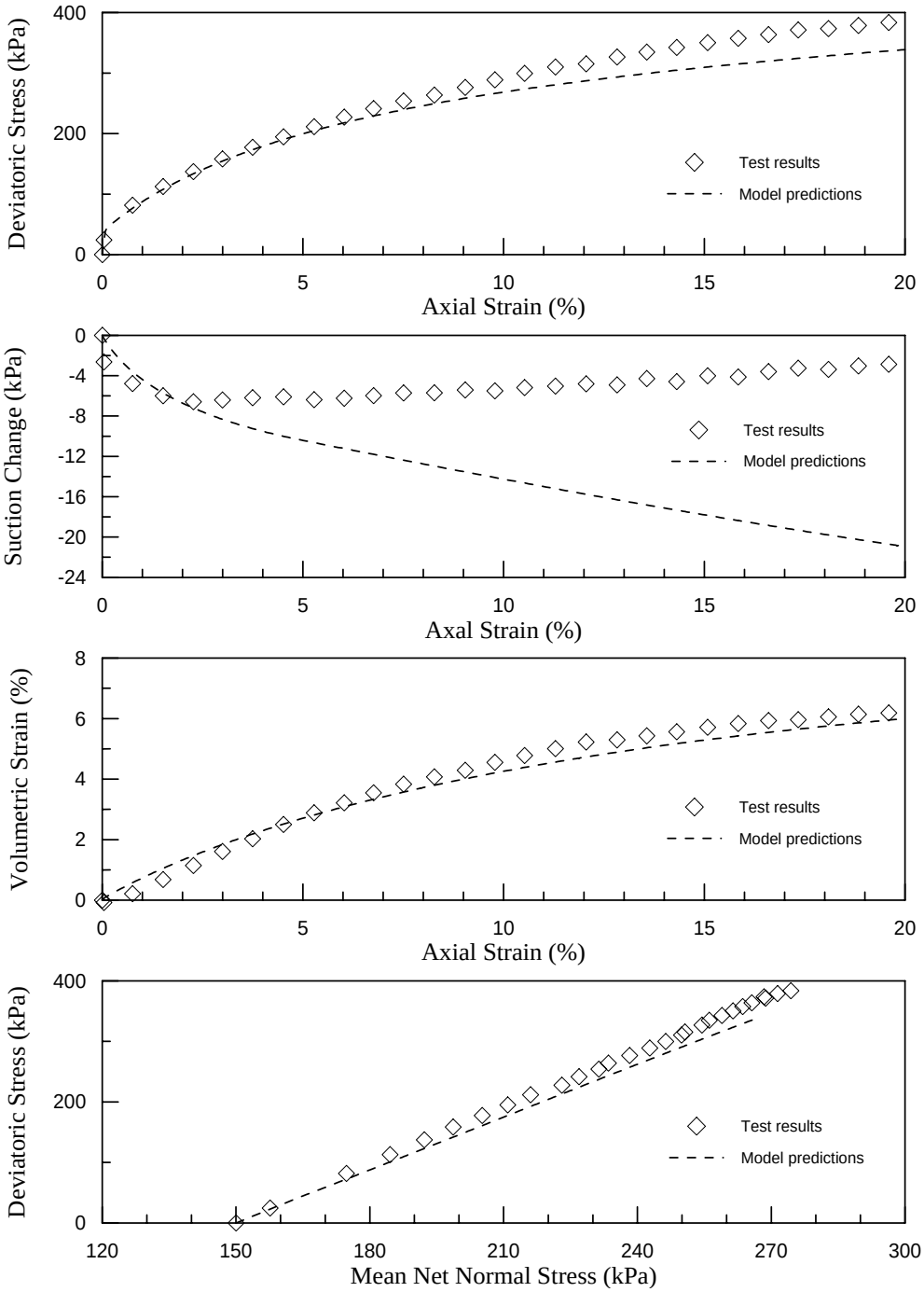


**Fig. 5.18a** Model predictions and CU test results for Test No.22 on Minco silt

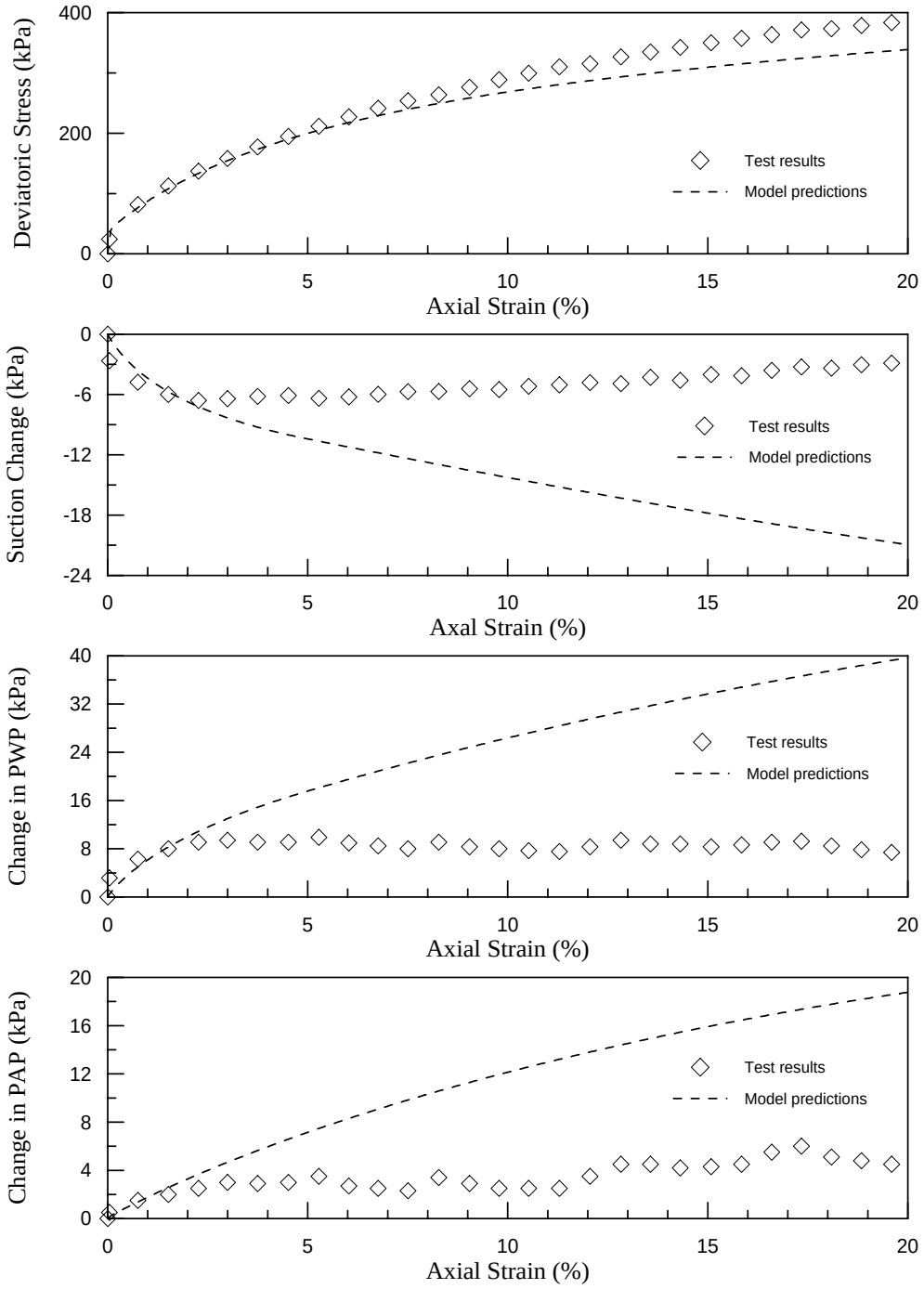


**Fig. 5.18b** Model predictions and CU test results for Test No.22 on Minco silt

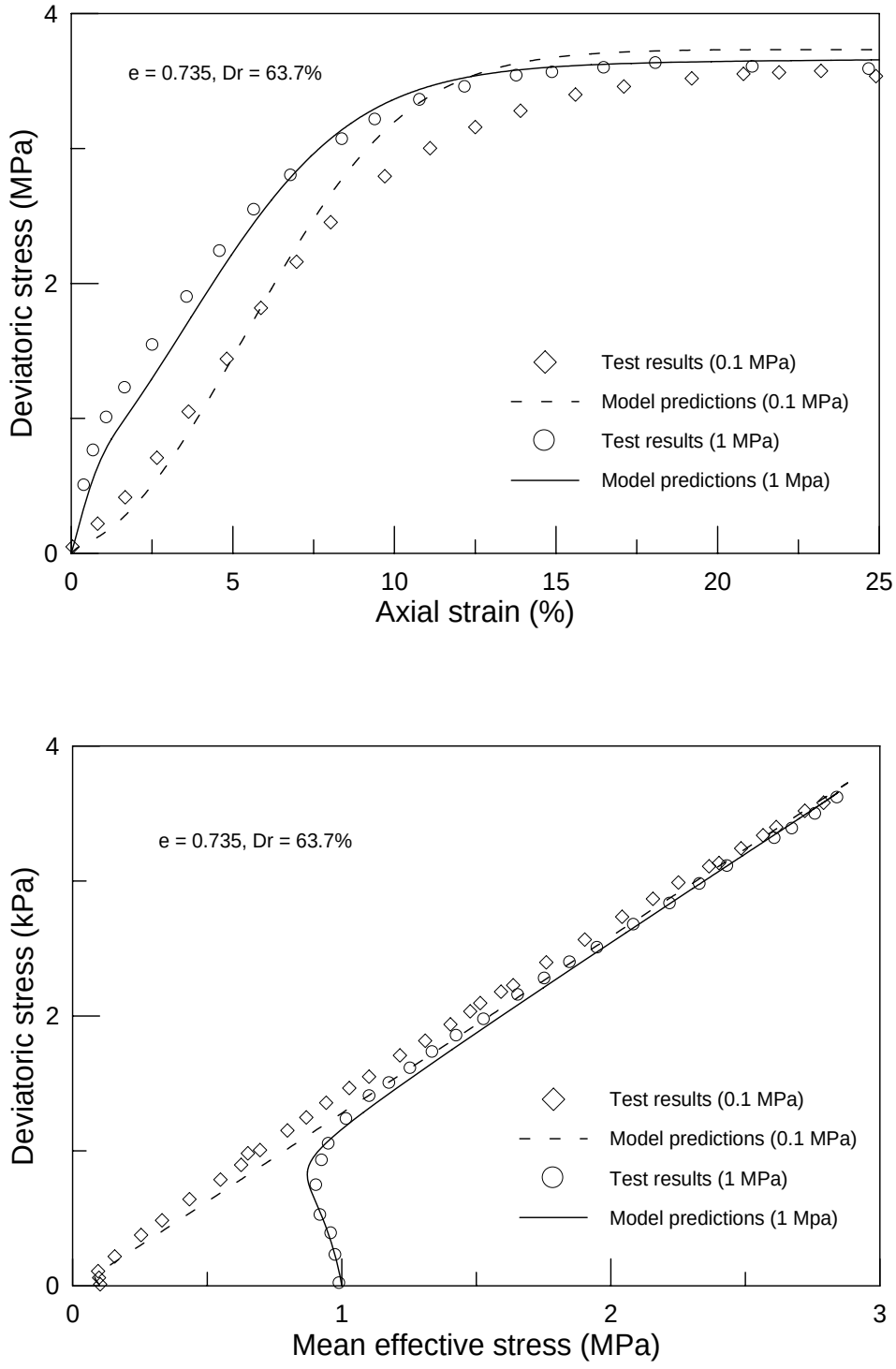


**Fig. 5.19** Saturated undrained Toyoura sand ($e$ = 0.735) behavior under initial effective stresses of 0.1 *MPa* and *1 MPa*

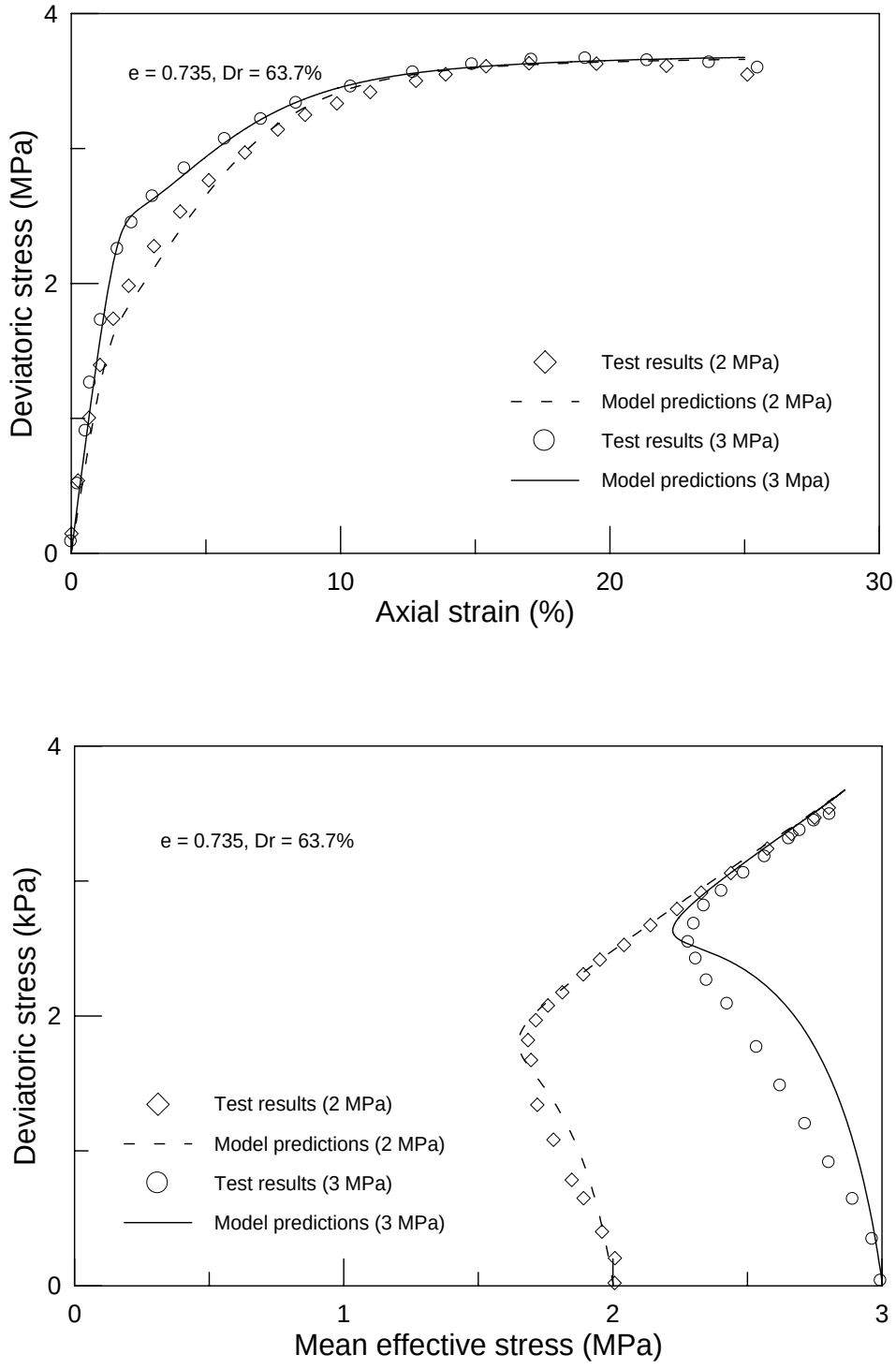


**Fig. 5.20** Saturated undrained Toyoura sand ($e$ = 0.735) behavior under initial effective stresses of 2 *MPa* and 3 *MPa*

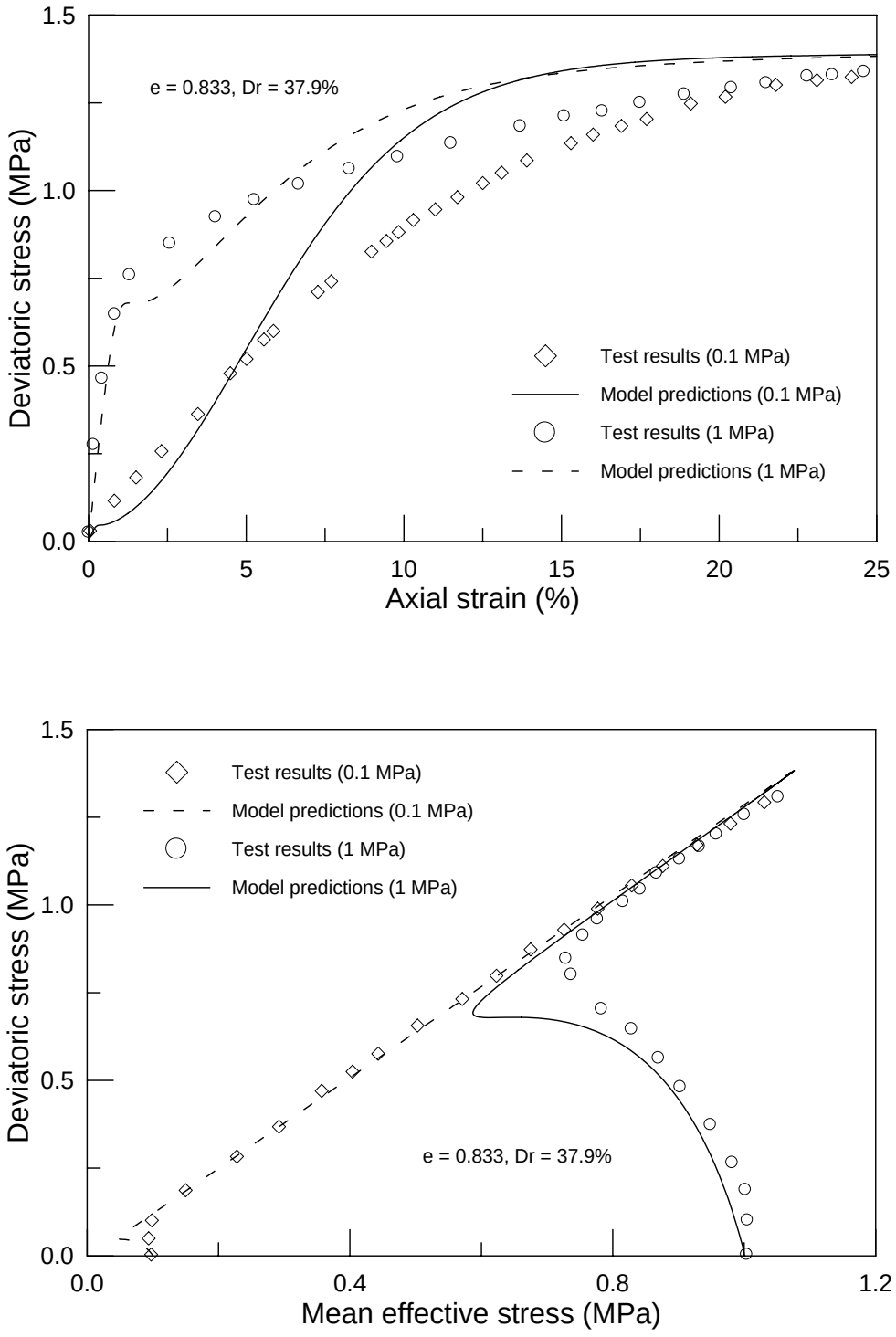


**Fig. 5.21** Saturated undrained Toyoura sand ($e$ = 0.833) behavior under initial effective stresses of 0.1 *MPa* and 1 *MPa*

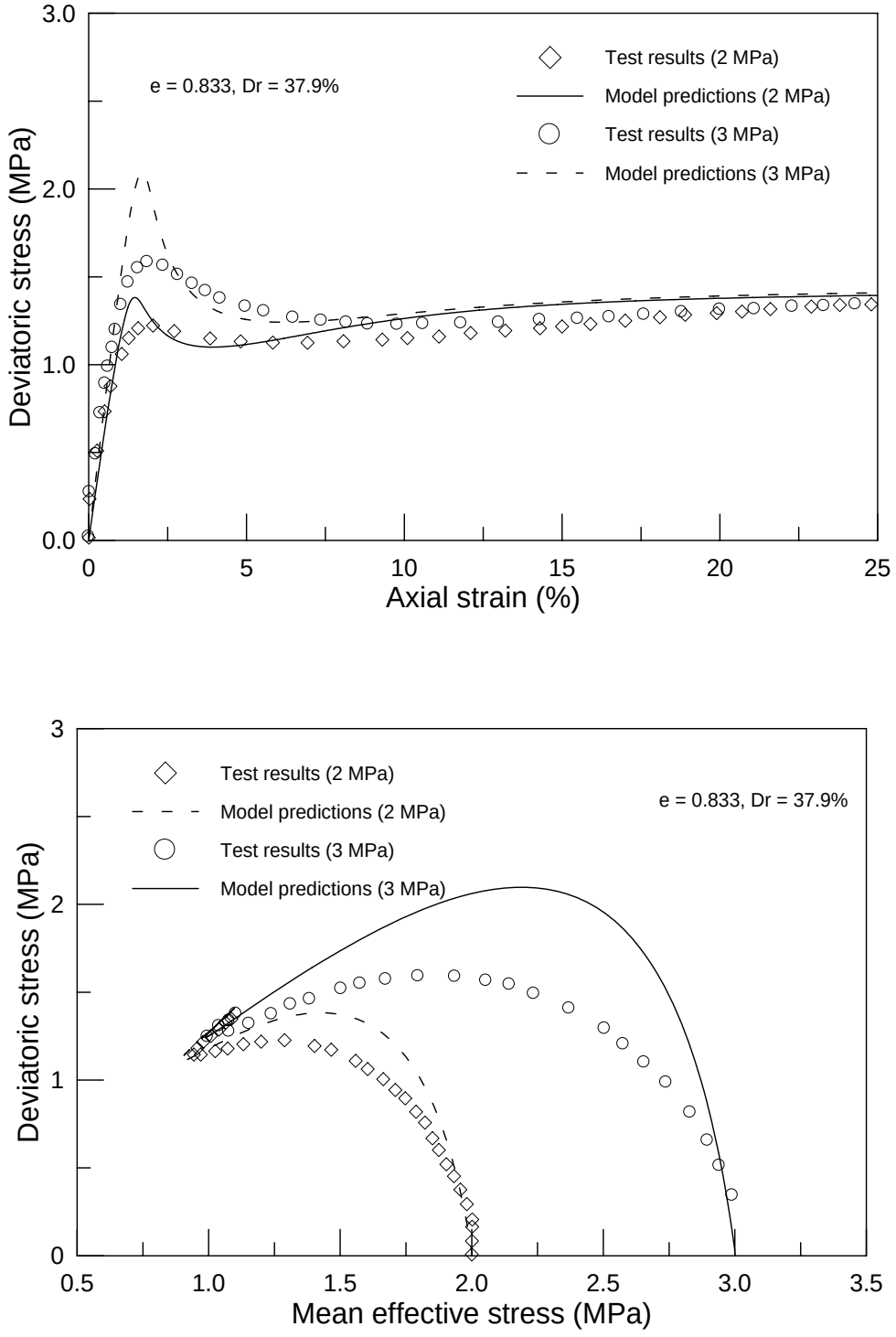


**Fig. 5.22** Saturated undrained Toyoura sand ($e$ = 0.833) behavior under initial effective stresses of 2 *MPa* and 3 *MPa*

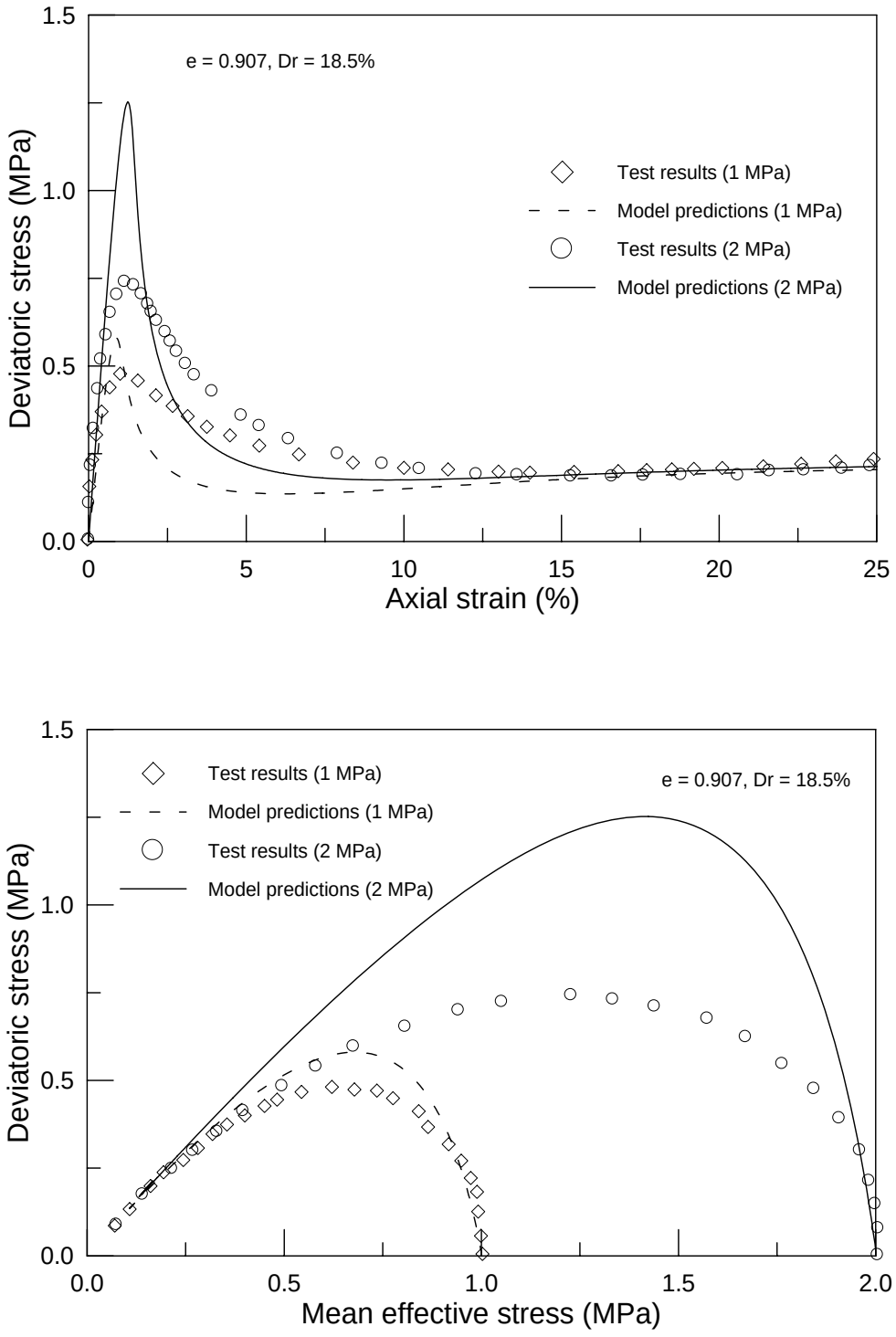


**Fig. 5.23** Saturated undrained Toyoura sand ($e$ = 0.907) behavior under initial effective stresses of 1 *MPa* and 2 *MPa*

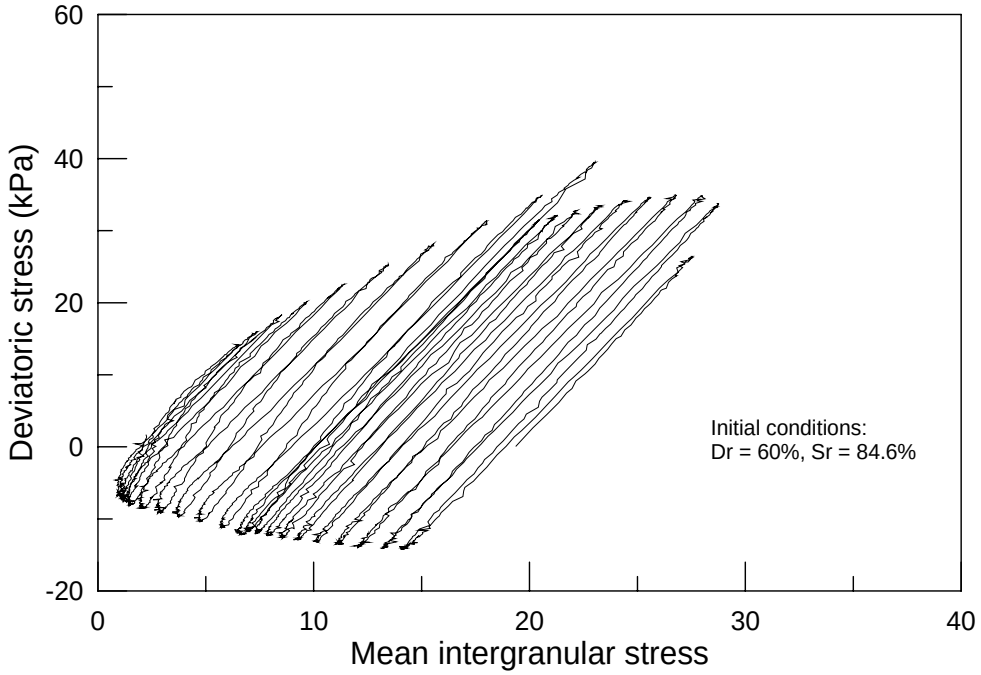


**Fig. 5.24a** Unsaturated test results ( $p' - q$ ) for Toyoura sand (Unno *et al.*, 2008)

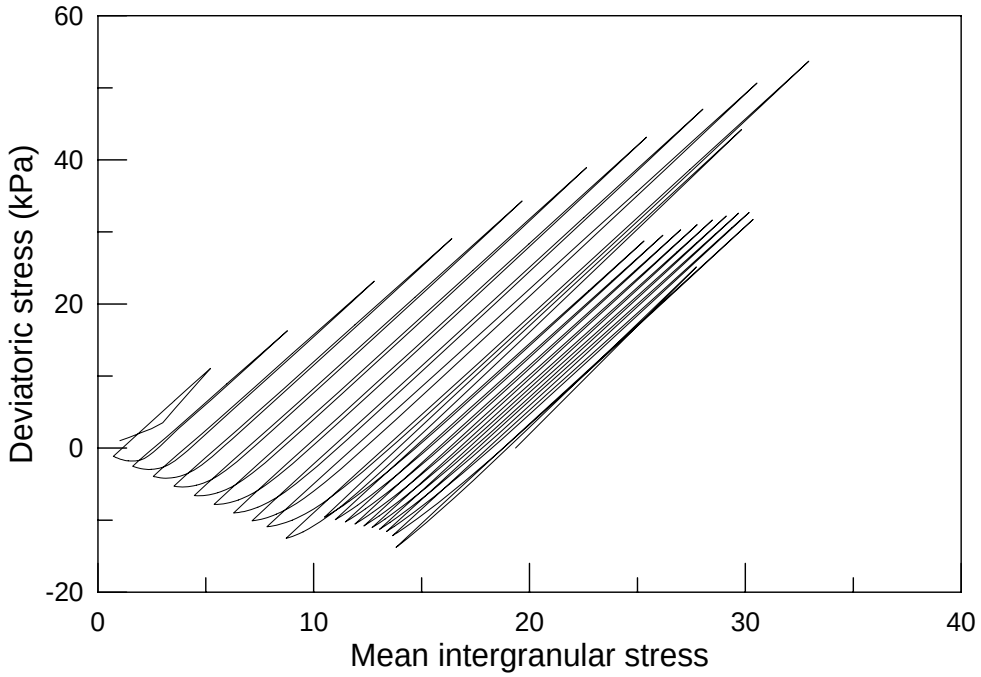


**Fig. 5.24b** Unsaturated model predictions ( $p' - q$ ) for Toyoura sand

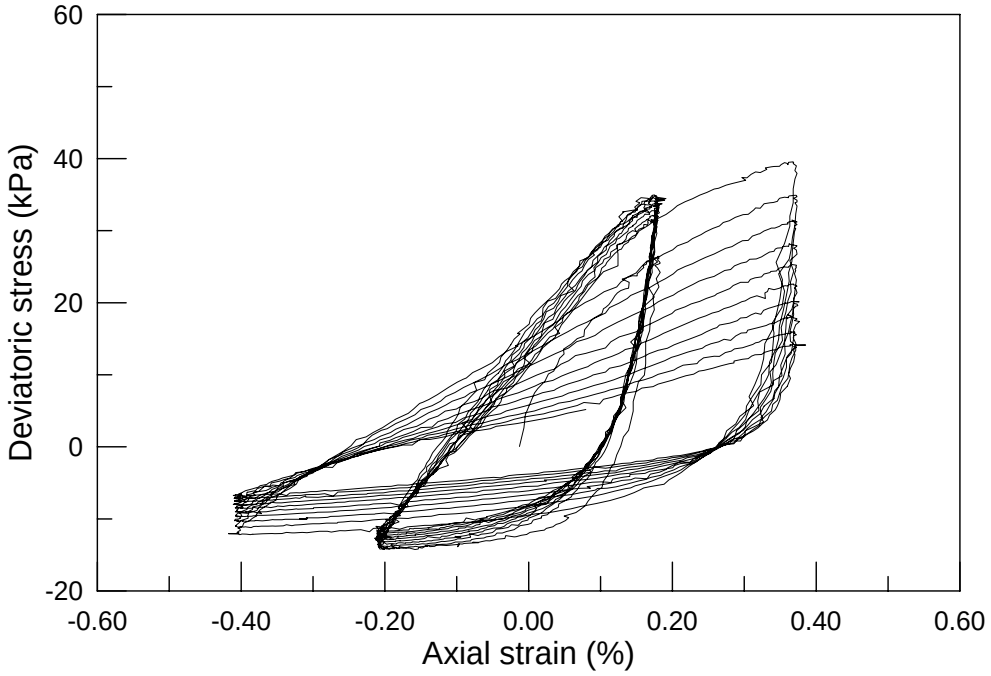


**Fig. 5.25a** Unsaturated test results ( $\varepsilon_a - q$ ) for Toyoura sand (Unno *et al.*, 2008)

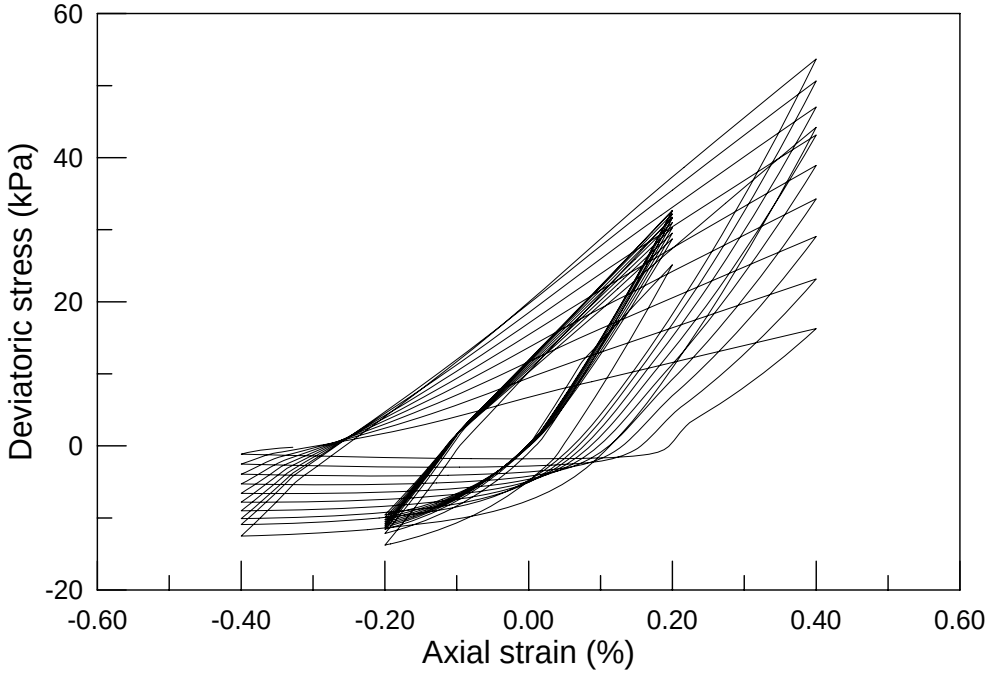


**Fig. 5.25b** Unsaturated model predictions ( $\varepsilon_a - q$ ) for Toyoura sand

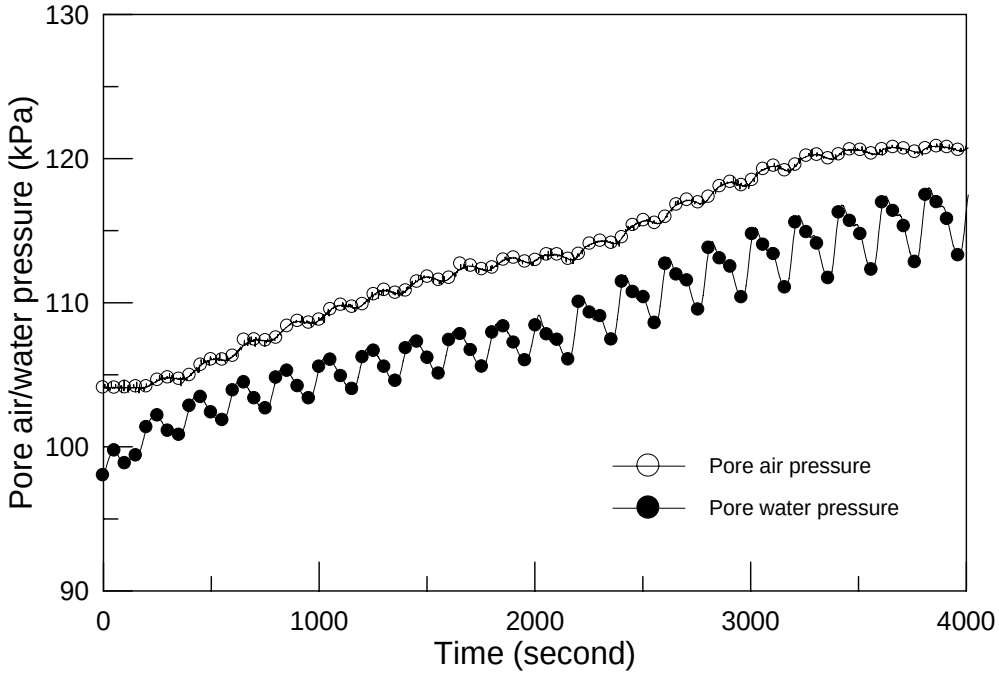


**Fig. 5.26a** Pore air/water pressure for Toyoura sand (Unno *et al.*, 2008)

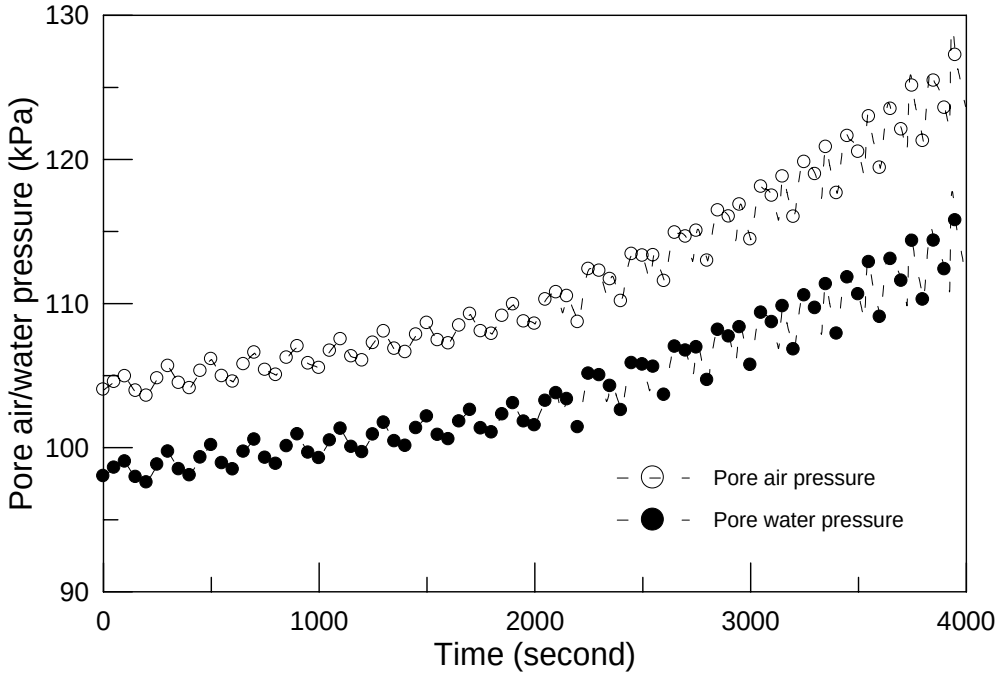


**Fig. 5.26b** Model predictions of pore air/water pressure for Toyoura sand

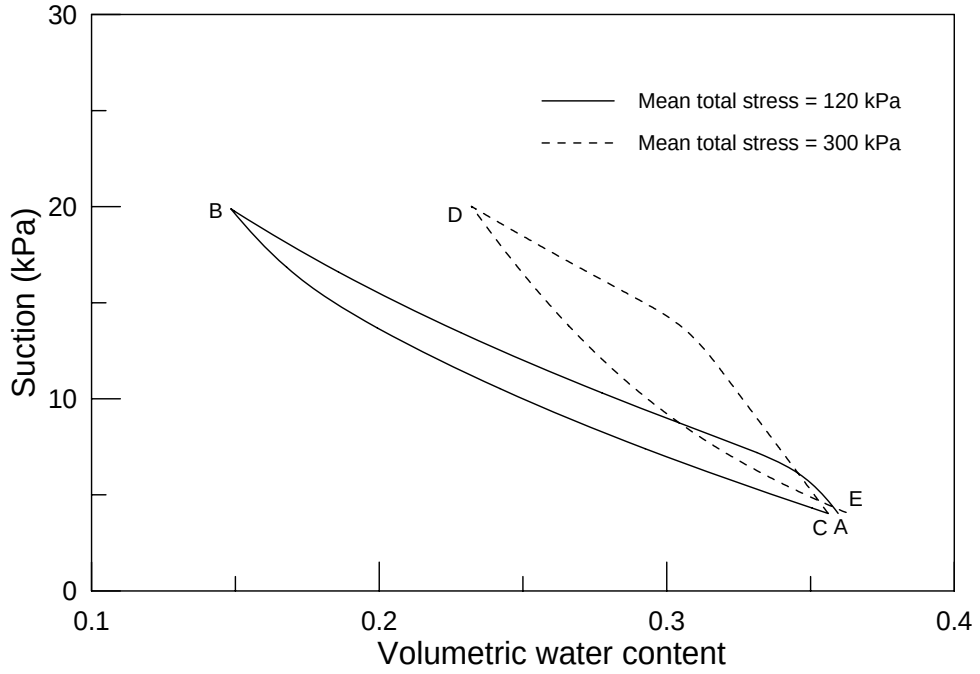


**Fig. 5.27** Demonstration of influence of stress state on SWCCs

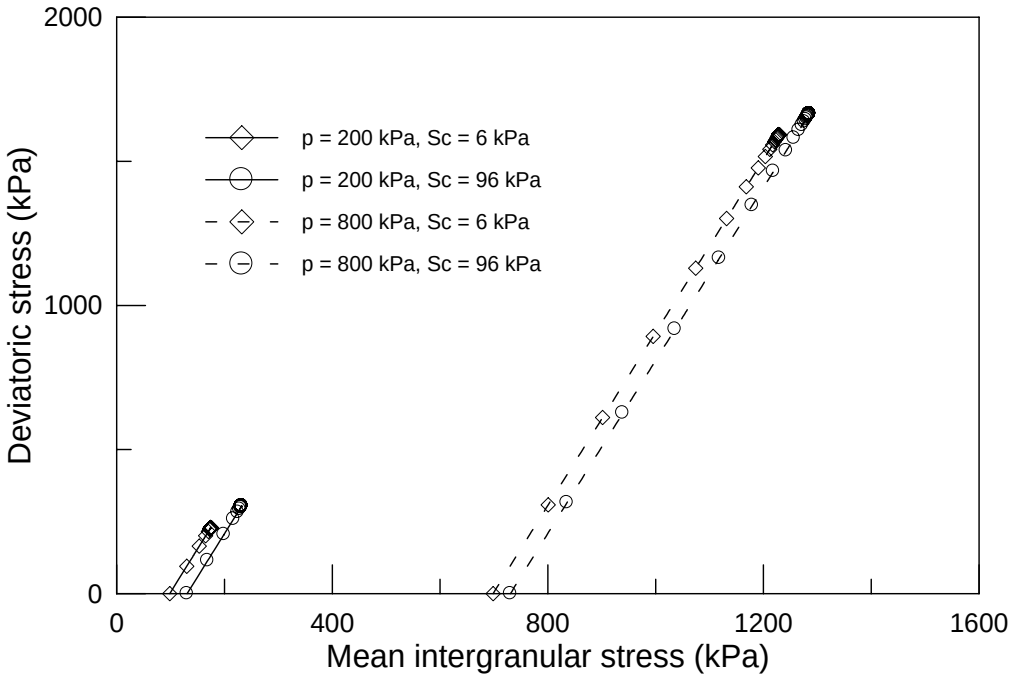


**Fig. 5.28** $p' - q$ under different total stresses and suctions

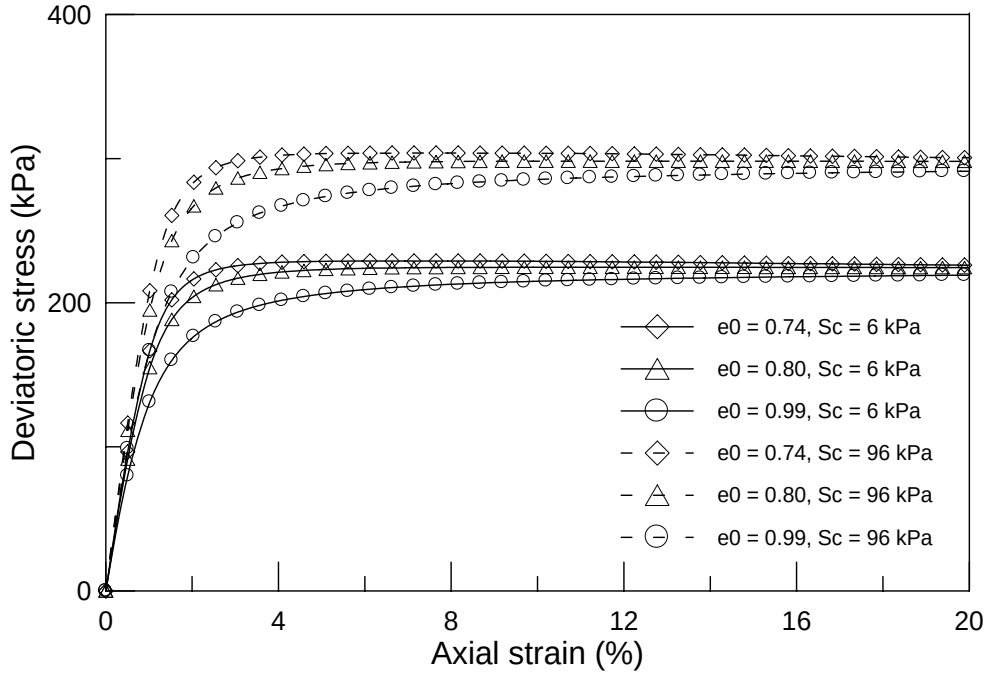


**Fig. 5.29** $\varepsilon_a - q$ under mean total stress of 200 *kPa*

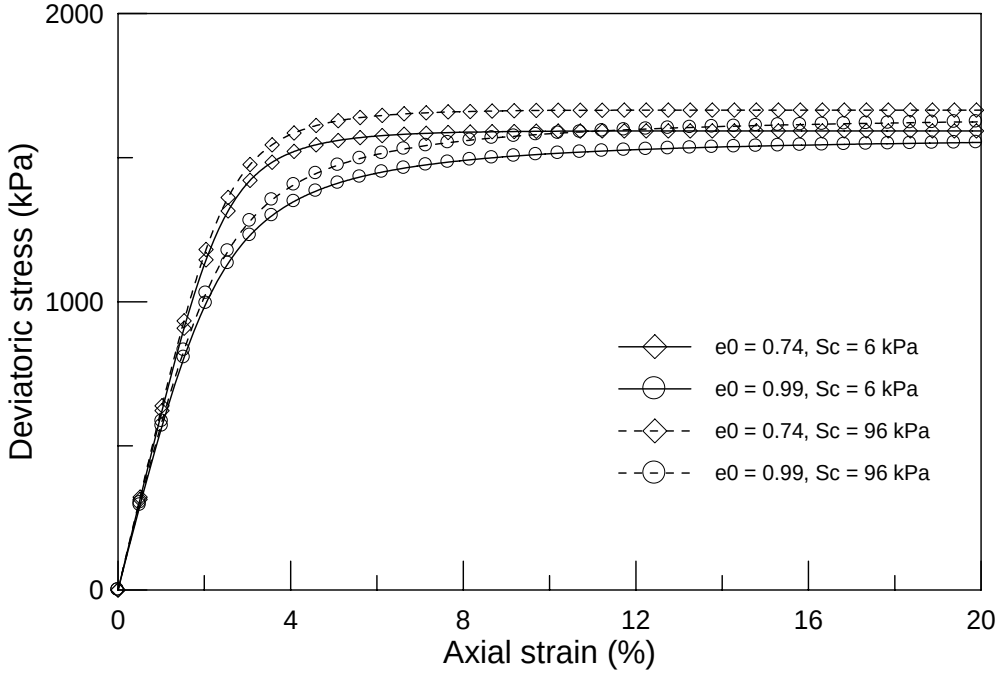


**Fig. 5.30** $\varepsilon_a - q$ under mean total stress of 800 *kPa*

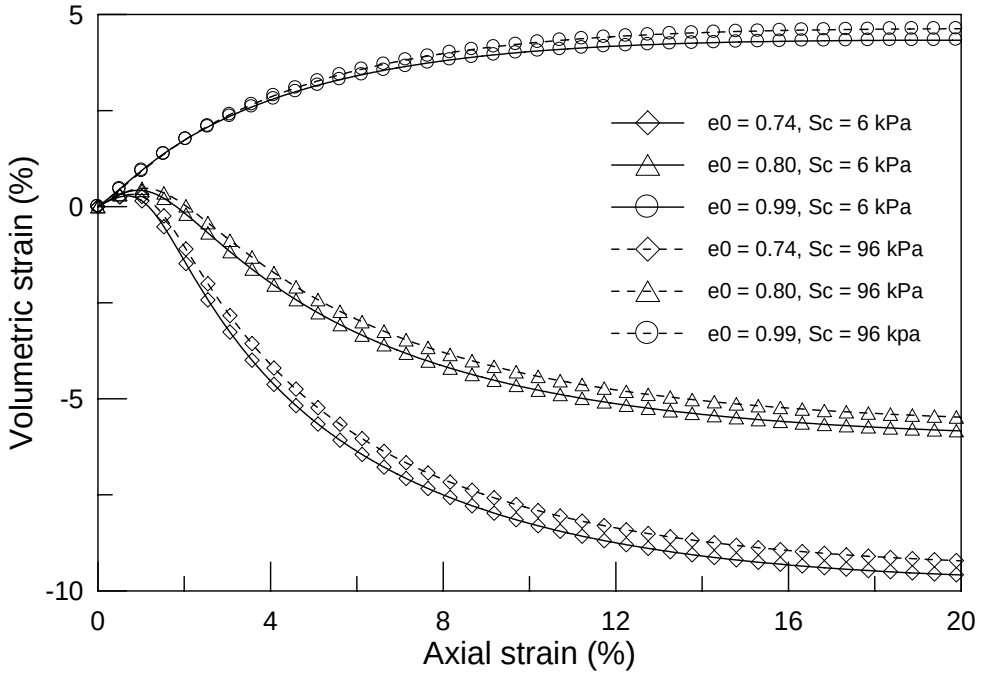


**Fig. 5.31** $\varepsilon_a - \varepsilon_v$ under mean total stress of 200 *kPa*

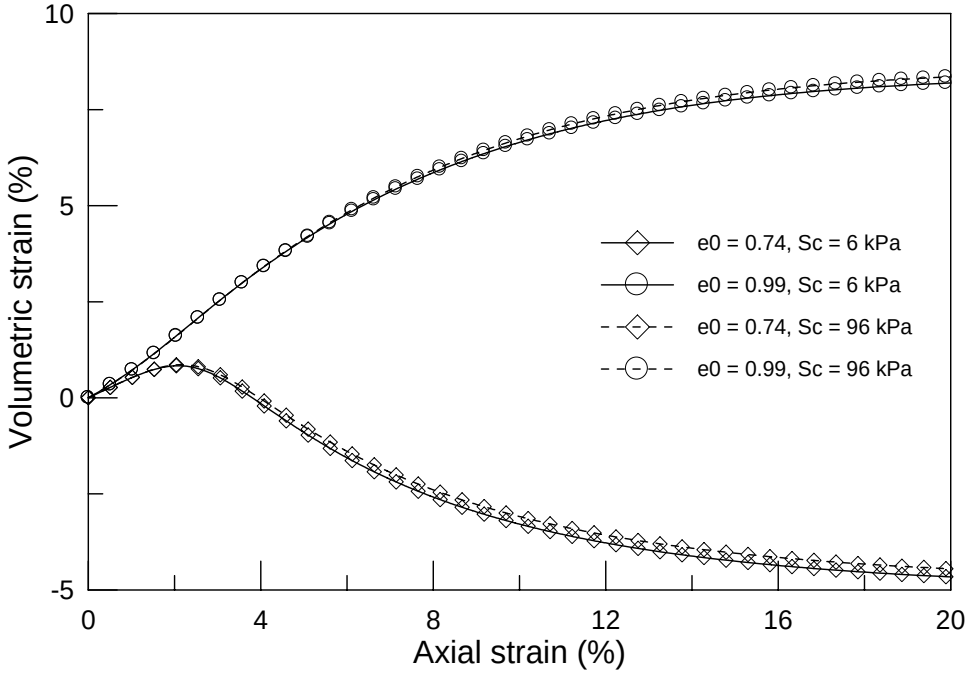


**Fig. 5.32** $\varepsilon_a - \varepsilon_v$ under mean total stress of 800 *kPa*

# CHAPTER 6

# CONCLUSIONS AND RECOMMENDATIONS

## 6.1 CONCLUSIONS

The following conclusions can be drawn based on the current research:

1. A comprehensive constitutive model for unsaturated sands/silts in general stress space has been presented for the first time;
2. The appropriate selection of stress-strain variables is one of the most important steps required in the development of a sound constitutive model for unsaturated soils. With the appropriate selection of stress-strain variables, some important concepts, such as critical state and phase transformation line can be directly extended from saturated soils to unsaturated soils. The stress-strain variables for modeling unsaturated soils should be consistent with thermodynamic considerations;
3. To account for the coupling effects between mechanical and hydraulic behavior of unsaturated soils, it is necessary to include a practical hysteresis model for SWCCs;

4. In addition to the appropriate selection of stress-strain variables and the hysteretic SWCCs model, the proposed hardening laws are the key to predicting the coupled hydraulic and mechanical behavior of unsaturated sands and silts;
5. The soil deformation has a strong influence on the evolution of SWCCs in unsaturated soils. The effect of suction on the sand deformation may not be as significant as the effect of soil deformation on the SWCCs in sands;
6. Liquefaction not only occurs in saturated sands, but also in unsaturated sands;
7. Under cyclic loadings, the stress-strain curves in unsaturated silts and sands show stabilization.

## 6.2 RECOMMENDATIONS FOR FUTURE RESEARCH

The following research may be carried out to improve current research on modeling unsaturated sands and silts:

1. In the proposed model, the capillary elastic modulus $\Gamma^e$ and residual volume fraction of water $n_{wr}$ are assumed to be constant for simplicity. As discussed in Chapters 3 and 5, $\Gamma^e$ may change with suction and $n_{wr}$ may be related to the soil deformation. Note that $n_{wr}$ had to be changed to make better predictions for the OU mixture. Although the new functional forms of $\Gamma^e$ and $n_{wr}$ will increase the complexity of the model, the model performance should definitely be enhanced.

2. Although the proposed SWCCs model can well simulate the suction-water content relationships for most of the soils, the thermodynamic basis of the hysteresis of SWCCs or the physical explanation on the hysteresis will definitely help understand the mechanism behind the hysteretic phenomenon. More experimental and theoretical research is needed to investigate the hysteresis of SWCCs. The related topic on SWCCs has a broad application in geotechnical engineering, geoenvironmental engineering, petroleum engineering and many other fields;
3. Given the fact that very limited test results are available on the coupling effects between the mechanical and hydraulic behavior of unsaturated soils, especially sands and silts, a systematic experimental investigation on unsaturated sands and silts is strongly suggested;
4. The proposed unsaturated soil model is basically for sands or silts, not clays. In near future, a unified unsaturated soil model, which covers sands, silts and especially clays, is desired. It is beneficial to treat all the soils in a unified framework;
5. The proposed unsaturated soil model has only been investigated on the single element level. It will be beneficial to implement the current model into a finite element program to examine some boundary and initial value problems. Some potential application in practice is highly desired;
6. Liquefaction in unsaturated sands has not been extensively investigated. The importance of liquefaction in unsaturated sands has not drawn enough attention in the geotechnical engineering community. It would be valuable to carry out more research on liquefaction in unsaturated sands and silts both experimentally and

theoretically. Liquefaction of unsaturated sands and silts has important practical applications, especially for geotechnical engineering structures subjected to earthquake;

7. Fabric has a strong effect on the sand and silt behavior, especially when liquefaction is of interest. Although some issues on the fabric have been studied recently, extensive investigation on the fabric of sands has not yet been carried out. Some topics, such as the selection of internal variables to capture the fabric effects and the evolution of the fabric tensor, are just beginning to get attention from soil science community and geotechnical community.

# REFERENCES


Adams, B.A., 1996. Critical state behaviour of an agricultural soil. Ph.D. dissertation, University of Saskatchewen, Saskatoon, Canada

Adamson, A.W., 1990. Physical chemistry of surfaces, 5th edition, Wiley Interscience, New York

Aitchison, G.D., 1967. Separate roles of site investigation, quantification of soil properties, and selection of operational environment in the determination of foundation design on expansive soils. *Proc. 3rd Asian Reg. Conf. Soil Mech. Found. Eng.*, Israel, Vol. 3, 72-77

Aitchison, G.D. and Donald, I.B., 1956. Some preliminary studies of unsaturated soils. *Proc. 2nd Australia-New Zealand Conf. Soil Mech. Found. Engng.*, Christchurch, 192-199

Alawaji, H.A.S., Runesson, K. and Sture, S., 1991. Integration of constitutive equations in soil plasticity. *ASCE J. Engng Mech.*, 117(8), 1771-1790

Alonso, E.E., Gens, A. and Josa, A., 1990. A constitutive model for partially saturated soils. *Géotechnique*, 40(3), 405-430

Alonso, E.E., Vaunat, J. and Gens, A., 1999. Modelling the mechanical behaviour of expansive clays. *Engng. Geol.*, 54, 173-183

Anandarajah, A. and Dafalias, Y.F., 1986. Bounding surface plasticity. III: application to anisotropic cohesive soils. *J. Engng. Mech.*, ASCE, 112(12), 1292-1318

Ananthanathan, P.J., 2002. Laboratory testing of unsaturated Minco silt. Master thesis, University of Oklahoma, Norman, Oklahoma

Arulmoli, K., Muraleetharan, K.K., Hossain, M.M. and Fruth, L.S., 1992. VELACS: Verification of liquefaction analysis by centrifuge studies, laboratory testing program, soil data report. Technical report, the Earth Technology Corporation, Irvine, California

Barbour, S.L., 1998. Nineteenth Canadian geotechnical colloquium: the soil-water characteristic curve: a historical perspective. *Can. Geotech. J.*, 35, 873-894

Barden, L., Madedor, A.O. and Sides, G.R., 1969. Volume change characteristics of unsaturated clay. *J. Soil Mech. Found. Engng.*., ASCE, 95(SM1), 33-52

Bardet, J.P., 1986. Bounding surface plasticity model for sands. *J. Engng. Mech.*, ASCE, 112(11), 1198-1217

Bardet, J.P., 1990. Hypoplastic model for sands. *J. Engng. Mech.*, ASCE, 116(9), 1973-1994

Bear, J., 1972. Dynamics of fluids in porous media. Dover Publications, Inc., New York.

Been, K. and Jefferies, M.G., 1985. A state parameter for sands. *Géotechnique*, 35(2), 99-112

Been, K., Crooks, J.H.A., Becker, D.E. and Jefferies, M.G., 1986. The cone penetration test in sands: Part I, state parameter interpretation. *Géotechnique*, 36(2), 239-249

Beese, F., van der Ploeg, R.R., 1976. Influence of hysteresis on moisture flow in an undisturbed soil monolith. *Soil Sci. Soc. Am. J.*, 40, 480-484

Biot, M.A., 1941. General theory of three-dimensional consolidation. *J. Applied Physics*, 12, 155-164

Bishop, A.W., 1959. The principle of effective stress. *Tek. Ukebl.*, 106(39), 113-143

Bishop, A.W. and Blight, G.E., 1963. Some aspects of effective stress in saturated and partly saturated soils. *Géotechnique*, 13, 177-197.

Bishop, A.W. and Donald, I.B., 1961. The experimental study of partly saturated soils in triaxial apparatus. *Proc. 5th Int. Conf. Soil Mech. Found. Engng.*, Vol. 1, 13-21

Blight, G.E., 1967. Effective stress evaluation for unsaturated soils. *J. Soil Mech. Found. Engng.*, ASCE, 93(SM2), 125-148

Bluhm, J. and de Boer, R., 1996. Effective stresses – a clarification. *Arch. Applied Mech.*, 66(7), 479-492

Bolzon, G., Schrefler, B.A. and Zienkiewicz, O.C., 1996. Elastoplastic soil constitutive laws generalized to partially saturated states. *Géotechnique*, 46(2), 279-289

Booth, A.R., 1975. The factors influencing collapse settlement in compacted soils. *Proc. 6th Regional Conf. for Africa on Soil Mech. Found. Engng.*, Durban, Vol. 1, 57-63

Borja, R.I., 1990. Cam-clay plasticity, Part I: implicit integration of constitutive relations. *Comp. Methd. Applied Mech. Engng.*, 78, 49-72

Borja, R.I., 1991. Cam-clay plasticity, Part II: implicit integration of constitutive equation based on a nonlinear elastic stress predictor. *Comp. Methd. Applied Mech. Engng.*, 88, 225-240

Borja, R.I., 2006. On the mechanical energy and effective stress in saturated and unsaturated porous continua. *Int. J. Solids Structures*, 43, 1764-1786

Braddock, R.D., Parlange, J.Y. and Lee, J., 2001. Application of a soil water hysteresis model to simple water retention curves. *Transport in Porous Media*, 44, 407-420

Braudel, H.J., Abouaf, M. and Chenot, J.L., 1986. An implicit and incremental formulation for the solution of elastoplastic problems by the finite element method. *Comp. Struct.*, 22, 801-814

Brooks, R.H. and Corey, A.T., 1964. Hydraulic properties of porous medium. *Hydrology paper No. 3*, Civil Engineering Department, Colorado State University

Celes, J.D., 1996. Measurement of soil suction and water coefficient of permeability as functions of moisture content in unsaturated soils. *A research paper presented at the University of Oklahoma Undergraduate Research Day*.

Chen, L.X., 2006. Hysteresis and dynamic effects in the relationship between capillary pressure, saturation, and air-water interfacial area in porous media. Ph.D. dissertation, University of Oklahoma, Norman, Oklahoma

Chen, L.X., Miller, G.A., Kibbey, T.C.G., 2007. Rapid pseudo-static measurement of hysteretic capillary pressure-saturation relationships in unconsolidated porous media. *ASTM Geotech. Test. J.*, 30(6), 1-10

Cheng, J.T., Pyrak-Nolte, L.J., Nolte, D.D. and Giordano, N.J., 2004. Linking pressure and saturation through interfacial areas in porous media. *Geophys. Res. Lett.*, 31, L08502

Chiu, C.F. and Ng, C.W.W., 2003. A state-dependent elasto-plastic model for saturated and unsaturated soils. *Géotechnique*, 53, 809-829

Clothier, B.E. and Smettem, K.R.J., 1990. Combining laboratory and field measurements to define the hydraulic properties of soil. *Soil Sci. Soc. Am. J.*, 54(2), 299-304

Coleman, J.D., 1962. Stress-strain relations for partially saturated soils. *Géotechnique*, 12(4), 348-350

Collins, I.F. and Kelly, P.A., 2002. A thermomechanical analysis of a family of soil models. *Géotechnique*, 52(7), 507-518

Coussy, O. and Dangla, P., 2002. Approche énergétique du comportement des sols non saturés. In *Mécanique des sols non saturés*, Coussy and Fleureau (ed.), Hermes Science Publications, Paris

Cox, D.W., 1978. Volume change of compacted clay fill. *Clay Fills*, 79-86, London

Croney, D., 1952. The movement and distribution of water in soils. *Géotechnique*, 3, 1-16

Croney, D. and Coleman, D.J., 1961. Pore pressure and suction in soils. In *Proceedings of the Conference on Pore Pressure and Suction in Soils*. Butterworths, London

Croney, D., Coleman, D.J. and Black, W.P.M., 1958. Movement and distribution of water in soil in relation to highway design and performance. *Water and Its Conduction in Soils,* Highway Res. Board, Special Report No. 40, Washington, DC, 226-252

Crouch, R.S. and Wolf, J.P., 1994a. Unified 3D critical-state bounding-surface plasticity model for soils incorporating continuous plastic loading under cyclic paths. Part I: constitutive relations. *Int. J. Numer. Anal. Meth. Geomech.*, 18(11), 735-758

Crouch, R.S. and Wolf, J.P., 1994b. Unified 3D critical-state bounding-surface plasticity model for soils incorporating continuous plastic loading under cyclic paths. Part II: calibration and simulations. *Int. J. Numer. Anal. Meth. Geomech.*, 18(11), 759-784

Crouch, R.S., Wolf, J.P. and Dafalias, Y.F., 1994. Unified critical-state bounding-surface plasticity model for soil. *J. Engng. Mech.*, ASCE, 120(11), 2251-2270

Cui, Y.J. and Delage, P., 1996. Yielding and plastic behaviour of an unsaturated compacted silt. *Géotechnique*, 46(2), 291-311

Dafalias, Y.F., 1986. Bounding surface plasticity. I: mathematical foundation and hypoplasticity. *J. Engng. Mech.*, ASCE, 112(9), 966-987

Dafalias, Y.F. and Herrmann, L.R., 1982. Bounding surface formulation of soil plasticity. In *Soil Mechanics-Transient and Cyclic Loads*, Pande and Zienkiewicz (ed.), John Wiley & Sons Ltd.

Dafalias, Y.F. and Herrmann, L.R., 1986. Bounding surface plasticity II: Application to isotropic cohesive soils. *J. Eng. Mech.*, ASCE, 112(12), 1263-1291

Dafalias, Y.F. and Manzari, M.T., 1999. Modeling of fabric effect on the cyclic loading response of granular soils. *Proc. ASCE 13$^{th}$ Engng. Mech. Conf.*, Baltimore, Maryland

Dafalias, Y.F. and Manzari, M.T., 2004. Simple plasticity sand model accounting for fabric change effects. *J. Engng. Mech.*, 130(6), 622-634

Dafalias, Y.F., Papadimitriou, A.G. and Li, X.S., 2004. Sand plasticity model accounting for inherent fabric anisotropy. *J. Engng. Mech.*, 130(11), 1319-1333

Dafalias, Y.F. and Popov, E.P., 1975. A model of nonlinearly hardening materials for complex loading. *Acta Mech.*, 21, 173-192

Dafalias, Y.F. and Popov, E.P., 1976. Plastic internal variables formalism of cyclic plasticity. *J. Appl. Mech.*, ASME, 43, 645-651

Dafalias, Y.F. and Popov, E.P., 1977. Cyclic loading for materials with vanishing elastic regions. *Nucl. Engng. Design*. 41, 293-302

Dane, J.H. and Hruska, S., 1983. In-situ determination of soil hydraulic properties during drainage. *Soil Sci. Soc. Am. J.*, 47, 619-624

Datcheva, M. and Schanz, T., 2003. Anisotropic bounding surface plasticity with rotational hardening for unsaturated frictional materials. *J. Phys. IV France*, 105, 305-312

de Boer, R. and Ehlers, W., 1990. The development of the concept of effective stresses. *Acta Mech.*, 83, 77-92

de F.N. Gitirana, G. and Fredlund, D.G., 2004. Soil-water characteristic curve equation with independent properties. *J. Geotech. Geoenviron. Engng.*, 130(2), 209-212

Desai, C.S., 1974. A consistent finite element technique for work-softening behavior. *Proc. Int. Conf. Comp. Meth. Nonlinear Mech.*, University of Texas at Austin, Texas

Deshpande, S.D., 1997. Static and dynamic centrifuge modeling of unsaturated soil embankment. MS thesis, University of Oklahoma, Norman, Oklahoma

Estabragh, A.R. and Javadi, A.A., 2008. Critical state for overconsolidated unsaturated silty soil. *Can. Geotech. J.*, 45, 408-420

Everett, D.H., 1954. A general approach to hysteresis. Part 3: a formal treatment of the independent domain model of hysteresis. *Trans. Faraday Soc.*, 50, 1077-1096

Everett, D.H., 1955. A general approach to hysteresis. Part 4: an alternative formulation of the domain model. *Trans. Faraday Soc.*, 51, 1551-1557

Farias, M.M., Pinheiro, M. and Neto, M.P.C., 2006. An elastoplastic model for unsaturated soils under general three-dimensional conditions. *Soils Found.*, 46(5), 613-628

Feng, M. and Fredlund, D.G., 1999. Hysteretic influence associated with thermal conductivity sensor measurements. *Proceeding from Theory to the Practice of Unsaturated Soil Mechanics*, in associated with 52nd Can. Geotech. Conference and Unsaturated Soil Group, Regina, 14:2:14-14:2:20

Fleureau, J.M., Kheirbeh-Saoud, S., Soemitro, R. and Taibi, S., 1993. Behavior of clayey soils on drying-wetting paths. *Can. Geotech. J.*, 30(2), 287-296

Fredlund, D.G. and Morgenstern, N.R., 1977. Stress state variables for unsaturated soils. *J. Geotech. Engng.*, ASCE, 103(GT5), 447-466

Fredlund, D.G. and Rahardjo, H., 1993. Soil mechanics for unsaturated soils. John Wiley & Sons, Inc.

Fredlund, D.G. and Xing, A., 1994. Equations for the soil-water characteristic curve. *Can. Geotech. J.*, 31, 521-532

Fredlund, D.G., Xing, A., Fredlund, M.D. and Barbour, S.L., 1995. The relationship of the unsaturated soil shear strength to the soil-water characteristic curve. *Can. Geotech. J.*, 32, 440-448

Gajo, A. and Muir Wood, D., 1999. A kinematic hardening constitutive model for sands: the multiaxial formulation. *Int. J. Numer. Anal. Meth. Geomech.*, 23, 925-965

Gallipoli, D., Gens, A., Chen, G. and D'Onza, F., 2008. Modelling unsaturated soil behaviour during normal consolidation and at critical state. *Computers and Geotechnics*, 35, 825-834

Gallipoli, D., Gens, A., Sharma, R. and Vaunat, J., 2003a. An elasto-plastic model for unsaturated soil incorporating the effects of suction and degree of saturation on mechanical behaviour. *Géotechnique*, 53(1), 123-135

Gallipoli, D., Gens, A., Sharma, R. and Vaunat, J., 2004. An elasto-plastic model for unsaturated soil incorporating the effects of suction and degree of saturation on mechanical behaviour (Discussion by Robles and Hoyos). *Géotechnique*, 54(4), 293-295

Gallipoli, D., Wheeler, S.J. and Karstunen, M., 2003b. Modelling the variation of degree of saturation in a deformable unsaturated soil. *Géotechnique*, 53(1), 105-112

Gandola, F., Debionne, S., Varado, N., Haverkamp, R., Ross, P.J., Sander, G. and Parlange, G.J.Y., 2004. Simple soil water hysteresis prediction model based on theory and geometric scaling. *Geophys. Res. Abs.* (European Geosciences Union), 6, 07289

Geiser, F., Laloui, L. and Vulliet, L., 2000. Modelling the behaviour of unsaturated silt. In *Experimental Evidence and Theoretical Approaches in Unsaturated Soils*, Trento, 155-175

Geiser, F., Laloui, L. and Vulliet, L., 2006. Elasto-plasticity of unsaturated soils: laboratory test results on a remoulded silt. *Soils Found.*, 46(5), 545-556

Gens, A. and Alonso, E.E., 1992. A framework for the behaviour of unsaturated expansive clays. *Can. Geotech. J.*, 29, 1013-1032

Gillham, R.W., Klute, A. and Heermann, D.F., 1976. Hydraulic properties of a porous medium: measurement and empirical representation. *Soil Sci. Soc. Am. J.*, 40(2), 203-207

Goddard, J.D., and Didwania, A.K., 1998. Computations of dilatancy and yield surfaces for assemblies of rigid frictional spheres. *Quarterly J. Mech. Applied Math.*, 51(1), 15-43

Gray, W.G. and Hassanizadeh, S.M., 1989. Averaging theorems and averaged equations for transport of interface properties in multiphase system. *Int. J. Multiphase Flow*, 15, 81-95

Gray, W.G. and Schrefler, B.A., 2001. Thermodynamic approach to effective stress in partially saturated porous media. *Eur. J. Mech. A/Solids*, 20, 521-538

Hashiguchi, K., 1978. Plastic constitutive equations of granular materials. *Proc. US-Japan Seminar Continuum Mech. Stast. Appr. Granular Materials*, 321-329

Hashiguchi, K., 1980. Constitutive equations of elastoplastic materials with elastic-plastic transition. *J. Appl. Mech.,* ASME, 47, 266-272

Hashiguchi. K., 1985. Subloading surface model of plasticity. *Proc. 11th Int. Conf. Soil Mech. Found. Eng.*, 127-130

Hashiguchi, K., 1989. Subloading surface model in unconventional plasticity. *Int. J. Solids Struct.*, 25, 917-945

Hashiguchi, K., 1993. Fundamental requirements and formulation of elastoplastic constitutive equations with tangential plasticity. *Int. J. Plasticity*, 9, 525-549

Hashiguchi, K., 2000. Fundamentals in constitutive equation: continuity and smoothness conditions and loading criterion, *Soils Found.*, 40(3), 155-161

Hashiguchi, K. and Chen, Z.P., 1998. Elastoplastic constitutive equation of soils with the subloading surface and the rotational hardening. *Int. J. Numer. Anal. Meth. Geomech.*, 22, 197-227

Hashiguchi, K. and Ueno, M., 1977. Elastoplastic constitutive laws of granular materials. *Proc. 5th Int. Conf. Soil Mech. Found. Engng.*, Tokyo, 73-82.

Hassanizadeh, S.M. and Gray, W.G., 1990. Mechanics and thermodynamics of multiphase flow in porous media including interphase boundaries. *Adv. Water Resour.*, 13(4), 169-186

Hassanizadeh, S.M. and Gray, W.G., 1993. Thermodynamic basis of capillary pressure in porous media. *Water Resour. Res.*, 29, 3389-3405

Haverkamp, R., Arrue, J.L. and Soet, M., 1997. Soil physical properties within the root zone of the vine area of Tomelloso. Local and spatial standpoint. In *Final integrated report of EFEDA II (European Field Experiment in a Desertification Area) Spain*. Santa Olalla (ed.), CEE project n˚ CT920090, Brussels

Haverkamp, R., Reggiani, P., Ross, P.J. and Parlange, J.-Y, 2002. Soil water hysteresis prediction model based on theory and geometric scaling. In: *Environmental Mechanics: Water, Mass and Energy Transfer in the Biosphere*, Raats, Smiles and Warrick (Eds.), AGU Geophysical Monograph, 129, 213-246

Held, R.J. and Celia, M.A., 2001. Modeling support of functional relationships between capillary pressure, saturation, interfacial area and common lines. *Adv. Water Resour.*, 24, 325-343

Henkel, D.J., 1960. The relationships between the effective stresses and water content in saturated clays. *Géotechnique*, 10(2), 41–54

Ho, K.M.Y., Ng, C.W.W., Ho, K.K.S. and Tang, W.H., 2006. State-dependent soil-water characteristic curves (SDSWCCs) of weathered soils. In *Unsaturated Soils 2006*, Miller, Zapata, Houston and Fredlund (ed.), *GSP No. 147*, *Proc. 4th Int. Conf. Unsat. Soils*, Geo-Institute, ASCE, Carefree, Arizona, 2, 1302-1313

Houlsby, G.T., 1979. The work input to a granular material. *Géotechnique*, 29(3), 354-358

Houlsby, G.T., 1997. The work input to an unsaturated granular material. *Géotechnique*, 47(1), 193-196

Hutter, K., Laloui, L. and Vulliet, L., 1999. Thermodynamically based mixture models for saturated and unsaturated soils. *Mech. Cohes. Frict. Mat.*, 4, 295–338

Hyodo, M., Murata, H., Yasufuku, N. and Fujii, T., 1991. Undrained cyclic shear strength and residual shear strain of saturated sand by cyclic triaxial tests. *Soils Found.*, 31(3), 60-76

Hyodo, M., Tanimizu, H., Yasufuku, N. and Murata, H., 1994. Undrained cyclic and monotonic triaxial behaviour of saturated loose sand. *Soils Found.*, 34(1), 19-32

Inel, S. and Lade, P.V., 1997. Rotational kinematic hardening model for sand. Part II characteristic work hardening law and predictions. *Comp. Geotech.*, 21(3), 217-234

Ishihara, K., 1993. Liquefaction and flow failure during earthquakes. *Géotechnique*, 43(3), 351-415

Ishihara, K., Tatsuoka, F. and Yasuda, S., 1975. Undrained deformation and liquefaction of sand under cyclic stresses. *Soils Found.*, 15(1), 29-44

Ishihara, K., Troncoso, J., Kawase, Y. and Takahashi, Y., 1980. Cyclic strength characteristics of tailings materials. *Soils Found.*, 20(4), 127-142

Jardine, R.J., Gens, A., Hight, D.W. and Coop, M.R., 2004. Developments in understanding soil behaviour. In *Advances in Geotechnical Engineering. The Skempton Conference*. Thomas Telford, London

Jennings, J.E., 1961. A revised effective stress law for use in the prediction of the behaviour of unsaturated soils. In *Symposium on pore pressure and suction in soils*, Butterworth: London, 26-30

Jennings, J.E. and Burland, J.B., 1962. Limitations to the use of effective stresses in partially saturated soils. *Géotechnique*, 12, 125-144

Jeremic, B. and Sture, S., 1997. Implicit integrations in elastoplastic geotechnics. *Mech. Cohe. Fric. Materials*, 2(2), 165-183

Josa, A., Alonso, E.E., Lloret, A. and Gens, A., 1987. Stress-strain behaviour of partially saturated soils. *Proc. 9th European Conf. on Soil Mech. Fdn. Engng.*, Dublin, Volume 2, 561-564

Kabilamany, K. and Ishihara, K., 1990. Stress dilatancy and hardening laws for rigid granular model of sand. *Soil Dyn. Earthquake Engng.*, 9(2), 66-77

Kaliakin, V.N., Dafalias, Y.F. and Herrmann, L.R., 1987. Time dependent bounding surface model for isotropic cohesive soils. Notes for a short course held in conjunction with *the 2nd Int. Conf. Constitutive Laws Engng. Materials: Theory and Application*, Tucson, AZ

Kaliakin, V.N. and Dafalias, Y.F., 1990. Verification of the elastoplastic-viscoplastic bounding surface model for cohesive soils. *Soils Found.*, 30(3), 25-36

Karube, D., 1988. New concept of effective stress in unsaturated soil and rock. *Special Technical Publication 977*, ASTM, Philadelphia, 539-552

Khalili, N., Habte, M.A. and Zargarbashi, S., 2008. A fully coupled flow deformation model for cyclic analysis of unsaturated soils including hydraulic and mechanical hystereses. *Computers and Geotechnics*, 35, 872-889

Khalili, N., Geiser, F. and Blight, G.E., 2004. Effective stress in unsaturated soils: review with new evidence. *Int. J. Geomech.*, 4(2), 115-126

Khalili, N. and Khabbaz, M.H., 1998. A unique relationship for $\chi$ for the determination of the shear strength of unsaturated soils. *Géotechnique*, 48(5), 681-687

Khalili, N., Witt, R., Laloui, L., Vulliet, L. and Koliji, A., 2005. Effective stress in double porous media with two immiscible fluids. *Geophys. Res. Lett.*, 32, L15309

Kim, M.K. and Lade, P.V., 1988. Single hardening constitutive model for frictional materials, I. plastic potential function. *Comp. Geotech.*, 5, 307-324

Kohgo, Y., 2008. A hysteresis model of soil water retention curves based on bounding surface concept. *Soils Found.*, 48(5), 633-640

Kohgo, Y., Nakano, M. and Miyazaki, T., 1993a. Theoretical aspects of constitutive modeling for unsaturated soils. *Soils Found.*, 33(4), 49-63

Kohgo, Y., Nakano, M. and Miyazaki, T., 1993b. Verification of the generalized elastoplastic model for unsaturated soils. *Soils Found.*, 33(4), 64-73

Kool, J.B. and Parker, J.C., 1987. Development and evaluation of closed-form expressions for hysteretic soil hydraulic properties. *Water Resour. Res.*, 23(1), 105-114

Kovacs, C., 1981. Seepage hydraulics. Elsevier Science Publishers, Amsterdam

Krieg, R.D., 1975. A practical two-surface plasticity theory. *J. Appl. Mech.* (transaction of the ASME), 42, 641-646

Lade, P.V., 1977. Elasto-plastic stress-strain theory for cohensionless soil with curved yield surfaces. *Int. J. Solids Structures*, 13, 1019-1035

Lade, P. V. and de Boer, R., 1997. The concept of effective stress for soil, concrete and rock. *Géotechnique*, 47(1), 61-78

Lade, P.V. and Duncan, J.M., 1975. Elastoplastic stress-strain theory for cohesionless soil. *J. Geotech. Engng.*, ASCE, 101(GT10), 1037-1053

Lade, P.V. and Inel, S., 1997. Rotational kinematic hardening model for sand. Part I concept of rotating yield and plastic potential surfaces. *Comp. Geotech.*, 21(3), 183-216

Lade, P.V. and Kim, M.K., 1988a. Single hardening constitutive model for frictional materials, II. yield criterion and plastic work contours. *Comp. Geotech.*, 6, 13-30

Lade, P.V. and Kim, M.K., 1988b. Single hardening constitutive model for frictional materials, III. Comparisons with experimental data. *Comp. Geotech.*, 6, 31-48

Laloui, L. and Nuth, M., 2009. On the use of the generalized effective stress in the constitutive modelling of unsaturated soils. *Computers and Geotechnics*, 36, 20-23

Lenhard, R.J., Parker, J.C., Kaluarachchi, J.J., 1991. Comparing simulated and experimental hysteretic two-phase transient fluid flow phenomena. *Water Resour. Res.*, 27(8), 2113-2124

Leong, E.C. and Rahardjo, H., 1997. Review of soil-water characteristic curve equations. *J. Geotech. Geoenviron. Engng.*, 123(12), 1106-1117

Li, X.S., 1997. Modelling of dilative shear failure. *J. Geotech. Geoenviron. Engng.*, ASCE, 123(7), 609-616

Li, X.S., 2002. A sand model with state-dependent dilatancy. *Géotechnique*, 52(3), 173-186

Li, X.S., 2003. Effective stress in unsaturated soil: a microstructural analysis. *Géotechnique*, 53(2), 273-277

Li, X.S., 2004. Modelling of hysteresis response for arbitrary wetting/drying paths. *Comput. Geotech.*, 32, 133-137

Li, X.S., 2007a. Thermodynamics-based constitutive framework for unsaturated soils 1: Theory. *Géotechnique*, 57 (5), 411 – 422

Li, X.S., 2007b. Thermodynamics-based constitutive framework for unsaturated soils 2: A basic triaxial model. *Géotechnique*, 57(5), 423 – 435

Li, X.S. and Dafalias, Y.F., 2000. Dilatancy for cohesionless soils. *Géotechnique*, 50(4), 449-460

Li, X.S. and Dafalias, Y.F., 2002. Constitutive modeling of inherently anisotropic sand behavior. *J. Geotech. Geoenviron. Engng.*, 128(10), 868-880

Li, X.S. and Dafalias, Y.F., 2004. A constitutive framework for anisotropic sand including non-proportional loading. *Géotechnique*, 54(1), 41-55

Li, X.S., Dafalias, Y.F. and Wang, Z.L., 1999. State-dependent dilatancy in critical-state constitutive modelling of sand. *Can. Geotech. J.*, 36, 599-611

Li, X.S. and Wang, Y., 1998. Linear representation of steady-state line for sand. *J. Geotech. Geoenviron. Engng.*, 124(12), 1215-1217

Li, X. and Zienkiewicz, O.C., 1992. Multiphase flow in deforming porous media and finite element solutions. *Comput. Struct.*, 45, 211-227

Ling, H.I., Yue, D., Kaliakin, V.N. and Themelis, N.J., 2002. Anisotropic elastoplastic bounding surface model for cohesive soils. *J. Engng. Mech.*, ASCE, 128(7), 748-758

Liu, C. and Muraleetharan, K.K., 2006. Description of soil water characteristic curves using the bounding surface plasticity theory. In *Unsaturated Soils 2006*, Miller, Zapata, Houston and Fredlund (ed.), *GSP No. 147*, *Proc. 4th Int. Conf. Unsat. Soils*, Geo-Institute, ASCE, Carefree, Arizona, 2, 2432-2440

Lloret, A. and Alonso, E.E., 1980. Consolidation of unsaturated soil including swelling and collapse behaviour. *Géotechnique*, 30(4), 499-477

Lloret, A. and Alonso, E.E., 1985. State surfaces for partially saturated soils. *Proc. 11th Int. Conf. Soil Mech. Found. Engng.*, Vol. 2, San Francisco, 557-562

Loret, B. and Khalili, N., 2000. A three-phase model for unsaturated soils. *Int. J. Numer. Anal. Meth. Geomech.*, 24, 893-927

Loret, B. and Khalili, N., 2002. An effective stress elastic-plastic model for unsaturated porous media. *Mech. Materials*, 34, 97-116

Lu, N. and Likos, W., 2004. Unsaturated soil mechanics. John Wiley & Sons, Inc., Hoboken, New Jersey

Lu, N. and Likos, W., 2006. Suction stress characteristic curve for unsaturated soil. *J. Geotech. Geoenviron. Engng.*, 132(2), 131-142

Maâtouk, A., Leroueil, S. and La Rochelle, P., 1995. Yielding and critical state of a collapsible unsaturated silty soil. *Géotechnique*, 45(3), 465-477

Macari, E.J., Hoyos, L.R. and Arduino, P., 2003. Constitutive modeling of unsaturated soil behavior under axisymmetric stress states using a stress/suction-controlled cubical test cell. *Int. J. Plasticity*, 19, 1481-1515

Macari, E.J., Weihe, S. and Arduino, P., 1997. Implicit integration of elasto-plastic constitutive Models for frictional materials with highly non-linear hardening functions. *J. Mech. Cohes. Fric. Materials*. 2, 1-29

Manzari, M.T. and Dafalias, Y.F., 1997. A critical state two-surface plasticity model for sands. *Géotechnique*, 47(2), 255-272

Manzari, M.T. and Prachathananukit, R., 2001. On integration of a cyclic soil plasticity model. *Int. J. Numer. Anal. Meth. Geomech.*, 25, 525-549

Maqsoud, A., Bussière, B., Aubertin, M. and Mbonimpa, M., 2006. Modification of the predictive MK model to integrate hysteresis of the water retention curve. In *Proc. 4th Int. Conf. Unsat. Soils*, Miller, Zapata, Houston, and Fredlund (Eds.), ASCE Geo-Institute Geotechnical Special Publication No. 147, 2465-2476

Maqsoud, A., Bussière, B., Mbonimpa, M. and Aubertin, M., 2004. Hysteresis effects on the water retention curve: a comparison between laboratory results and predictive models. In *Proc. 57th Can. Geotech. Conf./5th Joint CGS/IAH-CNC Conf.*, Quebéc, Canada

Maswoswe, J., 1985. Stress path for a compacted soil during collapse due to wetting. Ph.D. dissertation, Imperial College, London

Matsuoka, H., Sun, D., Kogane, A., Fukuzawa, N. and Ichihara, W., 2002. Stress-strain behaviour of unsaturated soil in true triaxial tests. *Can. Geotech. J.*, 39, 608-619

Matyas, E.L. and Radhakrishna, H.S., 1968. Volume change characteristics of partially saturated soils. *Géotechnique*, 18(4), 432-448

Miller, C.J., Yesiller, N., Yaldo, K. and Merayyan, S., 2002. Impact of soil type and compaction conditions on soil water characteristic. *J. Geotech. Geoenviron. Engng.*, 128(9), 733-742

Miller, G.A., Khoury, C.N., Muraleetharan, K.K., Liu, C. and Kibbey, T.C.G., 2008. Effects of soil skeleton deformations on hysteretic soil water characteristic curves: experiments and simulations. *Water Resour. Res.,* doi:10.1029/2007WR006492

Mooney, M.A., Finno, R.J. and Viggiani, G., 1998. A unique critical state for sand? *J. Geotech. Geoenviron. Engng.*, 124(11), 1100-1108

Morrow, N.R., 1970. Physics and thermodynamics of capillary. *Industr. Engng. Chem.*, 62(6), 32-56

Morrow, N.R. and Harris, C.C., 1965. Capillary equilibrium in porous materials. *Soc. Petrol. Engng. J.*, 5, 15-24

Mrŏz, Z., 1967. On the description of anisotropic workhardening. *J. Mech. Phys. Solids*, 15, 163-175

Mrŏz, Z., 1969. An attempt to describe the behavior of metals under cyclic loads using a more general workhardening model. *Acta Mech.*, 7, 199-212

Mrŏz, Z., 1980. On two limiting cases of multisurface hardening model. *Int. J. Numer. Anal. Meth. Geomech.*, 4(4), 389-391

Mrŏz, Z., Norris, V.A. and Zienkiewicz, O.C., 1978. An anisotropic hardening model for soils and its application to cyclic loading. *Int. J. Numer. Anal. Meth. Geomech.*, 2, 203-221

Mrŏz, Z., Norris, V.A. and Zienkiewicz, O.C., 1979. Application of an anisotropic hardening model in the analysis of elastoplastic deformation of soils. *Géotechnique*, 29(1), 1-34

Mrŏz, Z., Norris, V.A. and Zienkiewicz, O.C., 1981. An anisotropic, critical state model for soils subject to cyclic loading. *Géotechnique*, 31(1), 451-469

Mrŏz, Z. and Pietruszczak, S., 1983. A constitutive model for sand with anisotropic hardening rule. *Int. J. Numer. Anal. Meth. Geomech.*, 7, 305-320

Mualem, Y., 1973. Modified approach to capillary hysteresis based on a similarity hypothesis. *Water Resour. Res.*, 9, 1324-1331

Mualem, Y., 1974. A conceptual model of hysteresis. *Water Resour. Res.*, 10(3), 514-520

Mualem, Y., 1984. A modified dependent-domain theory of hysteresis. *Soil Sci.*, 137(5), 283-291.

Mualem, Y. and Miller, E.E., 1979. A hysteresis model based on an explicit domain-dependence function. *Soil Sci. Soc. Am. J.*, 43, 1067-1073

Mualem, Y. and Morel-Seytoux, H.J., 1978. Analysis of a capillary hysteresis model based on a one-variable distribution function. *Water Resour. Res.*, 14, 605-610

Muir Wood, D., Belkheir, K. and Liu, D.F., 1994. Strain softening and state parameters for sand modelling. *Géotechnique*, 44(2), 335-339

Muraleetharan, K.K., Liu, C., Wei, C.F., Kibbey, T.C.G. and Chen, L., 2008. An elastoplastic framework for coupling hydraulic and mechanical behavior of unsaturated soils. *Int. J. Plasticity*, 25, 473-490

Muraleetharan, K.K., Mish, K.D., Yogachandran, C. and Arulannandan, K., 1997. DYSAC2(Version 7.0): Dynamic Soil Analysis Code for 2-dimensional problems. *Technical report*, School of Civil Engineering and Environmental Science, University of Oklahoma, Norman, Oklahoma

Muraleetharan, K.K. and Nedunuri, P.R., 1998. A bounding surface elastoplastic constitutive model for monotonic and cyclic behavior of unsaturated soils. *Proc. 12$^{th}$ Engng. Mech. Conf.*, ASCE, La Jolla, CA, 1331-1334

Muraleetharan, K.K. and Wei, C.F., 1999. Dynamic behavior of unsaturated porous media: governing equations using the theory of mixtures with interfaces (TMI). *Int. J. Numer. Anal. Meth. Geomech.*, 23, 1579-1608

Murray, E.J., 2002. An equation of state for unsaturated soils. *Can. J. Geotech.*, 39, 125-140

Nimmo, J.R. and Miller, E.E., 1986. The temperature dependence of isothermal moisture vs. potential characteristics of soils. *Soil Sci. Soc. Am. J.*, 50, 1105-1113

Ng, W.W. and Pang, Y.W., 2000. Influence of stress state on soil-water characteristics and slope stability. *J. Geotech. Geoenviron. Engng.*, 126(2), 157-166

Nova, R. and Hueckel, T., 1981. A unified approach to the modelling of liquefaction and cyclic mobility of sands. *Soils Found.*, 21, 13-28

Nova, R. and Muir Wood, D., 1979. A constitutive model for sand in triaxial compression. *Int. J. Numer. Anal. Meth. Geomech.*, 3, 255-278

Nur, A. and Byerlee, J. D., 1971. An exact effective stress law for elastic deformation of rock with fluids. *J. Geophys. Res.*, 76(26), 6414–6419

Nuth, M. and Laloui, L., 2008a. Effective stress concept in unsaturated soils: clarification and validation of a unified framework. *Int. J. Numer. Anal. Meth. Geomech*., 32, 771-801

Nuth, M. and Laloui, L., 2008b. Advances in modelling hysteretic water retention curve in deformable soils. *Computers and Geotechnics*, 35, 835-844

Oda, M., Koishikawa, I. and Higuchi, T., 1978. Experimental study of anisotropic shear strength of sand by plane strain test. *Soils Found.*, 18(1), 25-38

Oda, M. and Nakayama, H., 1988. Introduction of inherent anisotropy of soils in the yield function. In *Micromechanics of granular materials*, Satake and Jenkins (ed.), Elsevier, Amsterdam

Ortiz, M. and Popov, E.P., 1985. Accuracy and stability of integration algorithms for elastoplastic constitutive relations. *Int. J. Numer. Meth. Engng.*, 21(9), 1561-1576

Parker, J.C. and Lenhard, R.J., 1987. A model of hysteretic constitutive relations governing multiphase flow, 1. saturation-pressure relationship. *Water Resour. Res.*, 23(12), 2187-2196

Parlange, J.Y., 1976. Capillary hysteresis and relationship between drying and wetting curves. *Water Resour. Res.*, 12, 224-228

Pastor, M., Zienkiewicz, O.C. and Chan, A.H.C., 1990. Generalized plasticity and the modelling of soil behaviour. *Int. J. Numer. Anal. Methods Geomech.*, 14, 151-190

Pastor, M., Zienkiewicz, O.C., and Leung, K.H., 1985. Simple model for transient soil loading in earthquake analysis. II. non-associative model for sands. *Int. J. Numer. Anal. Meth. Geomech.*, 9, 477-498

Pestana, J.M. and Whittle A.J., 1995. Compression model for cohesionless soils. *Géotechnique*, 45(4), 611-631

Pham, H.Q. and Fredlund, D.G., 2008. Equations for the entire soil-water characteristic curve for a volume change soil. *Can. Geotech. J.*, 45, 443-453

Pham, H.Q., Fredlund, D.G. and Barbour, S.L., 2003. A practical hysteresis model for the soil-water characteristic curve for soils with negligible volume change. *Géotechnique*, 53(2), 293-298

Pietruszczak, S. and Mrŏz, Z., 1983. On hardening anisotropy of K0-consolidated clays. *Int. J. Numer. Anal. Meth. Geomech.*, 7, 19-38

Poulovassilis, A., 1970a. Hysteresis of pore water in granular porous bodies. *Soil Sci.*, 109(1), 5-12

Poulovassilis, A., 1970b. The effect of the entrapped air on the hysteresis curve of a porous body and on its hydraulic conductivity. *Soil Sci.*, 109(3), 154-162

Poulovassilis, A. and Childs, E.C., 1971. The hysteresis of pore water: the non-independent of domains. *Soil Sci.*, 112, 301-312

Poulovassilis, A. and El-Ghamry, W.M., 1978. The dependent domain theory applied to scanning curves of any order in hysteretic soil water relationships. *Soil Sci.*, 126(1), 1-8

Prevost, J.H., 1982. Two-surface versus multi-surface plasticity theories: a critical assessment. *Int. J. Numer. Anal. Meth. Geomech.*, 6, 323-338

Pride, S.R., and Flekkøy, E.G., 1999. Two-phase through porous media in the fixed-contact-line regime. *Phys. Rev. E*, 60(4), 4285-4299

Rampino, C., Mancuso, C. and Vinale, F., 2000. Experimental behaviour and modeling of an unsaturated compacted soil. *Can. Geotech. J.*, 37, 748-763

Reeves, P.C. and Celia, M.A., 1996. A functional relationship between capillary pressure, saturation, and interfacial area as revealed by a pore-scale model. *Water Resour. Res.*, 32, 2345-2358

Richards, B.G., 1965. Measurement of the free energy of soil moisture by the psychrometeric technique using thermistors. In *Moisture equilibria and moisture changes in soils beneath covered areas*. Aitchison (ed.), Butterworth & Co. Ltd., Sydney, Australia

Richart, F.E., Hall, J.R. and Woods, R.D., 1970. Vibration of soils and foundations. *International series in theoretical and applied mechanics*. Prentice-Hall, Englewood Cliffs, New Jersey

Rojas, E. and Rojas, F., 2005. Modeling hysteresis of the soil-water characteristic curve. *Soils Found.*, 45(3), 135-145

Roscoe, K.H. and Schofield, A.N., 1963. Mechanical behaviour of an idealized wet clay. *Proc. 2nd Eur. Conf. Soil Mech. Found. Engng.*, 47–54

Roscoe, K.H., Schofield, A.N. and Wroth, C.P., 1958. On the yielding of soils. *Géotechnique*, 8, 22-53

Rowe, P.W., 1962. The stress-dilatancy relation for static equilibrium of an assembly of particles in contact. *Proc. Roy. Soc., Series A*, 269, 500-527

Santagiuliana, R. and Schrefler, B.A., 2006. Enhancing the Bolzon-Schrefler-Zienkiewicz constitutive model for partially saturated soil, *Transport in Porous Media*, 65, 1-30

Schofield, A.W. and Wroth, C.P., 1968. Critical state soil mechanics. McGraw-Hill Publication, London

Sharma, R.S., 1998. Mechanical behaviour of unsaturated highly expansive clays. Ph.D. dissertation, University of Oxford, UK

Sharma, R.S. and Wheeler, S.J., 2000. Behaviour of an unsaturated highly expansive clay during cycles of wetting and drying. *Proc. Asian Conf. Unsat. Soils*, Singapore, 721–726

Sheng, D., Fredlund, D.G. and Gens, A., 2008. A new modelling approach for unsaturated soils using independent stress variables. *Can. Geotech. J.*, 45, 511-534

Sheng, D., Gens, A., Fredlund, D.G. and Sloan, S.W., 2008. Unsaturated soils: From constitutive modelling to numerical algorithms. *Computers and Geotechnics*, 35, 810-824

Sheng, D., Sloan, S.W. and Gens, A., 2004. A constitutive model for unsaturated soils: thermomechanical and computational aspects. *Comput. Mech.*, 33(6), 453-465

Sillers, W.S., Fredlund, D.G. and Zakerzadeh, N., 2001. Mathematical attributes of some soil-water characteristic curve model. *Geotech. Geological Engng.*, 19, 243-283

Simo, J.C. and Ortiz, M.A., 1985. A unified approach to finite deformation elastoplastic analysis based on the use of hyper-elastic constitutive equations. *Compt. Meth. Applied Mech. Engng.*, 49, 221-245

Simo, J.C. and Taylor, R.L., 1985. Consistent tangent operators for rate-independent elasto-plasticity. *Compt. Meth. Applied Mech. Engng.*, 48, 101-118

Sivakumar, V., 1993. A critical state framework for unsaturated soil. Ph.D. dissertation, University of Sheffield, UK

Skempton, A.W., 1961. Effective stress in soils, concrete and rock. In *Symposium on pore pressure and suction in soils*, Butterworth: London, 4-16

Skempton, A.W. and Bjerrum, L., 1957. A contribution to the settlement analysis of foundations on clay. *Géotechnique*, 7, 168-178

Stauffer, F. and Dracos, T., 1984. Local infiltration into layered soil and response of the water table: Experiments and simulation. In *Frontiers in Hydrology*, Water Resources Publication, Littleton, Colorado, 228-242

Suklje, L., 1969. Rheological aspects of soil mechanics. Wiley: New York

Sun, D.A., Sheng, D., Cui, H.B. and Sloan, S.W., 2007a. A density-dependent elastoplastic hydro-mechanical model for unsaturated compacted soils. *Int. J. Numer. Anal. Meth. Geomech*., 31, 1257-1279

Sun, D.A., Sheng, D. and Sloan, S.W., 2007b. Elastoplastic modelling of hydraulic and stress-strain behaviour of unsaturated soils. *Mech. Materials*, 39, 212-221

Sun, D.A., Sheng, D., Xiang, L. and Sloan, S.W., 2008. Elastoplastic prediction of hydro-mechanical behaviour of unsaturated soils under undrained conditions. *Computers and Geotechnics*, 35, 845-852

Sun, D.A., Sheng, D., Xu, Y.F., 2007c. Collapse behaviour of unsaturated compacted soil with different initial densities. *Can. Geotech. J.*, 44, 673-686

Taiebat, M. and Dafalias, Y.F., 2008. SANISAND: simple anisotropic and plasticity model. *Int. J. Numer. Anal. Meth. Geomech.*, 32, 915-948

Talsma, T., 1970. Hysteresis in two sands and the independent domain model. *Water Resour. Res.*, 6(3), 964-970

Tan, N.K., 2005. Pressuremeter and cone penetrometer testing in a calibration chamber with unsaturated Minco silt. Ph.D. dissertation, University of Oklahoma, Norman, Oklahoma

Tarantino, A., 2007. A possible critical state framework for unsaturated compacted soils. *Géotechnique*, 57(4), 385-389

Tatsuoka, F. and Ishihara, K., 1974. Yielding of sand in triaxial compression. *Soils Found.*, 14(2), 63-76

Terzaghi, K., 1936. The shear resistance of saturated soils. *Proc. 1st Int. Conf. on Soil Mech. Fdn. Engng.*, Volume 1, 54-56

Thomas, H.R. and He, Y., 1998. Modeling the behaviour of unsaturated soil using an elastoplastic constitutive model. *Géotechnique*, 48(5), 589-603

Thu, T.M., Rahardjo, H. and Leong, E.C., 2007. Elastoplastic model for unsaturated soil with incorporation of the soil-water characteristic curve. *Can. Geotech. J.*, 44, 67-77

Tobita, Y., 1988. Yield condition of anisotropic granular materials. *Soils Found.*, 128(2), 113-126

Tobita, Y., 1989. Fabric tensors in constitutive equations for granular materials. *Soils Found.*, 129(4), 91-104

Toll, D.G., 1990. A framework for unsaturated soil behaviour. *Géotechnique*, 40(1), 31-44

Toll, D.G. and Ong, B.D., 2003. Critical-state parameters for an unsaturated residual sandy clay. *Géotechnique*, 53(1), 93-103

Toll, D.G. and Ong, B.D., 2004. Critical-state parameters for an unsaturated residual sandy clay (Discussion by Murray E.J. and Sivakumar, V.). *Géotechnique*, 54(1), 69-71

Topp, G.C., 1969. Soil-water hysteresis measured in a sandy loam and compared with the hysteretic domain model. *Soil Sci. Soc. Am. Proc.*, 33, 643-651

Topp, G.C., 1971a. Soil water hysteresis in silt loam and clay loam soils. *Water Resour. Res.*, 7(4), 914-920

Topp, G.C., 1971b. Soil-water hysteresis: the domain theory extended to pore interaction conditions. *Soil Sci. Soc. Am. J.*, 35, 219-225

Topp, G.C. and Miller, E.E., 1966. Hysteretic moisture characteristics and hydraulic conductivities for glass-bead media. *Soil Sci. Soc. Am. Proc.*, 30, 156-162

Uchida, K. and Stedman, J.D., 2001. Liquefaction behavior of Toyoura sand under cyclic strain controlled triaxial loading. *Proc. 11$^{th}$ Int. Offshore Polar Engng. Conf.*, Stavanger, Norway

Vachaud, G. and Thony, J.L., 1971. Hysteresis during infiltration and redistribution in a soil column at different initial water contents. *Water Resour. Res.*, 7, 111-127

van Genuchten, M.Th., 1980. A closed form equation predicting the hydraulic conductivity of unsaturated soils. *Soil Sci. Soc. Am. J.*, 44, 892-898

Verdugo, R. and Ishihara, K., 1996. The steady state of sandy soils. *Soils Found.*, 36(2), 81-91

Vermeer, P.A., 1978. A double hardening model for sands. *Géotechnique*, 28, 413-433

Viaene, P., Vereecken, H., Diels, J. and Feyen, J., 1994. A statistical analysis of six hysteresis models for the moisture retention characteristic. *Soil Sci.*, 157, 345–355

Vinayagam, T., 2004. Understanding the stress-strain behavior of unsaturated Minco silt using laboratory testing and constitutive modeling. Master thesis, University of Oklahoma, Norman, Oklahoma

Wan, R.G. and Guo, P.J., 1999. A pressure and density dependent dilatancy model for granular materials. *Soils Found.*, 39(6), 1-11

Wan, R.G. and Guo, P.J., 2001. Effect of microstructure on undrained behavior of sands. *Can. Geotech. J.*, 38, 16-28

Wang, Z.L., Dafalias, Y.F., Li, X. and Makdisi, F.I., 2002. State pressure index for modeling sand behavior. *J. Geotech. Geoenviron. Engng.*, 128(6), 511-519

Wang, Z.L., Dafalias, Y.F. and Shen, C.K., 1990. Bounding surface hypoplasticity model for sand. *J. Engng. Mech.*, ASCE, 116(5), 983-1001

Wei, C.F., 2001. Static and dynamic behavior of multiphase porous media: governing equations and finite element implementation. Ph.D. dissertation, University of Oklahoma, Norman, Oklahoma

Wei, C. and Dewoolkar, M.M., 2006. Formulation of capillary hysteresis with internal state variables. *Water Resour. Res.*, 42, W07405

Wei, C. and Muraleetharan, K.K. 2002a. A continuum theory of porous media saturated by multiple immiscible fluids: I. Linear poroelasticity. *Int. J. Eng. Sci.*, 40, 1807-1833

Wei, C. and Muraleetharan, K.K. 2002b. A continuum theory of porous media saturated by multiple immiscible fluids: II. Lagrangian description and variational structure. *Int. J. Eng. Sci.*, 40, 1835-1854

Wheeler, S.J., 1996. Inclusion of specific water volume within an elasto-plastic model for unsaturated soil. *Can. Geotech. J.*, 33, 42-57

Wheeler, S.J., Gallipoli, D. and Karstunen, M., 2002. Comments on use of the Barcelona Basic Model for unsaturated soils. *Int. J. Numer. Anal. Meth. Geomech*., 26, 1561-1571

Wheeler, S.J., Sharma, R.S. and Buisson, M.S.R., 2003. Coupling of hydraulic hysteresis and stress-strain behaviour in unsaturated soils. *Géotechnique*, 53(1), 41-54

Wheeler, S.J. and Sivakumar, V., 1995. An elasto-plastic critical state framework for unsaturated soil. *Géotechnique*, 45(1), 35-53

Wheeler, S.J. and Sivakumar, V., 2000. Influence of compaction procedure on the mechanical behaviour of an unsaturated compacted clay. Part 2: shearing and constitutive modelling. *Géotechnique*, 50(4), 369-376

Wilmanski, K., 1995. Lagrangean model of two-phase porous media. *J. Non-Equilib. Thermodyn.*, 20, 50-77

Wu, L., Vomocil, J.A. and Childs, S.W., 1990. Pore size, particle size, aggregate size, and water retention. *Soil Sci. Soc. Am. J.*, 54, 952-956

Yang, C., Cui, Y.J., Pereira, J.M. and Huang, M.S., 2008. A constitutive model for unsaturated cemented soils under cyclic loadings. *Computers and Geotechnics*, 35, 853-859

Yang, Y., 2003. The middle surface concept and its application to constitutive modeling of soils. Ph.D. dissertation, University of Oklahoma, Norman, Oklahoma

Yang, Y. and Muraleetharan, K.K., 2003. Middle surface concept and its application to elastoplastic behavior of saturated sands. *Géotechnique*, 53(4), 421-431

Yang, Y., Muraleetharan, K.K. and Yu, H.S., 2008. Generalized trapezoidal numerical integration of an advanced soil model. *Int. J. Numer. Anal. Mech. Geomech.*, 32, 43-64

Yoshimine, M., Ishihara, K. and Vargas, W., 1989. Effects of principal stress direction and intermediate principal stress on drained shear behavior of sand. *Soils Found.*, 38(3), 177-186

Yu, H.S., 1994. State parameter from self-boring pressuremeter tests in sand. *J. Geotech. Engng.*, ASCE, 120(12), 2118-2135

Yu, H.S., 1996. Interpretation of pressuremeter unloading tests in sand. *Géotechnique*, 46(1), 17-34

Yu, H.S., 1998. CASM: a unified state parameter model for clay and sand. *Int. J. Numer. Anal. Meth. Geomech*., 22, 621-653

Zienkiewicz, O.C., Leung, K.H. and Pastor, M., 1985. Simple model for transient soil loading in earthquake analysis. I. basic model and its application. *Int. J. Numer. Anal. Meth. Geomech.*, 9, 453-476

# APPENDIX I: STRESS UPDATE ALGORITHM

## (I-1) Elastic predictor

At step $n+1$, for iteration number zero:

$$\Delta\varepsilon_{v,n+1}^{p(0)} = \Delta\boldsymbol{\varepsilon}_{q,n+1}^{p(0)} = \Delta n_{w,n+1}^{p(0)} = \Delta\boldsymbol{\alpha}_{n+1}^{(0)} = \Delta m_{n+1}^{(0)} = 0 \tag{A.1}$$

The updated stresses:

$$I_{n+1}^{(0)} = \left[ \left(I_n\right)^{(1-b_1)} + \frac{K_0\left(1-b_1\right)}{p_{ref}^{b_1}} \Delta\varepsilon_{v,n+1} \right]^{1/(1-b_1)} \tag{A.2}$$

$$\mathbf{s}_{n+1}^{(0)} = \mathbf{s}_n + 2G_{n+1}\Delta\boldsymbol{\varepsilon}_{q,n+1}, \text{ with } G_{n+1} = G_0\left(\frac{I_{n+1}}{p_{ref}}\right)^{d_1} \tag{A.3}$$

$$s_{c,\,n+1}^{(0)} = s_{c,n} + \Gamma^e \Delta n_{w,n+1} \tag{A.4}$$

Wetting: $s_{c0w,\,n+1}^{(0)} = s_{c0w,n}$ (A.5)

Drying: $s_{c0d,\,n+1}^{(0)} = s_{c0d,n}$ (A.6)

## (I-2) Plastic corrector

The SWCCs are elastoplastic, so the plastic water content has to be introduced whenever suction changes. If the trial stresses are outside of the yield surface, i.e., $f\left(\boldsymbol{\sigma}', s_c; \boldsymbol{\alpha}, m\right) > 0$, it is also necessary to correct the elastic predictions by simultaneously satisfying all the rate equations:

$$I_{n+1}^{(m)} = \left[ \left(I_n\right)^{(1-b_1)} + \frac{K_0\left(1-b_1\right)}{p_{ref}^{b_1}} \left(\Delta\varepsilon_{v,n+1} - \Delta\varepsilon_{v,n+1}^{p(m)}\right) \right]^{1/(1-b_1)} \tag{B.1}$$

$$\Delta\varepsilon_{v,n+1}^{p(m)} = \Lambda_{n+1}^{(m)} D_{n+1}^{(m)} \tag{B.2}$$

$$\mathbf{s}_{n+1}^{(m)} = \mathbf{s}_n + 2G_{n+1}^{(m)}\left(\Delta\boldsymbol{\varepsilon}_{q,n+1} - \Delta\boldsymbol{\varepsilon}_{q,n+1}^{p(m)}\right) \tag{B.3}$$

$$\Delta\boldsymbol{\varepsilon}_{q,n+1}^{p(m)} = \Lambda_{n+1}^{(m)} \mathbf{n}_{n+1}^{(m)} \tag{B.4}$$

$$s_{c,n+1}^{(m)} = s_{c,n} + \Gamma^e\left(\Delta n_{w,n+1} - \Delta n_{w,n+1}^{p(m)}\right) \tag{B.5}$$

$$\Delta n_{w,n+1}^{p(m)} = \left(s_{c,n+1}^{(m)} - s_{c,n}\right) / \Gamma_{n+1}^{p(m)} \tag{B.6}$$

$$\boldsymbol{\alpha}_{n+1}^{(m)} = \boldsymbol{\alpha}_n + \Lambda_{n+1}^{(m)} h_{n+1}^{(m)} \mathbf{b}_{n+1}^{(m)} \tag{B.7}$$

$$m_{n+1}^{(m)} = m_n + c_m\left(1+e_0\right)\Lambda_{n+1}^{(m)} D_{n+1}^{(m)} + c_v\left(\frac{s_{c,n+1}^{(m)} n_{w,n+1}^{(m)}}{p_{ref}}\right)^{\varpi} \Delta n_{w,n+1}^{p(m)} \tag{B.8}$$

$$\mathbf{F}_{n+1}^{(m)} = \mathbf{F}_n - \Lambda_{n+1}^{(m)} c_f < -D_{n+1}^{(m)} > \left(F_{\max}\mathbf{n}_{n+1}^{(m)} + \mathbf{F}_{n+1}^{(m)}\right) \tag{B.9}$$

Wetting bound:

$$s_{c0w,n+1}^{(m)} = s_{c0w,n} \exp\left[ \zeta v_{n+1}^{(m)} \Delta\varepsilon_{v,n+1}^{p(m)} - \frac{1}{d_2} \frac{\left(n_{ws,n+1} - n_{wr,n+1}\right)\Delta n_{w,n+1}^{p(m)}}{\left(n_{ws,n+1} - n_{w,n+1}^{(m)}\right)\left(n_{w,n+1}^{(m)} - n_{wr,n+1}\right)} \right] \tag{B.10}$$

Drying bound:

$$s_{c0d,n+1}^{(m)} = s_{c0d,n} \exp\left[ \zeta v_{n+1}^{(m)} \Delta\varepsilon_{v,n+1}^{p(m)} - \frac{1}{d_3} \frac{\left(n_{ws,n+1} - n_{wr,n+1}\right)\Delta n_{w,n+1}^{p(m)}}{\left(n_{ws,n+1} - n_{w,n+1}^{(m)}\right)\left(n_{w,n+1}^{(m)} - n_{wr,n+1}\right)} \right] \tag{B.11}$$

$$\sqrt{\mathbf{r}_{n+1}^{(m)} : \mathbf{r}_{n+1}^{(m)}} - \sqrt{\frac{2}{3}} m_{n+1}^{(m)} I_{n+1}^{(m)} \sqrt{1 - \left(I_{n+1}^{(m)} / I_0\right)^{\beta}} = 0 \tag{B.12}$$

In the above plastic corrector, some important parameters are given as follows:

$$D_{n+1}^{(m)} = B_{n+1}^{(m)}\left[\mathbf{d}_{n+1}^{(m)} : \mathbf{n}_{n+1}^{(m)}\right],\ B_{n+1}^{(m)} = B_0\left(1+ < \mathbf{F}_{n+1}^{(m)} : \mathbf{n}_{n+1}^{(m)} >\right) \tag{B.13}$$

$$h_{n+1}^{(m)} = \frac{h_0\left|\mathbf{b}_{n+1}^{(m)} : \mathbf{n}_{n+1}^{(m)}\right|}{b_{ref,n+1}^{(m)} - \left|\mathbf{b}_{n+1}^{(m)} : \mathbf{n}_{n+1}^{(m)}\right|} = \frac{h_0\left|\mathbf{b}_{n+1}^{(m)} : \mathbf{n}_{n+1}^{(m)}\right|}{2\sqrt{2/3}\alpha_{c,n+1}^{b(m)} - \left|\mathbf{b}_{n+1}^{(m)} : \mathbf{n}_{n+1}^{(m)}\right|} \tag{B.14}$$

$$\mathbf{b}_{n+1}^{(m)} = \sqrt{\frac{2}{3}}\alpha_{\theta,n+1}^{b(m)}\mathbf{n}_{n+1}^{(m)} - \boldsymbol{\alpha}_{n+1}^{(m)},\ \mathbf{b}_{n+1}^{(m)} : \mathbf{n}_{n+1}^{(m)} = \sqrt{\frac{2}{3}}\alpha_{\theta,n+1}^{b(m)} - \boldsymbol{\alpha}_{n+1}^{(m)} : \mathbf{n}_{n+1}^{(m)} \tag{B.15}$$

$$\mathbf{d}_{n+1}^{(m)} = \sqrt{\frac{2}{3}}\alpha_{\theta,n+1}^{d(m)}\mathbf{n}_{n+1}^{(m)} - \boldsymbol{\alpha}_{n+1}^{(m)},\ \mathbf{d}_{n+1}^{(m)} : \mathbf{n}_{n+1}^{(m)} = \sqrt{\frac{2}{3}}\alpha_{\theta,n+1}^{d(m)} - \boldsymbol{\alpha}_{n+1}^{(m)} : \mathbf{n}_{n+1}^{(m)} \tag{B.16}$$

$$K_{n+1}^{(m)} = K_0\left(\frac{I_{n+1}^{(m)}}{p_{ref}}\right)^{b_1},\ G_{n+1}^{(m)} = G_0\left(\frac{I_{n+1}^{(m)}}{p_{ref}}\right)^{d_1} \tag{B.17}$$

$$\mathbf{r}_{n+1}^{(m)} = \mathbf{s}_{n+1}^{(m)} - \boldsymbol{\alpha}_{n+1}^{(m)}\boldsymbol{I}_{n+1}^{(m)},\ \bar{\mathbf{r}}_{n+1}^{(m)} = \frac{\mathbf{r}_{n+1}^{(m)}}{I_{n+1}^{(m)}},\ \mathbf{n}_{n+1}^{(m)} = \frac{\mathbf{r}_{n+1}^{(m)}}{\sqrt{\mathbf{r}_{n+1}^{(m)} : \mathbf{r}_{n+1}^{(m)}}} = \frac{\bar{\mathbf{r}}_{n+1}^{(m)}}{\sqrt{\bar{\mathbf{r}}_{n+1}^{(m)} : \bar{\mathbf{r}}_{n+1}^{(m)}}} \tag{B.18}$$

Wetting: $$\Gamma_{n+1}^{p(m)} = \Gamma_{0w,n+1}^{p(m)}\left(1+\frac{H\delta_{n+1}^{(m)}}{< \delta_{in} - g\delta_{n+1}^{(m)} >}\right) \tag{B.19}$$

Drying: $$\Gamma_{n+1}^{p(m)} = \Gamma_{0d,n+1}^{p(m)}\left(1+\frac{H\delta_{n+1}^{(m)}}{< \delta_{in} - g\delta_{n+1}^{(m)} >}\right) \tag{B.20}$$

Wetting: $$\delta_{n+1}^{(m)} = s_{c,n+1}^{(m)} - s_{c0w,n+1}^{(m)} \tag{B.21}$$

Drying: $$\delta_{n+1}^{(m)} = s_{c0d,n+1}^{(m)} - s_{c,n+1}^{(m)} \tag{B.22}$$

Wetting: $$\Gamma_{0,n+1}^{p(m)} = \Gamma_{0w,n+1}^{p(m)} = -\frac{1}{d_2}\frac{\left(n_{ws,n+1} - n_{wr,n+1}\right)s_{c0w,n+1}^{(m)}}{\left(n_{ws,n+1} - n_{w,n+1}^{(m)}\right)\left(n_{w,n+1}^{(m)} - n_{wr,n+1}\right)} \tag{B.23}$$

Drying: $$\Gamma_{0,n+1}^{p(m)} = \Gamma_{0d,n+1}^{p(m)} = -\frac{1}{d_3}\frac{\left(n_{ws,n+1} - n_{wr,n+1}\right)s_{c0d,n+1}^{(m)}}{\left(n_{ws,n+1} - n_{w,n+1}^{(m)}\right)\left(n_{w,n+1}^{(m)} - n_{wr,n+1}\right)} \tag{B.24}$$

Note: $\delta_{in}$ is not constant. In this model, $\delta_{in}$ changes whenever the suction loading direction is changed. In a given drying or wetting process, $\delta_{in}$ is treated as a constant.

**(I-3) Stress update algorithm**

Step 1: Initialize the local iteration number, $m$, loading index, $\Lambda$, and the incremental plastic strains, i.e.,

$$m=0,\ \Delta\varepsilon_{v,n+1}^{p(0)}=\Delta\boldsymbol{\varepsilon}_{q,n+1}^{p(0)}=\Delta n_{w,n+1}^{p(0)}=0,\ \Lambda_{n+1}^{(0)}=\Lambda_n \tag{C.1}$$

Step 2: Calculate the trial stress state using an elastic prediction

$$I_{n+1}^{(0)}=\left[\left(I_n\right)^{(1-b_1)}+\frac{K_0\left(1-b_1\right)}{p_{ref}^{b_1}}\Delta\varepsilon_{v,n+1}\right]^{1/(1-b_1)} \tag{C.2}$$

$$\mathbf{s}_{n+1}^{(0)}=\mathbf{s}_n+2G_{n+1}\Delta\boldsymbol{\varepsilon}_{q,n+1} \tag{C.3}$$

$$s_{c,\,n+1}^{(0)}=s_{c,n}+\Gamma^e\Delta n_{w,n+1} \tag{C.4}$$

$$s_{c0w,\,n+1}^{(0)}=s_{c0w,n} \tag{C.5}$$

$$s_{c0d,\,n+1}^{(0)}=s_{c0d,n} \tag{C.6}$$

Step 3: Check the suction path and yield condition:

$$f_{n+1}^{(0)}=\sqrt{\mathbf{r}_{n+1}^{(0)}:\mathbf{r}_{n+1}^{(0)}}-\sqrt{2/3}m_{n+1}^{(0)}I_{n+1}^{(0)}\sqrt{1-\left(I_{n+1}^{(0)}/I_0\right)^{\beta}}$$

(1) IF: {suction $s_c$ is constant} and { $f_{n+1}^{(0)}\le Tol_1$ }, THEN: EXIT

(2) ELSE IF: { $s_c$ is constant} and { $f_{n+1}^{(0)}>Tol_1$ }, THEN: Calculate the residuals:

$$\overline{R}_1=I_{n+1}^{(m)}-\left[\left(I_n\right)^{(1-b_1)}+\frac{K_0\left(1-b_1\right)}{p_{ref}^{b_1}}\left(\Delta\varepsilon_{v,n+1}-\Delta\varepsilon_{v,n+1}^{p(m)}\right)\right]^{1/(1-b_1)} \tag{C.7}$$

$$\overline{R}_2=\Delta\varepsilon_{v,n+1}^{p(m)}-\Lambda_{n+1}^{(m)}D_{n+1}^{(m)} \tag{C.8}$$

$$\overline{\mathbf{R}}_3=\mathbf{s}_{n+1}^{(m)}-\mathbf{s}_n-2G_{n+1}^{(m)}\left(\Delta\boldsymbol{\varepsilon}_{q,n+1}-\Delta\boldsymbol{\varepsilon}_{q,n+1}^{p(m)}\right) \tag{C.9}$$

$$\overline{\mathbf{R}}_4=\Delta\boldsymbol{\varepsilon}_{q,n+1}^{p(m)}-\Lambda_{n+1}^{(m)}\mathbf{n}_{n+1}^{(m)} \tag{C.10}$$

$$\overline{\mathbf{R}}_7 = \boldsymbol{\alpha}_{n+1}^{(m)} - \boldsymbol{\alpha}_n - \Lambda_{n+1}^{(m)} h_{n+1}^{(m)} \mathbf{b}_{n+1}^{(m)} \tag{C.11}$$

$$\overline{R}_8 = m_{n+1}^{(m)} - m_n - c_m \left(1 + e_0\right) \Lambda_{n+1}^{(m)} D_{n+1}^{(m)} \tag{C.12}$$

$$\overline{\mathbf{R}}_9 = \mathbf{F}_{n+1}^{(m)} - \mathbf{F}_n + \Lambda_{n+1}^{(m)} c_f < -D_{n+1}^{(m)} > \left(F_{\max} \mathbf{n}_{n+1}^{(m)} + \mathbf{F}_{n+1}^{(m)}\right) \tag{C.13}$$

$$\overline{R}_{12} = \sqrt{\mathbf{r}_{n+1}^{(m)} : \mathbf{r}_{n+1}^{(m)}} - \sqrt{2/3} m_{n+1}^{(m)} I_{n+1}^{(m)} \sqrt{1 - \left(I_{n+1}^{(m)} / I_0\right)^{\beta}} \tag{C.14}$$

IF: $\left\| \overline{\mathbf{R}}_{n+1}^{(m)} \right\| \le Tol_2$, THEN: Calculate the trial bounding suctions:

Wetting bound: $s_{c0w,n+1}^{(m)} = s_{c0w,n} \exp\left(\zeta v_{n+1}^{(m)} \Delta \varepsilon_{v,n+1}^{p(m)}\right)$

Drying bound: $s_{c0d,n+1}^{(m)} = s_{c0d,n} \exp\left(\zeta v_{n+1}^{(m)} \Delta \varepsilon_{v,n+1}^{p(m)}\right)$

IF: $s_{c0w,n+1}^{(m)} \le s_c \le s_{c0d,n+1}^{(m)}$, THEN:

IF: $\zeta v_{n+1}^{(m)} \Delta \varepsilon_{v,n+1}^{p(m)} \ge 0$, THEN: $\Delta n_{w,n+1}^{p(m)} = \left(s_{c0d,n+1}^{(m)} - s_{c0d,n}\right) / \Gamma_{0d,n+1}^{p(m)}$

ELSE IF: $\zeta v_{n+1}^{(m)} \Delta \varepsilon_{v,n+1}^{p(m)} < 0$, THEN: $\Delta n_{w,n+1}^{p(m)} = \left(s_{c0w,n+1}^{(m)} - s_{c0w,n}\right) / \Gamma_{0w,n+1}^{p(m)}$

END IF

ELSE IF: $s_{c0w,n+1}^{(m)} > s_c$, THEN:

$\Delta s_{c0w,n+1}^{(m)} = s_c - s_{c0w,n+1}^{(m)} < 0$ (i.e., $s_{c0w,n+1}^{(m)}$ decreases to $s_c$)

$\Delta n_{w,n+1}^{p(m)} = \Delta s_{c0w,n+1}^{(m)} / \Gamma_{0w,n+1}^{p(m)}$

$s_{c0w,n+1}^{(m)} = s_c$

$$s_{c0d,n+1}^{(m)} = s_{c0d,n} \exp\left[\zeta v_{n+1}^{(m)} \Delta \varepsilon_{v,n+1}^{p(m)} - \frac{1}{d_3} \frac{\left(n_{ws,n+1} - n_{wr,n+1}\right) \Delta n_{w,n+1}^{p(m)}}{\left(n_{ws,n+1} - n_{w,n+1}^{(m)}\right)\left(n_{w,n+1}^{(m)} - n_{wr,n+1}\right)}\right]$$

ELSE IF: $s_c > s_{c0d,n+1}^{(m)}$, THEN:

$\Delta s_{c0d,n+1}^{(m)} = s_c - s_{c0d,n+1}^{(m)} > 0$ (i.e., $s_{c0d,n+1}^{(m)}$ increases to $s_c$)

$$\Delta n_{w,n+1}^{p(m)} = \Delta s_{c0d,n+1}^{(m)} / \Gamma_{0d,n+1}^{p(m)}$$

$$s_{c0w,n+1}^{(m)} = s_{c0w,n} \exp\left[ \zeta v_{n+1}^{(m)} \Delta \varepsilon_{v,n+1}^{p(m)} - \frac{1}{d_2} \frac{\left(n_{ws,n+1} - n_{wr,n+1}\right) \Delta n_{w,n+1}^{p(m)}}{\left(n_{ws,n+1} - n_{w,n+1}^{(m)}\right)\left(n_{w,n+1}^{(m)} - n_{wr,n+1}\right)} \right]$$

$$s_{c0d,n+1}^{(m)} = s_c$$

END IF

ELSE IF: $\left\| \overline{\mathbf{R}}_{n+1}^{(m)} \right\| > Tol_2$, THEN: Obtain incremental plastic strains and internal variables by solving the system: $\mathbf{T}_{n+1}^{(m)} \Delta \mathbf{U}_{n+1}^{(m)} = -\overline{\mathbf{R}}_{n+1}^{(m)}$. $\Delta \mathbf{U}_{n+1}^{(m)}$ is a 28×28 matrix.

$$\Delta \mathbf{U}_{n+1}^{(m)} = \{ \Delta I_{n+1}^{(m)}, \Delta^2 \varepsilon_{v,n+1}^{p(m)}, \Delta \mathbf{s}_{n+1}^{(m)}, \Delta^2 \boldsymbol{\varepsilon}_{q,n+1}^{p(m)}, \Delta \boldsymbol{\alpha}_{n+1}^{(m)}, \Delta m_{n+1}^{(m)}, \Delta \mathbf{F}_{n+1}^{(m)}, \Delta \Lambda_{n+1}^{(m)} \}$$

Update stresses, plastic strains and internal variables:

$$I_{n+1}^{(m+1)} = I_{n+1}^{(m)} + \Delta I_{n+1}^{(m)}$$

$$\Delta \varepsilon_{v,n+1}^{p(m+1)} = \Delta \varepsilon_{v,n+1}^{p(m)} + \Delta^2 \varepsilon_{v,n+1}^{p(m)}$$

$$\mathbf{s}_{n+1}^{(m+1)} = \mathbf{s}_{n+1}^{(m)} + \Delta \mathbf{s}_{n+1}^{(m)}$$

$$\Delta \boldsymbol{\varepsilon}_{q,n+1}^{p(m+1)} = \Delta \boldsymbol{\varepsilon}_{q,n+1}^{p(m)} + \Delta^2 \boldsymbol{\varepsilon}_{q,n+1}^{p(m)}$$

$$\boldsymbol{\alpha}_{n+1}^{(m+1)} = \boldsymbol{\alpha}_{n+1}^{(m)} + \Delta \boldsymbol{\alpha}_{n+1}^{(m)}$$

$$m_{n+1}^{(m+1)} = m_{n+1}^{(m)} + \Delta m_{n+1}^{(m)}$$

$$\mathbf{F}_{n+1}^{(m+1)} = \mathbf{F}_{n+1}^{(m)} + \Delta \mathbf{F}_{n+1}^{(m)}$$

$$\Lambda_{n+1}^{(m+1)} = \Lambda_{n+1}^{(m)} + \Delta \Lambda_{n+1}^{(m)}$$

Set $m \rightarrow m+1$, and GO TO step 3

END IF

(3) ELSE IF: {suction $s_c$ changes} and { $f_{n+1}^{(0)} \le Tol_1$ }, THEN: Calculate the residuals:

$$\overline{R}_5 = s_{c,n+1}^{(m)} - s_{c,n} - \Gamma_{sc}^{e}\left(\Delta n_{w,n+1} - \Delta n_{w,n+1}^{p(m)}\right) \tag{C.15}$$

$$\overline{R}_6 = \Delta n_{w,n+1}^{p(m)} - \left(s_{c,n+1}^{(m)} - s_{c,n}\right)/\Gamma_{n+1}^{p(m)} \tag{C.16}$$

$$\overline{R}_8 = m_{n+1}^{(m)} - m_n - c_v\left(\frac{s_{c,n+1}^{(m)} n_{w,n+1}^{(m)}}{p_{ref}}\right)^{\varpi} \Delta n_{w,n+1}^{p(m)} \tag{C.17}$$

Wetting bound: $\overline{R}_{10} = s_{c0w,n+1}^{(m)} - s_{c0w,n} \exp\left[-\frac{1}{d_2}\frac{\left(n_{ws,n+1} - n_{wr,n+1}\right)\Delta n_{w,n+1}^{p(m)}}{\left(n_{ws,n+1} - n_{w,n+1}^{(m)}\right)\left(n_{w,n+1}^{(m)} - n_{wr,n+1}\right)}\right]$ (C.18)

Drying bound: $\overline{R}_{11} = s_{c0d,n+1}^{(m)} - s_{c0d,n} \exp\left[-\frac{1}{d_3}\frac{\left(n_{ws,n+1} - n_{wr,n+1}\right)\Delta n_{w,n+1}^{p(m)}}{\left(n_{ws,n+1} - n_{w,n+1}^{(m)}\right)\left(n_{w,n+1}^{(m)} - n_{wr,n+1}\right)}\right]$ (C.19)

IF: $\left\|\overline{\mathbf{R}}_{n+1}^{(m)}\right\| \le Tol_2$, THEN:

IF: $s_{c0w,n+1}^{(m)} \le s_c \le s_{c0d,n+1}^{(m)}$, THEN: EXIT;

ELSE IF: $s_{c0w,n+1}^{(m)} > s_c$, THEN:

$\Delta s_{c0w,n+1}^{(m)} = s_c - s_{c0w,n+1}^{(m)} < 0$ (i.e., $s_{c0w,n+1}^{(m)}$ decreases to $s_c$)

$\Delta n_{w,n+1}^{p(m)} = \Delta s_{c0w,n+1}^{(m)} / \Gamma_{0w,n+1}^{p(m)}$

$\Delta \varepsilon_{v,n+1}^{p(m)} = \Delta s_{c0w,n+1}^{(m)} / \left(s_{c0w,n+1}^{(m)} \zeta v_{n+1}^{(m)}\right)$

$s_{c0d,n+1}^{(m)} = s_{c0d,n} \exp\left[\zeta v_{n+1}^{(m)} \Delta \varepsilon_{v,n+1}^{p(m)} - \frac{1}{d_3}\frac{\left(n_{ws,n+1} - n_{wr,n+1}\right)\Delta n_{w,n+1}^{p(m)}}{\left(n_{ws,n+1} - n_{w,n+1}^{(m)}\right)\left(n_{w,n+1}^{(m)} - n_{wr,n+1}\right)}\right]$

ELSE IF: $s_c > s_{c0d,n+1}^{(m)}$, THEN:

$\Delta s_{c0d,n+1}^{(m)} = s_c - s_{c0d,n+1}^{(m)} > 0$ (i.e., $s_{c0d,n+1}^{(m)}$ increases to $s_c$)

$\Delta n_{w,n+1}^{p(m)} = \Delta s_{c0d,n+1}^{(m)} / \Gamma_{0d,n+1}^{p(m)}$

$$\Delta\varepsilon_{v,n+1}^{p(m)} = \Delta s_{c0d,n+1}^{(m)} / \left( s_{c0d,n+1}^{(m)} \zeta v_{n+1}^{(m)} \right)$$

$$s_{c0w,n+1}^{(m)} = s_{c0w,n} \exp\left[ \zeta v_{n+1}^{(m)} \Delta\varepsilon_{v,n+1}^{p(m)} - \frac{1}{d_2} \frac{\left( n_{ws,n+1} - n_{wr,n+1} \right) \Delta n_{w,n+1}^{p(m)}}{\left( n_{ws,n+1} - n_{w,n+1}^{(m)} \right) \left( n_{w,n+1}^{(m)} - n_{wr,n+1} \right)} \right]$$

END IF

ELSE IF: $\left\| \overline{\mathbf{R}}_{n+1}^{(m)} \right\| > Tol_2$, THEN: Obtain incremental plastic strains and internal variables by solving the system: $\mathbf{T}_{n+1}^{(m)} \Delta\mathbf{U}_{n+1}^{(m)} = -\overline{\mathbf{R}}_{n+1}^{(m)}$. $\Delta\mathbf{U}_{n+1}^{(m)}$ is a 5×5 matrix.

$$\Delta\mathbf{U}_{n+1}^{(m)} = \{ \Delta s_{c,n+1}^{(m)}, \Delta^2 n_{w,n+1}^{p(m)}, \Delta m_{n+1}^{(m)}, \Delta s_{0w,n+1}^{(m)}, \Delta s_{0d,n+1}^{(m)} \}$$

Update stresses, plastic strains and internal variables:

$$s_{c,n+1}^{(m+1)} = s_{c,n+1}^{(m)} + \Delta s_{c,n+1}^{(m)}$$

$$\Delta n_{w,n+1}^{p(m+1)} = \Delta n_{w,n+1}^{p(m)} + \Delta^2 n_{w,n+1}^{p(m)}$$

$$m_{n+1}^{(m+1)} = m_{n+1}^{(m)} + \Delta m_{n+1}^{(m)}$$

$$s_{c0w,n+1}^{(m+1)} = s_{c0w,n+1}^{(m)} + \Delta s_{c0w,n+1}^{(m)}$$

$$s_{c0d,n+1}^{(m+1)} = s_{c0d,n+1}^{(m)} + \Delta s_{c0d,n+1}^{(m)}$$

Set $m \rightarrow m$+1, and GO TO step 3

END IF

(4) ELSE IF: {suction $s_c$ changes} and { $f_{n+1}^{(0)} > Tol_1$ }, THEN: Calculate the residuals:

$$\overline{R}_1 = I_{n+1}^{(m)} - \left[ \left( I_n \right)^{(1-b_1)} + \frac{K_0 \left( 1 - b_1 \right)}{p_{ref}^{b_1}} \left( \Delta\varepsilon_{v,n+1} - \Delta\varepsilon_{v,n+1}^{p(m)} \right) \right]^{1/(1-b_1)} \tag{C.20}$$

$$\overline{R}_2 = \Delta\varepsilon_{v,n+1}^{p(m)} - \Lambda_{n+1}^{(m)} D_{n+1}^{(m)} \tag{C.21}$$

$$\overline{\mathbf{R}}_3 = \mathbf{s}_{n+1}^{(m)} - \mathbf{s}_n - 2G_{n+1}^{(m)} \left( \Delta\boldsymbol{\varepsilon}_{q,n+1} - \Delta\boldsymbol{\varepsilon}_{q,n+1}^{p(m)} \right) \tag{C.22}$$

$$\overline{\mathbf{R}}_4 = \Delta\boldsymbol{\varepsilon}_{q,n+1}^{p(m)} - \Lambda_{n+1}^{(m)}\mathbf{n}_{n+1}^{(m)} \tag{C.23}$$

$$\overline{R}_5 = s_{c,n+1}^{(m)} - s_{c,n} - \Gamma^e\left(\Delta n_{w,n+1} - \Delta n_{w,n+1}^{p(m)}\right) \tag{C.24}$$

$$\overline{R}_6 = \Delta n_{w,n+1}^{p(m)} - \left(s_{c,n+1}^{(m)} - s_{c,n}\right)/\Gamma_{n+1}^{p(m)} \tag{C.25}$$

$$\overline{\mathbf{R}}_7 = \boldsymbol{\alpha}_{n+1}^{(m)} - \boldsymbol{\alpha}_n - \Lambda_{n+1}^{(m)} h_{n+1}^{(m)}\mathbf{b}_{n+1}^{(m)} \tag{C.26}$$

$$\overline{R}_8 = m_{n+1}^{(m)} - m_n - c_m\left(1+e_0\right)\Lambda_{n+1}^{(m)} D_{n+1}^{(m)} - c_v\left(\frac{s_{c,n+1}^{(m)} n_{w,n+1}^{(m)}}{p_{ref}}\right)^{\varpi}\Delta n_{w,n+1}^{p(m)} \tag{C.27}$$

$$\overline{\mathbf{R}}_9 = \mathbf{F}_{n+1}^{(m)} - \mathbf{F}_n + \Lambda_{n+1}^{(m)} c_f < -D_{n+1}^{(m)} > \left(F_{\max}\mathbf{n}_{n+1}^{(m)} + \mathbf{F}_{n+1}^{(m)}\right) \tag{C.28}$$

Wetting bound:

$$\overline{R}_{10} = s_{c0w,n+1}^{(m)} - s_{c0w,n}\exp\left[\zeta\nu_{n+1}^{(m)}\Delta\varepsilon_{v,n+1}^{p(m)} - \frac{1}{d_2}\frac{\left(n_{ws,n+1} - n_{wr,n+1}\right)\Delta n_{w,n+1}^{p(m)}}{\left(n_{ws,n+1} - n_{w,n+1}^{(m)}\right)\left(n_{w,n+1}^{(m)} - n_{wr,n+1}\right)}\right] \tag{C.28}$$

Drying bound:

$$\overline{R}_{11} = s_{c0d,n+1}^{(m)} - s_{c0d,n}\exp\left[\zeta\nu_{n+1}^{(m)}\Delta\varepsilon_{v,n+1}^{p(m)} - \frac{1}{d_3}\frac{\left(n_{ws,n+1} - n_{wr,n+1}\right)\Delta n_{w,n+1}^{p(m)}}{\left(n_{ws,n+1} - n_{w,n+1}^{(m)}\right)\left(n_{w,n+1}^{(m)} - n_{wr,n+1}\right)}\right] \tag{C.29}$$

$$\overline{R}_{12} = \sqrt{\mathbf{r}_{n+1}^{(m)} : \mathbf{r}_{n+1}^{(m)}} - \sqrt{2/3}\, m_{n+1}^{(m)} I_{n+1}^{(m)}\sqrt{1 - \left(I_{n+1}^{(m)}/I_0\right)^{\beta}} \tag{C.30}$$

IF: $\left\|\overline{\mathbf{R}}_{n+1}^{(m)}\right\| \le Tol_2$, THEN:

IF: $s_{c0w,n+1}^{(m)} \le s_{c,n+1}^{(m)} \le s_{c0d,n+1}^{(m)}$, THEN: EXIT

ELSE IF: $s_{c0w,n+1}^{(m)} > s_{c,n+1}^{(m)}$, THEN:

$\Delta s_{c0w,n+1}^{(m)} = s_c - s_{c0w,n+1}^{(m)} < 0$ (i.e., $s_{c0w,n+1}^{(m)}$ decreases to $s_c$)

$\Delta n_{w,n+1}^{p(m)} = \Delta s_{c0w,n+1}^{(m)} / \Gamma_{0w,n+1}^{p(m)}$

$s_{c0w,n+1}^{(m)} = s_{c,n+1}^{(m)}$

$$s_{c0d,n+1}^{(m)} = s_{c0d,n} \exp\left[ \zeta v_{n+1}^{(m)} \Delta \varepsilon_{v,n+1}^{p(m)} - \frac{1}{d_3} \frac{\left(n_{ws,n+1} - n_{wr,n+1}\right) \Delta n_{w,n+1}^{p(m)}}{\left(n_{ws,n+1} - n_{w,n+1}^{(m)}\right)\left(n_{w,n+1}^{(m)} - n_{wr,n+1}\right)} \right]$$

ELSE IF: $s_{c,n+1}^{(m)} > s_{c0d,n+1}^{(m)}$, THEN:

$$\Delta s_{c0d,n+1}^{(m)} = s_c - s_{c0d,n+1}^{(m)} > 0 \text{ (i.e., } s_{c0d,n+1}^{(m)} \text{ increases to } s_c)$$

$$\Delta n_{w,n+1}^{p(m)} = \Delta s_{c0d,n+1}^{(m)} / \Gamma_{0d,n+1}^{p(m)}$$

$$s_{c0w,n+1}^{(m)} = s_{c0w,n} \exp\left[ \zeta v_{n+1}^{(m)} \Delta \varepsilon_{v,n+1}^{p(m)} - \frac{1}{d_2} \frac{\left(n_{ws,n+1} - n_{wr,n+1}\right) \Delta n_{w,n+1}^{p(m)}}{\left(n_{ws,n+1} - n_{w,n+1}^{(m)}\right)\left(n_{w,n+1}^{(m)} - n_{wr,n+1}\right)} \right]$$

$$s_{c0d,n+1}^{(m)} = s_{c,n+1}^{(m)}$$

END IF

ELSE IF: $\left\| \overline{\mathbf{R}}_{n+1}^{(m)} \right\| > Tol_2$, THEN: Obtain incremental plastic strains and internal variables by solving the system: $\mathbf{T}_{n+1}^{(m)} \Delta \mathbf{U}_{n+1}^{(m)} = -\overline{\mathbf{R}}_{n+1}^{(m)}$. $\Delta \mathbf{U}_{n+1}^{(m)}$ is a 32×32 matrix.

$$\Delta \mathbf{U}_{n+1}^{(m)} = \{ \Delta I_{n+1}^{(m)}, \Delta^2 \varepsilon_{v,n+1}^{p(m)}, \Delta \mathbf{s}_{n+1}^{(m)}, \Delta^2 \boldsymbol{\varepsilon}_{q,n+1}^{p(m)}, \Delta s_{c,n+1}^{(m)}, \Delta^2 n_{w,n+1}^{p(m)}, \Delta \boldsymbol{\alpha}_{n+1}^{(m)}, \Delta m_{n+1}^{(m)}, \Delta \mathbf{F}_{n+1}^{(m)}, \Delta s_{c0w,n+1}^{(m)}, \Delta s_{c0d,n+1}^{(m)} \Delta \Lambda_{n+1}^{(m)} \}$$

Update stresses, plastic strains and internal variables:

$$I_{n+1}^{(m+1)} = I_{n+1}^{(m)} + \Delta I_{n+1}^{(m)}$$

$$\Delta \varepsilon_{v,n+1}^{p(m+1)} = \Delta \varepsilon_{v,n+1}^{p(m)} + \Delta^2 \varepsilon_{v,n+1}^{p(m)}$$

$$\mathbf{s}_{n+1}^{(m+1)} = \mathbf{s}_{n+1}^{(m)} + \Delta \mathbf{s}_{n+1}^{(m)}$$

$$\Delta \boldsymbol{\varepsilon}_{q,n+1}^{p(m+1)} = \Delta \boldsymbol{\varepsilon}_{q,n+1}^{p(m)} + \Delta^2 \boldsymbol{\varepsilon}_{q,n+1}^{p(m)}$$

$$s_{c,n+1}^{(m+1)} = s_{c,n+1}^{(m)} + \Delta s_{c,n+1}^{(m)}$$

$$\Delta n_{w,n+1}^{p(m+1)} = \Delta n_{w,n+1}^{p(m)} + \Delta^2 n_{w,n+1}^{p(m)}$$

$$\boldsymbol{\alpha}_{n+1}^{(m+1)} = \boldsymbol{\alpha}_{n+1}^{(m)} + \Delta \boldsymbol{\alpha}_{n+1}^{(m)}$$

$$m_{n+1}^{(m+1)} = m_{n+1}^{(m)} + \Delta m_{n+1}^{(m)}$$

$$\mathbf{F}_{n+1}^{(m+1)} = \mathbf{F}_{n+1}^{(m)} + \Delta \mathbf{F}_{n+1}^{(m)}$$

$$s_{c0w,n+1}^{(m+1)} = s_{c0w,n+1}^{(m)} + \Delta s_{c0w,n+1}^{(m)}$$

$$s_{c0d,n+1}^{(m+1)} = s_{c0d,n+1}^{(m)} + \Delta s_{c0d,n+1}^{(m)}$$

$$\Lambda_{n+1}^{(m+1)} = \Lambda_{n+1}^{(m)} + \Delta \Lambda_{n+1}^{(m)}$$

Set $m \to m+1$, and GO TO Step 3

END IF

END IF

# APPENDIX II: COMPUTATION OF $\mathbf{T} = \dfrac{\partial \overline{\mathbf{R}}}{\partial \mathbf{U}}$

All variables in $\Delta \mathbf{U}_{n+1}^{(m)}$ are assumed to be independent basic variables except the mean intergranular confining stress $I$ is related to the matric suction $s_c$. When the matric suction is controlled to be constant, the mean intergranular confining stress is not a function of suction. From the algorithm in Appendix I, the selection of the residuals depends on the loading conditions. In the following calculation, only the general situation is treated. For simplicity, the local iteration number *m* and the step number *n*+1 are omitted.

$$\frac{\partial \overline{R}_1}{\partial I} = 1,\ \frac{\partial \overline{R}_1}{\partial \varepsilon_v^p} = \frac{K_0}{p_{ref}^{b_1}}\left[ \left(I_n\right)^{(1-b_1)} + \frac{K_0\left(1-b_1\right)}{p_{ref}^{b_1}}\left(\Delta\varepsilon_v - \Delta\varepsilon_v^p\right)\right]^{b_1/(1-b_1)} \tag{D.1}$$

$$\frac{\partial \overline{R}_1}{\partial \mathbf{s}} = 0,\ \frac{\partial \overline{R}_1}{\partial \boldsymbol{\varepsilon}_q^p} = 0,\ \frac{\partial \overline{R}_1}{\partial s_c} = \frac{\partial \overline{R}_1}{\partial I}\frac{\partial I}{\partial s_c} = \frac{\partial I}{\partial s_c},\ \frac{\partial \overline{R}_1}{\partial n_w^p} = 0 \tag{D.2}$$

$$\frac{\partial \overline{R}_1}{\partial \boldsymbol{\alpha}} = 0,\ \frac{\partial \overline{R}_1}{\partial m} = 0,\ \frac{\partial \overline{R}_1}{\partial \mathbf{F}} = 0,\ \frac{\partial \overline{R}_1}{\partial s_{0w}} = \frac{\partial \overline{R}_1}{\partial s_{0d}} = 0,\ \frac{\partial \overline{R}_1}{\partial \Lambda} = 0 \tag{D.3}$$

$$\frac{\partial \overline{R}_2}{\partial I} = -\frac{\partial D}{\partial I}\Lambda,\ \frac{\partial \overline{R}_2}{\partial \varepsilon_v^p} = 1,\ \frac{\partial \overline{R}_2}{\partial \mathbf{s}} = -\frac{\partial D}{\partial \mathbf{s}}\Lambda,\ \frac{\partial \overline{R}_2}{\partial \boldsymbol{\varepsilon}_q^p} = 0,\ \frac{\partial \overline{R}_2}{\partial s_c} = \frac{\partial \overline{R}_2}{\partial I}\frac{\partial I}{\partial s_c},\ \frac{\partial \overline{R}_2}{\partial n_w^p} = 0 \tag{D.4}$$

$$\frac{\partial \overline{R}_2}{\partial \boldsymbol{\alpha}} = -\frac{\partial D}{\partial \boldsymbol{\alpha}}\Lambda,\ \frac{\partial \overline{R}_2}{\partial m} = -\frac{\partial D}{\partial m}\Lambda,\ \frac{\partial \overline{R}_2}{\partial \mathbf{F}} = -\frac{\partial D}{\partial \mathbf{F}}\Lambda,\ \frac{\partial \overline{R}_2}{\partial s_{c0w}} = \frac{\partial \overline{R}_2}{\partial s_{c0d}} = 0,\ \frac{\partial \overline{R}_2}{\partial \Lambda} = -D \tag{D.5}$$

$$\frac{\partial \overline{\mathbf{R}}_3}{\partial I} = -2\left(\Delta\boldsymbol{\varepsilon}_q - \Delta\boldsymbol{\varepsilon}_q^p\right)\frac{\partial G}{\partial I},\ \frac{\partial \overline{\mathbf{R}}_3}{\partial \varepsilon_v^p} = 0,\ \frac{\partial \overline{\mathbf{R}}_3}{\partial \mathbf{s}} = \mathbf{I},\ \frac{\partial \overline{\mathbf{R}}_3}{\partial \boldsymbol{\varepsilon}_q^p} = 2G\mathbf{I} \tag{D.6}$$

$$\frac{\partial \overline{\mathbf{R}}_3}{\partial s_c} = \frac{\partial \overline{\mathbf{R}}_3}{\partial I}\frac{\partial I}{\partial s_c},\ \frac{\partial \overline{\mathbf{R}}_3}{\partial n_w^p} = 0,\ \frac{\partial \overline{\mathbf{R}}_3}{\partial \boldsymbol{\alpha}} = 0,\ \frac{\partial \overline{\mathbf{R}}_3}{\partial m} = 0 \tag{D.7}$$

$$\frac{\partial \overline{\mathbf{R}}_3}{\partial \mathbf{F}} = 0,\ \frac{\partial \overline{\mathbf{R}}_3}{\partial s_{c0w}} = \frac{\partial \overline{\mathbf{R}}_3}{\partial s_{c0d}} = 0,\ \frac{\partial \overline{\mathbf{R}}_3}{\partial \Lambda} = 0 \tag{D.8}$$

$$\frac{\partial \overline{\mathbf{R}}_4}{\partial I} = -\Lambda\frac{\partial \mathbf{n}}{\partial I},\ \frac{\partial \overline{\mathbf{R}}_4}{\partial \varepsilon_v^p} = 0,\ \frac{\partial \overline{\mathbf{R}}_4}{\partial \mathbf{s}} = -\Lambda\frac{\partial \mathbf{n}}{\partial \mathbf{s}},\ \frac{\partial \overline{\mathbf{R}}_4}{\partial \boldsymbol{\varepsilon}_q^p} = \mathbf{I},\ \frac{\partial \overline{\mathbf{R}}_4}{\partial s_c} = \frac{\partial \overline{\mathbf{R}}_4}{\partial I}\frac{\partial I}{\partial s_c} \tag{D.9}$$

$$\frac{\partial \overline{\mathbf{R}}_4}{\partial n_w^p} = 0,\ \frac{\partial \overline{\mathbf{R}}_4}{\partial \boldsymbol{\alpha}} = -\Lambda\frac{\partial \mathbf{n}}{\partial \boldsymbol{\alpha}},\ \frac{\partial \overline{\mathbf{R}}_4}{\partial m} = 0,\ \frac{\partial \overline{\mathbf{R}}_4}{\partial \mathbf{F}} = 0,\ \frac{\partial \overline{\mathbf{R}}_4}{\partial s_{c0w}} = \frac{\partial \overline{\mathbf{R}}_4}{\partial s_{c0d}} = 0,\ \frac{\partial \overline{\mathbf{R}}_4}{\partial \Lambda} = -\mathbf{n} \tag{D.10}$$

$$\frac{\partial \overline{R}_5}{\partial I} = 0,\ \frac{\partial \overline{R}_5}{\partial \varepsilon_v^p} = 0,\ \frac{\partial \overline{R}_5}{\partial \mathbf{s}} = 0,\ \frac{\partial \overline{R}_5}{\partial \boldsymbol{\varepsilon}_q^p} = 0,\ \frac{\partial \overline{R}_5}{\partial s_c} = 1,\ \frac{\partial \overline{R}_5}{\partial n_w^p} = \Gamma^e \tag{D.11}$$

$$\frac{\partial \overline{R}_5}{\partial \boldsymbol{\alpha}} = 0,\ \frac{\partial \overline{R}_5}{\partial m} = 0,\ \frac{\partial \overline{R}_5}{\partial \mathbf{F}} = 0,\ \frac{\partial \overline{R}_5}{\partial s_{c0w}} = \frac{\partial \overline{R}_5}{\partial s_{c0d}} = 0,\ \frac{\partial \overline{R}_5}{\partial \Lambda} = 0 \tag{D.12}$$

$$\frac{\partial \overline{R}_6}{\partial I} = 0,\ \frac{\partial \overline{R}_6}{\partial \varepsilon_v^p} = 0,\ \frac{\partial \overline{R}_6}{\partial \mathbf{s}} = 0,\ \frac{\partial \overline{R}_6}{\partial \boldsymbol{\varepsilon}_q^p} = 0 \tag{D.13}$$

$$\frac{\partial \overline{R}_6}{\partial s_c} = \frac{-1}{\Gamma^p} + \frac{\left(s_c - s_{c,n}\right)}{\left(\Gamma^p\right)^2}\frac{\partial \Gamma^p}{\partial s_c},\ \frac{\partial \overline{R}_6}{\partial n_w^p} = 1,\ \frac{\partial \overline{R}_6}{\partial \boldsymbol{\alpha}} = 0,\ \frac{\partial \overline{R}_6}{\partial m} = 0,\ \frac{\partial \overline{R}_6}{\partial \mathbf{F}} = 0 \tag{D.14}$$

$$\frac{\partial \overline{R}_6}{\partial s_{c0w}} = \frac{\left(s_c - s_{c,n}\right)}{\left(\Gamma^p\right)^2}\frac{\partial \Gamma^p}{\partial s_{c0w}},\ \frac{\partial \overline{R}_6}{\partial s_{c0d}} = \frac{\left(s_c - s_{c,n}\right)}{\left(\Gamma^p\right)^2}\frac{\partial \Gamma^p}{\partial s_{c0d}},\ \frac{\partial \overline{R}_6}{\partial \Lambda} = 0 \tag{D.15}$$

$$\frac{\partial \overline{\mathbf{R}}_7}{\partial I} = -\Lambda\left(\mathbf{b}\frac{\partial h}{\partial I} + h\frac{\partial \mathbf{b}}{\partial I}\right),\ \frac{\partial \overline{\mathbf{R}}_7}{\partial \varepsilon_v^p} = -\Lambda\frac{\partial (h\mathbf{b})}{\partial \varepsilon_v^p} = 0 \tag{D.16}$$

$$\frac{\partial \overline{\mathbf{R}}_7}{\partial \mathbf{s}} = -\Lambda\left(\mathbf{b}\frac{\partial h}{\partial \mathbf{s}} + h\frac{\partial \mathbf{b}}{\partial \mathbf{s}}\right),\ \frac{\partial \overline{\mathbf{R}}_7}{\partial \boldsymbol{\varepsilon}_q^p} = -\Lambda\frac{\partial (h\mathbf{b})}{\partial \boldsymbol{\varepsilon}_q^p} = 0 \tag{D.17}$$

$$\frac{\partial \overline{\mathbf{R}}_7}{\partial s_c} = -\Lambda\left(\mathbf{b}\frac{\partial h}{\partial s_c} + h\frac{\partial \mathbf{b}}{\partial s_c}\right),\ \frac{\partial \overline{\mathbf{R}}_7}{\partial n_w^p} = 0\,,\ \frac{\partial \overline{\mathbf{R}}_7}{\partial \boldsymbol{\alpha}} = \mathbf{I} - \Lambda\frac{\partial (h\mathbf{b})}{\partial \boldsymbol{\alpha}} \tag{D.18}$$

$$\frac{\partial \overline{\mathbf{R}}_7}{\partial m} = -\Lambda\frac{\partial (h\mathbf{b})}{\partial m},\ \frac{\partial \overline{\mathbf{R}}_7}{\partial \mathbf{F}} = -\Lambda\frac{\partial (h\mathbf{b})}{\partial \mathbf{F}},\ \frac{\partial \overline{\mathbf{R}}_7}{\partial s_{c0w}} = \frac{\partial \overline{\mathbf{R}}_7}{\partial s_{c0d}} = 0\,,\ \frac{\partial \overline{\mathbf{R}}_7}{\partial \Lambda} = -h\mathbf{b} \tag{D.19}$$

$$\frac{\partial \overline{R}_8}{\partial I} = -c_m(1+e_0)\Lambda\frac{\partial D}{\partial I},\frac{\partial \overline{R}_8}{\partial \varepsilon_v^p} = 0,\frac{\partial \overline{R}_8}{\partial \mathbf{s}} = -c_m(1+e_0)\Lambda\frac{\partial D}{\partial \mathbf{s}},\frac{\partial \overline{R}_8}{\partial \boldsymbol{\varepsilon}_q^p} = 0 \tag{D.20}$$

$$\frac{\partial \overline{R}_8}{\partial s_c} = -c_m(1+e_0)\Lambda\frac{\partial D}{\partial I}\frac{\partial I}{\partial s_c} - \varpi c_v\left(\frac{n_w}{p_{ref}}\right)^{\varpi} s_c{}^{(\varpi-1)}\Delta n_w^p\,,\ \frac{\partial \overline{R}_8}{\partial n_w^p} = -c_v\left(\frac{s_c n_w}{p_{ref}}\right)^{\varpi} \tag{D.21}$$

$$\frac{\partial \overline{R}_8}{\partial \boldsymbol{\alpha}} = -c_m(1+e_0)\Lambda\frac{\partial D}{\partial \boldsymbol{\alpha}},\ \frac{\partial \overline{R}_8}{\partial \mathbf{F}} = -c_m(1+e_0)\Lambda\frac{\partial D}{\partial \mathbf{F}} \tag{D.22}$$

$$\frac{\partial \overline{R}_8}{\partial m} = 1 - c_m(1+e_0)\Lambda\frac{\partial D}{\partial m}\,,\ \frac{\partial \overline{R}_8}{\partial s_{c0w}} = \frac{\partial \overline{R}_8}{\partial s_{c0d}} = 0\,,\ \frac{\partial \overline{R}_8}{\partial \Lambda} = -c_m(1+e_0)D \tag{D.23}$$

$$\frac{\partial \overline{\mathbf{R}}_9}{\partial I} = \Lambda c_f\left[< -D > F_{\max}\frac{\partial \mathbf{n}}{\partial I} + \frac{\partial < -D >}{\partial I}(F_{\max}\mathbf{n} + \mathbf{F})\right] \tag{D.24}$$

$$\frac{\partial \overline{\mathbf{R}}_9}{\partial \mathbf{s}} = \Lambda c_f\left[< -D > F_{\max}\frac{\partial \mathbf{n}}{\partial \mathbf{s}} + \frac{\partial < -D >}{\partial \mathbf{s}}(F_{\max}\mathbf{n} + \mathbf{F})\right] \tag{D.25}$$

$$\frac{\partial \overline{\mathbf{R}}_9}{\partial \boldsymbol{\alpha}} = \Lambda c_f\left[< -D > F_{\max}\frac{\partial \mathbf{n}}{\partial \boldsymbol{\alpha}} + \frac{\partial < -D >}{\partial \boldsymbol{\alpha}}(F_{\max}\mathbf{n} + \mathbf{F})\right] \tag{D.26}$$

$$\frac{\partial \overline{\mathbf{R}}_9}{\partial \varepsilon_v^p} = 0\,,\ \frac{\partial \overline{\mathbf{R}}_7}{\partial \boldsymbol{\varepsilon}_q^p} = 0\,,\ \frac{\partial \overline{\mathbf{R}}_9}{\partial s_c} = \frac{\partial \overline{\mathbf{R}}_9}{\partial I}\frac{\partial I}{\partial s_c}\,,\ \frac{\partial \overline{\mathbf{R}}_9}{\partial n_w^p} = 0\,,\ \frac{\partial \overline{\mathbf{R}}_9}{\partial s_{c0w}} = \frac{\partial \overline{\mathbf{R}}_9}{\partial s_{c0d}} = 0 \tag{D.27}$$

$$\frac{\partial \overline{\mathbf{R}}_9}{\partial m} = \Lambda c_f \frac{\partial < -D >}{\partial m}(F_{\max}\mathbf{n} + \mathbf{F}) \tag{D.28}$$

$$\frac{\partial \overline{\mathbf{R}}_9}{\partial \mathbf{F}} = \mathbf{I} + \Lambda c_f \left[ < -D > \mathbf{I} + \frac{\partial < -D >}{\partial \mathbf{F}}(F_{\max}\mathbf{n} + \mathbf{F}) \right], \frac{\partial \overline{\mathbf{R}}_9}{\partial \Lambda} = c_f < -D > (F_{\max}\mathbf{n} + \mathbf{F}) \tag{D.29}$$

$$\frac{\partial \overline{R}_{10}}{\partial I} = 0, \frac{\partial \overline{R}_{10}}{\partial \varepsilon_v^p} = -\zeta v s_{0w,n} \exp\left[ \zeta v \Delta \varepsilon_v^p - \frac{1}{d_2} \frac{(n_{ws} - n_{wr})\Delta n_w^p}{(n_{ws} - n_w)(n_w - n_{wr})} \right] \tag{D.30}$$

$$\frac{\partial \overline{R}_{10}}{\partial \mathbf{s}} = 0, \frac{\partial \overline{R}_{10}}{\partial \boldsymbol{\varepsilon}_q^p} = 0, \frac{\partial \overline{R}_{10}}{\partial s_c} = 0 \tag{D.31}$$

$$\frac{\partial \overline{R}_{10}}{\partial n_w^p} = \frac{1}{d_2} \frac{(n_{ws} - n_{wr})s_{0w,n}}{(n_{ws} - n_w)(n_w - n_{wr})} \exp\left[ \zeta v \Delta \varepsilon_v^p - \frac{1}{d_2} \frac{(n_{ws} - n_{wr})\Delta n_w^p}{(n_{ws} - n_w)(n_w - n_{wr})} \right] \tag{D.32}$$

$$\frac{\partial \overline{R}_{10}}{\partial \boldsymbol{\alpha}} = 0, \frac{\partial \overline{R}_{10}}{\partial m} = 0, \frac{\partial \overline{R}_{10}}{\partial \mathbf{F}} = 0, \frac{\partial \overline{R}_{10}}{\partial s_{c0w}} = 1, \frac{\partial \overline{R}_{10}}{\partial s_{c0d}} = 0, \frac{\partial \overline{R}_{10}}{\partial \Lambda} = 0 \tag{D.33}$$

$$\frac{\partial \overline{R}_{11}}{\partial I} = 0, \frac{\partial \overline{R}_{11}}{\partial \varepsilon_v^p} = -\zeta v s_{0d,n} \exp\left[ \zeta v \Delta \varepsilon_v^p - \frac{1}{d_3} \frac{(n_{ws} - n_{wr})\Delta n_w^p}{(n_{ws} - n_w)(n_w - n_{wr})} \right] \tag{D.34}$$

$$\frac{\partial \overline{R}_{11}}{\partial \mathbf{s}} = 0, \frac{\partial \overline{R}_{11}}{\partial \boldsymbol{\varepsilon}_q^p} = 0, \frac{\partial \overline{R}_{11}}{\partial s_c} = 0 \tag{D.35}$$

$$\frac{\partial \overline{R}_{11}}{\partial n_w^p} = \frac{1}{d_3} \frac{(n_{ws} - n_{wr})s_{0d,n}}{(n_{ws} - n_w)(n_w - n_{wr})} \exp\left[ \zeta v \Delta \varepsilon_v^p - \frac{1}{d_3} \frac{(n_{ws} - n_{wr})\Delta n_w^p}{(n_{ws} - n_w)(n_w - n_{wr})} \right] \tag{D.36}$$

$$\frac{\partial \overline{R}_{11}}{\partial \boldsymbol{\alpha}} = 0, \frac{\partial \overline{R}_{11}}{\partial m} = 0, \frac{\partial \overline{R}_{11}}{\partial \mathbf{F}} = 0, \frac{\partial \overline{R}_{11}}{\partial s_{c0w}} = 0, \frac{\partial \overline{R}_{11}}{\partial s_{c0d}} = 1, \frac{\partial \overline{R}_{11}}{\partial \Lambda} = 0 \tag{D.37}$$

$$\frac{\partial \overline{R}_{12}}{\partial I} = \frac{\partial \sqrt{\mathbf{r}:\mathbf{r}}}{\partial I} - \sqrt{2/3}m\left(\frac{2-(2+\beta)(I/I_0)^{\beta}}{2\sqrt{1-(I/I_0)^{\beta}}}\right) \tag{D.38}$$

$$\frac{\partial \overline{R}_{12}}{\partial \varepsilon_v^p} = 0,\ \frac{\partial \overline{R}_{12}}{\partial \mathbf{s}} = \frac{\partial \sqrt{\mathbf{r}:\mathbf{r}}}{\partial \mathbf{s}},\ \frac{\partial \overline{R}_{12}}{\partial \boldsymbol{\varepsilon}_q^p} = 0 \tag{D.39}$$

$$\frac{\partial \overline{R}_{12}}{\partial s_c} = \frac{\partial \overline{R}_{12}}{\partial I}\frac{\partial I}{\partial s_c},\ \frac{\partial \overline{R}_{12}}{\partial n_w^p} = 0,\ \frac{\partial \overline{R}_{12}}{\partial \boldsymbol{\alpha}} = \frac{\partial \sqrt{\mathbf{r}:\mathbf{r}}}{\partial \boldsymbol{\alpha}} \tag{D.40}$$

$$\frac{\partial \overline{R}_{12}}{\partial m} = -\frac{\sqrt{6}}{6} I\sqrt{1-(I/I_0)^{\beta}},\ \frac{\partial \overline{R}_{12}}{\partial \mathbf{F}} = 0,\ \frac{\partial \overline{R}_{12}}{\partial s_{c0w}} = \frac{\partial \overline{R}_{12}}{\partial s_{c0d}} = 0,\ \frac{\partial \overline{R}_{12}}{\partial \Lambda} = 0 \tag{D.41}$$

In the above-mentioned quantities, more calculations should be carried out to give more details and all the relationships are listed below:

$$\begin{aligned}\frac{\partial D}{\partial I} &= B_0\frac{\partial <\mathbf{F}:\mathbf{n}>}{\partial I}(\mathbf{d}:\mathbf{n}) + B\frac{\partial(\mathbf{d}:\mathbf{n})}{\partial I} \\ &= B_0\left(\mathbf{F}:\frac{\partial \mathbf{n}}{\partial I}\right)(\mathbf{d}:\mathbf{n}) + B\left[\sqrt{\frac{2}{3}}\frac{\partial(\alpha_\theta^d)}{\partial I} - \frac{\partial(\boldsymbol{\alpha}:\mathbf{n})}{\partial I}\right]\end{aligned} \tag{D.42}$$

$$\begin{aligned}\frac{\partial D}{\partial \mathbf{s}} &= B_0\frac{\partial <\mathbf{F}:\mathbf{n}>}{\partial \mathbf{s}}(\mathbf{d}:\mathbf{n}) + B\frac{\partial(\mathbf{d}:\mathbf{n})}{\partial \mathbf{s}_{n+1}} \\ &= B_0\left(\mathbf{F}:\frac{\partial \mathbf{n}}{\partial \mathbf{s}}\right)(\mathbf{d}:\mathbf{n}) + B\left[\sqrt{\frac{2}{3}}\frac{\partial(\alpha_\theta^d)}{\partial \mathbf{s}} - \frac{\partial(\boldsymbol{\alpha}:\mathbf{n})}{\partial \mathbf{s}}\right]\end{aligned} \tag{D.43}$$

$$\begin{aligned}\frac{\partial D}{\partial \boldsymbol{\alpha}} &= B_0\frac{\partial <\mathbf{F}:\mathbf{n}>}{\partial \boldsymbol{\alpha}}(\mathbf{d}:\mathbf{n}) + B\frac{\partial(\mathbf{d}:\mathbf{n})}{\partial \boldsymbol{\alpha}} \\ &= B_0\left(\mathbf{F}:\frac{\partial \mathbf{n}}{\partial \boldsymbol{\alpha}}\right)(\mathbf{d}:\mathbf{n}) + B\left[\sqrt{\frac{2}{3}}\frac{\partial(\alpha_\theta^d)}{\partial \boldsymbol{\alpha}} - \frac{\partial(\boldsymbol{\alpha}:\mathbf{n})}{\partial \boldsymbol{\alpha}}\right]\end{aligned} \tag{D.44}$$

$$\frac{\partial D}{\partial \mathbf{F}} = B_0 \frac{\partial < \mathbf{F} : \mathbf{n} >}{\partial \mathbf{F}} (\mathbf{d} : \mathbf{n}) + B \frac{\partial (\mathbf{d} : \mathbf{n})}{\partial \mathbf{F}}$$
$$= B_0 \frac{\partial < \mathbf{F} : \mathbf{n} >}{\partial \mathbf{F}} (\mathbf{d} : \mathbf{n}) + B \left[ \sqrt{\frac{2}{3}} \frac{\partial (\alpha_\theta^d)}{\partial \mathbf{F}} - \frac{\partial (\boldsymbol{\alpha} : \mathbf{n})}{\partial \mathbf{F}} \right] \tag{D.45}$$

$$\frac{\partial D}{\partial m} = B \frac{\partial (\mathbf{d} : \mathbf{n})}{\partial m} = \sqrt{\frac{2}{3}} B \frac{\partial (\alpha_\theta^d)}{\partial m}, \ \frac{\partial D}{\partial s_c} = \frac{\partial D}{\partial I} \frac{\partial I}{\partial s_c} \tag{D.46}$$

$$\frac{\partial G}{\partial I} = G_0 d_1 I^{d_1 - 1} p_{ref}^{-d_1}, \ \frac{\partial I}{\partial s_c} = n_w \tag{D.47}$$

New definition: $\hat{m} = \sqrt{\left( \frac{\mathbf{s}}{I} - \boldsymbol{\alpha} \right) : \left( \frac{\mathbf{s}}{I} - \boldsymbol{\alpha} \right)} = \sqrt{\bar{\mathbf{r}} : \bar{\mathbf{r}}}$, $\mathbf{n} = \frac{\bar{\mathbf{r}}}{\sqrt{\bar{\mathbf{r}} : \bar{\mathbf{r}}}}$

$$\frac{\partial \mathbf{n}}{\partial I} = \frac{-(\bar{\mathbf{r}} + \boldsymbol{\alpha})}{I \ \hat{m}} + \frac{\bar{\mathbf{r}} [\bar{\mathbf{r}} : (\bar{\mathbf{r}} + \boldsymbol{\alpha})]}{I \ \hat{m}^3}, \ \frac{\partial \mathbf{n}}{\partial \mathbf{s}} = \frac{\mathbf{I}}{I \ \hat{m}} - \frac{\bar{\mathbf{r}} \otimes \bar{\mathbf{r}}}{I \ \hat{m}^3} \tag{D.48}$$

$$\frac{\partial \mathbf{n}}{\partial \boldsymbol{\alpha}} = \frac{-\mathbf{I}}{\hat{m}} + \frac{\left( \frac{\mathbf{s}}{I} - \boldsymbol{\alpha} \right) \otimes \left( \frac{\mathbf{s}}{I} - \boldsymbol{\alpha} \right)}{\hat{m}^3} = \frac{-\mathbf{I}}{\hat{m}} + \frac{\bar{\mathbf{r}} \otimes \bar{\mathbf{r}}}{\hat{m}^3} \tag{D.49}$$

$$\frac{\partial \mathbf{b}}{\partial I} = \sqrt{\frac{2}{3}} \left( \alpha_\theta^b * \frac{\partial \mathbf{n}}{\partial I} + \mathbf{n} * \frac{\partial \alpha_\theta^b}{\partial I} \right), \ \frac{\partial \mathbf{b}}{\partial \mathbf{s}} = \sqrt{\frac{2}{3}} \left( \alpha_\theta^b * \frac{\partial \mathbf{n}}{\partial \mathbf{s}} + \mathbf{n} * \frac{\partial \alpha_\theta^b}{\partial \mathbf{s}} \right), \ \frac{\partial \mathbf{b}}{\partial s_c} = \frac{\partial \mathbf{b}}{\partial I} \frac{\partial I}{\partial s_c} \tag{D.50}$$

$$\frac{\partial \mathbf{b}}{\partial \boldsymbol{\alpha}} = \sqrt{\frac{2}{3}} \left( \alpha_\theta^b * \frac{\partial \mathbf{n}}{\partial \boldsymbol{\alpha}} + \mathbf{n} * \frac{\partial \alpha_\theta^b}{\partial \boldsymbol{\alpha}} \right) - \mathbf{I}, \ \frac{\partial \mathbf{b}}{\partial m} = \sqrt{\frac{2}{3}} \frac{\partial \alpha_\theta^b}{\partial m} * \mathbf{n}, \ \frac{\partial \mathbf{b}}{\partial \mathbf{F}} = \sqrt{\frac{2}{3}} \frac{\partial \alpha_\theta^b}{\partial \mathbf{F}} * \mathbf{n} \tag{D.51}$$

$$\frac{\partial h}{\partial I} = h_0 \left[ \frac{\frac{\partial |\mathbf{b} : \mathbf{n}|}{\partial I} * b_{ref} - \frac{\partial b_{ref}}{\partial I} * |\mathbf{b} : \mathbf{n}|}{\left( b_{ref} - |\mathbf{b} : \mathbf{n}| \right)^2} \right], \ \frac{\partial h}{\partial \mathbf{s}} = h_0 \left[ \frac{\frac{\partial |\mathbf{b} : \mathbf{n}|}{\partial \mathbf{s}} * b_{ref} - \frac{\partial b_{ref}}{\partial \mathbf{s}} * |\mathbf{b} : \mathbf{n}|}{\left( b_{ref} - |\mathbf{b} : \mathbf{n}| \right)^2} \right] \tag{D.52}$$

$$\frac{\partial h}{\partial \boldsymbol{\alpha}} = h_0 \left[ \frac{\frac{\partial |\mathbf{b} : \mathbf{n}|}{\partial \boldsymbol{\alpha}} * b_{ref} - \frac{\partial b_{ref}}{\partial \boldsymbol{\alpha}} * |\mathbf{b} : \mathbf{n}|}{\left( b_{ref} - |\mathbf{b} : \mathbf{n}| \right)^2} \right], \ \frac{\partial h}{\partial m} = h_0 \left[ \frac{\frac{\partial |\mathbf{b} : \mathbf{n}|}{\partial m} * b_{ref} - \frac{\partial b_{ref}}{\partial m} * |\mathbf{b} : \mathbf{n}|}{\left( b_{ref} - |\mathbf{b} : \mathbf{n}| \right)^2} \right] \tag{D.53}$$

$$\frac{\partial h}{\partial \mathbf{F}} = h_0 \left[ \frac{\dfrac{\partial |\mathbf{b}:\mathbf{n}|}{\partial \mathbf{F}} * b_{ref} - \dfrac{\partial b_{ref}}{\partial \mathbf{F}} * |\mathbf{b}:\mathbf{n}|}{\left(b_{ref} - |\mathbf{b}:\mathbf{n}|\right)^2} \right], \quad \frac{\partial h}{\partial s_c} = h_0 \left[ \frac{\dfrac{\partial |\mathbf{b}:\mathbf{n}|}{\partial s_c} * b_{ref} - \dfrac{\partial b_{ref}}{\partial s_c} * |\mathbf{b}:\mathbf{n}|}{\left(b_{ref} - |\mathbf{b}:\mathbf{n}|\right)^2} \right] \tag{D.54}$$

$$\frac{\partial \sqrt{\mathbf{r}:\mathbf{r}}}{\partial I} = \frac{(\mathbf{s} - I\boldsymbol{\alpha}):(-\boldsymbol{\alpha})}{\sqrt{(\mathbf{s} - I\boldsymbol{\alpha}):(\mathbf{s} - I\boldsymbol{\alpha})}} = -\hat{m}_1^{-1}\bar{\mathbf{r}}:\boldsymbol{\alpha}, \quad \frac{\partial \sqrt{\mathbf{r}:\mathbf{r}}}{\partial \mathbf{s}} = \frac{(\mathbf{s} - I\boldsymbol{\alpha})}{\sqrt{(\mathbf{s} - I\boldsymbol{\alpha}):(\mathbf{s} - I\boldsymbol{\alpha})}} = \hat{m}^{-1}\bar{\mathbf{r}} \tag{D.55}$$

$$\frac{\partial \sqrt{\mathbf{r}:\mathbf{r}}}{\partial \boldsymbol{\alpha}} == \frac{-I(\mathbf{s} - I\boldsymbol{\alpha})}{\sqrt{(\mathbf{s} - I\boldsymbol{\alpha}):(\mathbf{s} - I\boldsymbol{\alpha})}} = -I\ \hat{m}^{-1}\bar{\mathbf{r}} \tag{D.56}$$

More calculations are needed:

$$\frac{\partial \mathbf{d}}{\partial I} = \sqrt{\frac{2}{3}}\left( \alpha_\theta^d * \frac{\partial \mathbf{n}}{\partial I} + \mathbf{n} * \frac{\partial \alpha_\theta^d}{\partial I} \right), \quad \frac{\partial \mathbf{d}}{\partial \mathbf{s}} = \sqrt{\frac{2}{3}}\left( \alpha_\theta^d * \frac{\partial \mathbf{n}}{\partial \mathbf{s}} + \mathbf{n} * \frac{\partial \alpha_\theta^d}{\partial \mathbf{s}} \right) \tag{D.57}$$

$$\frac{\partial \mathbf{d}}{\partial \boldsymbol{\alpha}} = \sqrt{\frac{2}{3}}\left( \alpha_\theta^d * \frac{\partial \mathbf{n}}{\partial \boldsymbol{\alpha}} + \mathbf{n} * \frac{\partial \alpha_\theta^d}{\partial \boldsymbol{\alpha}} \right) - \mathbf{I}, \quad \frac{\partial \mathbf{d}}{\partial m} = \sqrt{\frac{2}{3}} \frac{\partial \alpha_\theta^d}{\partial m}\mathbf{n}, \quad \frac{\partial \mathbf{d}}{\partial s_c} = \sqrt{\frac{2}{3}}\left( \mathbf{n} * \frac{\partial \alpha_\theta^d}{\partial s_c} \right) \tag{D.58}$$

Recall the following relationships:

$$b_{ref} = 2\sqrt{2/3}\alpha_c^b, \ \alpha_c^b = M_c^c + k_c^b < -\psi > -m\sqrt{1-(I/I_0)^\beta} \tag{D.59}$$

$$\alpha_\theta^b = g(\theta, c)M_c^c + g(\theta, c_b)k_c^b < -\psi > -m\sqrt{1-(I/I_0)^\beta} \tag{D.60}$$

$$\alpha_\theta^d = g(\theta, c)M_c^c + g(\theta, c_d)k_c^d\psi - m\sqrt{1-(I/I_0)^\beta} \tag{D.61}$$

$$\psi = e - e_c = e - e_{cr} + \lambda\left( \frac{I}{p_{ref}} \right)^\xi \tag{D.62}$$

$$\frac{\partial b_{ref}}{\partial I} = 2\sqrt{\frac{2}{3}} \frac{\partial \alpha_c^b}{\partial I} = 2\sqrt{\frac{2}{3}}\left( k_c^b \frac{\partial < -\psi >}{\partial I} + \frac{m\beta}{I} \frac{(I/I_0)^\beta}{2\sqrt{1-(I/I_0)^\beta}} \right) \tag{D.63}$$

$$\frac{\partial b_{ref}}{\partial \mathbf{s}} = 2\sqrt{\frac{2}{3}}\frac{\partial \alpha_c^b}{\partial \mathbf{s}} = 2\sqrt{\frac{2}{3}}\left( k_c^b \frac{\partial < -\psi >}{\partial \mathbf{s}} \right),\ \frac{\partial b_{ref}}{\partial \boldsymbol{\alpha}} = 2\sqrt{\frac{2}{3}}\frac{\partial \alpha_c^b}{\partial \boldsymbol{\alpha}} = 0 \tag{D.64}$$

$$\frac{\partial b_{ref}}{\partial m} = 2\sqrt{\frac{2}{3}}\frac{\partial \alpha_c^b}{\partial m} = -2\sqrt{\frac{2}{3}}\sqrt{1-\left(I/I_0\right)^{\beta}} \tag{D.65}$$

$$\frac{\partial b_{ref}}{\partial \mathbf{F}} = 2\sqrt{\frac{2}{3}}\frac{\partial \alpha_c^b}{\partial \mathbf{F}} = 2\sqrt{\frac{2}{3}}\left( k_c^b \frac{\partial < -\psi >}{\partial \mathbf{F}} \right),\ \frac{\partial b_{ref}}{\partial s_c} = 2\sqrt{\frac{2}{3}}\frac{\partial \alpha_c^b}{\partial s_c} = 2\sqrt{\frac{2}{3}}k_c^b \frac{\partial < -\psi >}{\partial I}\frac{\partial I}{\partial s_c} \tag{D.66}$$

$$\frac{\partial \alpha_\theta^b}{\partial I} = \frac{\partial g(\theta,c)}{\partial I}M_c^c + \frac{\partial g(\theta,c_b)}{\partial I}k_c^b < -\psi > + g(\theta,c_b)k_c^b \frac{\partial < -\psi >}{\partial I} + \frac{m\beta}{I}\frac{\left(I/I_0\right)^{\beta}}{2\sqrt{1-\left(I/I_0\right)^{\beta}}} \tag{D.67}$$

$$\frac{\partial \alpha_\theta^b}{\partial \mathbf{s}} = \frac{\partial g(\theta,c)}{\partial \mathbf{s}}M_c^c + \frac{\partial g(\theta,c_b)}{\partial \mathbf{s}}k_c^b < -\psi > \tag{D.68}$$

$$\frac{\partial \alpha_\theta^b}{\partial \boldsymbol{\alpha}} = \frac{\partial g(\theta,c)}{\partial \boldsymbol{\alpha}}M_c^c + \frac{\partial g(\theta,c_b)}{\partial \boldsymbol{\alpha}}k_c^b < -\psi > \tag{D.69}$$

$$\frac{\partial \alpha_\theta^b}{\partial m} = -\sqrt{1-\left(I/I_0\right)^{\beta}},\ \frac{\partial \alpha_\theta^b}{\partial \mathbf{F}} = 0 \tag{D.70}$$

$$\frac{\partial \alpha_\theta^b}{\partial s_c} = \frac{\partial \alpha_\theta^b}{\partial I}\frac{\partial I}{\partial s_c} \tag{D.71}$$

$$\frac{\partial \alpha_\theta^d}{\partial I} = \frac{\partial g(\theta,c)}{\partial I}M_c^c + \frac{\partial g(\theta,c_d)}{\partial I}k_c^d \psi + g(\theta,c_d)k_c^d \frac{\partial \psi}{\partial I} + \frac{m\beta}{I}\frac{\left(I/I_0\right)^{\beta}}{2\sqrt{1-\left(I/I_0\right)^{\beta}}} \tag{D.72}$$

$$\frac{\partial \alpha_\theta^d}{\partial \mathbf{s}} = \frac{\partial g(\theta,c)}{\partial \mathbf{s}}M_c^c + \frac{\partial g(\theta,c_d)}{\partial \mathbf{s}}k_c^d \psi \tag{D.73}$$

$$\frac{\partial \alpha_\theta^d}{\partial \boldsymbol{\alpha}} = \frac{\partial g(\theta,c)}{\partial \boldsymbol{\alpha}}M_c^c + \frac{\partial g(\theta,c_d)}{\partial \boldsymbol{\alpha}}k_c^d \psi \tag{D.74}$$

$$\frac{\partial \alpha_\theta^d}{\partial m} = -\sqrt{1-\left(I/I_0\right)^{\beta}},\ \frac{\partial \alpha_\theta^d}{\partial \mathbf{F}} = 0 \tag{D.75}$$

$$\frac{\partial \alpha_\theta^d}{\partial s_c} = \frac{\partial \alpha_\theta^d}{\partial I}\frac{\partial I}{\partial s_c} \tag{D.76}$$

$$\frac{\partial g(\theta,c)}{\partial I}=\frac{\partial g(\theta,c)}{\partial(\cos 3\theta)}\frac{\partial(\cos 3\theta)}{\partial I}=\frac{2c(1-c)}{\left[(1+c)-(1-c)\cos 3\theta\right]^2}\frac{\partial(\cos 3\theta)}{\partial I} \tag{D.77}$$

$$\frac{\partial g(\theta,c)}{\partial \mathbf{s}}=\frac{\partial g(\theta,c)}{\partial(\cos 3\theta)}\frac{\partial(\cos 3\theta)}{\partial \mathbf{s}}=\frac{2c(1-c)}{\left[(1+c)-(1-c)\cos 3\theta\right]^2}\frac{\partial(\cos 3\theta)}{\partial \mathbf{s}} \tag{D.78}$$

$$\frac{\partial g(\theta,c)}{\partial \boldsymbol{\alpha}}=\frac{\partial g(\theta,c)}{\partial(\cos 3\theta)}\frac{\partial(\cos 3\theta)}{\partial \boldsymbol{\alpha}}=\frac{2c(1-c)}{\left[(1+c)-(1-c)\cos 3\theta\right]^2}\frac{\partial(\cos 3\theta)}{\partial \boldsymbol{\alpha}} \tag{D.79}$$

$$\frac{\partial(\cos 3\theta)}{\partial I}=\frac{\partial(\cos 3\theta)}{\partial \bar{S}}\frac{\partial \bar{S}}{\partial I}+\frac{\partial(\cos 3\theta)}{\partial \bar{J}}\frac{\partial \bar{J}}{\partial I}=\frac{9\sqrt{3}}{2}\left(\frac{\bar{S}^2}{\bar{J}^3}\frac{\partial \bar{S}}{\partial I}-\frac{\bar{S}^3}{\bar{J}^4}\frac{\partial \bar{J}}{\partial I}\right) \tag{D.80}$$

$$\frac{\partial(\cos 3\theta)}{\partial \mathbf{s}}=\frac{\partial(\cos 3\theta)}{\partial \bar{S}}\frac{\partial \bar{S}}{\partial \mathbf{s}}+\frac{\partial(\cos 3\theta)}{\partial \bar{J}}\frac{\partial \bar{J}}{\partial \mathbf{s}}=\frac{9\sqrt{3}}{2}\left(\frac{\bar{S}^2}{\bar{J}^3}\frac{\partial \bar{S}}{\partial \mathbf{s}}-\frac{\bar{S}^3}{\bar{J}^4}\frac{\partial \bar{J}}{\partial \mathbf{s}}\right) \tag{D.81}$$

$$\frac{\partial(\cos 3\theta)}{\partial \boldsymbol{\alpha}}=\frac{\partial(\cos 3\theta)}{\partial \bar{S}}\frac{\partial \bar{S}}{\partial \boldsymbol{\alpha}}+\frac{\partial(\cos 3\theta)}{\partial \bar{J}}\frac{\partial \bar{J}}{\partial \boldsymbol{\alpha}}=\frac{9\sqrt{3}}{2}\left(\frac{\bar{S}^2}{\bar{J}^3}\frac{\partial \bar{S}}{\partial \boldsymbol{\alpha}}-\frac{\bar{S}^3}{\bar{J}^4}\frac{\partial \bar{J}}{\partial \boldsymbol{\alpha}}\right) \tag{D.82}$$

Important notations related to the second and third invariants:

As to the vector $\begin{bmatrix}\bar{r}_1 & \bar{r}_4 & \bar{r}_6\\ \bar{r}_4 & \bar{r}_2 & \bar{r}_5\\ \bar{r}_6 & \bar{r}_5 & \bar{r}_3\end{bmatrix}$, $\bar{\mathbf{r}}=\frac{\mathbf{r}}{I}=\left(\frac{\mathbf{s}}{I}-\boldsymbol{\alpha}\right)$, $\bar{r}_i=\frac{s_i}{I}-\alpha_i$:

Its second invariant is calculated as $\bar{J}=\left[tr\left(\bar{\mathbf{r}}^2\right)/2\right]^{1/2}$ and the trace is:

$$tr\left(\bar{\mathbf{r}}^2\right)=\bar{r}_1^2+\bar{r}_2^2+\bar{r}_3^2+2(\bar{r}_4^2+\bar{r}_5^2+\bar{r}_6^2) \tag{D.83}$$

$$\frac{\partial tr\left(\bar{\mathbf{r}}^2\right)}{\partial \bar{r}_1}=2\bar{r}_1,\ \frac{\partial tr\left(\bar{\mathbf{r}}^2\right)}{\partial \bar{r}_2}=2\bar{r}_2,\ \frac{\partial tr\left(\bar{\mathbf{r}}^2\right)}{\partial \bar{r}_3}=2\bar{r}_3,\frac{\partial tr\left(\bar{\mathbf{r}}^2\right)}{\partial \bar{r}_4}=4\bar{r}_4,\ \frac{\partial tr\left(\bar{\mathbf{r}}^2\right)}{\partial \bar{r}_5}=4\bar{r}_5,\ \frac{\partial tr\left(\bar{\mathbf{r}}^2\right)}{\partial \bar{r}_6}=4\bar{r}_6 \tag{D.84}$$

Its third invariant is calculated as $\bar{S}=\left[tr\left(\bar{\mathbf{r}}^3\right)/3\right]^{1/3}$ and the trace is:

$$\begin{aligned}tr\left(\bar{\mathbf{r}}^3\right)=&\bar{r}_1(\bar{r}_1^2+\bar{r}_4^2+\bar{r}_6^2)+\bar{r}_2(\bar{r}_4^2+\bar{r}_2^2+\bar{r}_5^2)+\bar{r}_3(\bar{r}_3^2+\bar{r}_5^2+\bar{r}_6^2)\\&+2\bar{r}_4(\bar{r}_1\bar{r}_4+\bar{r}_2\bar{r}_4+\bar{r}_5\bar{r}_6)+2\bar{r}_5(\bar{r}_6\bar{r}_4+\bar{r}_2\bar{r}_5+\bar{r}_5\bar{r}_3)+2\bar{r}_6(\bar{r}_1\bar{r}_6+\bar{r}_5\bar{r}_4+\bar{r}_3\bar{r}_6)\end{aligned} \tag{D.85}$$

$$\frac{\partial tr\left(\bar{\mathbf{r}}^3\right)}{\partial \bar{r}_1} = 3(\bar{r}_1^2 + \bar{r}_4^2 + \bar{r}_6^2), \frac{\partial tr\left(\bar{\mathbf{r}}^3\right)}{\partial \bar{r}_2} = 3(\bar{r}_2^2 + \bar{r}_4^2 + \bar{r}_5^2), \frac{\partial tr\left(\bar{\mathbf{r}}^3\right)}{\partial \bar{r}_3} = 3(\bar{r}_3^2 + \bar{r}_5^2 + \bar{r}_6^2) \quad \text{(D.86)}$$

$$\frac{\partial tr\left(\bar{\mathbf{r}}^3\right)}{\partial \bar{r}_4} = 6(\bar{r}_1\bar{r}_4 + \bar{r}_2\bar{r}_4 + \bar{r}_5\bar{r}_6), \frac{\partial tr\left(\bar{\mathbf{r}}^3\right)}{\partial \bar{r}_5} = 6(\bar{r}_2\bar{r}_5 + \bar{r}_3\bar{r}_5 + \bar{r}_4\bar{r}_6), \frac{\partial tr\left(\bar{\mathbf{r}}^3\right)}{\partial \bar{r}_6} = 6(\bar{r}_1\bar{r}_6 + \bar{r}_3\bar{r}_6 + \bar{r}_4\bar{r}_5) \quad \text{(D.87)}$$

$$\frac{\partial \bar{J}}{\partial I} = \frac{\sum_{i=1}^{6}[\frac{\partial tr(\bar{\mathbf{r}}^2)}{\partial \bar{r}_i} \times \frac{\partial \bar{r}_i}{\partial I}]}{4\left[\frac{1}{2} tr\left(\bar{\mathbf{r}}^2\right)\right]^{1/2}} = -\frac{\sum_{i=1}^{6}[\frac{\partial tr(\bar{\mathbf{r}}^2)}{\partial \bar{r}_i} \times \frac{s_i}{I^2}]}{4\left[\frac{1}{2} tr\left(\bar{\mathbf{r}}^2\right)\right]^{1/2}} = -\frac{tr\left(\bar{\mathbf{r}} : \mathbf{s}\right)}{2\left[\frac{1}{2} tr\left(\bar{\mathbf{r}}^2\right)\right]^{1/2} I^2} \quad \text{(D.88)}$$

$$\frac{\partial \bar{J}}{\partial s_i} = \frac{\sum_{j=1}^{6}[\frac{\partial tr(\bar{\mathbf{r}}^2)}{\partial \bar{r}_j} \times \frac{\partial \bar{r}_j}{\partial s_i}]}{4\left[\frac{1}{2} tr\left(\bar{\mathbf{r}}^2\right)\right]^{1/2}} = \frac{\frac{\partial tr(\bar{\mathbf{r}}^2)}{\partial \bar{r}_i}}{4\left[\frac{1}{2} tr\left(\bar{\mathbf{r}}^2\right)\right]^{1/2} I}, \frac{\partial \bar{J}}{\partial \boldsymbol{\alpha}} = -I \frac{\partial \bar{J}}{\partial \mathbf{s}} \text{ (i=1,6)} \quad \text{(D.89)}$$

$$\frac{\partial \bar{S}}{\partial I} = \frac{\sum_{i=1}^{6}[\frac{\partial tr(\bar{\mathbf{r}}^3)}{\partial \bar{r}_i} \times \frac{\partial \bar{r}_i}{\partial I}]}{9\left[\frac{1}{3} tr\left(\bar{\mathbf{r}}^3\right)\right]^{2/3}} = -\frac{\sum_{i=1}^{6}[\frac{\partial tr(\bar{\mathbf{r}}^3)}{\partial \bar{r}_i} \times \frac{s_i}{I^2}]}{9\left[\frac{1}{3} tr\left(\bar{\mathbf{r}}^3\right)\right]^{2/3}} = -\frac{tr\left(\bar{\mathbf{r}}^2 : \mathbf{s}\right)}{3\left[\frac{1}{3} tr\left(\bar{\mathbf{r}}^3\right)\right]^{2/3} I^2} \quad \text{(D.90)}$$

$$\frac{\partial \bar{S}}{\partial s_i} = \frac{\sum_{j=1}^{6}[\frac{\partial tr(\bar{\mathbf{r}}^3)}{\partial \bar{r}_j} \times \frac{\partial \bar{r}_j}{\partial s_i}]}{9\left[\frac{1}{3} tr\left(\bar{\mathbf{r}}^3\right)\right]^{2/3}} = \frac{\frac{\partial tr(\bar{\mathbf{r}}^3)}{\partial \bar{r}_i}}{9\left[\frac{1}{3} tr\left(\bar{\mathbf{r}}^3\right)\right]^{2/3} I}, \frac{\partial \bar{S}}{\partial \boldsymbol{\alpha}} = -I \frac{\partial \bar{S}}{\partial \mathbf{s}} \text{ (i=1,6)} \quad \text{(D.91)}$$

$$\frac{\partial \psi}{\partial I} = \lambda \xi \frac{I^{\xi-1}}{p_{ref}^{\xi}}, \frac{\partial \psi}{\partial \boldsymbol{\alpha}} = 0, \frac{\partial \psi}{\partial \mathbf{s}} = 0, \frac{\partial \psi}{\partial \mathbf{F}} = 0 \quad \text{(D.92)}$$

$$\frac{\partial \Gamma^p}{\partial s_c} = \frac{\partial \Gamma^p}{\partial \Gamma_0^p} \frac{\partial \Gamma_0^p}{\partial s_c} + \Gamma_0^p H \frac{\partial\left(\delta / < \delta_{in} - g\delta >\right)}{\partial \delta} \frac{\partial \delta}{\partial s_c} \quad \text{(D.93)}$$

$$\frac{\partial \Gamma^p}{\partial s_{c0w}} = \frac{\partial \Gamma^p}{\partial \Gamma_0^p} \frac{\partial \Gamma_0^p}{\partial s_{c0w}} + \Gamma_0^p H \frac{\partial\left(\delta / < \delta_{in} - g\delta >\right)}{\partial \delta} \frac{\partial \delta}{\partial s_{c0w}} \quad \text{(D.94)}$$

$$\frac{\partial \Gamma^p}{\partial s_{c0d}} = \frac{\partial \Gamma^p}{\partial \Gamma_0^p}\frac{\partial \Gamma_0^p}{\partial s_{c0d}} + \Gamma_0^p H \frac{\partial\left(\delta / < \delta_{in} - g\delta >\right)}{\partial \delta}\frac{\partial \delta}{\partial s_{c0d}} \tag{D.95}$$

$$\frac{\partial \Gamma^p}{\partial \Gamma_0^p} = \left(1 + H \cdot \delta / < \delta_{in} - g\delta >\right),\ \frac{\partial \Gamma_0^p}{\partial s_c} = 0 \tag{D.96}$$

$$\frac{\partial \Gamma_0^p}{\partial s_{c0w}} = -\frac{1}{d_2}\frac{\left(n_{ws} - n_{wr}\right)}{\left(n_{ws} - n_w\right)\left(n_w - n_{wr}\right)},\ \frac{\partial \Gamma_0^p}{\partial s_{c0d}} = -\frac{1}{d_3}\frac{\left(n_{ws} - n_{wr}\right)}{\left(n_{ws} - n_w\right)\left(n_w - n_{wr}\right)} \tag{D.97}$$

$$\frac{\partial\left(\delta / < \delta_{in} - g\delta >\right)}{\partial \delta} = \frac{< \delta_{in} - g\delta > + g\delta < \delta_{in} - g\delta > /\left(\delta_{in} - g\delta\right)}{\left(< \delta_{in} - g\delta >\right)^2} \tag{D.98}$$

Wetting: $\partial\delta / \partial s_c = 1$, $\partial\delta / \partial s_{c0w} = -1$; Drying: $\partial\delta / \partial s_c = -1$, $\partial\delta / \partial s_{c0d} = 1$ (D.99)

# APPENDIX III: CONSISTENT TANGENT STIFFNESS MATRIX

The consistent tangent stiffness matrix is calculated following the procedure by Manzari and Prachathananukit (2001). The general stress-strain relation and its incremental form are given as follows:

$$\boldsymbol{\sigma}_{n+1} = \boldsymbol{\sigma}_n + \mathbf{D}^e_{n+1} : \left(\Delta\boldsymbol{\varepsilon}_{n+1} - \Lambda \mathbf{R}_{n+1}\right), \text{ with } \mathbf{R}_{n+1} = \mathbf{n}_{n+1} + \frac{1}{3} D_{n+1}\mathbf{I} \tag{E.1}$$

$$\begin{aligned} \underline{d\boldsymbol{\sigma}_{n+1}} &= \mathbf{D}^e_{n+1} : d\left(\Delta\boldsymbol{\varepsilon}_{n+1}\right) - d\Lambda \mathbf{D}^e_{n+1} : \mathbf{R}_{n+1} + \left( \left.\frac{\partial \mathbf{D}^e}{\partial \boldsymbol{\sigma}}\right|_{n+1} : \underline{d\boldsymbol{\sigma}_{n+1}} \right) : \left(\Delta\boldsymbol{\varepsilon}_{n+1} - \Lambda \mathbf{R}_{n+1}\right) \\ &- \Lambda \mathbf{D}^e_{n+1} : \left[ \left.\frac{\partial \mathbf{R}}{\partial \boldsymbol{\sigma}}\right|_{n+1} : \underline{d\boldsymbol{\sigma}_{n+1}} + \left.\frac{\partial \mathbf{R}}{\partial \boldsymbol{\alpha}}\right|_{n+1} : d\boldsymbol{\alpha}_{n+1} + \left.\frac{\partial \mathbf{R}}{\partial m}\right|_{n+1} dm_{n+1} + \left.\frac{\partial \mathbf{R}}{\partial \mathbf{F}}\right|_{n+1} : d\mathbf{F}_{n+1} \right] \end{aligned} \tag{E.2}$$

Rearrange (E-2) as:

$$\begin{aligned} &\left[ \mathbf{I} + \Lambda_{n+1} \mathbf{D}^e_{n+1} : \left.\frac{\partial \mathbf{R}}{\partial \boldsymbol{\sigma}}\right|_{n+1} + \Lambda_{n+1} \left.\frac{\partial \mathbf{D}^e}{\partial \boldsymbol{\sigma}}\right|_{n+1} : \mathbf{R}_{n+1} - \left.\frac{\partial \mathbf{D}^e}{\partial \boldsymbol{\sigma}}\right|_{n+1} : \Delta\boldsymbol{\varepsilon}_{n+1} \right] : d\boldsymbol{\sigma}_{n+1} \\ &= \mathbf{D}^e_{n+1} : \left\{ d\left(\Delta\boldsymbol{\varepsilon}_{n+1}\right) - d\Lambda \mathbf{R}_{n+1} - \Lambda \left[ \left.\frac{\partial \mathbf{R}}{\partial \boldsymbol{\alpha}}\right|_{n+1} : d\boldsymbol{\alpha}_{n+1} + \left.\frac{\partial \mathbf{R}}{\partial m}\right|_{n+1} dm_{n+1} + \left.\frac{\partial \mathbf{R}}{\partial \mathbf{F}}\right|_{n+1} : d\mathbf{F}_{n+1} \right] \right\} \end{aligned} \tag{E.3}$$

Rewrite (E.3) in a simplified form as: $d\boldsymbol{\sigma}_{n+1} = \mathbf{D}^*_{n+1} : \left(d\left(\Delta\boldsymbol{\varepsilon}_{n+1}\right) - d\Lambda \mathbf{R}^*_{n+1}\right)$ (E.4)

$$\mathbf{D}^*_{n+1} = \left[ \mathbf{I} + \Lambda_{n+1} \mathbf{D}^e_{n+1} : \left.\frac{\partial \mathbf{R}}{\partial \boldsymbol{\sigma}}\right|_{n+1} + \Lambda_{n+1} \left.\frac{\partial \mathbf{D}^e}{\partial \boldsymbol{\sigma}}\right|_{n+1} : \mathbf{R}_{n+1} - \left.\frac{\partial \mathbf{D}^e}{\partial \boldsymbol{\sigma}}\right|_{n+1} : \Delta\boldsymbol{\varepsilon}_{n+1} \right]^{-1} \mathbf{D}^e_{n+1} \tag{E.5.1}$$

$$\mathbf{R}^*_{n+1} = \mathbf{R}_{n+1} + h_{n+1} \left.\frac{\partial \mathbf{R}}{\partial \boldsymbol{\alpha}}\right|_{n+1} : \mathbf{b}_{n+1} + c_m (1+e_0) D_{n+1} \left.\frac{\partial \mathbf{R}}{\partial m}\right|_{n+1} - c_f \langle -D_{n+1} \rangle \left.\frac{\partial \mathbf{R}}{\partial \mathbf{F}}\right|_{n+1} : \left(F_{\max} \mathbf{n}_{n+1} + \mathbf{F}_{n+1}\right) \tag{E.5.2}$$

Note that Eq. (E.4) is very similar to the stress-strain relationship. From eq. (E.4):

$$
\begin{aligned}
d\boldsymbol{\sigma}_{n+1} &= \mathbf{D}^{*}_{n+1} : d\left(\Delta\boldsymbol{\varepsilon}_{n+1}\right) - d\Lambda \mathbf{D}^{*}_{n+1} : \mathbf{R}^{*}_{n+1} \\
&= \mathbf{D}^{*}_{n+1} : d\left(\Delta\boldsymbol{\varepsilon}_{n+1}\right) - \frac{1}{K_s^p} \mathbf{L}^{*}_{n+1} : d\boldsymbol{\sigma}_{n+1} \mathbf{D}^{*}_{n+1} : \mathbf{R}^{*}_{n+1}
\end{aligned}
\tag{E.6.1}
$$

$$
d\boldsymbol{\sigma}_{n+1} + \frac{1}{K_s^p} \mathbf{L}^{*}_{n+1} : d\boldsymbol{\sigma}_{n+1} \mathbf{D}^{*}_{n+1} : \mathbf{R}^{*}_{n+1} = \mathbf{D}^{*}_{n+1} : d\left(\Delta\boldsymbol{\varepsilon}_{n+1}\right) \tag{E.6.2}
$$

$$
\frac{d\boldsymbol{\sigma}_{n+1}}{d\left(\Delta\boldsymbol{\varepsilon}_{n+1}\right)} = \frac{\mathbf{D}^{*}_{n+1}}{1 + \frac{1}{K^{p}_{s,n+1}} \mathbf{L}^{*}_{n+1} : \mathbf{D}^{*}_{n+1} : \mathbf{R}^{*}_{n+1}} = \mathbf{D}^{ep}_{n+1} \tag{E.6.3}
$$

The consistent tangent operator is obtained using a standard procedure as:

$$
\mathbf{D}^{ep}_{n+1} = \left[ \mathbf{D}^{*}_{n+1} - \frac{\left(\mathbf{D}^{*}_{n+1} : \mathbf{R}^{*}_{n+1}\right) \otimes \left(\mathbf{L}^{*}_{n+1} : \mathbf{D}^{*}_{n+1}\right)}{K^{p}_{s,n+1} + \left(\mathbf{L}^{*}_{n+1} : \mathbf{D}^{*}_{n+1} : \mathbf{R}^{*}_{n+1}\right)} \right] \tag{E.7}
$$

$$
K^{p}_{s,n+1} = -\frac{1}{\Lambda} \left( \left. \frac{\partial f}{\partial \boldsymbol{\alpha}} \right|_{n+1} : \Delta\boldsymbol{\alpha}_{n+1} + \left. \frac{\partial f}{\partial m} \right|_{n+1} \Delta m_{n+1} \right) \tag{E.8.1}
$$

$$
\mathbf{L}^{*}_{n+1} = \frac{\partial f}{\partial \boldsymbol{\sigma}_{n+1}} = \mathbf{n}_{n+1} - \frac{1}{3} N_{n+1} \mathbf{I} = \mathbf{n}_{n+1} - \frac{1}{3} \left[ \left(\boldsymbol{\alpha}_{n+1} : \mathbf{n}_{n+1}\right) + \sqrt{\frac{2}{3}} m \left( \frac{2 - (2+\beta)\left(\frac{I}{I_0}\right)^{\beta}}{2\sqrt{1 - \left(\frac{I}{I_0}\right)^{\beta}}} \right) \right] \mathbf{I} \tag{E.8.2}
$$

Note: $\mathbf{D}^{e}$ is a fourth-order tensor and its second-order form is given below:

$$
\left[\mathbf{D}^{e}\right]_{6\times 6} = \begin{bmatrix}
(K + 4G/3) & (K - 2G/3) & (K - 2G/3) & 0 & 0 & 0 \\
(K - 2G/3) & (K + 4G/3) & (K - 2G/3) & 0 & 0 & 0 \\
(K - 2G/3) & (K - 2G/3) & (K + 4G/3) & 0 & 0 & 0 \\
0 & 0 & 0 & G & 0 & 0 \\
0 & 0 & 0 & 0 & G & 0 \\
0 & 0 & 0 & 0 & 0 & G
\end{bmatrix} \tag{E.9}
$$

In fact, the above consistent tangent operator in Eq. (E.7) and the elastic stiffness matrix in Eq. (E.9) are just for the soil skeleton. The hydraulic mechanism is not included and

they should be accounted for separately. In this way, the elastic stiffness matrix in Eq. (E.9) will be expanded to a 7x7 matrix with the element of $D^e(7,7) = \Gamma^e$, while the corresponding element in the consistent tangent modulus from the soil water characteristic curves is $D^{ep}(7,7) = 1/(1/\Gamma^e + 1/\Gamma^p) = \Gamma^e\Gamma^p/\left(\Gamma^e + \Gamma^p\right)$.